UNIVERSITY OF CALIFORNIA

Santa Barbara

Fabrication of Polymer Brushes via Light-Mediated Polymerization and Polymerization of Acrylic Acid

A dissertation submitted in partial satisfaction of the

requirements for the degree Doctor of Philosophy

in Chemistry

by

Benjaporn Narupai

Committee in charge:

Professor Craig J. Hawker, Chair

Professor Javier Read de Alaniz

Professor R. Daniel Little

Professor Michael L. Chabinyc

December 2018

The dissertation of Benjaporn Narupai is approved.

_____
Javier Read de Alaniz

_____
R. Daniel Little

_____
Michael L. Chabinyc

_____
Craig J. Hawker, Committee Chair

November 2018

Fabrication of Polymer Brushes via Light-Mediated Polymerization

and Polymerization of Acrylic Acid

ACKNOWLEDGEMENTS

First of all, I would like to thank my advisor, Craig Hawker. I still remember how excited I was when I received the offer to join his group. Craig has been very supportive throughout my Ph.D. He has inspired me to become a better scientist. Craig has taught me to be self-critical with every result, to make sure that they are convincing and impactful and has taught me tirelessly to improve my scientific thinking, creativity, presentation and writing skills, always putting a lot of effort teaching me to make my work more valuable and unique. He always encourages me to talk to people including those who are not in the polymer field to get opinions from different perspectives. Craig has created a good environment in the group by having people with a variety of backgrounds, different expertise and encourages everyone to help each other. I feel so lucky to be part of the group and cannot thank Craig enough for all opportunities and support that he gave me not only as his graduate student but will also continue to give throughout my future career.

I would like to thank my committee members, Prof. Javier Read de Alaniz, Prof. R. Daniel Little and Prof. Michael L. Chabinyc for their help and support. I appreciate the many helpful discussions and useful advice given during my candidacy and proposal exams, and the continued guidance and encouragement throughout my Ph.D.

I would like to thank Justin Poelma. Justin was a senior graduate student when I joined the group. He helped me for a smooth start in the group during my first year, showed me my way around the lab, taught me to grow polymer brushes from the surface, and how to use a glovebox. I enjoyed working with Justin a lot, and I am forever grateful for his patience to kindly teach me when I had no experience. He also encouraged me and helped me apply for

my first ACS conference in San Francisco. Building on the expertise I learned from Justin, I ended up leading and/or participating in so many more projects related to polymer brushes after he graduated.

Zak Page was a former postdoc in the group. I thank Craig a lot for pairing me with him. Zak is an incredible postdoc. He is smart, hard-working and highly motivated. Zak was always the first one in the lab in the morning. Zak was a great resource for me not only in fundamental organic synthesis but also from a materials viewpoint. Every time I needed help, Zak was the first person that I went and talked to. Zak has been an amazing mentor, his encouragement and compassion helped me during the difficult times. I cannot thank him enough for everything he has done for me. I feel so lucky to have worked with such a great scientist like Zak for the last two years of my Ph.D.

I am thankful to all Hawker group members. I have been surrounded by so many talented people. I benefited from working alongside Jing Ren and Johannes Willenbacher on a poly(acrylic acid) project, where I learned a lot from them. The video of the rapid polymerization we made together was one of my favorite videos in graduate school. For the last two months before my defense, I worked with Reggie Bou Zerdan on the branched poly(acrylic acid) polymers. I had so much fun and laughed so hard when we worked together in Blab. I would like to thank Reggie for all the joy she brought. I would also like to thank Christian Pester for helping me with many surface characterization techniques. I appreciated fruitful discussion with Athina Anastasaki on ATRP and thank her for teaching me Cu(0)-mediated polymerization. I would like to thank Alaina McGrath for her useful advice and the time spent in her office discussing random topics. I appreciated scientific discussion with Jia Niu and his help on cell work. I am grateful to Stephanie Barbon for her help with scientific

writing and helpful advice. I greatly appreciate her willingness to help. I am also very thankful for former and current group members including Nicolas Treat, Brett Fors, Revital Kaminker, Jimmy Lawrence, Yingdong Luo, In-Hwan Lee, Abby Knight, Morgan Schulze, Neil Dolinski, Allison Abdilla, Caitlin Sample, Yvonne Diaz, Emre Discekici, Akira Watanabe, Zhishuai (Frank) Geng and Eileen Seo for all their help and making my life at UCSB so enjoyable.

As an international student, I live far away from my home and family. A group of Thai students at UCSB including Piyatida Klumphu, Varistha Chobpattana, Pinn Siraprapasiri, Krittiya Carter, Preeti Overtcjaiyapong, Chatarin Wangsanuwat, Jakkarin Limwongyut, and John Carter have made studying abroad so fun. We got together almost every Friday night to play board games, hang out and cook Thai food that you cannot get at any restaurants in Santa Barbara. Probably though, my most favorite time was playing with the kids and teaching them to speak Thai. My life at UCSB was filled with lots of memorable experiences. Without them, I would have been homesick staying away from home. I am thankful for their support and care.

Lastly, the most important people that I would like to acknowledge is my family. They have supported me on every step in my life. Thanks to all technology that made it so easy to talk to them! I thank my family for always being there for me to share all difficult and happy times together. I was extremely ecstatic when my family came to the US to celebrate my graduation. Seeing their smile at that special event is priceless. With understanding, caring and loving from my family, I would not ask for anything more.

VITA OF BENJAPORN NARUPAI

December 2018

Education

2013 - 2018 Ph.D. Materials Chemistry

Chemistry and Biochemistry Department, University of California Santa Barbara

2008 – 2012 B.Sc. Chemistry (Honors Program, First-Class Honors)

Chemistry Department, Chulalongkorn University, Thailand

Research Experience

2013 - Present Advisor: Prof. Craig J. Hawker

Graduate Researcher, Materials Research Laboratory

University of California Santa Barbara

- Developed synthetic strategies to prepare well-defined, multifunctional polymer brush patterns via light-mediated controlled radical polymerization
- Developed a novel strategy for the synthesis of branched polymer brushes by sequential light-mediated polymerization
- Synthesized multicolored arrays of polymer brushes with micron feature resolution for organic light emitting diode - *in collaboration with the Dow Chemical Company*
- Synthesized hierarchical polymer brush patterns to engineer surface properties in a continuous manner

- Established an iodine transfer radical polymerization of acrylic acid – *in collaboration with the Dow Chemical Company*

2011 Advisor: Prof. Thomas J. McCarthy
Visiting Researcher, Polymer Science and Engineering Department
University of Massachusetts Amherst

- Prepared chemically patterned surfaces using photolithography for surface-supported crystal arrays

2008 – 2012 Advisor: Assoc. Prof. Voravee P. Hoven
Undergraduate Researcher, Chemistry Department
Chulalongkorn University, Thailand

- Synthesized and polymerized a methyl red-derived monomer for colorimetric DNA sequence detection on a paper-based platform
- Prepared polymer brushes for protein patterning using photolithography

Technical Skills: Atomic force microscopy, X-ray photoelectron spectroscopy, Secondary ion mass spectrometry, Profilometry, Scanning electron microscopy, Transmission electron microscopy, Fluorescent microscopy, UV-Vis spectroscopy, NMR spectroscopy, Fourier-transform infrared spectroscopy, Gel permeation chromatography, Contact angle goniometry, Optical reflectometry, Gas chromatography mass spectrometry, Optical microscopy

Publications

9. **Narupai, B**; Willenbacher, J.; Ren, M. J.; Barbon, S. M.; Schulze. M. W.; Bou Zerdan, R.; Lee, I. H.; Discekici, E. H.; Anastasaki, A.; McGrath, A. J.; Laitar, D. S.; Van Dyk, A. K.; Hawker, C. J. "Low Temperature, Rapid Copolymerization of Acrylic Acid and Sodium Acrylate in Water." *Manuscript available upon request.*

8. **Narupai, B**; Page, Z. A.; Treat, N. J.; McGrath, A. J.; Pester. C. W.; Discekici, E. H.; Dolinski, N. D.; Meyers, G. F.; Read De Alaniz, J.; Hawker, C. J. "Simultaneous Preparation of Multiple Polymer Brushes under Ambient Conditions using Microliter Volumes." *Angew. Chem. Int. Ed.* **2018**, *57,* 13433-13438. DOI: 10.1002/anie.201805534

7. Page, Z. A.; **Narupai, B**.; Pester, C. W.; Bou Zerdan, R.; Sokolov, A.; Laitar, D. S.; Mukhopadhyay, S.; Sprague, S.; McGrath, A. J.; Kramer, J. W.; Trefonas, P.; Hawker, C. J. "Novel Strategy for Photopatterning Emissive Polymer Brushes for Organic Light Emitting Diode Applications." *ACS Cent. Sci.* **2017,** *3*, 654-661. DOI: 10.1021/acscentsci.7b00165

6. Page, Z. A.; Chiu, C.-Y.; **Narupai, B.**; Laitar, D. S.; Mukhopadhyay, S.; Sokolov, A.; Hudson, Z. M.; Bou Zerdan, R.; McGrath, A. J.; Kramer, J. W.; Barton, B. E.; Hawker, C. J. "Highly Photoluminescent Nonconjugated Polymers for Single-Layer Light Emitting Diodes." *ACS Photonics* **2017**, *4*, 631-641. DOI: 10.1021/acsphotonics.6b00994

5. Pester, C. W.; **Narupai, B.**; Mattson, K. M.; Bothman, D. P.; Klinger, D.; Lee, K. W.; Discekici, E. H.; Hawker, C. J. "Engineering Surfaces through Sequential Stop-Flow Photopatterning." *Adv. Mater.* **2016,** *28*, 9292-9300. DOI: 10.1002/adma.201602900

4. **Narupai, B.**; Poelma, J. E.; Pester, C. W.; McGrath, A. J.; Toumayan, E. P.; Luo, Y.; Kramer, J. W.; Clark, P. G.; Ray, P. C.; Hawker, C. J. "Hierarchical Comb Brush Architectures via Sequential Light-Mediated Controlled Radical Polymerizations." *J. Polym. Sci. Part A: Polym. Chem.* **2016,** *54*, 2276-2284. DOI: 10.1002/pola.28128 – *Front cover*

3. Discekici, E. H.; Pester, C. W.; Treat, N. J.; Lawrence, J.; Mattson, K. M.; **Narupai, B.**; Toumayan, E. P.; Luo, Y.; McGrath, A. J.; Clark, P. G.; Read De Alaniz, J.; Hawker, C. J. "Simple Benchtop Approach to Polymer Brush Nanostructures Using Visible-Light-Mediated Metal-Free Atom Transfer Radical Polymerization." *ACS Macro Lett.* **2016,** *5*, 258-262. DOI: 10.1021/acsmacrolett.6b00004

2. Pester, C. W.; Poelma, J. E.; **Narupai, B.**; Patel, S. N.; Su, G. M.; Mates, T. E.; Luo, Y.; Ober, C. K.; Hawker, C. J.; Kramer, E. J. "Ambiguous Anti-Fouling Surfaces: Facile Synthesis by Light-Mediated Radical Polymerization." *J. Polym. Sci. Part A: Polym. Chem.* **2016,** *54*, 253-262. DOI: 10.1002/pola.27748 – *Front cover*

1. Sangsuwan, A.; **Narupai, B.**; Sae-ung, P.; Rodtamai, S.; Rodthongkum, N.; Hoven, V. P. "Patterned Poly(acrylic acid) Brushes Containing Gold Nanoparticles for Peptide Detection by Surface-Assisted Laser Desorption/Ionization Mass Spectrometry." *Anal. Chem.* **2015,** *87*, 10738-10746. DOI: 10.1021/acs.analchem.5b00734

Patents

2. Hawker, C. J.; Page, Z. A.; Trefonas III, P.; Sokolov, A. N.; Kramer, J.; Laitar, D. S.; Mukhopadhyay, S.; **Narupai, B.**; Pester, C. W. "Photopatterned growth of electronically active brush polymers for light emitting diode displays." U.S. Patent Application No. 15476492 filed March 31, **2017**.

1. Hawker, C. J.; Page, Z. A.; Trefonas III, P.; Sokolov, A. N.; Kramer, J.; Laitar, D. S.; Mukhopadhyay, S.; **Narupai, B.**; Pester, C. W. "Photopatterned growth of electronically active brush polymers for light emitting diode displays." U.S. Patent Application No. 15476470 filed March 31, **2017**.

Honors and Awards

2013 – Present	Full Scholarship for Graduate Study from the Royal Thai Government, awarded to 4 students under the Development and Promotion of Science and Technology Talents Project
2008 – 2012	Full Scholarship for Undergraduate Study from the Royal Thai Government, awarded to 60 students under the Development and Promotion of Science and Technology Talents Project
2012	Poster Presentation Award from the 7th Conference on Science and Technology for Youths
2012	Selected Representative from the Department of Chemistry, Chulalongkorn University to attend the Hitachi Trophy 2012 Oral Presentation

2009	Oral Presentation Award from the Development and Promotion of Science and Technology Talents Project Conference
2007	Science and Technology Research Grant from the 10th Young Scientist Competition: YSC 2007, National Electronics and Computer Technology Center
2007	Selected Representative of Thai Students to attend the 34th Professor Harry Messel Australia International Science School, The University of Sydney

Professional Presentations

Jan 2018	Materials Research Outreach Symposium, University of California Santa Barbara, CA "Metal-Free Visible Light-Induced Growth of Polymer Brushes under Ambient Conditions"
Mar 2016	251st National ACS Meeting, San Diego, CA "Hierarchical Comb Brush Architectures via Sequential Light-Mediated Controlled Radical Polymerizations"
Feb 2016	Materials Research Outreach Symposium, University of California Santa Barbara, CA "Hierarchical Comb Brush Architectures via Sequential Light-Mediated Controlled Radical Polymerizations"
Nov 2015	UTEP-UCSB-PREM Workshop on Materials Chemistry Energy Conversion and Storage, University of California Santa Barbara, CA "Hierarchical Comb Brush Architectures via Sequential Light-Mediated Controlled Radical Polymerizations"

Jul 2015	15th SSCC&MS Conference, Jackson State University, MS – *Invited talk* "Hierarchical Comb Brush Architectures via Sequential Light-Mediated Controlled Radical Polymerizations"
Jun 2015	Gordon Research Conference: Polymer, South Hadley, MA "Control of Comb Brush Architectures via Light-mediated Controlled Radical Polymerization"
Feb 2015	Materials Research Outreach Symposium, University of California Santa Barbara, CA "Spatial Control over Polymer Brush Grafting Density using Visible Light"
Aug 2014	248th National ACS Meeting, San Francisco, California, CA "Spatial Control over Polymer Brush Grafting Density using Visible Light"

Teaching Experience

2015 - 2017	Teaching Assistant, General Chemistry, University of California Santa Barbara
2011	Science Instructor for 14th Chulalongkorn University Academic Exhibition
2010	Chemistry Instructor for the 3rd Scientist Camp, Chulalongkorn University
2009	Tutor for Math Chem, Department of Chemistry, Chulalongkorn University

Outreach Activities

2016 – 2017 Chemistry graduate recruitment committee

Organized recruitment activities, guided potential UCSB graduate students around campus and presented research opportunities in the Department of Chemistry

2016 "Build a Buckyball" workshop

Mentored K-12 students on construction of Buckminsterfullerene molecular models as part of MESA Science & Technology Day at UCSB

2015 "Build a Solar Car" workshop

Lead students with building and racing solar cars for the MESA Science & Technology Day at UCSB

2014 – 2015 "It's a Material World!" workshop

Participated in outreach events at Hollister and Foothill Elementary Schools for students in learning through hands-on activities highlighting Materials Science

ABSTRACT

Fabrication of Polymer Brushes via Light-Mediated Polymerization

and Polymerization of Acrylic Acid

by

Benjaporn Narupai

The development of polymer synthesis is of great significance towards the preparation of functional materials. Polymers have been used in surface modifications ranging from antifouling, antifogging to chemical sensing. Surfaces are often modified by a variety of techniques such as spin-coating, painting or dipping. However, these physisorption techniques lack stability against erosion. Covalent chemical attachment overcomes this disadvantage and offers chemical robustness with synthetic flexibility. Surface-initiated polymerizations are one of the most efficient strategies to modify surface properties via covalent attachment while providing high grafting density of a variety of functional groups as well as the ability to pattern the surfaces. This dissertation will highlight the development of three synthetic strategies. First, a novel strategy to synthesize branched polymer brushes by sequential light-mediated polymerization is demonstrated. Stepwise synthesis including linear copolymerization, deactivation of active chain ends and secondary graft polymerization is described affording branched polymer brush architectures. Secondly, the fabrication of well-defined, multifunctional polymer brushes using microliter volumes under ambient conditions is

reported. This simple synthetic strategy uses photoinduced polymerization with metal-free photoredox catalyst which acts as both an oxygen scavenger and polymerization catalyst. Finally, the rapid copolymerization of acrylic acid and sodium acrylate is demonstrated. This polymerization uses an alkyl iodide/sodium iodide as a mediator in water affording copolymers with a moderate control over molecular weight and dispersity.

TABLE OF CONTENTS

LIST OF FIGURES

LIST OF SCHEMES

LIST OF TABLES

I. Introduction and Literature Review

1.1 Applications of Surface Modification

Surface modification is an important strategy to change surface properties without altering the bulk material. Surface modification is essential for the preparation of materials, for example, biomedical devices where high mechanical toughness against degradation is required for the bulk material while biocompatibility is required for surface interacting with proteins.[1] Surface modification in general is widely used in many applications such as sensors, actuators, lubricants, and for properties such as anti-fouling or anti-fogging. Surfaces can be modified by a variety of techniques. Often, physisorption-based techniques such as spin-coating, dipping and spraying are used, however these strategies do not provide the ability to pattern the surface and lack stability against erosion.[1-2] Other surface modification techniques rely on covalent chemical attachment, which overcome some of the disadvantages of physisorption such as solvent or thermal instabilities, as well as offer chemical robustness with synthetic flexibility to incorporate a variety of functional groups on the surface.[3-4]

1.2 Polymer brushes via grafting-to and grafting-from strategies

Polymer brushes are thin polymer coatings consisting of polymer chains that have one chain end tethered to a surface by covalent chemical attachment. Polymer brushes have become interesting in stimuli responsive polymer coatings especially regarding sensors and actuators. This is because polymer brushes offer low chain entanglement due to terminally attached polymer chains which can immediately respond to environmental changes such as solvent, temperature, pH and ionic strength etc.[3] There are two strategies to prepare polymer brushes: 1) "grafting-to" and 2) "grafting-from" strategies. The "grafting to" strategy involves the preparation of preformed polymer with functional end groups designed to react with an appropriate substrate (Figure 1). With this strategy, the polymers can be well characterized via many characterization methods such as nuclear magnetic resonance spectroscopy (NMR) and size exclusion chromatography (SEC) to determine molecular weight and dispersity. However, the "grafting to" strategy suffers from low grafting density and thin polymer films. This is because polymer molecules have to diffuse through an existing attached polymer layer to reach the active sites on the surface. The steric hindrance of the attached polymers increase as the film thickness increases resulting in low grafting density.[3]

Because of these limitations, the "grafting from" strategy has become the preferred option to prepare polymer brushes with higher polymer grafting density and thicker polymer films. This alternative strategy can precisely control the functionality, polymer brush grafting density and the thickness of polymer film.[4] The "grafting from" strategy starts with the modification of the surface with an initiator-bearing self-assembled monolayer followed by surface-initiated polymerization. The self-assembled monolayers can be prepared on a variety of surfaces such as thiols on gold, silanes on glass/Si/SiO_2 etc.[4] Many controlled

polymerization techniques have been used to prepare polymer brushes including anionic polymerization, cationic polymerization and ring-opening polymerization.[5] Among the controlled polymerization techniques, controlled radical polymerization such as atom transfer radical polymerization (ATRP), reversible addition fragmentation chain transfer (RAFT) polymerization and nitroxide-mediated polymerization (NMP) are the most widely used to prepare polymer brushes because of their compatibility with both aqueous and organic solvents and high tolerance toward a wide range of functional groups.[5] Atom transfer radical polymerization (ATRP) will be described in more detail later in this chapter.

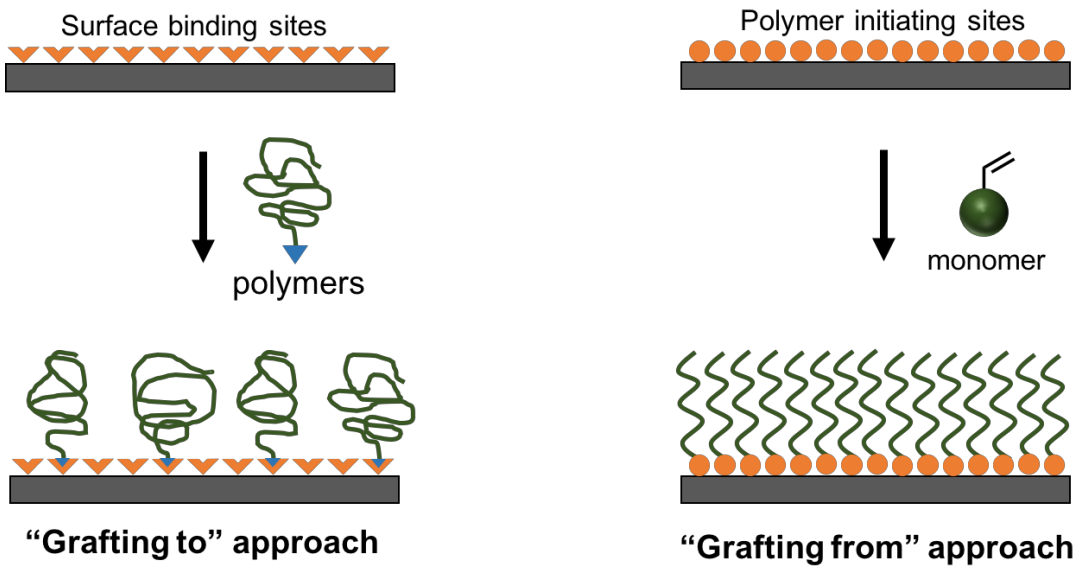

Figure 1. The fabrication of polymer brushes: "Grafting to" approach and "Grafting from" approach.

1.3 Regimes of brush formation

Grafting density (σ) of the polymers at the surface can dictate the structure of surface-immobilized polymers. The grafted polymer chains will overlap when the size of the polymer chains approach the distance between the grafting sites. According to theoretical and experimental studies, there are two regimes in brush formation including "mushroom" or "brush" regimes (Figure 2). In the "mushroom" regime, the polymer brush thickness, H, scales as $H \sim N\sigma^0$ in a good solvent, where N is the degree of polymerization of the grafted polymer. In the "brush" regime, H scales as $H \sim N\sigma^{1/3}$ where grafted polymer chains become more crowded and highly stretched.[6-7]

Figure 2. Regimes of brush formation: "mushroom" and "brush" regimes.

In 2002, Genzer and coworkers reported the mushroom-to-brush crossover in surface anchored polyacrylamide.[8] The gradient of initiator coverage on a silicon substrate was prepared by differential vapor diffusion. Then, surface-initiated polymerization was performed affording an array of grafted polymers with a variety of grafting densities. The relationship between polymer brush thickness and initiator density was studied demonstrating the crossover between mushroom and brush regimes occurs at $\sigma \approx 0.065$ chains/nm^2 (Figure 3).

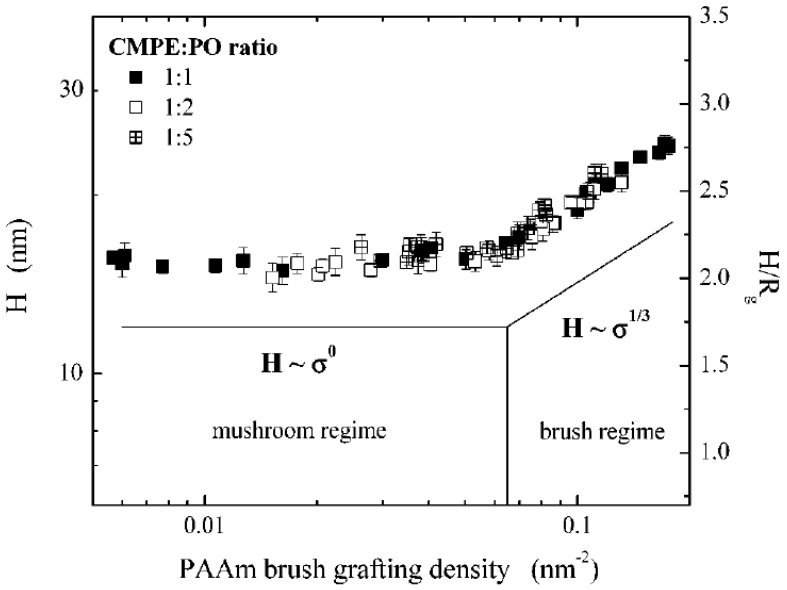

Figure 3. The wet thickness of polyacrylamide brushes (H) as a function of polymer brush grafting density demonstrating the crossover between "mushroom" and "brush" regimes. Reprinted with permission from reference 8. Copyright 2002 American Chemical Society.

1.4 Atom transfer radical polymerization (ATRP)

Atom transfer radical polymerization (ATRP) has been the most extensively used method to prepare polymer brushes. The advantages of ATRP over other techniques include the use of commercially available reagents, chemical versatility, compatibility with a variety of monomers and functional groups and tolerance to impurities.[5] ATRP relies on the reversible redox activation of a dormant halide-terminated polymer with a transition metal complex (metal/ligand) and deactivation of the resulting propagating radical species. A lower oxidation state of Cu^{I}/ligand reacts with an ATRP initiator to generate radical species that can initiate the polymerization. This propagating radical species can then be deactivated with a higher oxidation state Cu^{II}/ligand deactivator to generate the corresponding halogen-capped dormant

species to avoid termination events. This polymerization is based on the equilibrium of activation and deactivation processes (Figure 4). The parameters, including initiators, ligands, ratio of metal/ligand and solvents, can be varied to tune the polymerization. Surface-initiated atom transfer radical polymerization (SI-ATRP) is an efficient polymerization method to prepare polymer brushes. This method starts from the surface modification with initiator-bearing self-assembled monolayers. Then, this initiator-functionalized substrate is used to grow polymer brushes from the surface. There are several types of ATRP that have been used for this, that differ slightly from conventional ATRP. For example, Activators Regenerated by Electron Transfer (ARGET-ATRP) has been developed to reduce the amount of metal catalyst in the polymerization by using ppm level of metal in the presence of reducing agents.[9] Supplemental Activation Reducing Agent (SARA-ATRP)/Cu(0)-mediated living radical polymerization has been reported using Cu(0) as a metal catalyst in the polymerization.[10] Light-mediated ATRP has been developed by using light to regulate the activation and deactivation steps during the polymerization.[11-13] The following section will describe photo-induced polymerization techniques in more detail.

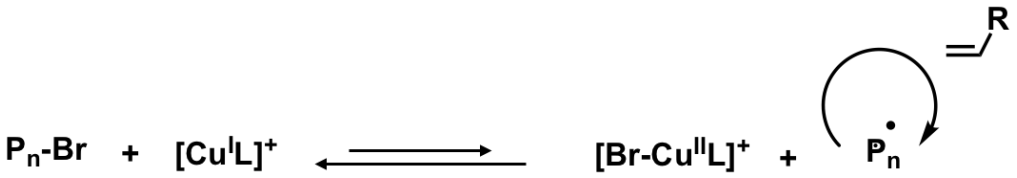

Figure 4. The mechanism of atom transfer radical polymerization based on Cu-based catalyst.

1.5 Light-mediated controlled radical polymerizations

External stimuli such as chemical, mechanical, electrochemical and photochemical stimuli have been used to regulate activation and deactivation steps of polymerizations. Light is the most attractive external stimulus due to the ability to tune the wavelength and the intensity of light. Moreover, light offers excellent spatial and temporal control during the polymerization.

In 2012, Matyjaszewski and coworkers reported photoinduced ATRP with ppm levels of the Cu catalyst using visible light and sunlight.[12] Photoreduction of the X-Cu^{II}/ligand deactivator complex yielded a Cu^{I}/ligand activator and a halogen radical that could initiate the polymerization (Figure 5). Irradiation of the reaction mixture with 392 nm, 450 nm and sunlight yielded polymerization. However, no polymerization occurred with lower energy red light (631 nm). The polymerization showed excellent control with both acrylate and methacrylate monomers. Moreover, chain extension could also be performed to yield block copolymers. This photoinduced ATRP has been shown to be environmentally benign due to low metal catalyst loading and mild radiation sources.

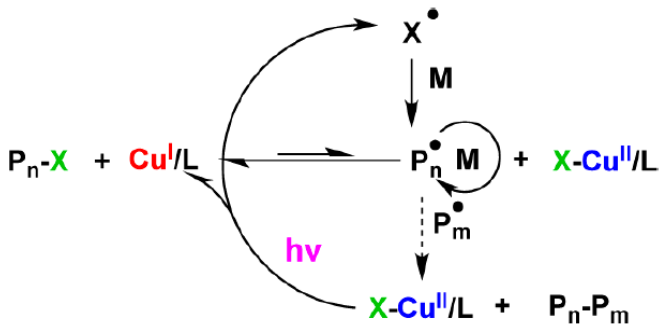

Figure 5. The mechanism of photoinduced ATRP based on Cu-based catalyst. Reprinted with permission from reference 12. Copyright 2012 American Chemical Society.

In 2014, Haddleton and coworkers reported photoinduced sequence-controlled living radical polymerization of acrylates in one pot.[14] The polymerization was performed using low concentration of $CuBr_2$ with Tris[2-(dimethylamino)ethyl]amine (Me_6Tren) as a ligand under 360 nm UV irradiation. The undecablock copolymers were prepared using alternating blocks of four different acrylate monomers yielding polymers with narrow dispersity (Đ <1.2), and importantly, with quantitative conversion achieved between the iterative monomer additions. This strategy offers a versatile and inexpensive platform for the preparation of multiblock copolymers demonstrating excellent end group fidelity and very low rates of termination.

In 2012, Hawker and coworkers reported photocontrolled polymerizations of methacrylates using iridium-based catalyst (non-copper-based catalyst system).[11] The photoredox catalyst, *fac*-[$Ir(ppy)_3$], is highly responsive to visible light (Figure 6a). The proposed mechanism of this polymerization starts from visible light irradiation to afford excited Ir^{III}* species, *fac*-[$Ir(ppy)_3$]*, which can reduce an alkyl bromide initiator to generate an alkyl radical that can initiate polymerization. Then, the highly oxidized Ir^{IV} complex can react with the propagating radical to generate the ground state Ir^{III} complex plus a dormant halogen-capped polymer chain. The cyclic process of propagation and halogen recapping can be regulated by visible light (Figure 6b).

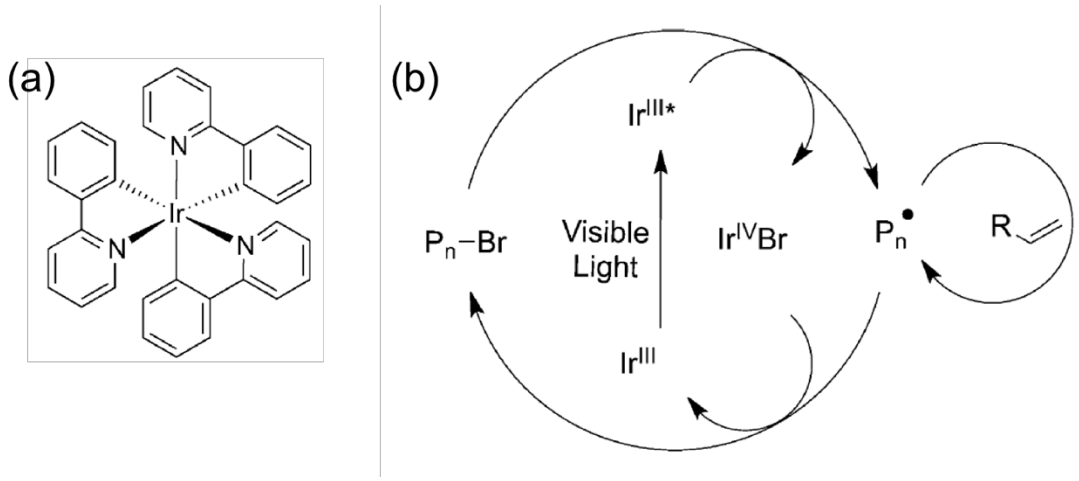

Figure 6. (a) The photoredox catalyst *fac*-[Ir(ppy)$_3$] (b) Proposed mechanism of a light-mediated controlled radical polymerization using Ir-based photoredox catalyst. Reprinted with permission from reference 11. Copyright 2012 John Wiley and Sons.

The polymerization of methyl methacrylate with 0.005 mol% of *fac*-[Ir(ppy)$_3$] resulted in a controlled polymerization with Đ < 1.3. The control experiments were performed without *fac*-[Ir(ppy)$_3$] catalyst or in the absence of light, showing no polymerization in both cases. The attractive feature of this strategy is the ability to activate and deactivate the polymerization immediately by switching "on" or "off" the light source. The polymerization with "on"/ "off" cycles (light off 1 hour, light on 2 hours) was performed. In the presence of light, monomer conversion was observed, while the polymerization stopped immediately and no conversion was observed during the dark period. The polymerization of the 2nd, 3rd and 4th light "on" cycle suggested that termination does not occur during the dark period and the halogen remains intact on the polymer chain ends (Figure 7). Chain extension were performed by sequential photocontrolled polymerization affording a well-defined poly(methacrylate)-*b*-(benzyl methacrylate) diblock copolymer. Unlike the copper-based system, the polymerization using

fac-[Ir(ppy)$_3$] is extremely tolerant to a variety of functional groups. Copolymerization of methacrylic acid and benzyl methacrylate were prepared affording excellent control over molecular weight and a low Đ.

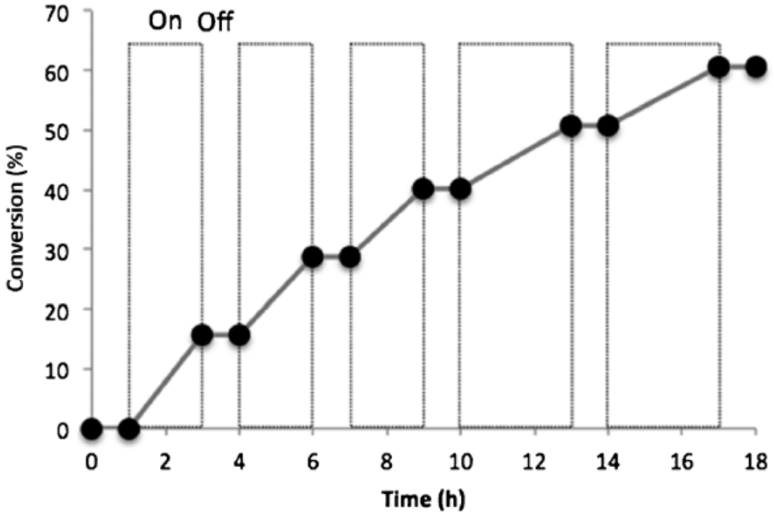

Figure 7. Polymerization of methyl methacrylate using *fac*-[Ir(ppy)$_3$] in the presence (on) and in the absence (off) of light. Plot of conversion vs. time during the polymerization. Reprinted with permission from reference 11. Copyright 2012 John Wiley and Sons.

1.6 Patterned polymer brushes

The fabrication of patterned polymer brushes is important in biotechnology applications such as model substrates for tissue engineering, biosensors, cell-surface interaction and cell patterning. [3,15-16] These applications require a well-defined spatial arrangement of chemical functionality on the surface. One of the strategies to prepare patterned polymer brushes is a top-down approach where uniform polymer brushes are destructively patterned by selective lithography. However, this strategy suffers from the debris of removed material and lateral

resolution limitation. The alternative strategy is using a pre-patterned initiator surface which can provide patterning at a wider range scale. Initiator-functionalized surface can be prepared by self-assembled monolayers (SAMs) for surface-initiated polymerization. SAMs can be formed on a variety of substrates with appropriate surface modifications such as attachment of silanes with hydroxylated surfaces (glass/silicon wafer), or thiols on gold, etc. [3,15-16] The fabrications of patterned initiator surface will be described below.

Photolithography is a widely-used technique to prepare micro and nanostructured materials. This strategy is based on the transfer of a mask pattern onto a substrate using a light sensitive photoresist.[3] For example, Ober and coworkers demonstrated the potentials of this strategy by creating poly(acrylic acid) brush patterns.[15] The photoresist was deposited on SAMs of poly(ethylene glycol) (PEG) on silicon wafer. The substrate was then exposed to UV light through a photomask to generate patterned photoresist. After that, the substrate was exposed to oxygen plasma to create patterned PEG (Figure 8a). Subsequently, the etched regions were back-filled with ATRP initiator-terminated dimethylchlorosilane for surface-initiated polymerization. The polymerization of sodium acrylate was performed in aqueous media via conventional ATRP resulting in patterned polymer brushes (Figure 8b).

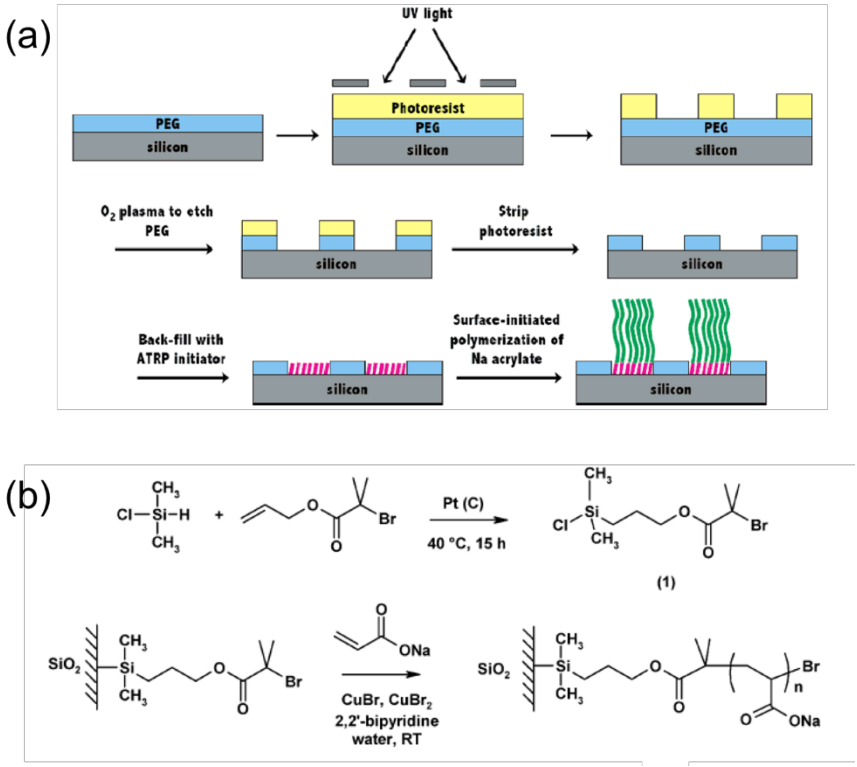

Figure 8. (a) The fabrication of patterned polymer brushes using photolithography technique (b) The deposition of ATRP initiator-terminated dimethylchlorosilane onto silicon surface and subsequent polymerization of sodium acrylate via ATRP. Reprinted with permission from reference 15. Copyright 2007 American Chemical Society.

Microcontact printing (μCP) is one of the most frequently used methods to prepare patterned polymer brushes with a micron scale resolution. Using this technique, Huck and coworkers reported growing multicomponent polymer brushes on gold via repetition of surface patterning.[16] Patterned initiator-terminated thiol monolayer was prepared on gold substrate by microcontact printing followed by surface-initiated ATRP. Then, the bromine chain ends are deactivated by the reaction with NaN_3. A new initiator pattern can be deposited onto the same substrate using microcontact printing in the area that was in contact with the stamp but did not contain polymer brushes. Subsequently, the second set of polymer brushes

with different monomer is grown from the second initiator pattern followed by deactivation of polymer chain ends. Repetition of patterned initiator deposition via microcontact printing, SI-ATRP and deactivation of chain ends up to quaternary brushes was demonstrated (Figure 9).

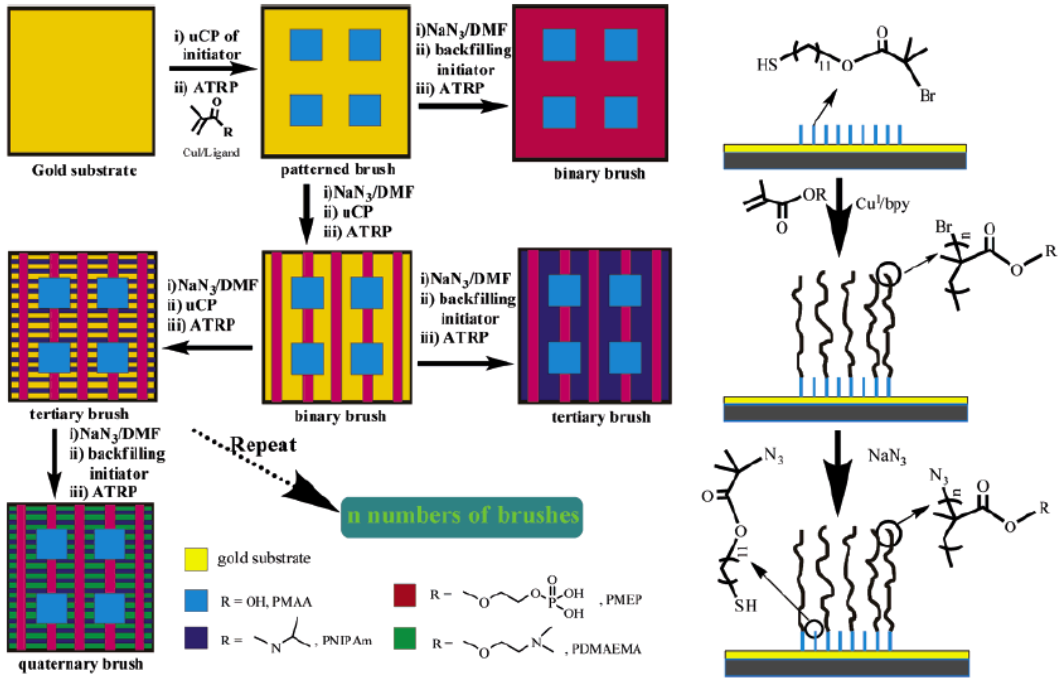

Figure 9. The stepwise synthesis of multiple patterned polymer brushes via repetition of microcontact printing, SI-ATRP and deactivation of polymer chain ends. Reprinted with permission from reference 16. Copyright 2006 American Chemical Society.

In 2013, Hawker and coworker have reported the fabrication of patterned polymer brushes via light-mediated living radical polymerization.[17] Unlike photolithography or microcontact printing, this strategy prepared patterned polymer brushes from a uniform initiator layer. ATRP initiator-terminated trichlorosilane was immobilized onto silicon substrate followed by surface-initiated polymerization. Light-mediated living radical polymerization using an Ir-

based photoredox catalyst was performed to prepare a variety of complex polymer brushes including patterned polymer brushes, gradient polymer brush nanostructures and diblock copolymer brushes. The *fac*-[Ir(ppy)$_3$] is highly responsive to visible light as mentioned early in this chapter. In the presence of light, excited Ir^{III}* species, *fac*-[Ir(ppy)$_3$]*, reduces the alkyl bromide initiator to generate radical that can initiate the polymerization. In the absence of light, the propagating polymer chains are returned to the dormant species and can be reinitiated upon re-exposure to light. Hence, the most attractive feature of this system is the direct spatial and temporal control over polymer brush growth from the uniform initiating layer. Using a photomask, brush growth can be restricted to the exposed region (Figure 10a-b). While no polymer brushes growth occurs in the unexposed regions, they still contain active initiating sites that can be utilized for further patterning. Moreover, gradient polymer brush nanostructures can be prepared using a grayscale lithography masks which is difficult to achieve using other techniques (Figure 10c).

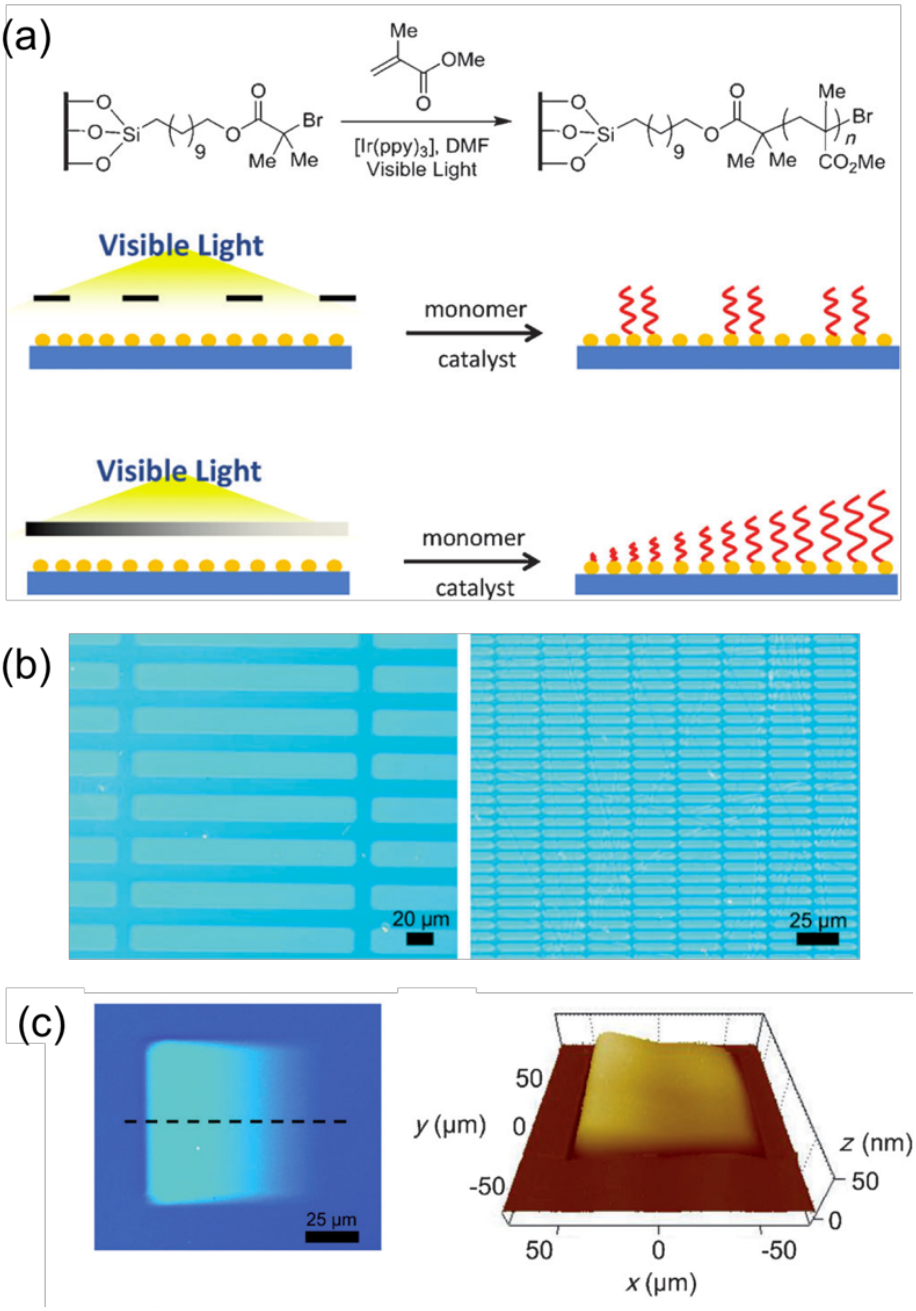

Figure 10. (a) Synthetic scheme illustrating the fabrication of patterned and gradient polymer brushes (b) Optical micrographs of patterned polymer brushes (c) Optical micrograph and 3D atomic force microscopy (AFM) image of gradient polymer brush nanostructure. Reprinted with permission from reference 17. Copyright 2013 John Wiley and Sons.

1.7 Metal-free atom transfer radical polymerizations

The conventional ATRP requires large concentrations of Cu-based catalyst (1,000 – 10,000 ppm) to achieve controlled polymerization. This conventional ATRP suffers from metal contamination which could be problematic in some applications such as microelectronics and biomedical materials.[18] Activators Regenerated by Electron Transfer for Atom Transfer Radical Polymerization (ARGET ATRP) has been developed to reduce the amount of metal catalyst down to ppm level in the presence of reducing agents.[9] Despite these efforts in reducing catalyst loading, metal-free polymerization remains highly desirable.

In 2014, Hawker and coworker reported organic-based photoredox catalyst, *N*-phenylphenothiazine (PTH), for light-mediated controlled radical polymerization (Figure 11a).[18] The proposed mechanism of this polymerization starts from excitation of PTH to PTH* upon exposure to light at 380 nm. This excited state PTH can reduce alkyl bromide to generate alkyl radical that can initiate the polymerization plus stable radical cation species. Then, this radical cation can react with the propagating radical affording the ground state PTH and a bromide-capped polymer chain. The cycle of the monomer adding to the radical chain end and bromide recapping the chain end can be regulated by light (Figure 11b).

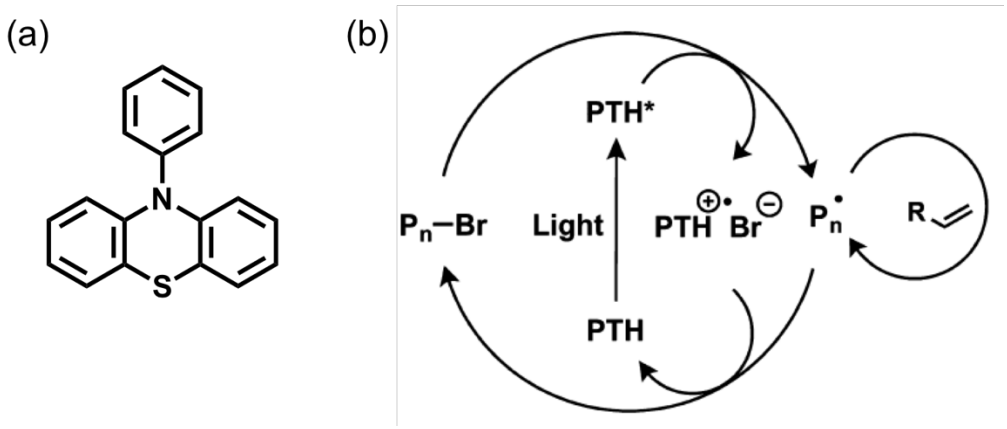

Figure 11. (a) Metal-free photoredox catalyst, *N*-phenylphenothiazine (PTH) (b) Proposed mechanism of light-mediated polymerization using PTH as a photoredox catalyst. Reprinted with permission from reference 18. Copyright 2014 American Chemical Society.

The polymerization of methyl methacrylate afforded a well-controlled polymerization with Đ < 1.4. The control experiments performed in the absence of light, initiator, or the photoredox catalyst led to no or uncontrolled polymerization. A key feature of light-mediated polymerization is the "on-off" experiment. In the presence of light, monomer conversion was obtained while no monomer conversion was observed during the dark periods. This result demonstrated efficient activation and deactivation of the polymerization process regulated by light (Figure 12). Unlike Ir-based photoredox system, the polymerization using PTH allows for a wider selection of functional monomers. The polymerization of stimuli responsive monomer, 2-(dimethylamino)ethyl methacrylate (DMAEMA,) afforded a controlled polymerization. Moreover, chain extension was performed affording poly(methyl methacrylate-*b*-benzyl methacrylaye) block copolymer, demonstrating that bromide chain end remained intact. Matyjaszewski and coworkers also reported the mechanism of photoinduced

metal-free ATRP using several phenothiazine derivatives by experimental and computational studies.[19]

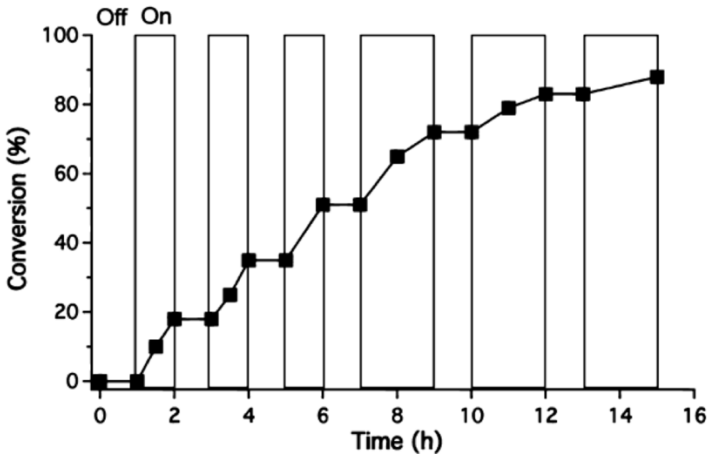

Figure 12. Polymerization of benzyl methacrylate using *N*-phenylphenothiazine (PTH) in the presence (on) and in the absence (off) of light. Reprinted with permission from reference 18. Copyright 2014 American Chemical Society.

Miyake and coworker reported organocatalyzed ATRP driven by visible light using diaryl dihydrophenazines as photoredox catalysts.[20] Polymerization of methyl methacrylate using diaryl dihydrophenazines with white LED or sunlight afforded controlled polymerization with tunable molecular weight and low dispersity. This system offered high initiation efficiencies through activation via visible light. Moreover, chain extension was performed to prepare block copolymer demonstrating high chain-end group fidelity.

In 2016, Hawker and coworker reported surface-initiated polymerization using *N*-phenyl phenothiazine as a photoredox catalyst.[21] This light-mediated polymerization provided the potential to pattern polymer brushes down to 1 μm features resolution. Moreover, patterned block copolymer can be achieved by simply using photomask in the chain extension process

(Figure 13a). In addition, the fabrication of polymer brushes from nanoparticles has been demonstrated supporting the ability to synthesize polymer brushes from curved surfaces (Figure 13b).

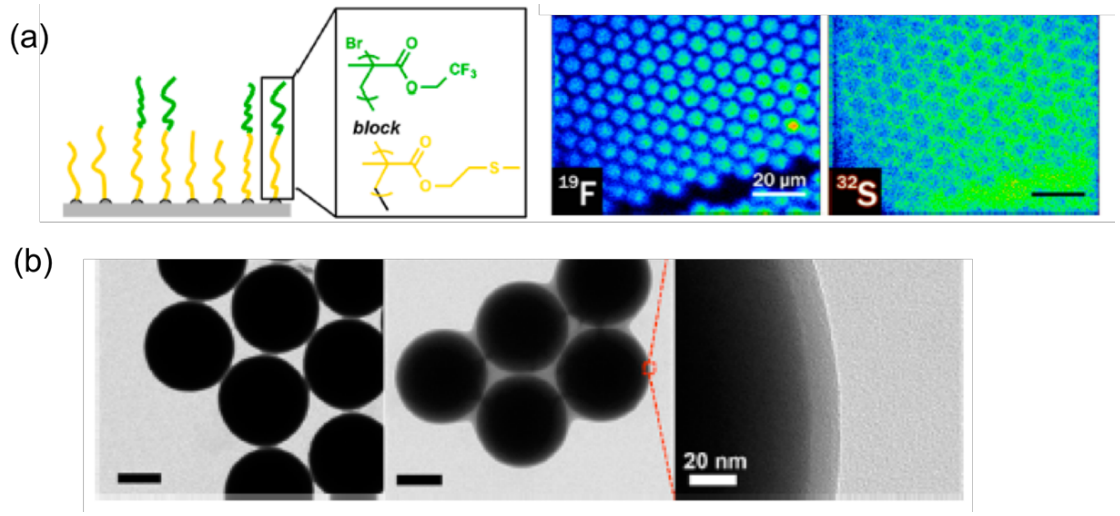

Figure 13. The fabrication of polymer brushes via metal-free light-mediated polymerization (a) Patterned block copolymer brushes on a flat silicon wafer confirmed by secondary ion mass spectrometry (SIMS) (b) Transmission electron microscopy (TEM) image of polymer brushes on SiO_2 nanoparticles. Reprinted with permission from reference 21. Copyright 2016 American Chemical Society.

1.8 Oxygen tolerance in controlled radical polymerization

Oxygen tolerance has gained continuous interest in controlled radical polymerization. Oxygen can react with the carbon-centered radical to form peroxy radicals and hydroperoxides which inhibit controlled radical polymerization. The requirement to remove oxygen from the reaction by freeze-pump-thaw or degassing limits its widespread implementation especially

in an industrial scale production. Moreover, special equipment such as glovebox to keep inert atmosphere also reduces the accessibility of these techniques.[22]

In 2007, Matyjaszewski and coworker reported the synthesis of polymer brushes via ARGET ATRP in the presence of air.[23] The polymerization was performed without deoxygenation using ppm level of copper catalyst and appropriate reducing agent. Reducing agents such as metallic copper, tin^{II} 2-ethylhexanoate or ascorbic acid can consume oxygen in the polymerization. The activator, Cu^{I} species, was oxidized by oxygen to generate deactivator, Cu^{II} species. This Cu^{II} species was then reduced to Cu^{I} species in the presence of a reducing agent (Figure 14a). The induction period when all oxygen was consumed was observed before the polymerization starts. Surface-initiated polymerization without deoxygenation was performed by adding reducing agent in the reaction solution affording densely grafted polymer brushes (0.4 chains/nm^2). The polymerization was stopped by opening the reaction to air and could be restarted by adding the reducing agent in the reaction solution. This strategy offered control over polymer brush growth without the need for deoxygenation.

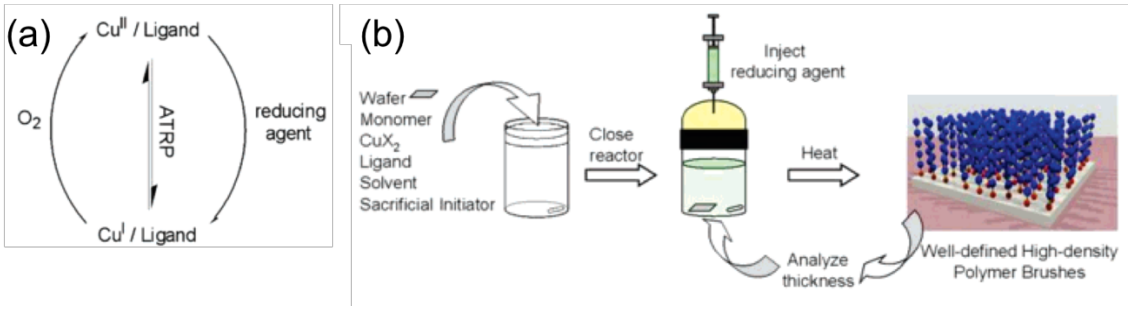

Figure 14. (a) Proposed mechanism of ARGET ATRP in the presence of air with a reducing agent (b) The fabrication of polymer brushes via ARGET ATRP without

deoxygenation. Reprinted with permission from reference 23. Copyright 2007 American Chemical Society.

In 2014, Hozumi and coworkers reported large-scale synthesis of pH-responsive polymer brushes under ambient conditions.[24] The fabrication of poly(2-(dimethylamino)ethyl methacrylate) brushes was performed in water under ambient condition affording a very thick polymer film (~700 nm). This synthetic strategy has been developed as "paint on" method, which directly pastes reaction solution onto the substrate to grow polymer brushes. Ascorbic acid was used as a reducing agent in ARGET ATRP allowing polymer brush growth under ambient conditions. Moreover, polymer brushes have been successfully prepared on a large-scale substrate (30 x 10 cm^2) through "paint on" strategy demonstrating the practicality of the surface coating method. Unfortunately, this strategy is limited to only poly(2-(dimethylamino)ethyl methacrylate).

In 2015, Jordan and coworkers reported wafer-scale synthesis of polymer brushes under ambient conditions using a copper plate.[25] The surface-initiated Cu(0)-mediated controlled radical polymerization was performed at room temperature and exposed to air affording high grafting density polymer brushes (~1 chains/nm^2). The copper plate acted as a lid to prevent oxygen diffusion and savage of oxygen by $Cu^{0/I}$ oxidation with an infinite Cu^0 reservoir. This air tolerant method allowed polymerization from a broad variety of monomers, such as (methacryloyloxy)ethyl trimethylammonium chloride, *N*-isopropylacrylamide, 2-hydroxyethyl methacrylate, 3-sulfopropyl methacrylate potassium salt, 2-(dimethylamino)ethyl methacrylate, etc. This strategy also provided the ability to prepare polymer brushes on entire wafer, which can be cleaved from the surface for NMR and SEC

characterizations yielding high molar mass polymer with narrow dispersity (Đ = 1.1). In addition, chain extension was performed on the wafer-scale under ambient condition affording tetrablock copolymer brushes demonstrating high end group fidelity of this strategy (Figure 15).

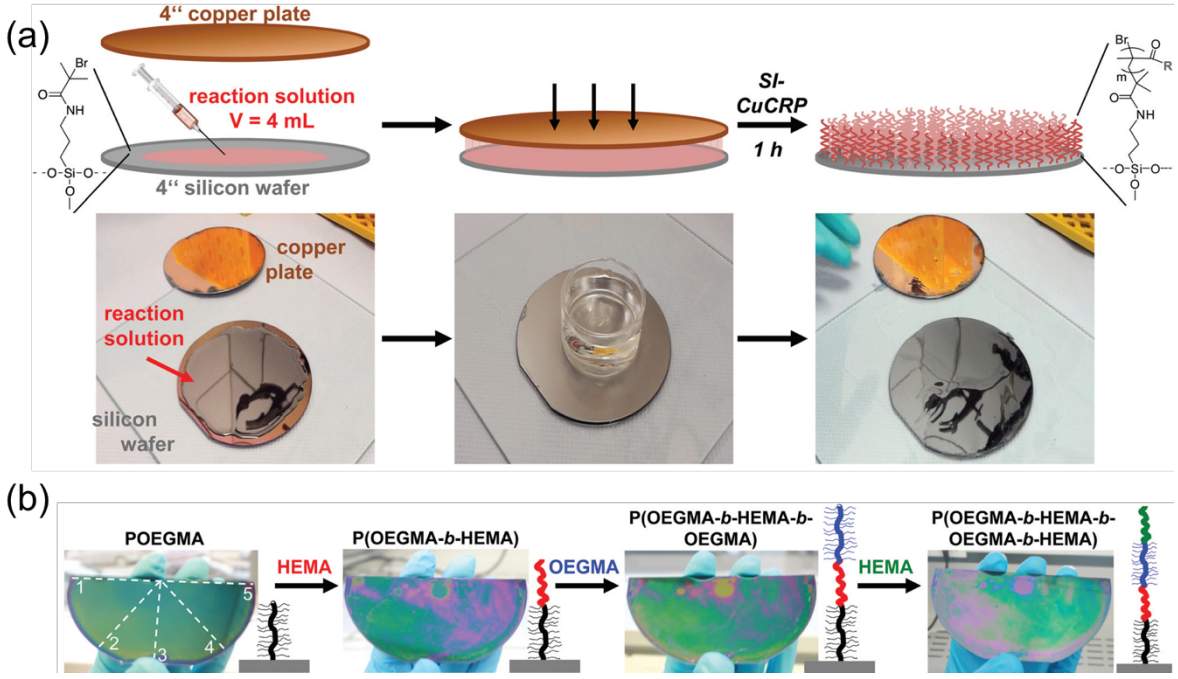

Figure 15. (a) Schematic illustration and photographs of experimental set up for the surface-initiated Cu(0)-mediated polymerization under ambient conditions on the entire wafer (b) The fabrication of homo, di-, tri- and tetrablock copolymer brushes. Adapted from reference 25, 2015 Published by The Royal Society of Chemistry.

1.9 Polymerization of acrylic acid

Poly(acrylic acid) (PAA) and related copolymers are widely used in industry ranging from adhesives, superabsorbents to coatings. The preparation of PAA is challenging due to the high reactivity of the monomer. In this section, two synthetic strategies to prepare PAA are described.

In 2000, Matyjaszewski and coworkers reported the indirect preparation of PAA via atom transfer radical polymerization.[26] The polymerization was performed using *tert*-butyl acrylate as a monomer coupled with Cu/ligand, alkyl bromide initiator and acetone as a solvent. Low molecular weight polymer with narrow dispersity was obtained. Subsequently, deprotection of *tert*-butyl ester was performed using HCl to generate poly(acrylic acid). Moreover, chain extension was performed followed by deprotection affording amphiphilic block copolymer.

In 2013, Lansalot and coworker reported the direct polymerization of acrylic acid in water via reversible addition fragmentation chain transfer (RAFT) polymerization.[27] The polymerization employed water soluble trithiocarbonates as chain transfer agent and azobis(4-cyanopentanoic acid) as a water soluble initiator. The polymerization was performed at different pHs ranging from 1.8 to 7, affording well-defined poly(acrylic acid) with $Đ < 1.1$. The poly(acrylic acid) macromolecular RAFT agent was further used to polymerize styrene in water via emulsion polymerization to generate block copolymer particles. This dissertation will highlight the novel synthetic strategy to prepare PAA in Chapter 4.

1.10 References

1) M. H. Stenzel, L. Zhang, W. T. S. Huck, *Macromol. Rapid Commun.* **2006**, *27*, 1121-1126.
2) C. W. Pester, B. Narupai, K. M. Mattson, D. P. Bothman, D. Klinger, K. W. Lee, E. H. Discekici, C. J. Hawker, *Adv. Mater.* **2016**, *28*, 9292-9300.
3) T. Chen, I. Amin, R. Jordan, *Chem. Soc. Rev.* **2012**, *41*, 3280-3296.
4) S. Edmondson, V. L. Osborne, W. T. S. Huck, *Chem. Soc. Rev.* **2004**, *33*, 14-22.
5) R. Barbey, L. Lavanant, D. Paripovic, N. Schüwer, C. Sugnaux, S. Tugulu, H.-A. Klok, *Chem. Rev.* **2009**, *109*, 5437-5527.
6) W. J. Brittain, S. Minko, *J. Polym. Sci. Part A: Polym. Chem.* **2007**, *45*, 3505-3512.
7) B. Zhao, W. J. Brittain, *Prog. Polym. Sci.* **2000**, *25*, 677-710.
8) T. Wu, K. Efimenko, J. Genzer, *J. Am. Chem. Soc.* **2002**, *124*, 9394-9395.
9) W. Jakubowski, K. Min, K. Matyjaszewski, *Macromolecules* **2006**, *39*, 39-45.
10) A. Anastasaki, V. Nikolaou, G. Nurumbetov, P. Wilson, K. Kempe, J. F. Quinn, T. P. Davis, M. R. Whittaker, D. M. Haddleton, *Chem. Rev.* **2016**, *116*, 835-877.
11) B. P. Fors, C. J. Hawker, *Angew. Chem. Int. Ed.* **2012**, *124*, 8980-8983.
12) D. Konkolewicz, K. Schröder, J. Buback, S. Bernhard, K. Matyjaszewski, *ACS Macro Lett.* **2012**, *1*, 1219-1223.
13) A. Anastasaki, V. Nikolaou, Q. Zhang, J. Burns, S. R. Samanta, C. Waldron, A. J. Haddleton, R. McHale, D. Fox, V. Percec, P. Wilson, D. M. Haddleton, *J. Am. Chem. Soc.* **2014**, *136*, 1141-1149.
14) A. Anastasaki, V. Nikolaou, G. S. Pappas, Q. Zhang, C. Wan, P. Wilson, T. P. Davis, M. R. Whittaker, D. M. Haddleton, *Chem. Sci.* **2014**, *5*, 3536-3542.

15) R. Dong, S. Krishnan, B. A. Baird, M. Lindau, C. K. Ober, *Biomacromolecules* **2007**, *8*, 3082-3092.

16) F. Zhou, Z. Zheng, B. Yu, W. Liu, W. T. S. Huck, *J. Am. Chem. Soc.* **2006**, *128*, 16253-16258.

17) J. E. Poelma, B. P. Fors, G. F. Meyers, J. W. Kramer, C. J. Hawker, *Angew. Chem. Int. Ed.* **2013**, *52*, 6844-6848.

18) N. J. Treat, H. Sprafke, J. W. Kramer, P. G. Clark, B. E. Barton, J. Read de Alaniz, B. P. Fors, C. J. Hawker, *J. Am. Chem. Soc.* **2014**, *136*, 16096-16101.

19) X. Pan, C. Fang, M. Fantin, N. Malhotra, W. Y. So, L. A. Peteanu, A. A. Isse, A. Gennaro, P. Liu, K. Matyjaszewski, *J. Am. Chem. Soc.* **2016**, *138*, 2411-2425.

20) J. C. Theriot, C.-H. Lim, H. Yang, M. D. Ryan, C. B. Musgrave, G. M. Miyake, *Science* **2016**, *352*, 1082.

21) E. H. Discekici, C. W. Pester, N. J. Treat, J. Lawrence, K. M. Mattson, B. Narupai, E. P. Toumayan, Y. Luo, A. J. McGrath, P. G. Clark, J. Read de Alaniz, C. J. Hawker, *ACS Macro Lett.* **2016**, *5*, 258-262.

22) J. Yeow, R. Chapman, A. J. Gormley, C. Boyer, *Chem. Soc. Rev.* **2018**, *47*, 4357-4387.

23) K. Matyjaszewski, H. Dong, W. Jakubowski, J. Pietrasik, A. Kusumo, *Langmuir* **2007**, *23*, 4528-4531.

24) G. J. Dunderdale, C. Urata, D. F. Miranda, A. Hozumi, *ACS Appl. Mater. Interfaces* **2014**, *6*, 11864-11868.

25) T. Zhang, Y. Du, J. Kalbacova, R. Schubel, R. D. Rodriguez, T. Chen, D. R. T. Zahn, R. Jordan, *Polym. Chem.* **2015**, *6*, 8176-8183.

26) K. A. Davis, K. Matyjaszewski, *Macromolecules* **2000**, *33*, 4039-4047.

27) I. Chaduc, A. Crepet, O. Boyron, B. Charleux, F. D'Agosto, M. Lansalot, *Macromolecules* **2013**, *46*, 6013-6023.

2. Hierarchical Comb Brush Architectures via Sequential Light-Mediated Controlled Radical Polymerizations[1]

2.1 Abstract

A novel strategy for the synthesis and characterization of branched polymer brushes by sequential light-mediated controlled radical polymerizations is described. Initially, linear brushes are prepared by surface-initiated copolymerization of methyl methacrylate and 2-hydroxyethyl methacrylate (HEMA). In a subsequent step, the HEMA side chains are functionalized with initiating groups for secondary graft polymerization, leading to hierarchical, branched architectures. The increased steric bulk due to the polymer side chains results in a dramatic increase in film thickness when compared to the starting linear brushes.

[1] Reproduced with permission: **Narupai, B.**; Poelma, J. E.; Pester, C. W.; McGrath, A. J.; Toumayan, E. P.; Luo, Y.; Kramer, J. W.; Clark, P. G.; Ray, P. C.; Hawker, C. J. "Hierarchical Comb Brush Architectures via Sequential Light-Mediated Controlled Radical Polymerizations." *J. Polym. Sci. Part A: Polym. Chem.* **2016,** *54*, 2276-2284. DOI: 10.1002/pola.28128. Copyright 2016, Wiley. License Number: 4440480606526.

This strategy also allows chemical gradient and complex three-dimensional structures to be obtained by employing grayscale photomasks in combination with controlled radical polymerization.

2.2 Introduction

The Surface-initiated polymerizations provide a robust and versatile strategy for modifying surface properties.[1–6] The advent of controlled radical polymerization (CRP) techniques such as atom transfer radical polymerization (ATRP),[7–11] nitroxide-mediated radical polymerization (NMP),[12–14] and reversible addition fragmentation chain transfer (RAFT) polymerization[15–17] have revolutionized this field and provide access to end-tethered polymer structures from a wide range of monomers and surfaces. Advantages associated with CRP techniques also allow for the fabrication of polymer brushes with precise control over brush height, grafting density and molecular architecture.[18] This design versatility has allowed polymer brushes to emerge as a major area of study, finding diverse applications in anti-fouling,[19–21] sensing,[22–25] bio/nanotechnology,[26–31] and lubrication.[32,33]

As the polymer brush field has evolved from simple homopolymer systems to block copolymers, a wide range of applications have also developed. For example, stimuli-responsive surfaces based on block copolymer brushes are now a major area of study.[34–36] Architectures with additional complexity, such as comb or branched polymer brushes, offer greater design flexibility to engineer specific properties. Unfortunately, these systems are poorly studied. Synthetically more challenging, this class of brushes consists of a main polymer chain with grafted side chains (branches) of the same, or different repeat units. Early experimental studies of comb polymer brushes employed photoiniferter chemistries; however, these systems suffer from a lack of control over molecular weight and chain density.[37–41]

Subsequent studies employed CRP techniques such as ATRP and RAFT,[42,43] which do not allow the effect of chain density and the two-dimensional patterning of the grafted chains to be investigate. Perhaps the most relevant study was the synthesis of surface-initiated hyperbranched polymers by Huck and coworkers. In this work, highly branched brush structures were achieved by ring opening polymerization, where the brush height was found to increase with the number of branching generations; however accurate control over molecular dimensions could not be achieved.[44] From these limited examples, characterization studies have revealed the potential of grafted, branched polymer structures to improve antifouling performance.[37,38,45]

To further understand the effect of branching in polymer brushes and to bring both control and tunability to these structures,[46–48] a sequential light-mediated approach was considered. From a synthetic viewpoint, our attention was directed to the recently developed photoredox-catalyzed light-mediated CRPs using *fac*-[Ir(ppy)$_3$][49,50] or organocatalytic phenothiazine systems.[51,52] The tunable nature of light-mediated polymerizations have significant implications for surface-initiated polymerizations. In addition to the traditional benefits of a controlled radical process, spatial control over brush growth is possible by simply employing a photomask.[53]

Light is not the only method that can achieve spatial control over brush growth. For example, Li et al. demonstrated that gradient brush structures can be accomplished electrochemically.[62] Although useful, arbitrary spatial control of complex polymer brush architectures could not be achieved by this method. For arbitrary patterning, lithographic techniques such as photolithography,[54] electron beam lithography,[55–58] and soft lithography[59–

[61,63] have been extensively used and offer excellent capabilities; however, these methods are often time-consuming, expensive, and destructive in nature.[47]

Herein, light-mediated polymerization was chosen as a simple way to achieve complex and arbitrary three-dimensional (3D) structures that may be difficult to access otherwise. These can be accomplished by simply modulating the rate of brush growth using a grayscale photomask and by the introduction of discrete backbone and grafted arm growth steps. By easily accessing well-defined branched polymer brush structures, systematic studies can be devised to better understand their physical properties.

The comb polymer brushes were prepared according to the synthetic strategy presented in Schemes 1 and 2. From a silicon substrate functionalized with surface-immobilized ATRP initiators, methyl methacrylate (MMA) and 2-hydroxyethyl methacrylate (HEMA) were copolymerized at varying ratios to obtain random copolymer brushes. The ability to vary the incorporation of HEMA ultimately allows for the density of grafted chains to be controlled in the resulting comb polymer architecture. For our studies, the percentage of HEMA units was varied between 1 and 9 mol % in the initial linear P(MMA-*co*-HEMA) copolymer brushes. It should be noted that the propagating alkyl bromide chain ends resulting from the surface-initiated living polymerization were deactivated by reaction with ethyl vinyl ether (EVE) using light-mediated atom-transfer radical addition (ATRA) to prevent subsequent chain end extension (Scheme 1).

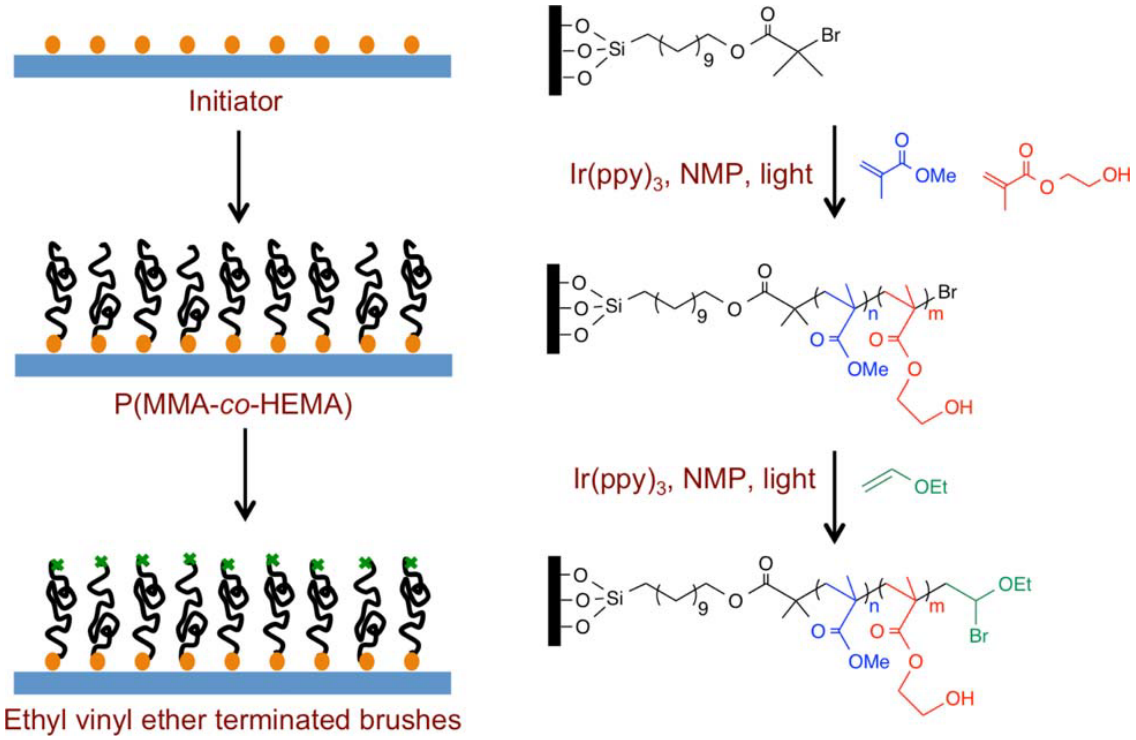

Scheme 1. Schematic representation and synthetic scheme illustrating the preparation of traditional linear, hydroxyl functionalized polymer brushes.

As a result, all subsequent polymer growth only occurs from the brush backbone. For growth of the grafted arms, the HEMA units were secondarily functionalized with initiating sites by reaction with ∞-bromoisobutyryl bromide in dichloromethane (DCM). The initiator-functionalized brushes were subjected to the same polymerization conditions that we used for initial brush growth, resulting in comb brush polymers. Each stage of the growth process lead to homogeneous films, further illustrating the robust nature of the photo-mediated chemistry.

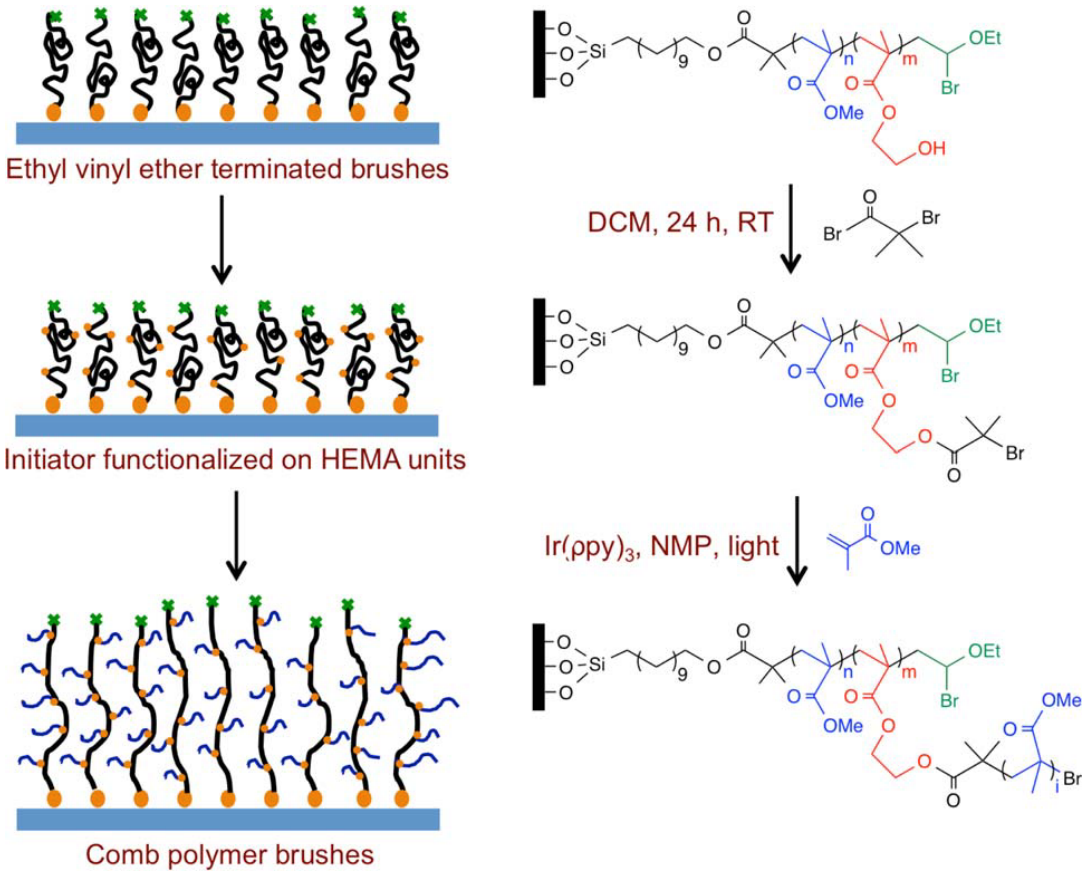

Scheme 2. Schematic representation and synthetic scheme illustrating the preparation of branched, comb brushes by a sequential functionalization and comb growth approach.

2.3 Results and Discussion

The relationship between P(MMA-*co*-HEMA) brush height, polymerization time and the level of HEMA incorporation was initially explored using light-mediated surface-initiated polymerization techniques. This modular, step-wise approach was applied to the preparation of grafted comb-based polymer brushes as outlined in Schemes 1 and 2. The incorporation of HEMA was varied between 1 and 9 mol % and for all incorporations studied, polymer brush

height was found to increase linearly with polymerization time (Figure 1). This result is consistent with previous reports of photomediated, CRP of linear chains initiated from surfaces. The ability to control the height of the initial brush layer is an important feature for subsequent fabrication of well-defined comb-based, polymer brush nanostructures. In general, brush heights between 10 and 100 nm could be obtained for polymerization times of 10–60 min, respectively. To ensure that subsequent polymer growth only occurs from the backbone and not the original propagating chain end, the initial polymer brushes were deactivated by reaction with ethyl vinyl ether (EVE). As a control, we attempted to chain extend P(MMA-*co*-HEMA) brushes containing 1 mol % HEMA before and after reaction with EVE. For the initial polymer brush, chain extension with MMA resulted in an increase in brush thickness from 12 to 23 nm, while after deactivation with EVE, chain extension with MMA gave no measureable increase in thickness, clearly illustrating capping and deactivation of the initial propagating chain end.

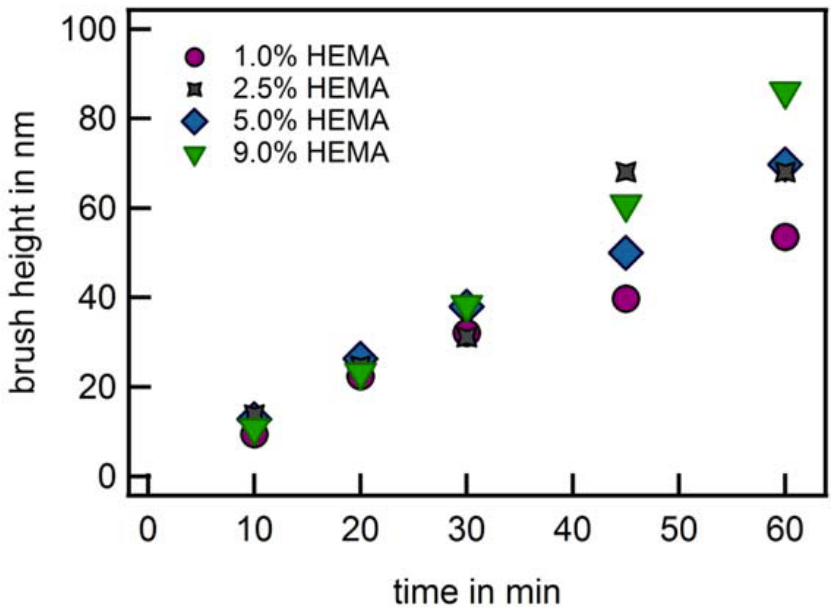

Figure 1. Relationship between brush height of P(MMA-*co*-HEMA) with 1, 2.5, 5, and 9 mol % incorporation of HEMA and polymerization time.

From these initial polymer brush scaffolds, the next step in this modular approach was to introduce initiating sites along the backbone by reaction of ∞-bromoisobutyryl bromide with the HEMA hydroxyl groups. Growth of the grafted arms could then be initiated from these groups using the reaction conditions described previously. Significantly, a controlled linear brushes are prepared by surface-initiated copolymerization of methyl methacrylate and 2-hydroxyethyl methacrylate (HEMA). In a subsequent step, the HEMA side chains are functionalized with initiating groups for secondary graft polymerization, leading to hierarchical, branched architectures. The increased steric bulk due to the polymer side chains results in a dramatic increase in film thickness when compared to the starting linear brushes. This strategy also allows chemical gradient and complex three-dimensional structures to be obtained by employing grayscale photomasks in combination with controlled radical

polymerization. increase in brush thickness could be observed for various levels of HEMA/initiator incorporation. The thickness increase can be attributed to polymerization time as well as the level of initiator incorporation along the backbone. As noted above, the polymer chain ends are deactivated, therefore, any increase in overall brush height is the result of graft polymerization only. One feature of this change in macromolecular architecture is the extension of the tethered linear polymer from an initial random coil structure to a significantly more extended configuration. The degree of extension was dictated by the increased steric volume associated with the grafted polymer chains.

To illustrate the ability to change brush structure and level of branching in more detail, a series of polymer brushes containing 1 mol % of initiator-functionalized HEMA repeat units along the backbone were prepared. For these systems, light-mediated controlled polymerization of MMA under the same conditions defined above resulted in a constant increase in final comb brush height with polymerization time. Remarkably, height increases in excess of 400% were observed even at this low level of initiator incorporation. For higher levels of initiator incorporation, the brush height also increased in an approximately linearly fashion; however, the time required to reach a brush height increase of 300–400% was reduced upon going from 2.5 mol % (~15 min) to 5 mol % (~10 min) and finally 9 mol % (~8 min) (Supporting Information Figure S1). It should also be noted that for the 5 and 9 mol % samples, longer reaction times led to visually inhomogeneous layers (Supporting Information Figure S3). We attribute this apparent loss of control to the high grafting density of the side chains which may lead to increased termination events and chain–chain coupling.

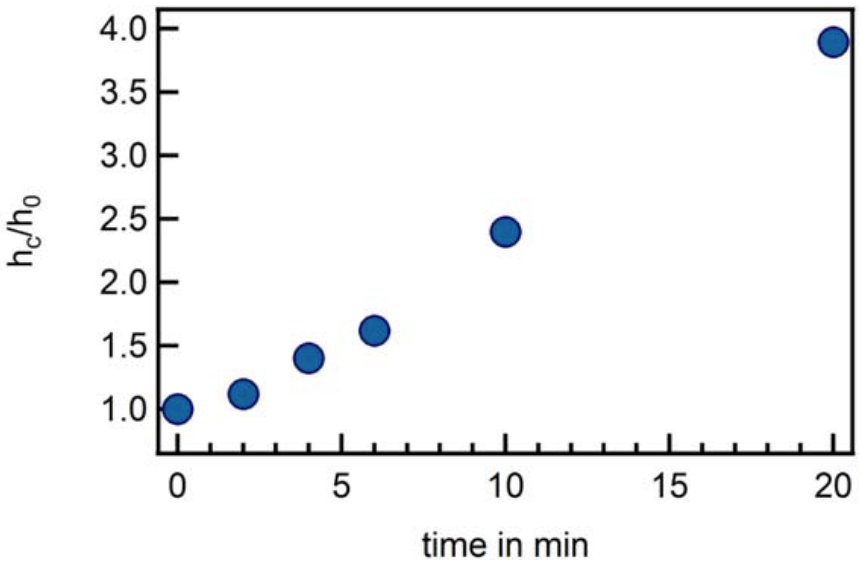

Figure 2. Relationship between normalized brush height and exposure time in minutes for 1 mol % grafted chains (h_c and h_0 refer to brush heights with, and without grafted chains, respectively). Results for 2.5 mol %, 5 mol %, and 9 mol % grafted chains are reported in the Supporting Information Figure S1).

A significant advantage of light-mediated polymerization for the fabrication of polymer brushes is the opportunity for spatial control, coupled with the ability to tune chain growth through modulation of light intensity. As a consequence, brushes and grafted chains of different lengths can be prepared on the same substrate, permitting fabrication of complex and arbitrary 3D polymer brush nanostructures. This feature also allows the molecular weight of both the tethered linear chains and the attached grafted chains to be independently controlled. To demonstrate spatial control, grafted comb brushes were prepared using a simple photomask (20×200 μm rectangles). Optical microscropy (Supporting Information Figure S4) revealed a regular pattern of rectangular features directly correlating to the original photomask. However, the more interesting and novel application of light-mediated polymerization

systems is the use of a grayscale mask to grow polymer chains of different molecular weights on the same substrate at the same time. This allows complex 3D nanostructures to be prepared in a single step. To illustrate the potential of this approach, PMMA brushes with 9 mol % HEMA were prepared as described above to give an initial brush height of ca. 23 nm. After capping the chain ends with EVE and introduction of initiating units along the backbone, comb growth could be performed with a grayscale mask as depicted schematically in Figure 3a, leading again to a pattern correlating with the original mask. To investigate the influence of a grayscale mask in greater detail, the heights of the patterned regions were measured using profilometry and plotted against the optical density of the grayscale mask (Figure 3b). In agreement with the controlled nature of this process, comb brush height was found to be inversely proportional to the optical density of the mask, which further illustrates the ability to tune brush height and backbone extension through control of the side chain molecular weight. Regions of the substrate which received more light exhibited a faster rate of grafted chain growth, resulting in increased molecular weights. This leads to increased steric interactions and higher chain extension of the backbones. This finding is consistent with our previous report.[53]

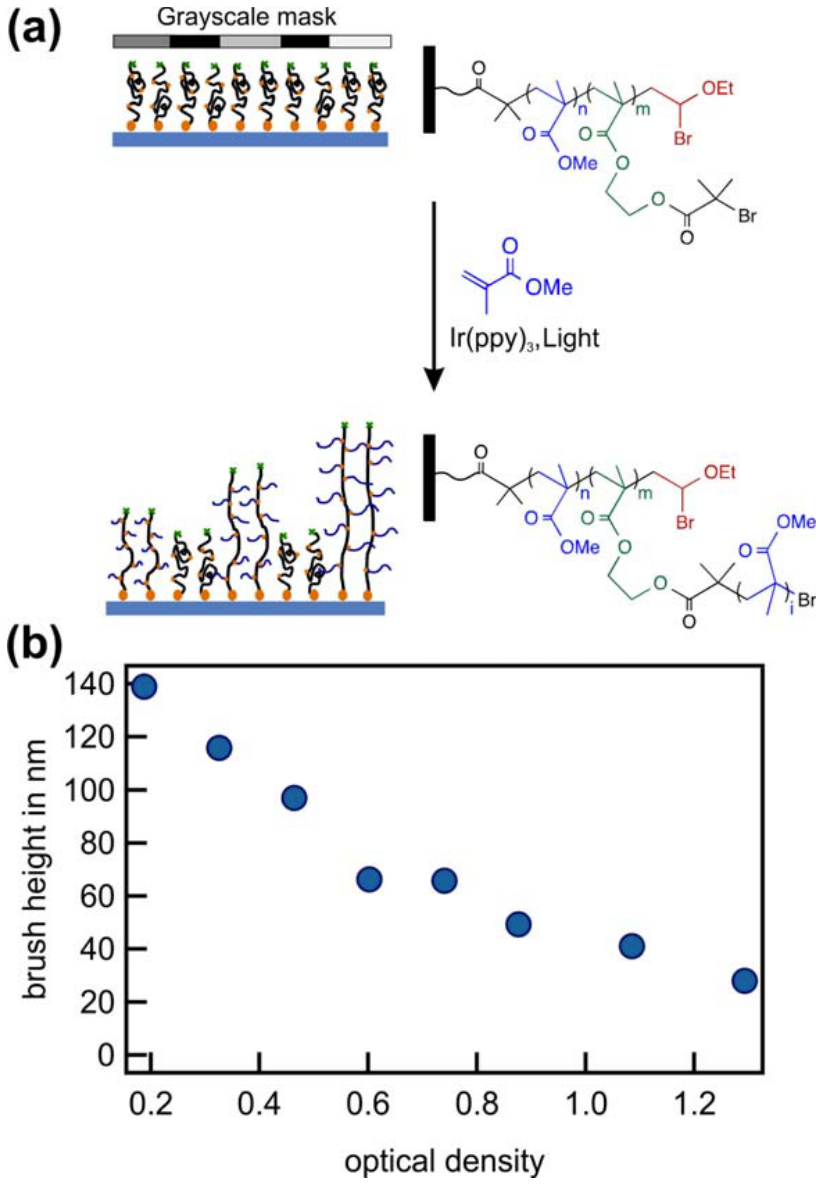

Figure 3. (a) Schematic representation of the patterning of comb polymer brush formation by modulating the rate of graft polymerization using a grayscale photomask; (b) relationship of brush height (measured by profilometry) as a function of the grayscale mask optical density.

The modular nature of this approach, combined with the ability to tune the molecular characteristics of each component, allows a novel range of 3D structures to be fabricated. To illustrate this aspect, unique comb brush structures were prepared from a uniform brush layer containing 9 mol % initiating sites along the backbone. Using a grayscale mask containing 100-μm gradient features, a simple wedge shaped structure was targeted. The optical density gradient in the photomask varied linearly from 0.22 to 1.29 as shown schematically in Figure 4a. After polymerization for 10 min, gradient structures were indeed visible to the naked eye with optical microscopy confirming the gradient structures (Figure 4b). Figure 4b presents profilometry measurements of the resulting microstructures. These measurements further confirm the formation of wedge shaped polymer brush features and importantly, the slope of the wedge is roughly linear and mimics the original linear grayscale photomask. The efficiency of this process allows feature heights in excess of 100 nm to be accessed with relatively short polymerization times (10 min) and suggests that custom grayscale masks with arbitrary optical density patterns could be used to produce a variety of 3D structures for specific applications.

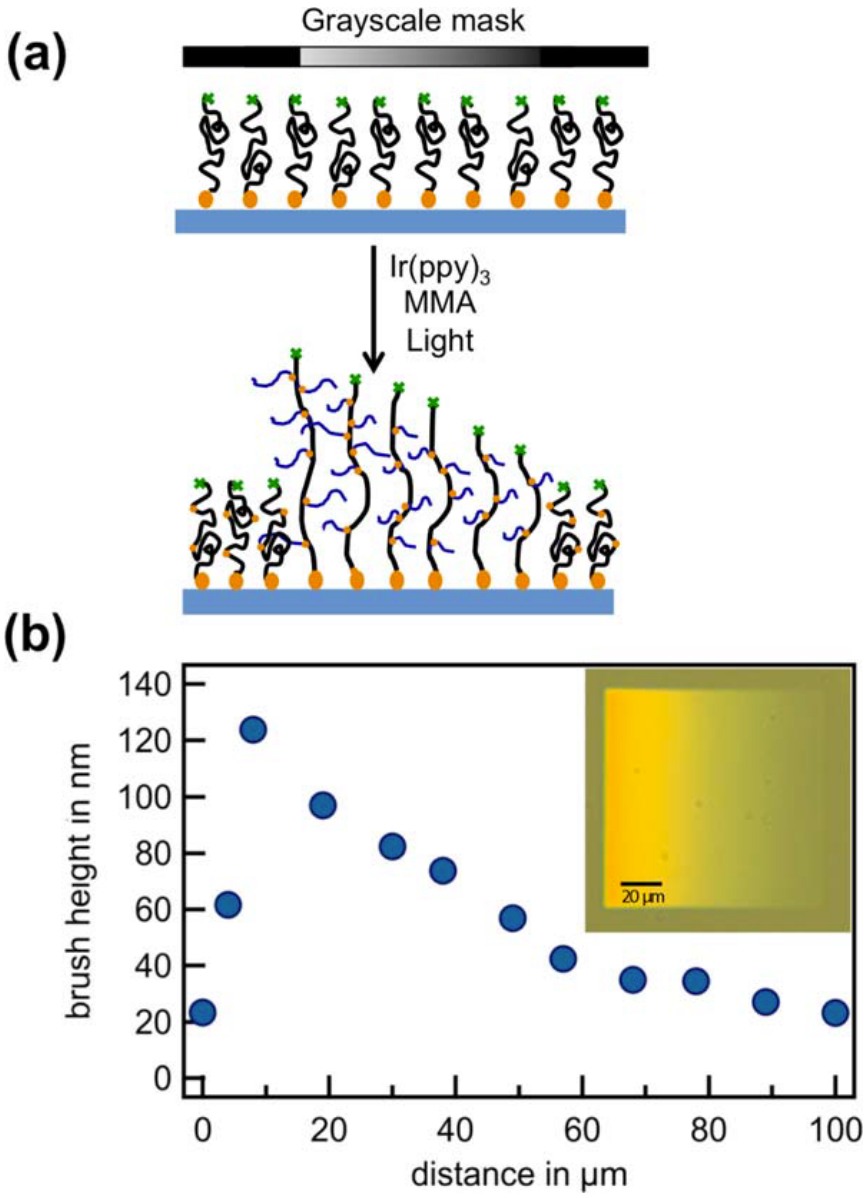

Figure 4. (a) Schematic representation of the formation of wedge-shaped nanoscale patterns using a gradient photomask with 100×100 µm prisms of variable slope; (b) optical micrograph of comb brushes using photomasks with prisms of a linear variation of optical density from 0.22 to 1.29; and relationship of brush height as a function of distance, measured across the 3D comb brush feature by profilometry.

Next, the potential of photomediated CRP for the fabrication of unique brush structures based on functional and branched block copolymer architectures was examined (Figure 5). Again the synthetic strategy starts with the preparation of a traditional linear PMMA polymer brush (Figure 5a). However in this case, the propagating chain end was not deactivated by reaction with EVE; instead, a second block of MMA and HEMA was grown to give a diblock copolymer brush (Figure 5b). Modification of the hydroxyl groups with initiating units, then allows for the growth of grafted polymer chains from the second block of the brush backbone only, leading to novel branched, block copolymer brush architectures (Figure 5c). Significantly, this multistep modular approach allows for different monomers to be incorporated at various stages of the synthesis, leading to responsive and functional surfaces. At the same time, the spatial control afforded by the light-mediated processes allows all components of the brush to be patterned.

To demonstrate this concept, a uniform PMMA brush was initially grown from the surface and shown to have a brush height of 44 nm. These PMMA brushes were then used as macroinitiators for the re-initiation and growth of a random copolymer block of MMA-*co*-HEMA containing 2.5 mol % HEMA. After growth of this second block, the resulting polymer brush had an overall brush height of 95 nm, indicating successful block copolymer brush formation. After terminating the linear brush chains with EVE, the HEMA units in the second block were functionalized with initiating units using the chemistry developed above. This sequence of steps then allows a third monomer, *t*-BuMA, to be grown specifically from the random copolymer block leading to grafted poly(*t*-butyl methacrylate) chains and the generation of novel branched, block copolymer brushes as depicted in Figure 5c.

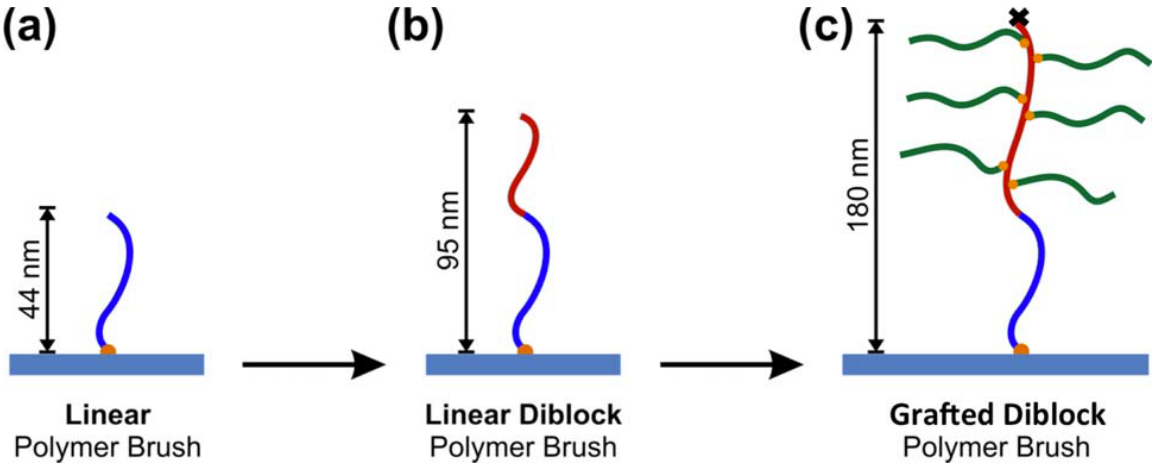

Figure 5. Fabrication of a multicomponent block copolymer structure starting from (a) linear polymer brush (PMMA); chain extension to give (b) linear diblock polymer brush (P[MMA-*b*-(MMA-*co*-HEMA)]); and finally comb growth leading to novel (c) grafted diblock polymer brush (P[MMA-*b*-(MMA-*co*-HEMA)-*g*-*t*-BuMA]) structures.

From this sequence of reactions, *t*-butyl esters are only contained in the graft arms and are susceptible to hydrolysis by immersion in trifluoroacetic acid (TFA) and DCM for 1 hour. This gives the corresponding methacrylic acid grafted chains, neutralization of which affords sodium poly(methacrylic acid) chains (Figure 6). This sequence of chemical modifications is confirmed by the changing surface properties for these polymer brushes. The sessile drop water contact angle for P[MMA-*b*-(MMA-*co*-HEMA)-*g*-*t*-BuMA] changes from 82º to 54 º upon deprotection of the t-butyl ester groups. A further reduction in contact angle (to 22 º) is observed after neutralization, demonstrating the utility of this modular approach for precise control over surface properties.

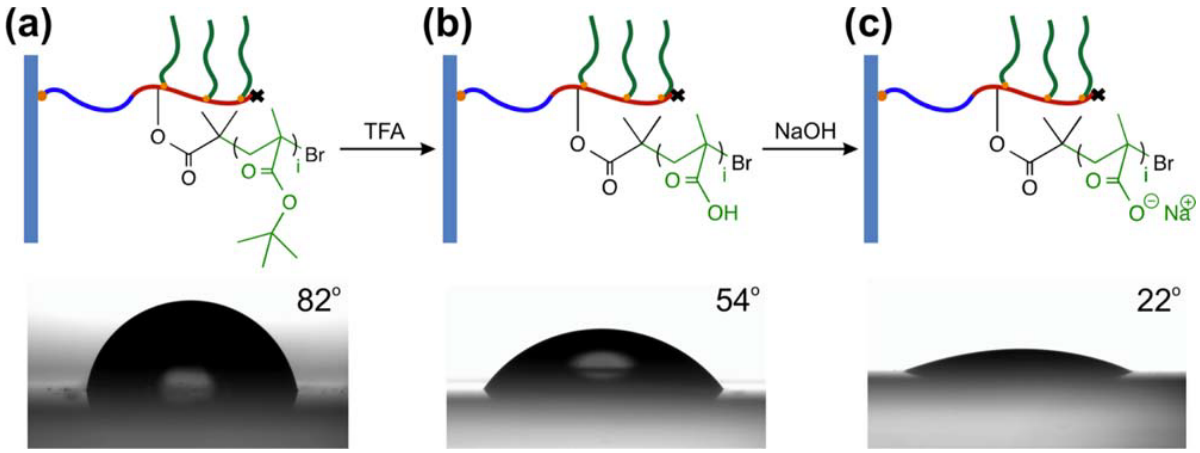

Figure 6. Water contact angles, droplet images, and structures for the branched, block copolymer brushes with (a) poly(*t*-BuMA) side chains; (b) poly(methacrylic acid) side chains after deprotection of the *t*-butyl esters with TFA; (c) poly(sodium methacrylate) side chains after neutralization by NaOH.

2.4 Conclusion

In conclusion, we have developed a straightforward approach to hierarchical comb brush architectures using light-mediated CRP. The modular and step-wise nature of this process allows the density of grafted chains along the tethered linear backbone to be controlled from 1 to 9 mol % through the initial monomer feed ratio of MMA to HEMA. A major consequence of this strategy is a rapid increase in brush layer thickness on secondary formation of the grafted polymer chains (up to 400%). This increase arises solely from the added steric requirements of the grafted chains and results in significant elongation of the tethered backbone polymer. In addition, spatial control over these unique molecular architectures could be achieved using photomasks, leading to complex 3D polymer brush structures and tunable

surface properties. By combining the ability to pattern using photomasks with the tunability of light as an external stimulus, we envision a high degree of synthetic flexibility and structural control for these novel macromolecular systems.

2.5 Supporting Information

Materials and Methods. Silicon substrates with 100 nm oxide were purchased from Silicon Quest International. Photomasks containing transparent rectangles (20x200 μm) were obtained from Photronics. A HEBS5N grayscale photomask was purchased from Canyon Materials containing squares of varying optical density and prisms of variable slope. UV 405 nm collimated LED lights 1.1 $\mu W/cm^2$ (Olympus BX & 1X, 1000 mA) were purchased from Thorlabs. Chemicals and solvents were purchased from commercial sources. Toluene was dried using a Pure-Solv MD-5 solvent purification system from Innovative Technology. 1-Methyl-2-pyrrolidinone (NMP) was freeze-pump-thaw degassed before use. HEMA, MMA, EVE, and *t*-butyl methacrylate (*t*-BuMA) were passed through aluminum oxide to remove inhibitor and freeze-pump-thaw degassed before polymerization.

Instrumentation. Film thicknesses were measured with a Filmetrics F20 optical reflectometer by setting silicon oxide (100 nm) as the first layer and the polymer brush as the second layer. Film thicknesses were measured with a Dektak IIA Profilometer by setting the scan length to 200 μm and the speed to medium. Profilometry was used to measure patterned and gradient polymer surfaces. Contact angle measurements were performed using OCA 15 Pro Data Physics Contact Angle. Deionized water, HCl (pH 4) and NaOH (pH 10) drops (2 μL) were dispensed from a 250-μL syringe with a needle diameter of 520 μm. Deionized water was used for the comb brushes with t-butyl ester containing grafted chains, HCl was

used for those with poly(methacrylic acid) grafted chains and NaOH was used for those with poly(sodium methacrylate) grafted chains. Optical micrographs were captured with a Nikon Elipse E600 optical microscope. Tapping mode AFM experiments were performed using a MFP-3D system (Asylum Research, Santa Barbara, CA). The measurements were conducted using commercial Si cantilevers. The height and phase images were acquired simultaneously at the set-point ratio $A/A_0 = 0.8$, where A and A_0 are the "tapping" and "free" cantilever amplitudes, respectively. X-ray photoelectron spectroscopy (XPS) measurements were conducted using a Kratos Axis Ultra Spectrometer (Kratos Analytical, Manchester, U.K.) with a monochromatic aluminum K_∞ X-ray source (1486.6 eV) operating at 225 W under a vacuum of 1028 Torr.

Uniform Alkyl Bromide-Functionalization of Silicon Surfaces. Silicon substrates were cleaned by sonication in acetone, followed by isopropyl alcohol and dried under a stream of nitrogen gas. Silicon substrates were placed in an air plasma cleaner (PDC-001, Harrick Plasma) for 20 min. A stock solution was then prepared by mixing 30 mL of a solution containing 125 μL of 11-(trichlorosilyl)undecyl 2-bromo-2- methylproanoate[53,64] in 250 mL of dry toluene (0.05% v/v) and 50 μL of dry triethylamine. The substrates were placed in petri dishes and covered with the stock solution under nitrogen gas and left overnight. The initiator-functionalized substrates were finally cleaned with toluene followed by ethanol and dried under a stream of nitrogen gas.

Synthesis of P(MMA-co-HEMA) Brushes. A 400 μL degassed solution of 2.5% HEMA and 97.5% MMA (MMA 2 mL, 18.7 mmol and HEMA 66.9 μL, 0.479 mmol) was mixed with 100 μL of a 1.2 mg/mL *fac*-[$Ir(ppy)_3$] stock solution (1.2 mg, 1.8 μmol in 1 mL degassed NMP) in a nitrogen atmosphere glove box. The monomer and catalyst solutions were pipetted

onto a silicon substrate and a glass coverslip was placed on top of the solution. The substrate was placed 1.13 cm below UV 405 nm collimated LED lights for 30 minutes and immersed in degassed NMP immediately after polymerization and removed from the glove box. Subsequently, the substrate was rinsed with dichloromethane (DCM) and dried under a stream of nitrogen.

End-capping of Initial Brush Layer with EVE. 100 μL of degassed EVE (1.04 mmol) was mixed with 100 μL of a 1.2 mg/mL *fac*-[Ir(ppy)$_3$] stock solution (1.2 mg, 1.8 μmol in 1 mL degassed NMP) in a nitrogen atmosphere glove box. The resulting solution was pipetted onto a silicon substrate and a glass coverslip was placed on top of the solution. The substrate was placed 1.13 cm below 405 nm collimated LED lights for 1 hour and immersed in NMP immediately after reaction and removed from the glove box. Subsequently, the substrate was rinsed with DCM and dried under a stream of nitrogen.

Functionalization of HEMA units with α-Bromoisobutyryl Bromide. The substrate was immerged in a solution of α-bromoisobutyryl bromide (1 mL, 8.09 mmol) in 1 mL DCM and allowed to react overnight. The substrate was rinsed with DCM and dried under a stream of nitrogen.

Synthesis of PMMA Pattern Side Chain. Degassed MMA (400 μL, 3.74 mmol) was mixed with 100 μL of a 1.2 mg/mL *fac*-[Ir(ppy)$_3$] stock solution (1.2 mg, 1.8 μmol in 1 mL degassed NMP) in a nitrogen atmosphere glove box. The monomer and catalyst solutions were pipetted onto a silicon substrate and a photomask containing transparent rectangles 20 μm×200 μm was placed on top of the solution. The substrate was placed 1.13 cm below 405 nm collimated LED lights for 8 minutes and immersed in degassed NMP immediately after polymerization and removed from the glove box. The substrate was rinsed with DCM and dried under a stream

of nitrogen. The rectangular regions of the comb brushes were visualized under an optical microscope.

Surface Roughness of Comb Brush Layers

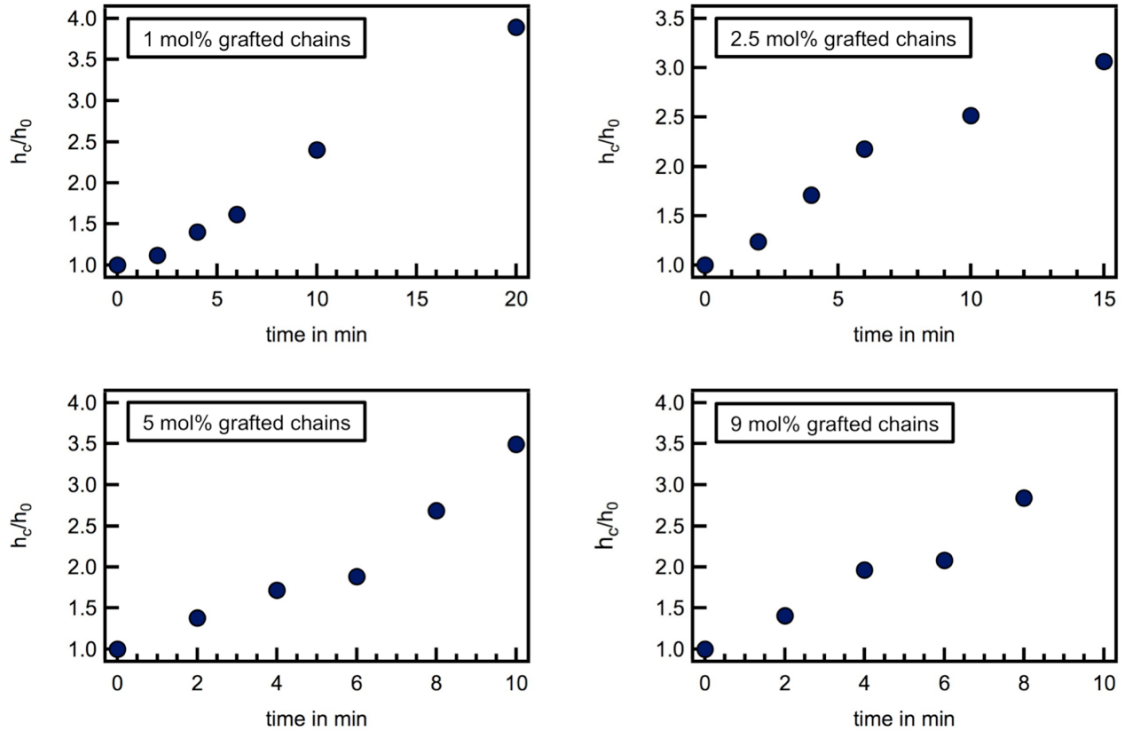

Figure S1. Relationship between normalized brush height and exposure time to light (h_c is brush height with side chains and h_0 is brush height without side chains) of 1 mol% grafted chains, 2.5 mol% grafted chains, 5 mol% grafted chains and 9 mol% grafted chains.

Surface Roughness of Comb Brush Layers

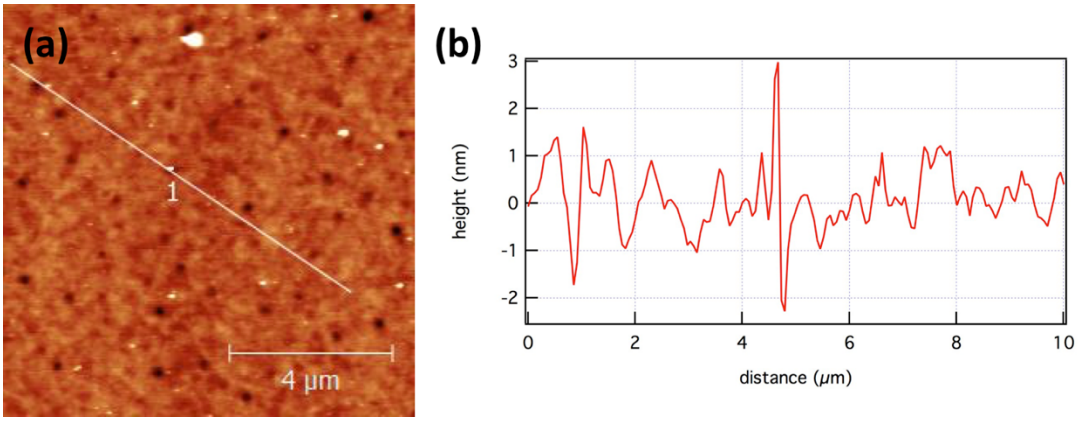

Figure S2. Atomic-force microscopy data of 2.5 mol% grafted chain after 2 min of side chain polymerization a) AFM image with rms roughness = 0.88 nm b) surface cross-section analysis of thin film.

Optical Micrographs of Homogeneous and Inhomogeneous Layers

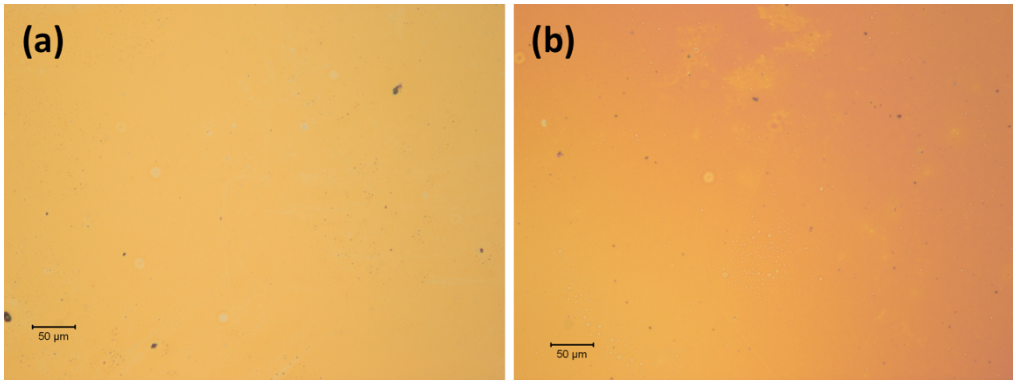

Figure S3. Optical micrographs for 5 mol% grafted chains; a) shows homogeneous layers after 10 min of side chain polymerization and b) shows inhomogeneous layers after 15 min of side chain polymerization.

Patterning with Rectangles Photomask

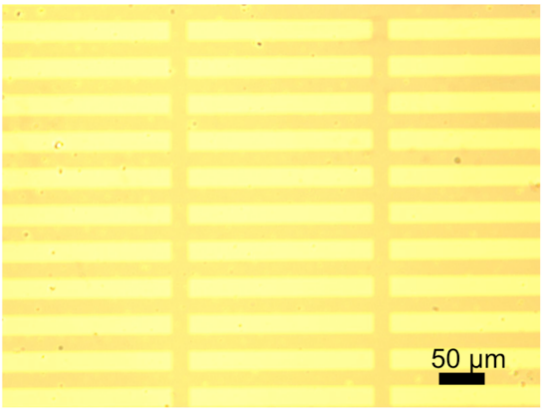

Figure S4. Optical micrograph of rectangles comb brushes using transparent rectangles 20 µm × 200 µm photomask.

Patterning with a Photomask Containing Squares of Varying Optical Density

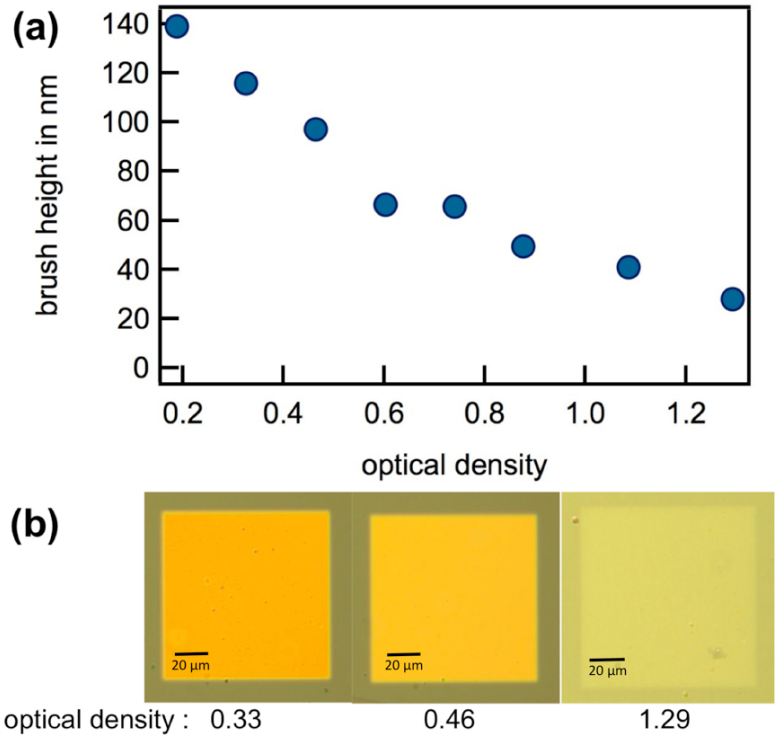

Figure S5. Using a grayscale mask to control the growth of grafted comb polymer brushes a) relationship of brush height (measured by profilometry) as a function of the grayscale mask

optical density b) Optical micrograph of comb brushes using 100 μm × 100 μm squares of 0.33, 0.46 and 1.29 optical density photomask.

Synthesis of P(MMA-co-HEMA) Brushes. The synthetic procedure was performed following the same procedure except the solution composition was changed to 9% HEMA and 91% MMA (MMA 2 mL, 18.7 mmol and HEMA 258 μL, 1.85 mmol). The substrate was placed 1.13 cm below 405 nm collimated LED lights for 20 minutes in a nitrogen atmosphere glove box.

End-capping of Initial Brush Layer with EVE and Functionalization of HEMA units with α-Bromoisobutyryl Bromide. Procedures were performed following the same procedure.

Synthesis of PMMA Pattern Side Chain. Synthetic procedures were performed following the same procedure. The monomer and catalyst solutions were pipetted onto a silicon substrate and a photomask containing 100 μm×100 μm squares of varying optical density was placed on top of the solution. The substrate was placed 1.13 cm below 405 nm collimated LED lights for 10 minutes in a nitrogen atmosphere glove box. The square regions of comb brushes were visualized under an optical microscope and the film thickness was measured by profilometry.

Patterning with Gradient Photomask

Synthesis of P(MMA-co-HEMA) Brushes. Synthetic procedures were performed following the same procedure. The solution composition was changed to 9% HEMA and 91% MMA (MMA 2 mL, 18.7 mmol and HEMA 258 μL, 1.85 mmol). The substrate was placed 1.13 cm below 405 nm collimated LED lights for 20 minutes in a nitrogen atmosphere glove box.

End-capping of Initial Brush Layer with EVE and Functionalization of HEMA units with α-Bromoisobutyryl Bromide. Synthetic procedures were performed following the same procedure.

Synthesis of PMMA Patterned Side Chain. Synthetic procedures were performed following the same procedure. The monomer and catalyst solutions were pipetted onto a silicon substrate and a photomask containing prisms of variable slope was placed on top of the solution. The substrate was placed 1.13 cm below 405 nm collimated LED lights for 10 minutes in a nitrogen atmosphere glove box. The prism regions of comb brushes were visualized under an optical microscope and the film thickness was measured by profilometry.

Synthesis of Complex Architectures

Synthesis of P(MMA) Brushes. 400 μL (3.74 mmol) of degassed MMA was mixed with 100 μL of a 1.2 mg/mL *fac*-[$Ir(ppy)_3$] stock solution (1.2 mg, 1.8 μmol in 1 mL degassed NMP) in a nitrogen atmosphere glove box. The monomer and catalyst solutions were pipetted onto a silicon substrate and a glass coverslip was placed on top of the solution. The substrate was placed 1.13 cm below 405 nm collimated LED lights for 30 minutes and the substrate was immersed in degassed NMP immediately after polymerization and removed from the glove box. Subsequently, the substrate was rinsed with DCM and dried under a stream of nitrogen.

Synthesis of P(MMA-co-HEMA) Brushes. Synthetic procedures were performed following the same procedure except for the polymerization time (changed to 45 minutes).

End-capping of Initial Brush Layer with EVE and Functionalization of HEMA units with α-Bromoisobutyryl Bromide. Synthetic procedures were performed following the same procedure.

Synthesis of t-BuMA Side Chain. Synthetic procedures were performed following the same procedure except the monomer was changed to *t*-BuMA. The catalyst solutions were pipetted onto a silicon substrate and a glass coverslip was placed on top of the solution. The substrate was then placed 1.13 cm below 405 nm collimated LED lights for 8 minutes in a nitrogen atmosphere glove box. After polymerization, the film thickness was measured by optical reflectometry. The contact angle goniometer was used to measure hydrophobicity by dispensed deionized water on the surface.

Modification of Hydrophilic Properties on Surface

Deprotection of t-Butyl Methacrylate. The substrate containing (P[MMA-*b*-(MMA-*co*-HEMA)-*g*-*t*-BuMA]) was placed in a 1:1 v/v solution of trifluoroacetic acid (TFA) and DCM (1 mL TFA (13.1 mmol) in 1 mL DCM) for 1 hour to cleave the *t*-butyl esters and generate poly(methacrylic acid) (PMAA). The substrate was cleaned with DCM and dried under a stream of nitrogen. The substrate was dipped in HCl pH 4 for 10 minutes to ensure complete protonation of poly(methacrylic acid). The contact angle goniometer was used to measure hydrophilicity by dispensed HCl pH 4 on the surface.

Neutralization of Poly(methacrylic acid). The substrate was neutralized by dipping in NaOH pH 10 for 10 minutes to generate the poly(sodium methacrylate) salt. The contact angle goniometer was used to measure hydrophilicity by dispensed NaOH pH 10 on the surface.

X-Ray Photoelectron Spectroscopy (XPS) Plots

XPS data was used to confirm elemental modifications of the surface-tethered polymer brushes. Specifically, the C1s and Na1s peaks are consistent the proposed polymer structure and corroborates our contact angle measurements. The grafted diblock polymer brushes with

poly(*t*-BuMA) side chains, and the subsequent modifications yielding poly(methacrylic acid) side chains, and poly(sodium methacrylate) side chains, were examined by XPS. First the C1s regions of the spectra were analyzed, as shown in Figure S6 below.

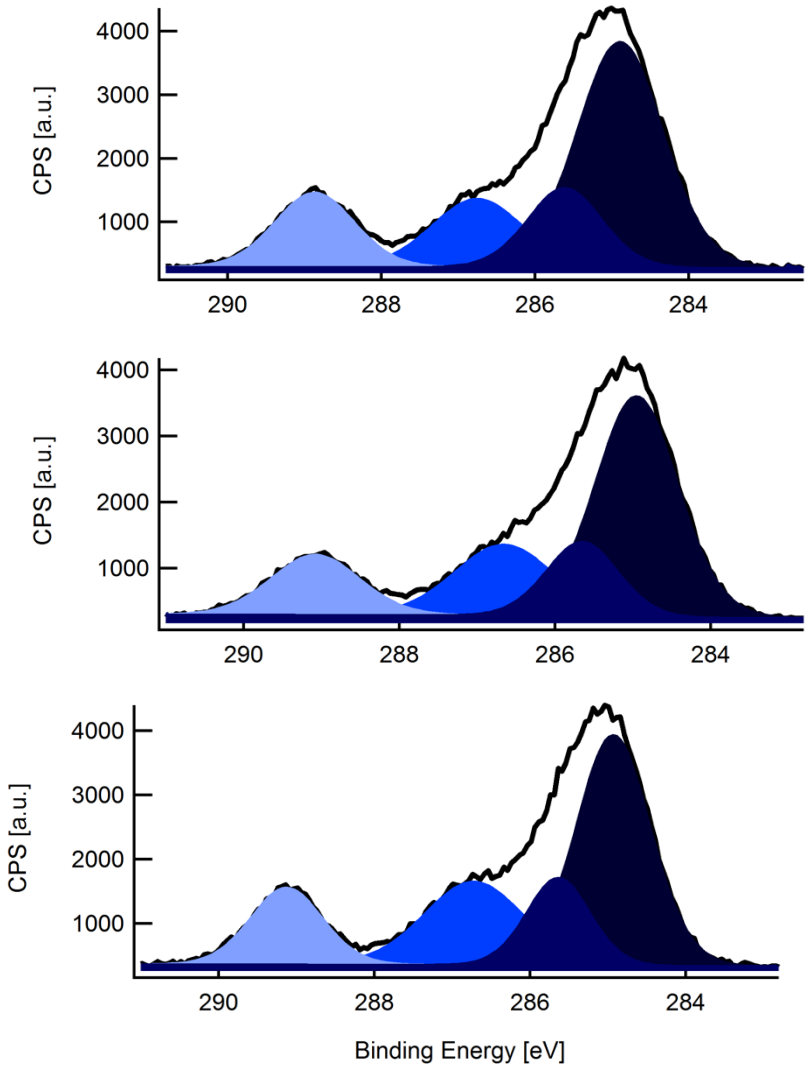

Figure S6. High-resolution C1s scans of grafted diblock polymer brushes with poly(*t*-BuMA), poly(methacrylic acid), and poly(sodium methacrylate) side chains in order from top to bottom. The C1s region is fitted using four Gaussians corresponding to the C-C (dark blue), CR_4 (navy blue), C-O (blue), and C=O (light blue) peaks.

The XPS spectra were processed using the CasaXPS software. Figure S6 shows the expected functionalities in the polymer films. Namely, the C-C, CR_4, C-O and C=O peaks are consistent with the expected spectra of our polymers and suggests preservation of the backbone chemistry. The successful conversion of the methacrylic acids to sodium methacrylates was confirmed by the Na1s region around 1071 eV as shown in Figure S7 below.

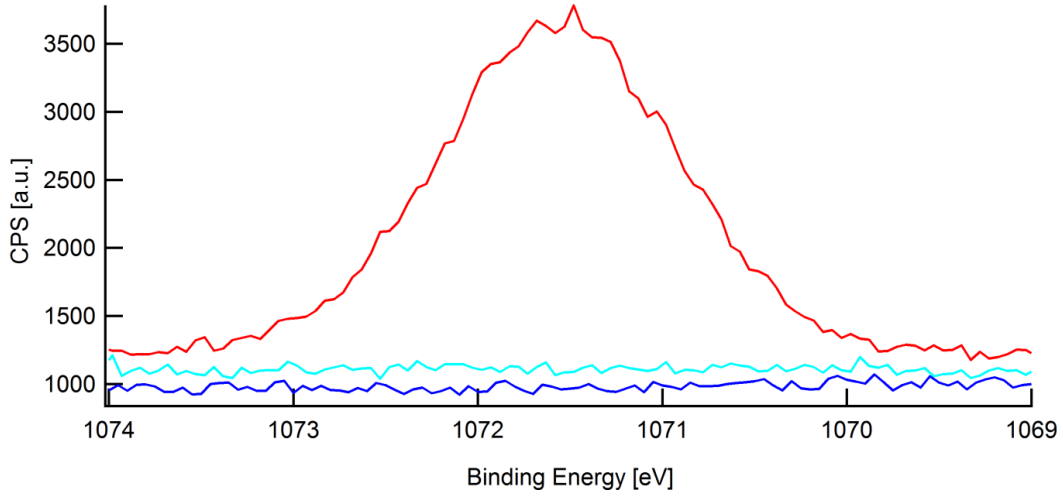

Figure S7. High-resolution scan of the Na1s peak, structures for the branched, block copolymer brushes with poly(*t*-BuMA) side chains (blue), poly(methacrylic acid) side chains (light blue), poly(sodium methacrylate) side chains (red). The characteristic Na1s peak centered around 1070 eV is only present for the sample neutralized using NaOH.

The red trace, corresponding to the grafted diblock polymer brushes with poly(sodium methacrylate) side chains, indicates the presence of the Na counter-ion within the film. This

is evidence of the successful deprotonation of the methacrylic acid to form the sodium methacrylate.

2.6 References

1) H. A. Klok and J. Genzer, *ACS Macro Letters*, **2015**, *28*, 636-9.
2) J. Lawrence and T. S. Emrick, *ACS Appl. Mater. & Inter*. **2016**, *8*, 2393-2398.
3) M. E. Welch, T. Doublet, C. Bernard, G. G. Malliaras and C. K. Ober *J. Polym. Sci. Part A Polym. Chem*. **2015**, *53*, 372–377.
4) R. Barbey, L. Lavanant, D. Paripovic, N. Schuwer, C. Sugnaux, S. Tugulu, H. A. Klok, *Chem. Rev*. **2009**, *109*, 5437-5527.
5) C. M. Hui, J. Pietrasik, M. Schmitt, C. Mahoney, J. Choi, M. R. Bockstaller and K. Matyjaszewski, *Chem. Mater.* **2014**, *26*, 745–762.
6) B. Li, B. Yu, Q. Ye and F. Zhou, *Acc. Chem. Res*. **2015**, *48*, 229–237.
7) J. Pyun, T. Kowalewski and K. Matyjaszewski, *Macromol. Rapid Commun*. **2003**, *24*, 1043–1059.
8) K. J. Peng, K. H. Wang, K. Y. Hsu, Y. L. Liu, *J. Polym. Sci. Part A Polym. Chem*. **2014**, *52*, 1588-1596.
9) R. R. Shah, D. Merreceyes, M. Husemann, I. Rees, N. L. Abbott, C. J. Hawker and J. L. Hedrick, *Macromolecules*, **2000**, *33*, 597–605.
10) X. Fan, L. Lin, J. L. Dalsin and P. B. Messersmith, *J. Am. Chem. Soc*. **2005**, *127*, 15843–15847.
11) M. Ejaz, S. Yamamoto, K. Ohno, Y. Tsujii and T. Fukuda, *Macromolecules* **1998**, *31*, 5934–5936.
12) M. Husseman, E. E. Malmström, M. McNamara, M. Mate, D. Mecerreyes, D. G. Benoit, J. L. Hedrick, P. Mansky, E. Huang, T. P. Russell and C. J. Hawker, *Macromolecules* **1999**, *32*, 1424–1431.

13) W. Devonport, L. Michalak, E. Malmstrom, M. Mate, B. Kurdi, C. J. Hawker, G. G. Barclay, R. Sinta, *Macromolecules* **1997**, *30*, 1929-1934.

14) C. Konn, F. Morel, E. Beyou, P. Chaumont and E. Bourgeat-Lami, *Macromolecules* **2007**, *40*, 7464–7472.

15) M. Baum and W. J. Brittain, *Macromolecules* **2002**, *35*, 610–615.

16) B. de Boer, H. K. Simon, M. P. L. Werts, E. W. van der Vegte and G. Hadziioannou, *Macromolecules* **2000**, *33*, 349–356.

17) N. Luo, J. B. Hutchison, K. S. Anseth and C. N. Bowman, *J. Polym. Sci. Part A Polym. Chem.* **2002**, *40*, 1885–1891.

18) C. Schuh, S. Santer, O. Prucker and J. Rühe, *Adv. Mater*. **2009**, *21*, 4706–4710.

19) H. Ma, J. Hyun, P. Stiller and A. Chilkoti, *Adv. Mater*. **2004**, *16*, 338–341.

20) A. Asatekin, S. Kang, M. Elimelech and A. M. Mayes, *J. Memb. Sci*. **2007**, *298*, 136–146.

21) J. L. Dalsin, B. H. Hu, B. P. Lee and P. B. Messersmith, *J. Am. Chem. Soc*. **2003**, *125*, 4253–4258.

22) L. Ionov, N. Houbenov, A. Sidorenko, M. Stamm and S. Minko, *Adv. Funct. Mater*. **2006**, *16*, 1153–1160.

23) H. C. McCaig, E. Myers, N. S. Lewis and M. L. Roukes, *Nano Lett*. **2014**, *14*, 3728–3732.

24) T. Chen, R. Ferris, J. Zhang, R. Ducker and S. Zauscher, *Prog. Polym. Sci*. **2010**, *35*, 94–112.

25) S. Kurosawa, H. Aizawa, Z. A. Talib, B. Atthoff and J. Hilborn, *Biosens. Bioelectron.* **2004**, *20*, 1165–1176.

26) W. Senaratne, L. Andruzzi and C. K. Ober, *Biomacromolecules* **2005**, *6*, 2427–2548.

27) R. Iwata, P. Suk-In, V. P. Hoven, A. Takahara, K. Akiyoshi and Y. Iwasaki, *Biomacromolecules* **2004**, *5*, 2308–2314.

28) P. M. Mendes, *Chem. Soc. Rev*. **2008**, *37*, 2512–29.

29) R. R. Bhat, B. N. Chaney, J. Rowley, A. Liebmann-Vinson and J. Genzer, *Adv. Mater.* **2005**, *17*, 2802–2807.

30) N. A. Hutter, M. Steenackers, A. Reitinger, O. A. Williams, J. a. Garrido and R. Jordan, *Soft Matter* **2011**, *7*, 4861–4867.

31) E. N. Chiang, R. Dong, C. K. Ober and B. a. Baird, *Langmuir* **2011**, *27*, 7016–7023.

32) M. Chen, W. H. Briscoe, S. P. Armes and J. Klein, *Science* **2009**, *323*, 1698–1701.

33) M. T. Müller, X. Yan, S. Lee, S. S. Perry and N. D. Spencer, *Macromolecules* **2005**, *38*, 5706–5713.

34) Ku, K.H.; Yang, H.; Jang, S.G.; Bang, J.; Kim, B.J., *J. Polym. Sci. Part A Polym. Chem.* **2016**, *54*, 228-237.

35) Prehn, F.C.; Boyes S.G., *Macromolecules* **2015**, *26*, 4269-80.

36) Orski S.V.; Sheridan R.J.; Chan E.P.; Beers K.L., *Polymer*, **2015**, *18*, 471-8.

37) X. Xu, D. J. Cao, *Chem. Phys*. **2009**, *130*, 164901.

38) W. M. De Vos, F. A. M. Leermakers, S. Lindhoud, S. W. Prescott, *Macromolecules* **2011**, *44*, 2334-2342.

39) T. Otsu and M. Yoshida, *Macromol. Rapid Commun.* **1982**, *3*, 127–132.

40) H. J. Lee, Y. Nakayama and T. Matsuda, *Macromolecules* **1999**, *32*, 6989–6995.

41) Y. Nakayama, M. Sudo, K. Uchida and T. Matsuda, *Langmuir* **2002**, *18*, 2601–2606.

42) S. Morsch, W. C. E. Schofield and J. P. S. Badyal, *Langmuir* **2011**, *27*, 14151–14159.

43) D. Wu, C. Zhao, J. Tian and H. Zhao, *Polym. Int.* **2009**, *58*, 1335–1340.

44) M. Khan and W. T. S. Huck, *Macromolecules* **2003**, *36*, 5088–5093.

45) O. V. Borisov and E. B. Zhulina, *Macromolecules* **2015**, *48*, 1499–1508.

46) T. Chen, I. Amin and R. Jordan, *Chem. Soc. Rev.* **2012**, *41*, 3280–3296.

47) M. E. Welch and C. K. Ober, *J. Polym. Sci. Part B Polym. Phys.* **2013**, *51*, 1457–1472.

48) W. Sheng, B. Li, X. Wang, B. Dai, B. Yu, X. Jia and F. Zhou, *Chem. Sci*. **2015**, *6*, 2068–2073.

49) B. P. Fors and C. J. Hawker, *Angew. Chem. Int. Ed. Engl*. **2012**, *51*, 8850–8853.

50) N. J. Treat, B. P. Fors, J. W. Kramer, M. Christianson, C. Chiu, J. R. De Alaniz and C. J. Hawker, *ACS Macro Lett*. **2014**, *3*, 580–584.

51) N. J. Treat, H. Sprafke, J. W. Kramer, P. G. Clark, B. E. Barton, J. R. de Alaniz, B. P. Fors and C. J. Hawker, *J. Am. Chem. Soc.* **2014**, *136*, 16096–16101.

52) X. Pan, M. Lamson, J. Yan and K. Matyjaszewski, *ACS Macro Lett*. **2015**, *4*, 192–196.

53) J. E. Poelma, B. P. Fors, G. F. Meyers, J. W. Kramer and C. J. Hawker, *Angew. Chem. Int. Ed. Engl.* **2013**, *52*, 6844–6848.

54) R. Dong, S. Krishnan, B. a. Baird, M. Lindau and C. K. Ober, *Biomacromolecules* **2007**, *8*, 3082–3092.

55) S. J. Ahn, M. Kaholek, W. K. Lee, B. LaMattina, T. H. LaBean and S. Zauscher, *Adv. Mater*. **2004**, *16*, 2141–2145.

56) N. Ballav, S. Schilp and M. Zharnikov, *Angew. Chem. Int. Ed. Engl.* **2008**, *120*, 1443–1446.

57) M. N. Khan, V. Tjong, A. Chilkoti and M. Zharnikov, *Angew. Chem. Int. Ed. Engl.* **2012**, *124*, 10449–10452.

58) M. Y. Paik, Y. Xu, A. Rastogi, M. Tanaka, Y. Yi and C. K. Ober, *Nano Lett*. **2010**, *10*, 3873–3879.

59) F. Zhou, Z. Zheng, B. Yu, W. Liu and W. T. S. Huck, *J. Am. Chem. Soc*. **2006**, *128*, 16253–16258.

60) T. Chen, R. Jordan and S. Zauscher, *Soft Matter* **2011**, *7*, 5532–5535.

61) O. Azzaroni, S. E. Moya, A. a. Brown, Z. Zheng, E. Donath and W. T. S. Huck, *Adv. Funct. Mater*. **2006**, *16*, 1037–1042.

62) B. Li, B. Yu, W. T. S. Huck, W. Liu and F. Zhou, *J. Am. Chem. Soc*. **2013**, *135*, 1708–1710.

63) T. Zhang, Y. Du, J. Kalbacova, R. Schubel, R. D. Rodriguez, T. Chen, D. R. T. Zahn and R. Jordan, *Polym. Chem*. **2015**, *6*, 8176-8183.

64) K. Matyjaszewski, P. J. Miller, N. Shukla, B. Immaraporn, A. Gelman, B. B. Luokala, T. M. Siclovan, G. Kickelbick, T. Vallant, H. Hoffmann and T. Pakula, *Macromolecules* **1999**, *32*, 8716–8724.

3. Simultaneous Preparation of Multiple Polymer Brushes under Ambient Conditions using Microliter Volumes[2]

3.1 Abstract

The fabrication of well-defined, multifunctional polymer brushes under ambient conditions is described. This facile methodology uses light-mediated, metal-free atom transfer radical polymerization (ATRP) to grow polymer brushes with only microliter volumes required. Key to the success of this strategy is the dual action of *N*-phenylphenothiazine (PTH) as both an oxygen scavenger and polymerization catalyst. Use of simple glass cover slips results in a high degree of spatial and temporal control and allows for multiple polymer brushes to be grown simultaneously. The preparation of arbitrary 3-D patterns and

[2] Reproduced with permission: **Narupai, B**; Page, Z. A.; Treat, N. J.; McGrath, A. J.; Pester. C. W.; Discekici, E. H.; Dolinski, N. D.; Meyers, G. F.; Read De Alaniz, J.; Hawker, C. J. "Simultaneous Preparation of Multiple Polymer Brushes under Ambient Conditions using Microliter Volumes." *Angew. Chem. Int. Ed.* **2018***, 57,* 13433-13438. DOI: 10.1002/anie.201805534. Copyright 2018, Wiley. License Number: 4440480905604.

functional/emissive polymer brushes demonstrates the practicality and versatility of this novel strategy.

3.2 Introduction

The ability to precisely control polymer brush growth[1-6] has enabled applications in areas ranging from anti-fouling,[7-8] anti-fog,[9-10] sensing,[11-13] to lubrication.[14] Key to these advances has been the development of surface-initiated controlled radical polymerization (SI-CRP)[15-21] strategies involving the growth of polymer brushes from initiator-functionalized surfaces. While successful, major challenges prevent the widespread adoption of SI-CRP. These include the use of air-free conditions, requirement for large reaction volumes (e.g., complete submergence of the substrate in monomer solution) and elaborate strategies for patterning brush growth.[22-27] To increase the versatility of SI-CRP, our group recently reported a visible light-mediated methodology for the preparation of polymer brushes using either iridium[28-30] or organic photoredox catalysts (*N*-phenylphenothiazine, PTH).[31-33] While these techniques enable access to patterned and gradient 3-dimensional polymer brush nanostructures, the need for an inert atmosphere and special equipment (e.g. glovebox, custom-made chambers) for brush growth significantly limits wide-spread implementation. Additives that regenerate the catalyst[34-35] or the use of an overlying copper-plate[36] provide partial solutions, however, no methodology allows well-defined polymer brush patterns to be simultaneously produced from microliter reaction volumes under ambient conditions.

Herein, we report a simple strategy for growing polymer brush structures using a simple glass cover slip as an oxygen barrier. Under ambient conditions, this method is shown to be robust and user-friendly, employing microliter amounts of reagents and visible light-mediation to achieve polymer brush growth over large surface areas. Key to the success of

this strategy is the use of organic photoredox systems (PTH) as both a catalyst and oxygen scavenger. By masking light activation, complex surface patterns with excellent spatial resolution (~1 μm) can be achieved while the use of specifically shaped cover slips allows multiple features to be prepared on a single substrate.

3.3 Results and Discussion

The procedure for controlled polymer brush growth under ambient conditions is graphically illustrated in Scheme 1. First, ~20 μL of monomer/PTH solution (*N,N*-dimethylacetamide, DMA, 4.7 M) is deposited onto an ATRP initiator-functionalized silicon wafer. A glass cover slip is subsequently placed on the wafer to uniformly spread the solution and provide a vertical barrier to oxygen diffusion. Under ambient conditions, irradiation with visible light (e.g., LEDs, natural sunlight, or a compact fluorescent lamp, Figure S2) excites the PTH, which acts as a scavenger to remove dissolved oxygen as well as a catalyst for brush polymerization. Significantly, growth of polymer brushes occurs without degassing and can be controlled by either the concentration of PTH or by the physical dimensions of the cover slip.

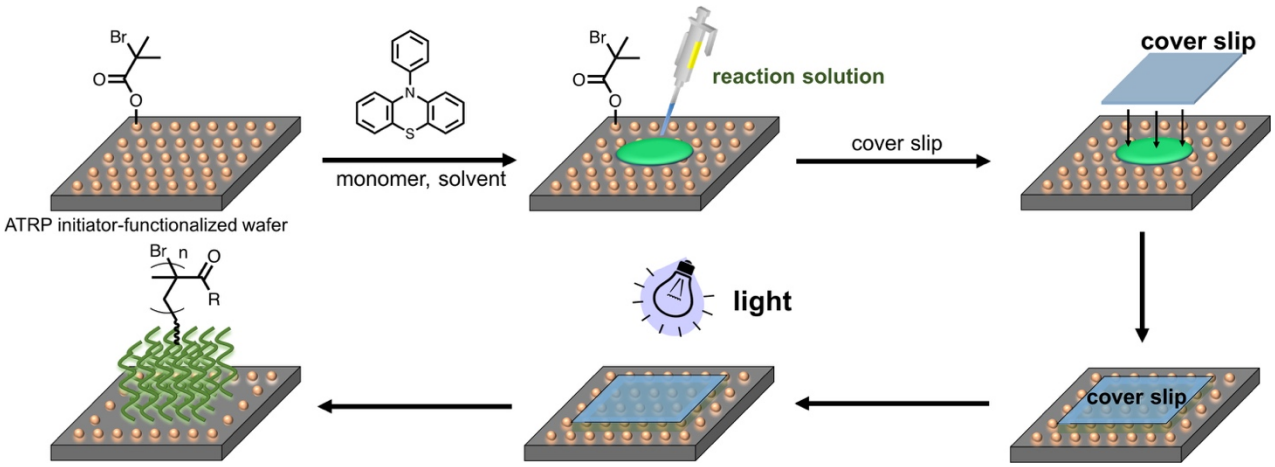

Scheme 1. Graphical representation of visible light mediated polymer brush growth under ambient conditions. *N*-phenylphenothiazine (PTH) acts as both a scavenger for oxygen and as a catalyst for SI-CRP, while the glass cover slip acts as a vertical barrier for the diffusion of oxygen.

In the following studies, silicon wafers functionalized with undecyl-2-bromo-2-methylpropanoate initiator and a visible LED excitation source (λmax = 405 nm) were utilized (details in SI). Initial studies examined the influence of oxygen on polymer brush growth with two variables being systematically changed: wafer size from 7×7 to 10×10 to 14×14 and 18×18 mm (glass cover slip was kept constant at 18×18 mm) and the concentration of PTH (0.5, 1.0 and 5.0 mol%). As shown in Figure 1, for all 7×7 and 10×10 mm wafers, polymerization of 2-(dimethylamino)ethyl methacrylate (DMAEMA) resulted in homogenous brush growth across the entire wafer. In contrast, for the 14×14 mm wafers, only the 5 mol% PTH concentration showed homogenous brush growth over the entire wafer surface, with "edge effects" (no polymer growth) being observed for the 0.5 and 1.0 mol% PTH samples.

This “edge effect” is further pronounced for the 18×18 mm substrates (glass cover slip is the same size as the silicon wafer), with this region increasing in size with decreasing PTH concentration (Figure 1c). Excluding “edge effect” regions, optical reflectometry indicated uniform polymer brush thicknesses ranging from 40 to 90 nm (Table S1).

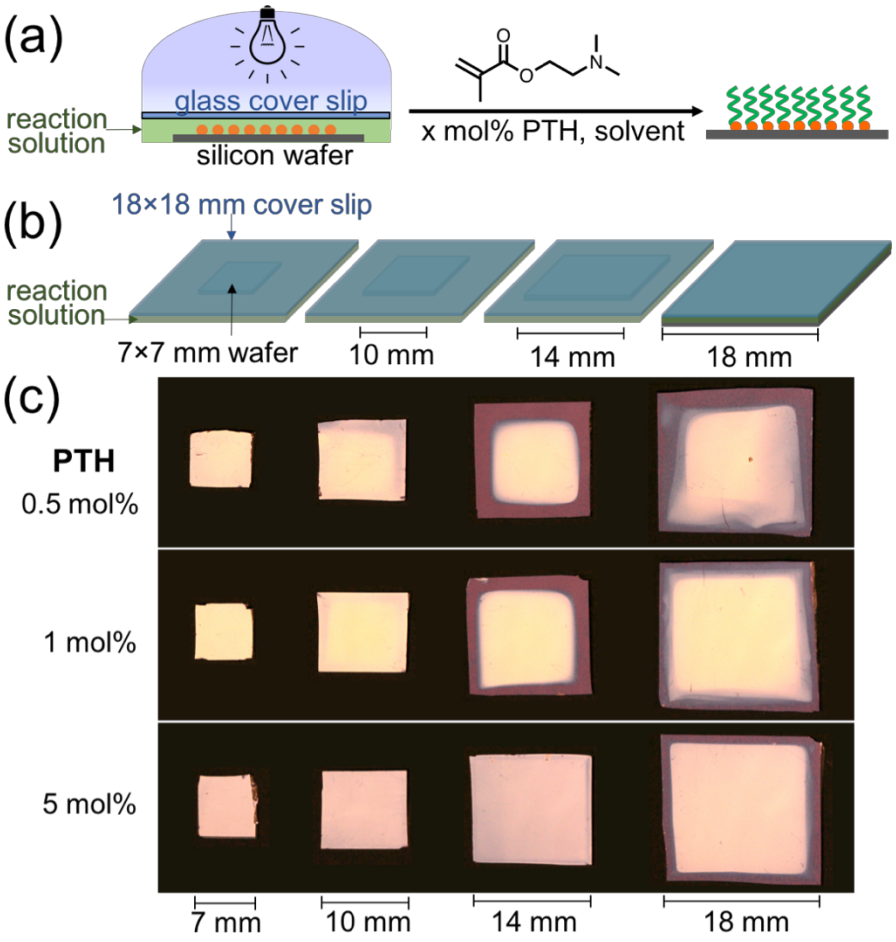

Figure 1. (a) Schematic representation of P(DMAEMA) brush growth in the presence of PTH, (b) Graphical representation of the experimental dimensions using wafers of different size and 18×18 mm glass cover slips, (c) Effect of wafer size and catalyst loading on the “edge effect.”

Having demonstrated the growth of polymer brushes under ambient conditions, we examined the extent of initiator retention in the "edge effect" regions. Using a substrate with a defined "edge effect", secondary brush growth over the full wafer was performed (Figure 2). Specifically, benzyl methacrylate (BnMA) polymer brushes were first prepared using an 18×18 mm ATRP initiator-functionalized silicon wafer, an 18×18 mm cover slip, and 1 mol% PTH to create the expected polymer brush functionalized substrate with a well-defined "edge effect" as depicted in Figure 2a. Subsequent irradiation of the entire substrate (both regions) through a photomask consisting of 20×200 μm transparent rectangles, resulted in patterned P(DMAEMA) brushes across both regions as evidenced by optical microscopy (Figure 2b). Moreover, characterization using atomic force microscopy (AFM) further confirmed patterned polymer brushes on the "edge effect" region (X) (Figure 2c) and on P(BnMA) brush region (Y) (Figure 2d) showing oxygen tolerance and retention of initiating ability in the "edge effect" regions.

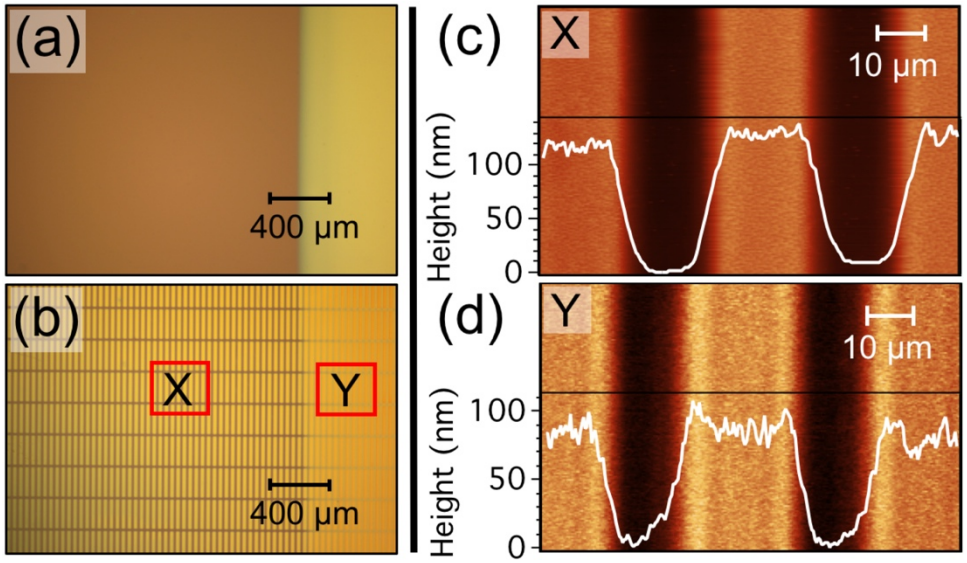

Figure 2. (a) Optical image of initial P(BnMA) brush showing the "edge effect" region (no polymer brush growth - brown region), (b) Growth of P(DMAEMA) using a photomask with transparent 20×200 µm rectangles over full wafer, (c) AFM topography images and height profiles for patterned P(DMAEMA) brushes on the "edge effect" region (X) and, (d) on P(BnMA) region (Y).

From these experiments, we hypothesize that larger cover slips (relative to the size of the wafer) and increased PTH loading allows for enhanced scavenging of the initial dissolved oxygen present in the solutions, as well as any oxygen that subsequently diffuses in from the edges of the cover slip/silicon wafer during polymerization. The relationship between brush growth and irradiation time was then examined using a traditional, multi-wafer approach as well as a single wafer, multiple cover slip strategy. In the first approach, a 1 mol% PTH/DMAEMA mixture was added to multiple 6×6 mm silicon wafers, each wafer covered with 18×18 mm cover slips and was irradiated for different lengths of time. At a PTH catalyst loading of 1 mol%, an inhibition period of 1 hour was observed, followed by a steady increase

in thickness over time resulting in a maximum brush height of approximately 160 nm (6 hours) (Figure S4). This SI-CRP behavior was further confirmed through a novel single wafer kinetic study. In this approach, P(DMAEMA) brush growth kinetics was investigated on a single, 2-inch silicon wafer, by sequentially placing individual drops (~10 μL) of a 5 mol% PTH polymerization mixture together with 0.5-inch diameter circular glass cover slips on the wafer at different time periods after starting irradiation (15, 30, 45, 60, 120, and 180 minutes). Significantly, a reproducible and controlled increase in brush thickness with increasing time is again observed and at this higher PTH loading level, little or no incubation period is observed (Figure S5). These results further illustrate the dual role of PTH, acting initially as an oxygen scavenger, and in the absence of oxygen, functioning as a photoredox polymerization catalyst for SI-CRP.[31]

An enabling feature of this novel strategy is the central role of a transparent cover slip for mediating brush growth. The presence of a cover slip opens up new opportunities for controlling SI-CRP and the resulting brush features. For example, extension of transparent cover slips to photomask allows patterned P(BnMA) brushes with feature resolution down to ~1 μm to be obtained. AFM confirmed the presence of patterned brushes with varied surface topography and corresponding height profiles. (Figure S6). Furthermore, the use of gradient photomasks leads to more unique 3-dimensional polymer brush archtectures. The gradient profile was confirmed through AFM and profilometry demonstrating the expected linear increase in brush height along the length of the structure (Figure S7). The success of these photomodulated experiments prompted a broadening of this cover slip concept to multiple cover slips and arbitrary shapes. Initial studies with mm-sized hexagon-, circle-, star-, diamond-, and triangle-shaped cover slips (5 mol% PTH) allows brushes of P(DMAEMA) to

be prepared with a high degree of fidelity, reproducing the original shape of the glass cover slips (Figure S8). Significantly, this strategy permits multiple cover slips of arbitrary shape to be employed simultaneously on the same silicon wafer. In demonstrating this additional level of control, M-, R-, and L-shaped cover slips were fabricated, and used to control brush growth of P(DMAEMA) from select areas of a 4-inch diameter silicon wafer. As shown in Figure 3a-d, reproduction of the "MRL" cover slips as a polymer brush pattern is achieved by adding monomer droplets to an initiator-functionalized silicon wafer. Placement of the individual M-, R- and L-cover slips then conformally spreads the monomer solution under the cover slips, and brush growth is achieved by irradiation at 405 nm. These results clearly illustrate the ability to spatially control the synthesis of polymer brushes under ambient conditions.

Of equal importance is the ability to prepare these polymer brushes over large surface areas. Uniform coverage of a 4-inch silicon wafer could be achieved using only 200 μL of reaction solution and a 4-inch diameter glass cover slip (~2.5 μL/cm^2). Significantly, optical reflectometry indicates formation of a uniform polymer brush layer (41 nm, Figure S9) which demonstrates the scalability of this approach. The versatility of this platform was also exemplified by the growth of a wide variety of functional polymer brushes. Importantly, the monomer scope is not limited by the solubility of PTH in this system. As shown in Table S2, hydrophobic, hydrophilic, and reactive methacrylate derivatives could be polymerized under ambient conditions, resulting in uniform polymer brush thicknesses (20-60 nm). By measuring the ratio between swollen and dry polymer brush heights of poly(methyl methacrylate) P(MMA), the grafting density was estimated to be 0.28 chains/nm^2 (see Figure S11 for detailed calculations).[37]

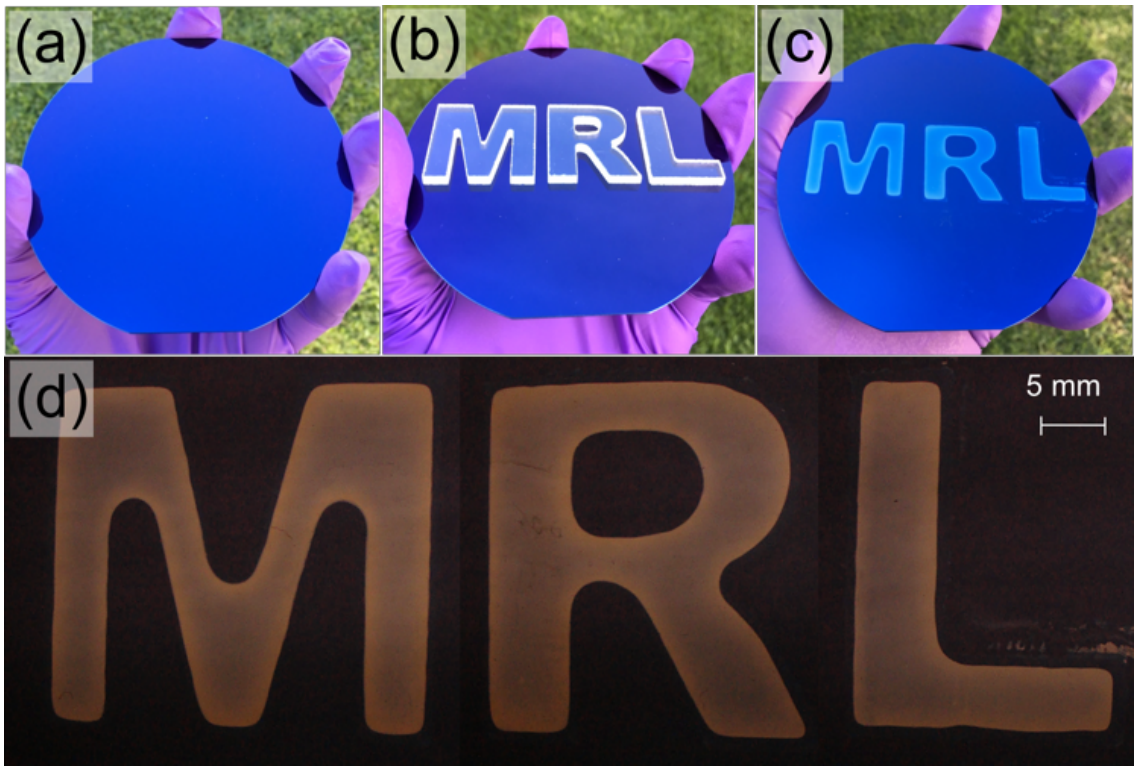

Figure 3. Patterning using glass cover slips of different shape. Digital images showing the preparation of "MRL" brushes on a 4-inch diameter ATRP-initiator functionalized silicon wafer (a) Initiator-functionalized silicon wafer, (b) "MRL" shaped glass cover slips on the wafer prior to brush growth, (c) Resulting polymer brushes after removal of cover slips and extensive washing and (d) Digital micrograph of purified polymer brushes illustrating fidelity with "MRL" shaped cover slips.

The versatility of this platform then opens up the possibility of simultaneously growing multiple polymer brushes from minimal reaction volumes, a critical feature for expensive or synthetically challenging monomers. To demonstrate this advantage, the one-step synthesis of multiple, emissive copolymer brushes from sub-milligram quantities of iridium-based monomers was examined. Taking advantage of a library of Ir-complexes recently developed

in our group,[39] four different monomer solutions (10-15 μL), each containing a distinct Ir-complex (0.5 mol% relative to benzyl methacrylate), were placed on a functionalized 2-inch silicon wafer and covered with four individual cover slips. Irradiation at 405 nm for 2 hours, followed by extensive washing, led to four well-defined features composed of different photoluminescent polymer brushes with colors (orange, blue, green and red) spanning the visible spectrum (λ_{ex} = 254 nm) (Figure 4). It should be noted that the combined mass of Ir-complexes used, less than 1.0 mg, is sufficient for the synthesis of ~cm^2 areas of functional polymer brushes with the phosphorescent properties of the emitting chains being defined by the different Ir-comonomers used. This ability to simultaneously perform multiple polymerizations on the same wafer using minimal amounts of functional building blocks highlights a major advantage of this strategy.

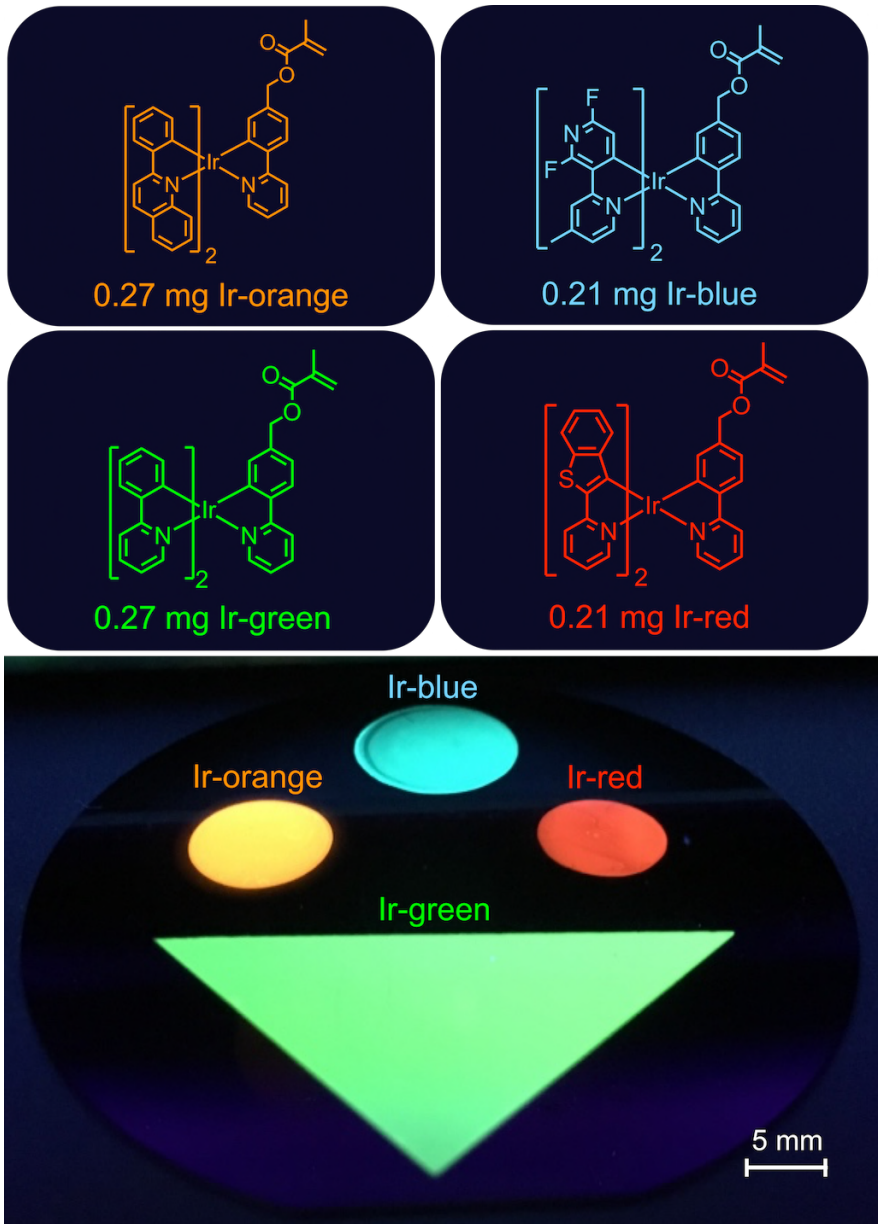

Figure 4. Chemical structures of the different monomeric Ir-complexes used for copolymer brushes formation (top), Fluorescence image (254 nm UV excitation) of the four copolymer brushes P(BnMA-*co*-Ir-complex). Brushes were simultaneously prepared under ambient conditions on a 2-inch ATRP initiator-functionalized silicon wafer using individual cover slips (bottom).

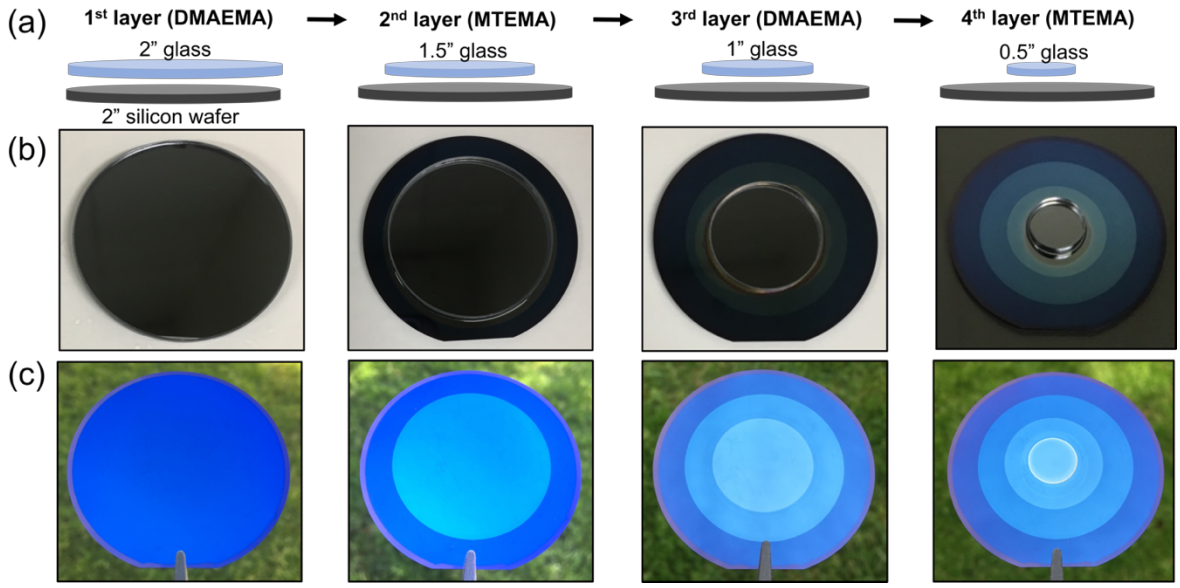

Figure 5. Sequential polymerization of DMAEMA-MTEMA-DMAEMA-MTEMA under ambient conditions (a) Graphical representation of the stepwise synthesis, (b) Corresponding digital images of the polymerization process, (c) Digital images of polymer brushes on a 2-inch ATRP initiator-functionalized silicon wafer during stepwise brush growth.

The controlled nature of this polymerization process was then examined through a step-wise sequence of growth-washing-reinitiation steps using progressively smaller cover slips and different monomers. This is illustrated in Figure 5, where DMAEMA (5 mol% PTH) was initially polymerized from a 2-inch diameter wafer using a 2-inch diameter circular glass cover slip followed by extensive washing to give a homogeneous P(DMAEMA) brush. Addition of a droplet of 2-(methylthio)ethyl methacrylate (MTEMA) (~30 μL, 5 mol% PTH) followed by placement of a 1.5-inch diameter cover slip then leads to growth of a second P(MTEMA) layer after irradiation at 405 nm. This sequence was then repeated using DMAEMA (1.0-inch diameter cover slip) and MTEMA (0.5-inch diameter cover slip) to give a novel, 3-dimensionally patterned polymer brush. As shown in Figure 5c, the size and shape

of the different cover slips is reproduced with a high degree of fidelity. This sequential growth could also be monitored by optical reflectometry and profilometry, which confirms the step-wise increase in brush thickness, while x-ray photoelectron spectroscopy (XPS) and secondary ion mass spectrometry (SIMS) shows the expected order of monomer incorporation (Figure S15-19) with the change in monomer functionality being clearly identified through the presence/absence of the N1s signal for DMAEMA and the S2s and S2p signals for MTEMA in XPS (Figure S15, 18-19). Significantly, other monomer sequences such as DMAEMA-BnMA-DMAEMA-BnMA or combination of shapes (square-circle) could also be realized, with the thickness of each layer being controlled by the irradiation time (Figures S16-18). This merger of efficient reinitiation with simple cover slip patterning clearly illustrates the retention of active bromine chain ends and opens up the design space available to this strategy.

3.4 Conclusion

In summary, this work demonstrates the simplicity of using metal-free ATRP (PTH acting as both an oxygen scavenger as well as a polymerization catalyst) in combination with transparent cover slips for the synthesis of complex and arbitrary 3-dimensional polymer brush structures. Key advantages include minimal reaction volumes, applicability to large area substrates and ambient conditions. In addition, the use of visible light and multiple cover slips of arbitrary shape allows isolated and spatially defined functional polymer brushes to be concurrently prepared on the same wafer. This straightforward and versatile synthetic platform will allow non-experts access to polymer brush architectures that are difficult to achieve using other techniques.

3.5 Supporting Information

General Reagent Information. All polymerizations were carried out in the presence of air. Silicon substrates with a 100 nm oxide layer were purchased from WaferPro and UniversityWafer, Inc. Photomasks containing transparent rectangles (20×200 μm) and polygons were obtained from Photronics, Inc. A HEBS5N grayscale photomask was purchased from Canyon Materials, Inc. containing squares of varying optical density and prisms of variable slope. 18×18 mm glass cover slips were purchased from VWR International. Circular glass cover slips were purchased from McMaster-Carr. Custom glass cover slips were cut out of a larger piece of glass using a diamond pen. The 405 nm collimated LED (3 mW•cm^{-2}, Olympus BX&1X, 1000 mA) and plano-convex lens (Ø50.8 mm, f = 60.0 mm, AR Coating: 350-700 nm) were purchased from Thorlabs Inc. 2-(methylthio)ethyl methacrylate (MTEMA) (96%), benzyl methacrylate (BnMA) (96%), 2-hydroxyethyl methacrylate (97%), furfuryl methacrylate (97%), and poly(ethylene)glycol methyl ether methacrylate, Mn 300 were purchased from Sigma-Aldrich. 2-(dimethylamino)ethyl methacrylate (DMAEMA) (99%) was purchased from Fisher Scientific. Dodecyl methacrylate (>97%), glycidyl methacrylate (>95%), tert-butyl methacrylate (98%), and 10-undecen-1-ol (98%) were purchased from TCI America. Methyl methacrylate (99%) was purchased from Alfa Aesar. All monomers were passed through a plug of basic alumina to remove inhibitor prior to use. *N,N*-dimethylacetamide (DMA, 99.9%) was purchased from Chem-Impex International. Phenothiazine (≥98%), RuPhos (95%), sodium tert-butoxide (NaOtBu) (97%), dioxane (anhydrous, 99.8%), chlorobenzene (anhydrous, 99.8%), 2-bromoisobutyryl bromide (98%), trichlorosilane (99%), Karstedt's catalyst (Pt ~2% in xylene), RuPhos Pd G1 methyl t-butyl ether adduct (95%), triethylamine (anhydrous,

≥99.5%), 2-ethoxyethanol (99%), 1,2-dimethoxyethane (DME) (99.5%, anhydrous), sodium borohydride (NaBH4) (99%), ethyl ∝-bromoisobutyrate (98%) and methacryloyl chloride (97%) were purchased from Sigma-Aldrich and used as received. 2,6-difluoropyridine-3-boronic acid (96%), 2-chloro-4-methylpyridine (96%), and 2-(4-formylphenyl)pyridine (97%) were purchased from Combi-Blocks. Iridium(III) chloride hydrate (99.9%-Ir) and *trans*-dichlorobis(triphenylphosphine)palladium(II) (99.9+%-Pd) were purchased from STREM Chemicals, Inc. Silver trifluoromethanesulfonate (99%) was purchased from Acros Organics. Magnesium sulfate (anhydrous), pyridine, ethyl acetate, hexane, acetone, dichloromethane (CH_2Cl_2), tetrahydrofuran, toluene and isopropanol were purchased from Fisher Scientific. Hydrochloric acid was purchased from EMD Millipore Corporation. Ethanol (200 proof) was purchased from Gold Shield. Dry toluene was obtained from a Pure Solv Innovative Technology, Inc. solvent purification system. Ir-orange, Ir-red and Ir-green were synthesized according to literature procedures.[39]

General Analytical Information. Nuclear magnetic resonance spectra were recorded on a Varian 400, 500 or 600 MHz spectrometer. Chemical ionization/Field desorption mass spectrometry were performed on a Waters GCT Premier time-of-flight mass spectrometer. Electrospray ionization mass spectrometry was performed on a Waters Xevo G2-XS time-of-flight mass spectrometer. Gas chromatography-mass spectrometry was performed on an Agilent 7890A equipped with a Waters GCT Premier time-of-flight mass spectrometer. Infrared spectra were recorded on a Thermo Nicolet iS10 FTIR Spectrometer. Size exclusion chromatography (SEC) was performed on a Waters Acquity Advanced Polymer Characterization (APC) equipped with Acquity UPLC refractive index detector eluting with 0.25% trimethylamine in chloroform and calibrated relative to polystyrene standards.

Filmetrics F20 optical reflectometer was used to measure polymer brush thickness. Keyence VHX-5000 microscope was used to image polymer brushes on silicon wafers. Optical micrographs were captured with a Nikon Elipse E600 optical microscope to identify patterned and gradient polymer brushes. Tapping mode atomic force microscopy (AFM) experiments were performed using a MFP-3D system (Asylum Research, Santa Barbara, CA) to identify patterned polymer brushes and determine brush thicknesses. The measurements were conducted using commercial Si cantilevers. 3D profiles were obtained on a KLA-Tencor P17 stylus profilometer (Profiler software v8.0) equipped with a 2 μm radius diamond tip and 60 degree cone angle. The 3D images were post-processed and analyzed using Scanning Probe Image Processor (SPIP v6.6.3, Image Metrology, Denmark). X-ray photoelectron spectroscopy (XPS) was performed using a Kratos Axis Ultra Spectrometer (Kratos Analytical, Manchester, UK) with a monochromatic aluminum K_∞ X-ray source (1486.6 eV) operating at 225 W under a vacuum of 10-8 Torr and spectra were analyzed using CasaXPS software. Secondary ion mass spectrometry (SIMS) imaging was performed using a Camera IMS 7f system (Camera SAS, Gennevilliers, France). A 10 kV Cs^+ ion beam and 5 kV negative sample potential were used, for a total impact energy of 15 kV.

Irradiation Setup for Large Scale Brush Growth

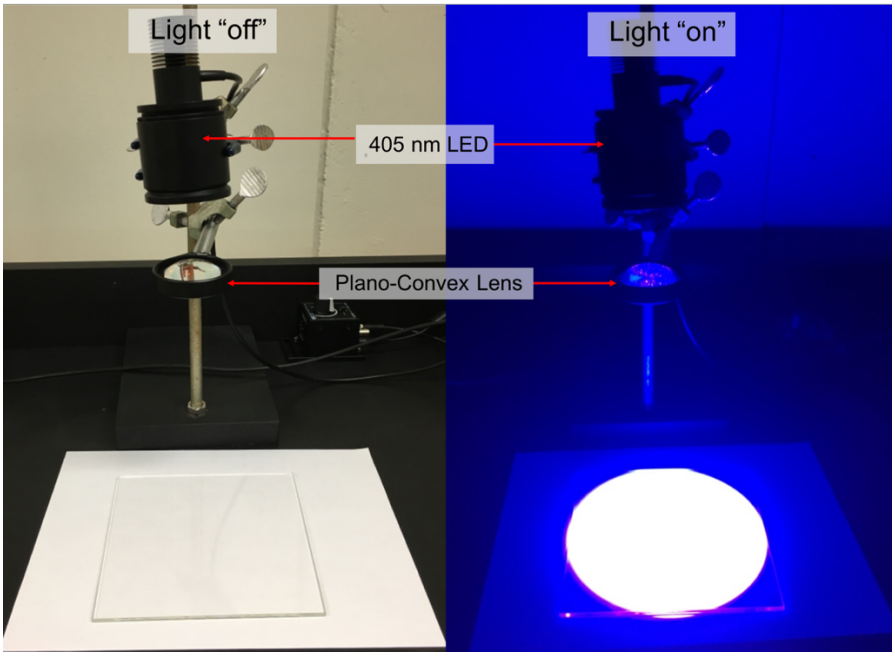

Figure S1. Images showing the setup used for 4-inch and 2-inch wafer grafting. A Plano-convex lens was used to expand the 405 nm LED light to cover a larger area.

Synthesis of *N*-phenylphenothiazine

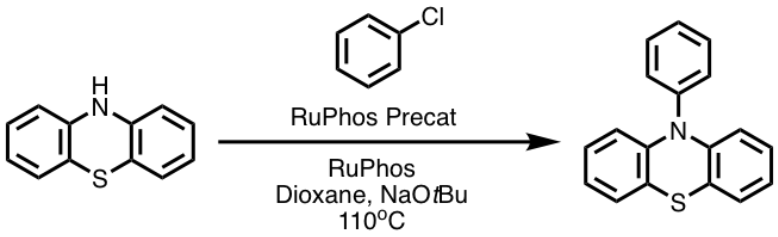

Scheme S1. Synthetic route to *N*-phenylphenothiazine.

To a 2-neck, 100 mL round-bottom flask equipped with a magnetic stir bar, inlet adapter, condenser and septum was added NaO*t*Bu (1.34 g, 14.0 mmol), phenothiazine (1.99 g, 9.99 mmol), RuPhos Precat (140 mg, 0.17 mmol, 1.7 mol%), and RuPhos (80 mg, 0.17 mmol, 1.7 mol%). The flask was evacuated and backfilled with argon 3x before adding dioxane (10 mL, anhydrous) and chlorobenzence (anhydrous) (1.43 mL, 14.1 mmol), followed by heating to 110 °C for 5 hours. The flask was then cooled to room temperature, diluted with CH_2Cl_2, washed with water and brine, dried with Mg_2SO_4, and run through a silica plug with 95:5 Hex:EtOAc. The product was dried under reduced pressure to yield 2.74 g of a light yellow solid (>95% yield). ^{1}H NMR (400 MHz, $CDCl_3$) δ 7.61 (t, *J* = 7.7 Hz, 2H), 7.48 (t, *J* = 7.4 Hz, 1H), 7.40 (d, *J* = 7.5 Hz, 2H), 7.03 (d, *J* = 8.9 Hz, 2H), 6.90 – 6.76 (m, 4H), 6.21 (d, *J* = 9.2 Hz, 2H). ^{13}C NMR (101 MHz, $CDCl_3$) δ 144.37, 141.08, 130.97, 130.86, 128.31, 126.94, 126.83, 122.57, 120.25, 116.14. IR (ATR) ν 3058, 2922, 2849, 1584, 1568, 1489, 1458, 1441, 1297, 1254, 1236, 1166, 1125,1080, 1070, 1042, 1022, 1003, 969, 935, 898, 853, 739, 714, 703, 692, 630, 617 cm^{-1}. LRMS (EI+) calculated for $[M]^+$ $C_{18}H_{13}NS$: 275.08, found: 275.08.

Uniform Alkyl Bromide (ATRP-Initiator) Functionalization of Silicon Surfaces

Undec-10-en-1-yl 2-bromo-2-methylpropanoate:

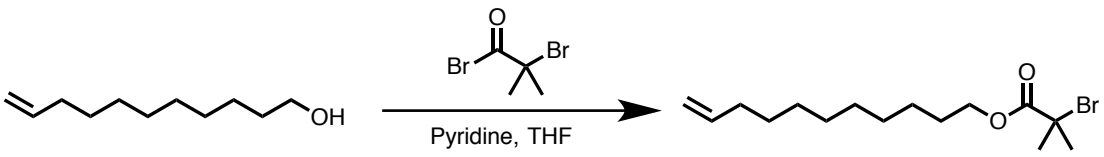

Scheme S2. Synthetic route to ATRP initiator precursor.

A 250 mL Schlenk flask equipped with a magnetic stir bar and a rubber septum, was evacuated and backfilled with argon. Then, undec-10-enol (3.3 mL, 16.5 mmol), pyridine (1.6 mL, 19.8 mmol), and tetrahydrofuran (75 mL) were added to the Schlenk flask, followed by cooling the flask in an ice bath and adding 2-bromoisobutyryl bromide (2.2 mL, 18.1 mmol) dropwise over 10 minutes. The solution was stirred overnight at room temperature, then diluted with hexane, washed with 1 N $HCl_{(aq)}$, dried with $MgSO_4$ (anhydrous), and concentrated in vacuo. The crude product was purified using column chromatography on silica gel with 25:1 Hex:EtOAc to yield 3.37 g of a colorless oil (64% yield). ^{1}H NMR (600 MHz, $CDCl_3$) δ 5.85 - 5.73 (m, 1H), 5.04 – 4.84 (m, 2H), 4.15 (t, J = 6.7 Hz, 2H), 2.02 (q, J = 6.9 Hz, 2H), 1.91 (s, 6H), 1.70 – 1.61 (m, 2H), 1.40 – 1.23 (m, 12H). ^{13}C NMR (101 MHz, $CDCl_3$) δ 171.47, 138.91, 113.93, 65.90, 55.72, 33.58, 30.56, 29.20, 29.15, 28.93, 28.86, 28.69, 28.12, 25.56. IR (ATR) ν 2925, 2854, 2360, 1734, 1641, 1463, 1389, 1371, 1273, 1160, 1108, 1010, 992, 909, 763, 722, 644 cm^{-1}.

11-(Trichlorosilyl)undecyl 2-bromo-2-methylpropanoate:

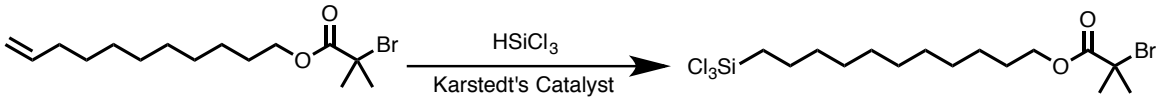

Scheme S3. Synthetic route to 11-(trichlorosilyl)undecyl 2-bromo-2-methylpropanoate.

A 50 mL Schlenk flask equipped with a magnetic stir bar and a rubber septum, was evacuated and backfilled with argon and charged with undec-10-en-1-yl-2-bromo-2-methylpropanoate (1.35 g, 4.2 mmol), trichlorosilane (4.2 mL, 41.6 mmol) and a solution of

Karstedt's catalyst in xylene (5 μL, 2 wt% Pt in xylene). The solution was stirred at room temperature for 4 hours. The reaction mixture was then concentrated under reduced pressure to yield 1.51 g of a clear oil (79% yield). The compound was used without further purification. ^{1}H NMR (400 MHz, $CDCl_3$) δ 4.16 (t, J = 6.6 Hz, 2H), 1.93 (s, 6H), 1.72 – 1.62 (m, 2H), 1.61 – 1.52 (m, 2H), 1.46 – 1.21 (m, 16H). ^{13}C NMR (101 MHz, $CDCl_3$) δ 171.57, 65.97, 55.83, 31.63, 30.61, 29.28, 29.24, 29.12, 28.97, 28.82, 28.16, 25.60, 24.12, 22.07. IR (ATR) ν 3005, 2926, 2855, 1734, 1463, 1389, 1371, 1274, 1160, 1108, 1011, 969, 917, 829, 764, 722, 691, 645, 560 cm^{-1}. GCMS (EI+) calculated for [M]+ $C_{15}H_{28}BrCl_3O_2Si$: 454.01, found: 454.01.

SiO_2 Surface Functionalization:

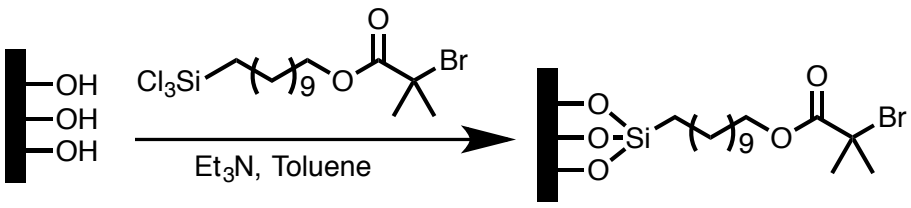

Scheme S4. ATRP-initiator functionalization on silicon wafer.

Silicon substrates were cleaned by sonication in acetone, followed by isopropanol for 10 minutes each and dried under a stream of nitrogen. Silicon substrates were placed in an air plasma cleaner (PDC-001, Harrick Plasma) for 15 minutes. A stock solution was then prepared by mixing 250 μL of 11-(trichlorosilyl)undecyl 2-bromo-2-methylpropanoate in 500 mL of dry toluene (0.05% v/v) and 100 μL of dry triethylamine. 2-inch diameter silicon wafers were placed in 3.5-inch diameter petri dishes and covered with 40 mL of stock solution under

nitrogen gas, while 4-inch diameter silicon wafers were placed in 5.5-inch diameter petri dishes and covered with 150 mL of stock solution under nitrogen gas. The reaction was left overnight at room temperature, and then cleaned with toluene then ethanol, and dried under a stream of nitrogen gas.

Synthesis of Ir-blue:

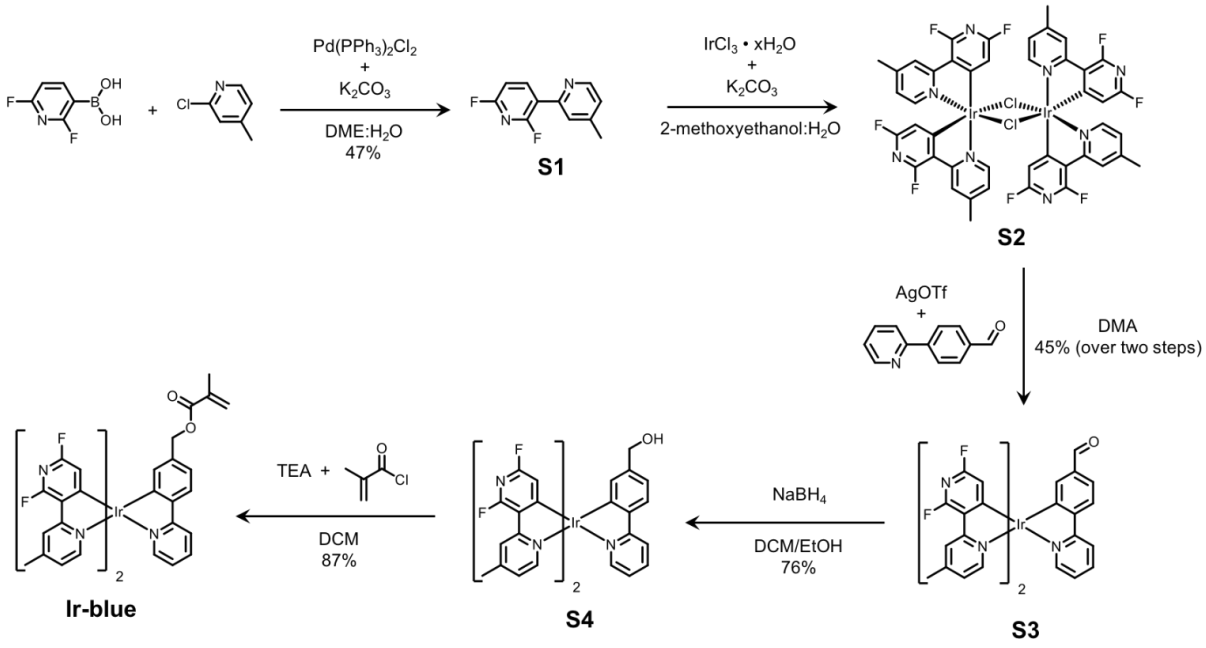

Scheme S5. General five step synthetic procedure to Ir-blue.

2',6'-difluoro-4-methyl-2,3'-bipyridine (S1):

To a 2-neck, 250 mL round-bottom flask equipped with a Vigreux column, inlet adapter, magnetic stir bar and septum was added 2,6-difluoropyridine-3-boronic acid (4.50 g, 28.3 mmol), 2-chloro-4-methylpyridine (4.34 g, 34.0 mmol), bis(triphenylphosphine)palladium(II) dichloride (0.20 g, 0.3 mmol), potassium carbonate (10.96 g, 79.3 mmol), DME (85 mL), and H_2O (40 mL). The mixture was degassed with argon for 10 minutes, heated to 80 °C, stirred

for 6 hours, cooled to room temperature, extracted with EtOAc, dried with $MgSO_4$ (anhydrous), filtered and concentrated under reduced pressure. The crude product was purified by column chromatography on silica gel, eluting with a gradient from 95:5 to 80:20 Hex:EtOAc. The solvent was removed by rotary evaporation to obtain 2.76 g (47% yield) of the desired product, **S1**, as a white fluffy crystalline solid. ^{1}H NMR (400 MHz, CD_2Cl_2) δ 8.66 (dt, *J* = 9.6, 8.1 Hz, 1H), 8.54 (d, *J* = 5.0 Hz, 1H), 7.66 (s, 1H), 7.14 (d, *J* = 5.0 Hz, 1H), 6.97 (dd, *J* = 8.2, 3.0 Hz, 1H), 2.42 (s, 3H). ^{13}C NMR (101 MHz, CD_2Cl_2) δ 162.75, 162.61, 160.29, 160.14, 159.99, 157.67, 157.53, 150.77, 150.71, 150.07, 148.77, 146.84, 146.80, 146.76, 146.72, 125.21, 125.11, 124.58, 120.02, 119.96, 119.78, 119.73, 107.49, 107.43, 107.15, 107.09, 21.50. ^{19}F NMR (376 MHz, CD_2Cl_2) δ -69.69, -70.29. IR (ATR) ν 3041, 1604, 1588, 1482, 1459, 1415, 1392, 1303, 1294, 1265, 1208, 1192, 1127, 1116, 1054, 990, 893, 854, 842, 819, 764, 731, 668, 628, 585, 562, 552 cm^{-1}. LRMS (ESI) calculated for $[M+H]^+$ $C_{11}H_9F_2N_2$: 207.07, found: 207.09.

Dichlorotetrakis[2-(2',6'-difluoro-4-methyl-2,3'-bipyridine)]diiridium(III) (S2):

To a 2-neck, 100 mL round-bottom flask equipped with a magnetic stir bar, inlet adapter, condenser and septum was added iridium(III) chloride hydrate (1.00 g, 3.16 mmol), **S1** (1.43 g, 6.95 mmol), 2-ethoxyethanol (24 mL), and H_2O (8 mL). The mixture was degassed with argon for 10 minutes and heated to 120 °C for 16 hours. The reaction was cooled to room temperature, H_2O (30 mL) was added and the precipitate was filtered, washed with H_2O then MeOH, then dried under reduced pressure to obtain 1.78 g of a green-yellow solid, **S2**. Due to poor solubility, the compound was used directly for the next reaction.

Bis[[2-(2',6'-difluoro-4-methyl-2,3'-bipyridine)]4-(pyridin-2-yl)benzaldehyde]-iridium(III) (S3):

To a 2-neck, 100 mL round-bottom flask equipped with a magnetic stir bar, inlet adapter, condenser and septum was added **S2** (1.00 g, 0.78 mmol), silver triflate (1.01 g, 3.92 mmol), and dimethylacetamide (15 mL, anhydrous). The mixture was degassed with argon for 10 minutes, heated to 100°C for 30 minutes, followed by the addition of 4-(2-pyridyl)benzaldehyde (0.36 g, 1.96 mmol) under a stream of argon. The reaction was then heated to 130 °C for 5 hours, cooled to room temperature, filtered, and washed with acetonitrile to remove silver salts. The filtrate was added to deionized H_2O and the resulting precipitate was filtered, then dissolved in CH_2Cl_2 and washed with deionized H_2O. The organic layer was dried over $MgSO_4$ (anhydrous), filtered and concentrated under reduced pressure to yield a light yellow solid. The crude product was purified by column chromatography on silica gel, eluting with a gradient starting at 7:3 CH_2Cl_2:Hex and ending with CH_2Cl_2. The solvent was removed by rotary evaporation and the resulting solid was precipitated from CH_2Cl_2 into hot hexanes to provide the desired product, **S3**, after filtration as a light yellow solid (0.59 g, 45% yield over two steps). ^{1}H NMR (400 MHz, DMSO-d_6) δ 9.77 (s, 1H), 8.43 (d, J = 8.2 Hz, 1H), 8.18 (d, J = 8.1 Hz, 1H), 8.09 – 7.93 (m, 3H), 7.87 (d, J = 5.5 Hz, 1H), 7.79 (d, J = 6.0 Hz, 1H), 7.51 (d, J = 8.0 Hz, 1H), 7.47 (d, J = 6.0 Hz, 1H), 7.33 (t, J = 6.4 Hz, 1H), 7.16 (s, 1H), 7.02 (d, J = 5.7 Hz, 2H), 5.95 (s, 1H), 5.75 (s, 1H), 2.43 (s, 6H). ^{13}C NMR (101 MHz, DMSO-d_6) δ 198.52, 194.01, 181.52, 170.91, 164.87, 162.73, 162.63, 162.06, 161.93, 161.63, 161.48, 160.34, 160.23, 159.54, 159.41, 159.16, 159.01, 158.82, 158.70, 158.33, 158.16, 156.28, 156.14, 155.83, 155.66, 152.02, 151.19, 151.02, 150.60, 149.26, 147.92, 139.06, 136.37, 136.12, 125.50, 125.27, 125.03, 124.61, 124.07, 123.89, 123.49, 123.32, 121.74, 108.52, 108.25, 106.69, 106.40, 20.88, 20.77. ^{19}F NMR (376

MHz, DMSO-d_6) δ -69.50 (d, J = 8.6 Hz), -70.40 (d, J = 9.6 Hz), -72.95 (d, J = 6.6 Hz), -73.51 (d, J = 9.6 Hz). IR (ATR) ν 2818, 1686, 1617, 1589, 1525, 1472, 1432, 1401, 1382, 1358, 1311, 1265, 1194, 1134, 1064, 1051, 1005, 890, 875, 862, 838, 822, 812, 784, 752, 737, 694, 629, 610, 586, 574, 562 cm^{-1}. LRMS (FD+) calculated for $C_{34}H_{22}F_4IrN_5O$: 785.14, found: 785.14.

Bis[[2-(2',6'-difluoro-4-methyl-2,3'-bipyridine)](4-(pyridin-2-yl)phenyl (S4):

To a 1-neck 250 mL round-bottom flask equipped with a magnetic stir bar and septum was added **S3** (450 mg, 0.57 mmol), CH_2Cl_2 (40 mL) and EtOH (40 mL), degassed with argon for 10 minutes, followed by the addition of $NaBH_4$ (43 mg, 1.15 mmol). The mixture was stirred for 12 hours at room temperature. The solvent was removed under reduced pressure and the resulting yellow solid was re-dissolved in CH_2Cl_2 and washed with deionized H_2O. The organic layer was dried over $MgSO_4$ (anhydrous), filtered and concentrated under reduced pressure to yield a yellow solid. The crude product was further purified by flash column chromatography on silica gel, eluting with CH_2Cl_2. The solvent was removed by rotary evaporation and the resulting solid was precipitated from CH_2Cl_2 into hot hexanes to provide the desired product, **S4**, after filtration as a light yellow solid (342 mg, 76% yield). ^{1}H NMR (400 MHz, DMSO-d_6) δ 8.23 (d, J = 8.2 Hz, 1H), 8.01 (d, J = 14.1 Hz, 2H), 7.95 – 7.82 (m, 3H), 7.76 (d, J = 5.1 Hz, 1H), 7.47 (d, J = 6.0 Hz, 1H), 7.18 (t, J = 6.4 Hz, 1H), 7.03 (t, J = 6.8 Hz, 2H), 6.97 (d, J = 7.9 Hz, 1H), 6.61 (s, 1H), 5.94 (s, 1H), 5.71 (s, 1H), 4.95 (t, J = 5.7 Hz, 1H), 4.34 – 4.15 (m, 2H), 2.44 (s, 6H). ^{13}C NMR (101 MHz, DMSO-d_6) δ 199.93, 182.52, 170.51, 166.54, 162.87, 162.76, 162.09, 161.96, 161.58, 161.44, 160.51, 160.40, 159.57, 159.44, 159.13, 158.97, 158.83, 158.69, 158.28, 158.12, 156.28, 156.14, 155.78, 155.61,

151.90, 150.38, 148.87, 147.81, 143.94, 143.45, 138.63, 133.89, 125.24, 124.90, 124.83, 124.69, 124.53, 123.95, 123.77, 123.71, 123.34, 123.18, 121.27, 120.05, 108.46, 108.22, 106.52, 106.26, 63.24, 20.87, 20.77. ^{19}F NMR (376 MHz, DMSO-d_6) δ -69.69 (d, J = 8.6 Hz), -70.80 (d, J = 9.8 Hz), -73.22 (d, J = 6.6 Hz), -74.00 (d, J = 9.7 Hz). IR (ATR) ν 3431, 2862, 1585, 1524, 1472, 1430, 1403, 1381, 1280, 1263, 1196, 1166, 1134, 1044, 1006, 876, 856, 837, 811, 778, 753, 735, 637, 584 cm^{-1}. LRMS (FD+) calculated for $C_{34}H_{24}F_4IrN_5O$: 787.15, found: 787.16.

Bis[[2-(2',6'-difluoro-4-methyl-2,3'-bipyridine)](4-(pyridin-2-yl)phenyl)oxymethylmethacrylate]-iridium(III) (Ir-blue):

To a dry 6 mL Schlenk tube equipped with a magnetic stir bar and septum was added **S4** (200 mg, 0.25 mmol), CH_2Cl_2 (4 mL, anhydrous) and trimethylamine (177 μL, 1.27 mmol). The mixture was degassed with argon for 10 minutes and cooled to 0 °C, followed by addition of methacryloyl chloride (49 μL, 0.51 mmol) using a syringe. The reaction mixture was stirred at 0 °C for 10 minutes under argon then allowed to warm to room temperature and stirred for an additional hour. The reaction mixture was concentrated and added to a silica gel column, wet packed with 70:29:1 Hex:CH_2Cl_2:TEA. The product was eluted with a gradient starting at 1:1 and ending at 0:1 Hex:CH_2Cl_2, concentrated under reduced pressure then precipitated from CH_2Cl_2 into hot hexanes to provide the desired product, **Ir-blue**, after filtration as a light yellow powder (189 mg, 87% yield). ^{1}H NMR (400 MHz, CD_2Cl_2) δ 8.05 (d, J = 12.0 Hz, 2H), 7.99 (d, J = 8.2 Hz, 1H), 7.90 (d, J = 5.9 Hz, 1H), 7.85 (d, J = 5.4 Hz, 1H), 7.77 (t, J = 8.4 Hz, 2H), 7.44 (d, J = 5.9 Hz, 1H), 7.00 (t, J = 6.7 Hz, 2H), 6.83 (s, 1H), 6.78 – 6.67 (m, 2H), 6.06 (s, 1H), 6.00 (s, 1H), 5.79 (s, 1H), 5.57 (s, 1H), 5.04 (s, 2H), 2.46 (s, 6H), 1.89 (s, 3H). ^{13}C NMR (101 MHz, CD_2Cl_2) δ 199.69, 181.80, 181.75, 172.58, 167.75, 167.45, 164.62,

164.51, 163.48, 163.35, 163.02, 162.86, 162.43, 162.33, 160.95, 160.82, 160.55, 160.39, 160.12, 159.98, 159.67, 159.50, 157.57, 157.43, 157.17, 156.99, 153.05, 151.28, 150.30, 149.04, 148.05, 145.05, 138.69, 138.31, 136.93, 135.51, 125.78, 125.17, 124.97, 124.73, 124.55, 124.40, 124.30, 124.13, 123.60, 121.80, 120.39, 109.54, 109.50, 109.28, 109.24, 107.53, 107.48, 107.24, 107.20, 66.67, 21.69, 21.62, 18.55. ^{19}F NMR (376 MHz, CD_2Cl_2) δ -70.21 (d, J = 8.9 Hz), -71.11 (d, J = 9.7 Hz), -74.01 (d, J = 9.0 Hz), -74.60 (d, J = 9.8 Hz). IR (ATR) ν 3068, 2952, 1714, 1588, 1525, 1473, 1432, 1404, 1381, 1312, 1280, 1263, 1195, 1147, 1134, 1050, 999, 966, 940, 904, 876, 842, 829, 809, 782, 750, 741, 675, 647, 586, 558, 535 cm^{-1}. LRMS (FD+) calculated for $C_{38}H_{28}F_4IrN_5O_2$: 855.18, found: 855.19.

Synthesis of Polymer Brushes using Different Light Sources

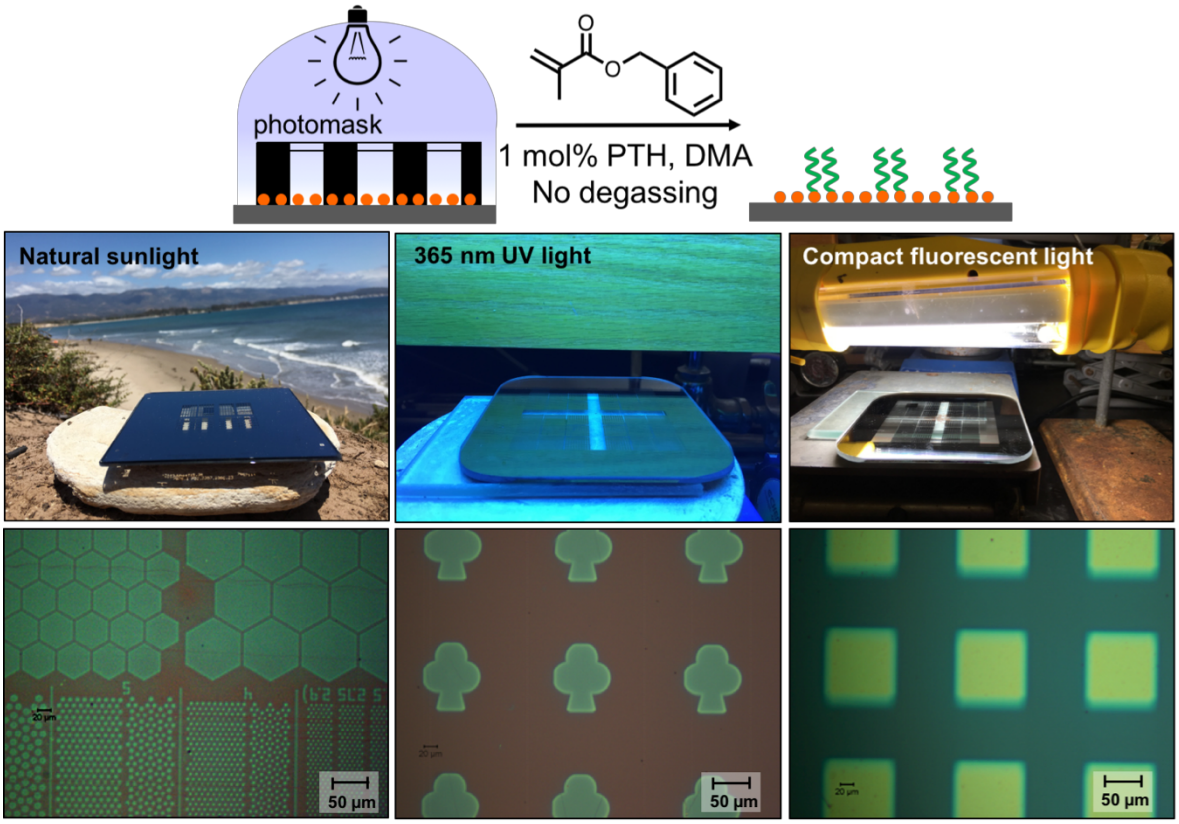

Figure S2. P(BnMA) brushes grafted from ATRP initiator-functionalized silicon wafers through various photomasks using different light sources: natural sunlight, 365 nm UV light, and compact fluorescent light. The corresponding optical reflectance micrographs of the patterned brushes are provided below.

An ATRP initiator-functionalized silicon substrate was placed on top of a glass plate. A solution containing *N*-phenylphenothiazine (PTH) (3.25 mg, 11.8 µmol, 1 mol%), benzyl methacrylate (BnMA) (200 µL, 1.18 mmol) and 50 µL *N,N*-dimethylacetamide (DMA) was pipetted onto the silicon substrate directly until it was completely covered without any deoxygenation. Then, a photomask was placed on top of the solution to form a thin layer in

contact with the substrate. The wafer was placed under natural sunlight for 20 minutes. To show the versatility of this system, different light sources, including 365 nm UV light (90 minutes) and compact fluorescent light (13.5 hours) were used to grow patterned polymer brushes. After irradiation, the samples were cleaned using Soxhlet extraction with CH_2Cl_2 for 24 hours and then dried under a stream of nitrogen. Optical microscopy indicated the successful formation of patterned polymer brushes using the different light sources.

Study of Buffer Region and Catalyst Loading

ATRP initiator-functionalized wafers were cut into 7×7 mm, 10×10 mm, 14×14 mm, and 18×18 mm pieces. The wafer was placed on top of a glass plate. A solution containing 0.5 mol% PTH was prepared by mixing PTH (1.63 mg, 5.93 μmol), 2-(dimethylamino)ethyl methacrylate (DMAEMA) (200 μL, 1.19 mmol), and 51.5 μL DMA in a vial. The reaction solution was pipetted onto the silicon substrate directly without any deoxygenation, followed by placing an 18×18 mm glass cover slip on top of the solution to form a thin layer in contact with the substrate, while also filling the space underneath the glass cover slip. The wafer was placed below a 405 nm collimated LED for 4.5 hours in the presence of air. To prepare the 1 and 5 mol% PTH solutions, the synthetic procedure for 0.5 mol% PTH was followed, changing only the PTH quantities to 3.26 mg (11.9 μmol) and 16.3 mg (59.3 μmol), respectively. After irradiation, the substrates were cleaned using Soxhlet extraction with CH_2Cl_2 for 24 hours and then dried under a stream of nitrogen. Polymer brushes were observed by eye on the silicon wafers and brush heights were determined inside polymer brush regions using optical reflectometry.

Table S1. Film thickness of P(DMAEMA) brushes determined using optical reflectometry after varying the wafer size and catalyst loading

PTH loading (mol%)	Polymer brush height (nm)			
	Silicon wafer size			
	7×7 mm	10×10 mm	14×14 mm	18×18 mm
0.5	67	78	76	68
1	82	92	85	86
5	52	49	44	58

Synthesis of Patterned Polymer Brushes in the "Edge Effect" Region

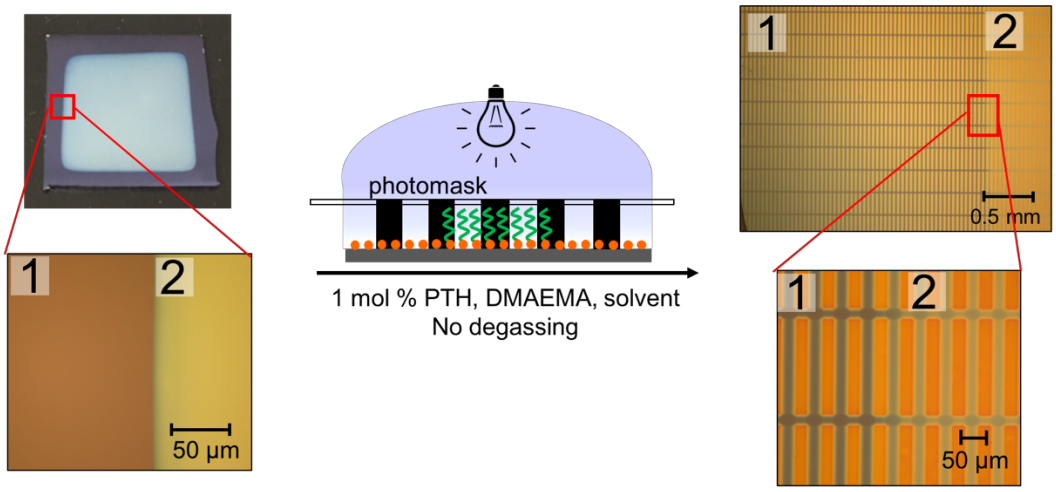

Figure S3. Synthesis of patterned polymer brushes in the "edge effect" region supports retention of ATRP initiator functionality.

An 18×18 mm ATRP initiator-functionalized silicon substrate was placed on top of a glass plate. A homogenous reaction solution was prepared by mixing PTH (3.25 mg, 11.8 µmol, 1

mol%), BnMA (200 μL, 1.18 mmol), and 50 μL DMA in a vial, followed by pipetting onto the silicon substrate directly without any deoxygenation. Then, an 18×18 mm glass cover slip was placed on top of the solution to form a thin layer in contact with the substrate. The wafer was placed below a 405 nm collimated LED for 2 hours in the presence of air. The substrate was rinsed with CH_2Cl_2 and then dried under a stream of nitrogen. The film thickness was measured to be 57 nm with optical reflectometry. An "edge effect" was observed on the wafer as shown in Figure S3.3. Subsequently, a new homogenous reaction solution containing PTH (3.26 mg, 11.9 μmol, 1 mol%), DMAEMA (200 μL, 1.19 mmol) and 51.5 μL DMA was prepared and pipetted onto the P(BnMA) brush functionalized substrate. Then, a photomask containing 20×200 μm transparent rectangle was placed on top of the solution to form a thin layer in contact with the substrate. It should be noted that the photomask is larger than the wafer to prevent the "edge effect". The wafer was placed below a 405 nm collimated LED for 15 hours in the presence of air. The substrate was cleaned using Soxhlet extraction with CH_2Cl_2 for 24 hours and then dried under a stream of nitrogen. The patterned polymer brushes were clearly visible by optical microscopy on the entire wafer, both on the "edge effect" region (1) and on P(BnMA) (2). AFM was used to image surface topography showing the height profile of patterned P(DMAEMA) brushes on the "edge effect" region and on P(BnMA) brushes.

Kinetic Study of P(DMAEMA) Brushes (1 mol% PTH)

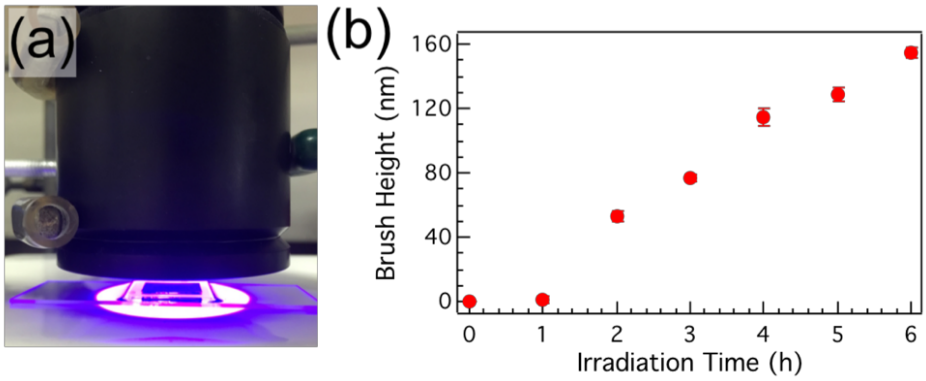

Figure S4. Temporal study of P(DMAEMA) brush growth under ambient conditions (room temperature and in the presence of air). (a) Image of the polymerization setup. (b) Relationship of brush height as a function of irradiation time. Error bars represent ± one standard deviation.

A 6×6 mm ATRP initiator-functionalized silicon substrate was placed on top of a glass plate. The reaction solution was prepared by mixing PTH (3.26 mg, 11.9 μmol, 1 mol%), DMAEMA (200 μL, 1.19 mmol) and 51.5 μL DMA in a glass vial, followed by pipetting onto the silicon substrate directly without any deoxygenation. Then, an 18 × 18 mm glass cover slip was placed on top of the solution to form a thin layer in contact with the substrate, while also filling the space underneath the glass cover slip. The wafer was placed below a 405 nm collimated LED. Polymerization time was varied between 1 and 6 hours. This experiment was repeated 3 times to get average brush thicknesses. The substrate was thoroughly washed using CH_2Cl_2 via Soxhlet extraction and subsequently dried under a stream of nitrogen. Brush height was determined using optical reflectometry. It should be noted that the upper limit of achievable film thickness is ~160 nm under these conditions. According to previous reports,

P(DMAEMA) polymer brush heights of ~700 nm could be achieved via metal-catalyzed ATRP.

Kinetic Study of P(DMAEMA) Brushes (5 mol% PTH)

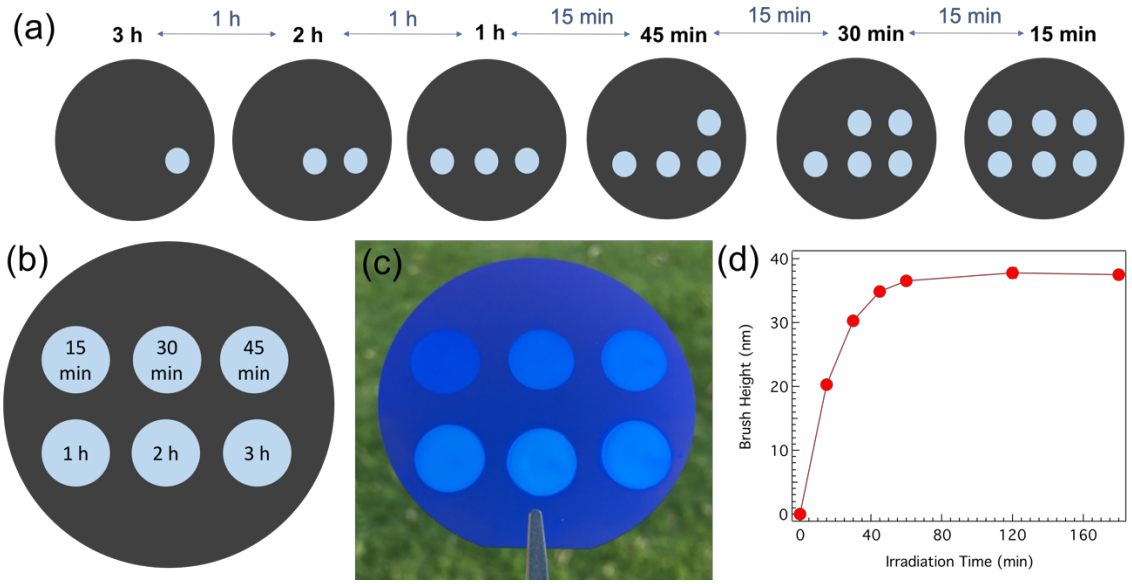

Figure S5. (a) Graphical representation of the polymerization setup at various time points. (b) Graphical representation of the kinetic study, showing 6 polymerization time points on a single 2-inch diameter ATRP initiator-functionalized silicon wafer. (c) Digital images of polymer brushes for the 6 polymerization time points. (d) Relationship of brush height as a function of irradiation time.

A homogeneous stock solution containing PTH (6.53 mg, 23.7 μmol, 5 mol%), DMAEMA (80 μL, 0.47 mmol) and 20.6 μL DMA was prepared, and 10 μL was pipetted onto the 3-hour position of a 2-inch diameter ATRP initiator-functionalized silicon substrate directly without any deoxygenation. Then, a 0.5-inch diameter glass cover slip was placed on top of the

solution to form a thin layer in contact with the substrate. The wafer was placed below a 405 nm collimated LED for 1 hour in the presence of air, followed by addition of another 10 μL of reaction solution onto the 2-hour position on the same wafer and another 0.5-inch diameter glass cover slip placed on top of that solution, without altering the excitation light. The synthetic procedure was repeated to prepare the other polymer brushes to provide the 1 hour, 45 minute, 30 minute, and 15 minute time points, that all finished at the same time. The substrate was submerged in CH_2Cl_2 and the glass cover slips were removed. The substrate was washed with CH_2Cl_2 and then dried under a stream of nitrogen. Brush height was determined by optical reflectometry.

Fabrication of Patterned Polymer Brushes

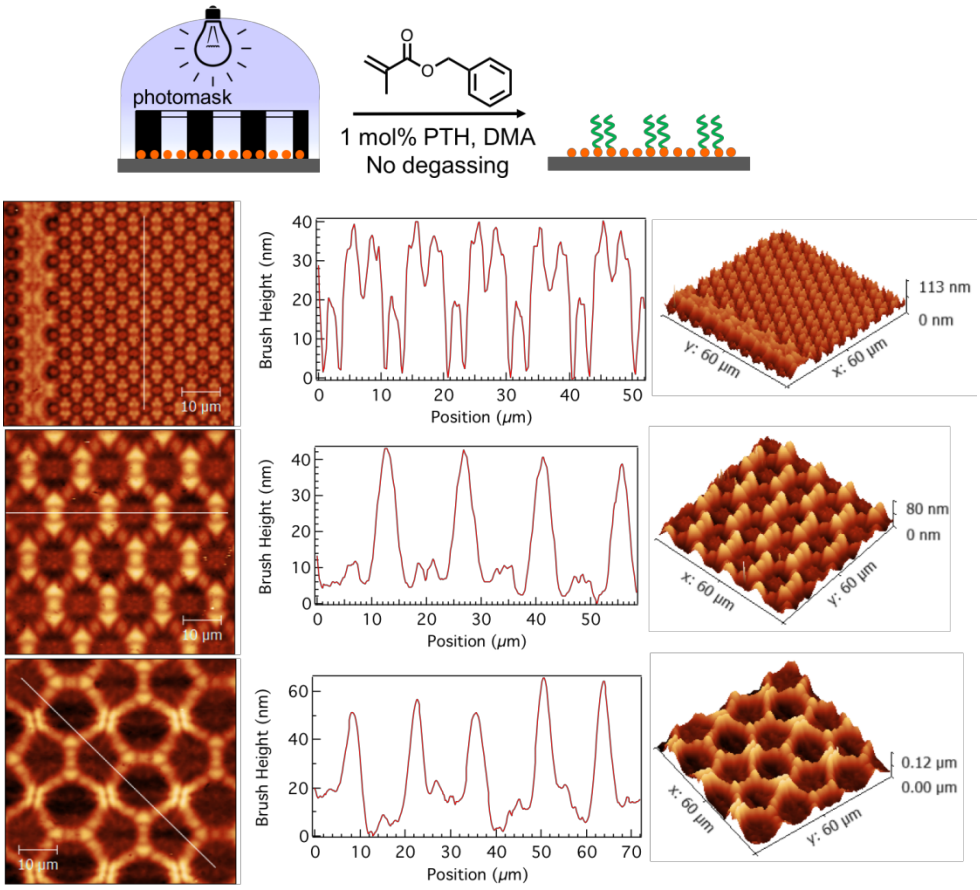

Figure S6. Schematic representation of the setup used to synthesize patterned polymer brushes, AFM topography with height profile, and corresponding 3D images of patterned polymer brushes.

An ATRP initiator-functionalized silicon substrate was placed on top of a glass plate. A homogeneous solution containing PTH (3.25 mg, 11.8 μmol, 1 mol%), BnMA (200 μL, 1.18 mmol), and 50 μL DMA was prepared and pipetted onto the silicon substrate directly until it was completely covered without any deoxygenation. Subsequently, a photomask containing polygon features was placed on top of the solution to form a thin layer in contact with the

substrate. The wafer was placed below a 405 nm collimated LED for 3 hours. After irradiation, the substrate was cleaned using Soxhlet extraction with CH_2Cl_2 for 24 hours and then dried under a stream of nitrogen. AFM was used to image surface topography with height profile and 3D images.

Fabrication of Gradient Polymer Brushes

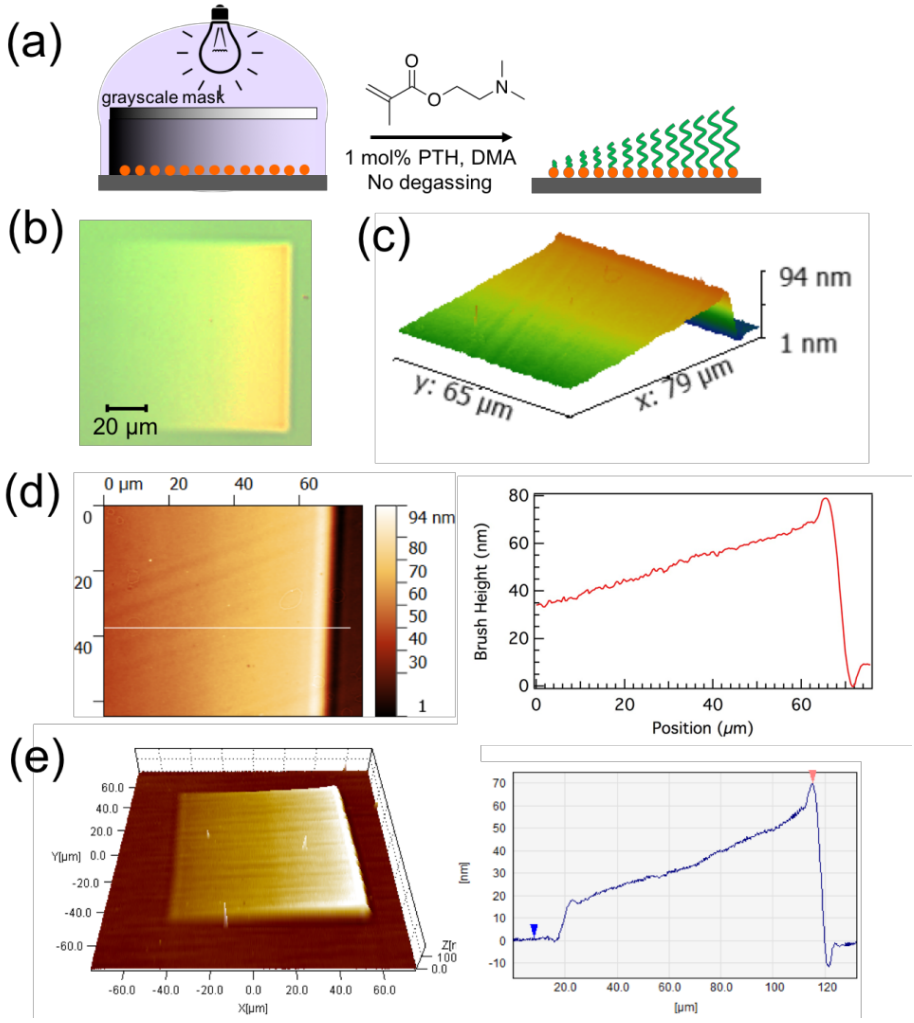

Figure S7. (a) Schematic representation of the setup used to synthesize gradient polymer brushes under a gray scale photomask (b) Optical micrograph of gradient polymer

brushes (c) 3D gradient polymer brush nanostructure of AFM image (d) AFM topography and height profile across the feature (e) Profilometry indicated 3D gradient polymer brush nanostructure and height profile across the image.

An ATRP initiator-functionalized silicon substrate was placed on top of a glass plate. A homogeneous solution containing PTH (3.26 mg, 11.9 μmol, 1 mol%), DMAEMA (200 μL, 1.19 mmol) and 51.5 μL DMA was prepared and pipetted onto the silicon substrate directly until it was completely covered without any deoxygenation. Then, a photomask containing inclined planes was placed on top of the solution to form a thin layer in contact with the substrate. The wafer was placed below a 405 nm collimated LED for 14 hours. The substrate was cleaned using Soxhlet extraction with CH_2Cl_2 for 24 h and then dried under a stream of nitrogen. Optical microscopy indicated the presence of gradient polymer brushes, which was further confirmed using AFM and profilometry, showing 3D gradient polymer brushes and height profiles with a linear relationship between brush height and position across the feature.

Grafting Polymer Brushes under Different Shapes of Cover Glass

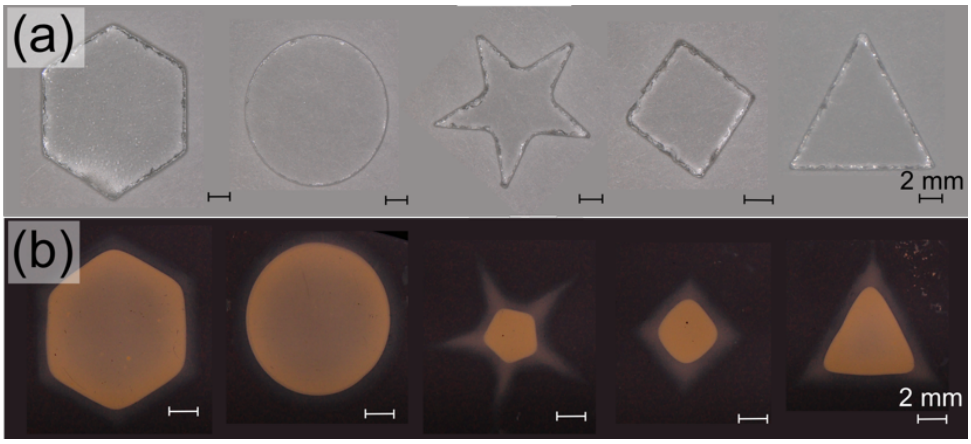

Figure S8. Patterning using different shaped glass cover slips. (a) Digital images of the glass cover slips used: hexagon, circle, star, diamond and triangle and (b) The corresponding polymer brushes.

A homogeneous solution containing PTH (16.4 mg, 59.5 μmol, 5 mol%), DMAEMA (200 μL, 1.19 mmol) and 51.5 μL DMA was prepared and pipetted onto an ATRP initiator-functionalized silicon substrate directly without any deoxygenation. Then, a glass hexagon was placed on top of the solution to form a thin layer in contact with the substrate. The wafer was placed below a 405 nm collimated LED for 14 hours in the presence of air. This same procedure was used to prepare polymer brushes using other glass shapes, (e.g., glass circle, glass star, glass diamond, and glass triangle). After irradiation, the substrate was submerged in CH_2Cl_2 and the glass was removed. The substrate was further cleaned with CH_2Cl_2 and then dried under a stream of nitrogen.

To prepare polymer brushes using "MRL" shaped glasses, a solution containing PTH (65.5 mg, 0.24 mmol, 5 mol%), DMAEMA (800 µL, 4.75 mmol), and 206 µL DMA was mixed in a vial and pipetted onto a 4-inch diameter ATRP initiator-functionalized wafer without any deoxygenation. "MRL" shaped cover slips were placed on top of the solution and irradiated with a 405 nm LED for 21 hours. After irradiation, the substrate was submerged in CH_2Cl_2 and the glass pieces were removed. The substrate was cleaned using CH_2Cl_2 and dried under a stream of nitrogen.

Synthesis of Polymer Brushes on a Large-Scale Surface

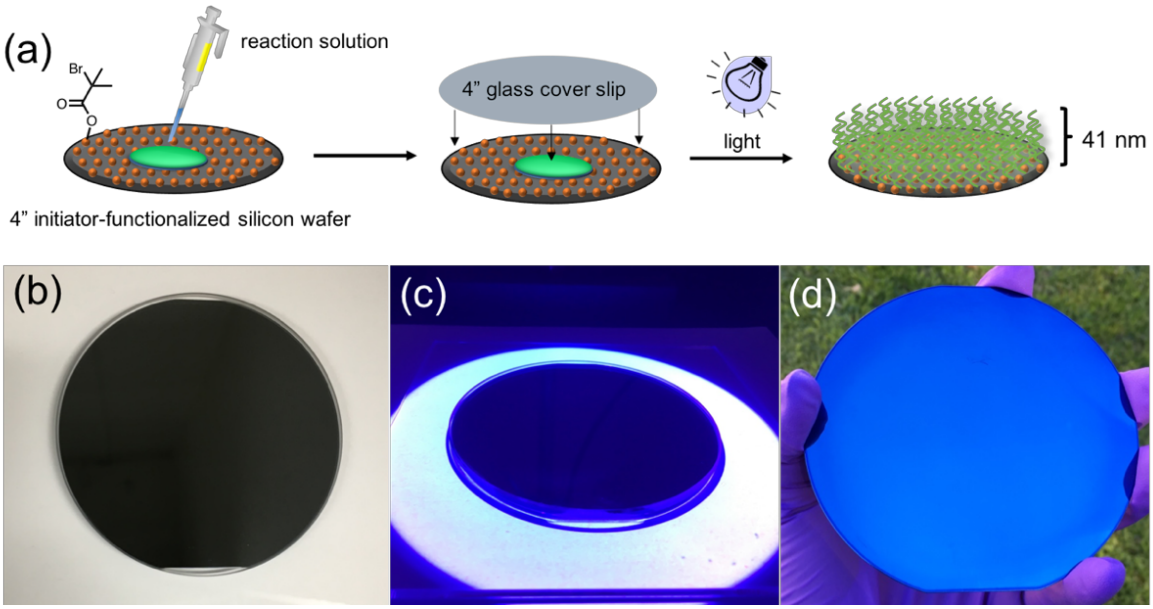

Figure S9. (a) Schematic representation of the polymer brush grafting-from procedure on a large-scale silicon wafer (4-inch diameter) under ambient conditions. Digital images of (b) The setup using a small amount of solution under a glass cover slip, (c) Irradiation with 405 nm light, and (d) Resulting polymer brushes after washing and drying.

A homogeneous solution containing PTH (16.3 mg, 0.06 mmol, 5 mol%), DMAEMA (200 µL, 1.19 mmol), and 51.1 µL DMA was prepared and 200 µL was pipetted onto a 4-inch ATRP initiator-functionalized silicon substrate directly without any deoxygenation. Then, a 4-inch diameter glass cover was placed on top of the solution to form a thin layer in contact with the substrate. The wafer was placed below a 405 nm LED for 2 hours in the presence of air. The substrate was submerged in CH_2Cl_2 and the glass was removed. The substrate was washed with CH_2Cl_2 and then dried under a stream of nitrogen. Uniform polymer brushes were observed on the 4-inch silicon wafer and brush height was determined to be 41 ± 1 nm by optical reflectometry.

Monomer Screening

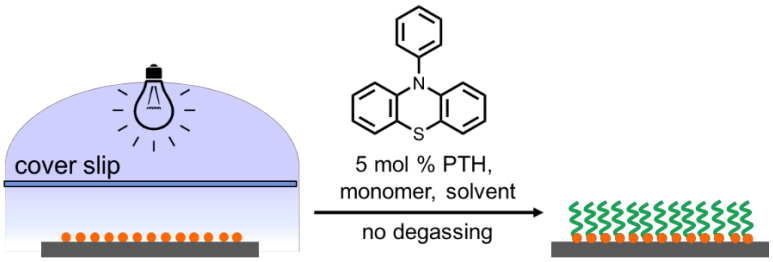

Figure S10. Schematic representation of the general setup used to graft polymer brushes from ATRP initiator-functionalized SiO_2 substrates using 5 mol% PTH and various monomers.

An 8×8 mm ATRP initiator-functionalized silicon substrate was placed on top of a glass plate. A stock solution containing PTH (5.14 mg, 18.7 µmol, 5 mol%), methyl methacylate (MMA) (40 µL, 0.37 mmol) and 38.4 µL DMA was prepared in a glass vial, from which 50 µL was

pipetted onto the silicon substrate without any deoxygenation. Then, a glass cover slip was placed on top of the solution to form a thin layer in contact with the substrate. The wafer was placed below a 405 nm collimated LED for 2 hours. The substrate was cleaned by washing thoroughly with CH_2Cl_2 and then dried under a stream of nitrogen. Brush height was determined by optical reflectometry. To showcase the versatility of this system, the same procedure was repeated using a variety of different monomers at a 5 mol% PTH loading.

Table S2. Polymerization time and film thickness of various polymer brushes grafted from SiO_2

Monomer	Polymerization time (h)	Brush thickness (nm)
Methyl methacrylate (MMA)	2	24
Benzyl methacrylate (BnMA)	1	44
2-(methylthio)ethyl methacrylate (MTEMA)	1	49
2-(dimethylamino)ethyl methacrylate (DMAEMA)	1	32
Poly(ethylene)glycol methyl ether methacrylate M_n 300	0.5	61
Dodecyl methacrylate	2	30
Furfuryl methacrylate	1	44
Glycidyl methacrylate	1	56
2-hydroxyethyl methacrylate	0.5	29
tert-butyl methacrylate	2	26

Determination of Grafting Density

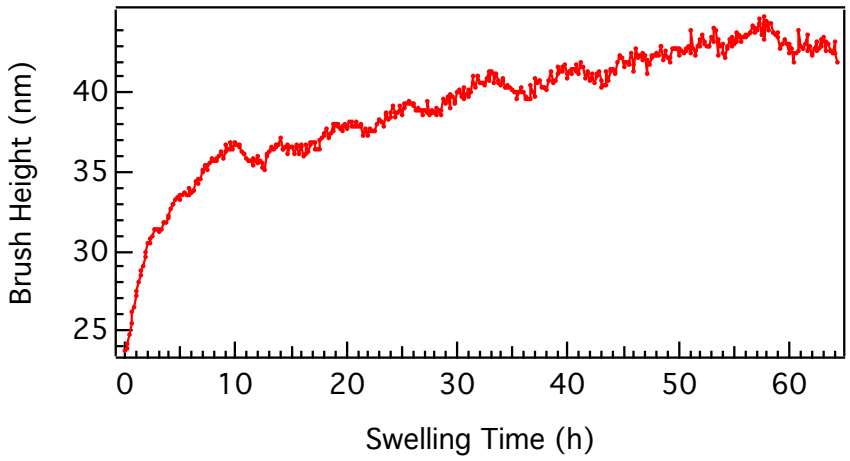

Figure S11. Plot depicting change in swollen P(MMA) brush height as a function of swelling time in THF.

A 10×10 mm ATRP initiator-functionalized silicon substrate was placed on top of a glass plate. A stock solution containing PTH (5.1 mg, 18.7 μmol, 5 mol%), methyl methacrylate (MMA) (40 μL, 0.37 mmol) and 38.4 μL of DMA was prepared in a glass vial. 50 μL of this solution was pipetted onto the silicon substrate without any deoxygenation. Following this, a glass cover slip was placed on top of the solution to form a thin layer in contact with the substrate. The wafer was placed below a 405 nm collimated LED and irradiated for 2 hours. The substrate was cleaned by washing thoroughly with CH_2Cl_2 and then dried under a stream of nitrogen. The dry polymer brush height was measured to be 24 nm by optical reflectometry. The sample was then placed in a chamber filled with tetrahydrofuran (THF) vapor and the brush height was measured every 500 seconds by optical reflectometry until a constant brush

thickness was reached (approximately 43 nm). The grafting density was estimated using a previously reported model (*Macromolecules* **2006**, *39*, 2764-2772).

$$N = \frac{1.074 \times h_s^{3/2}}{h_d^{1/2}}$$

$$\sigma = \frac{\rho_b h_d N_A}{m_0 N}$$

$$D = \left(\frac{4}{\pi\sigma}\right)^{1/2}$$

(N: degree of polymerization, h_s: swollen height, h_d: dry height, σ: grafting density, ρ_b: bulk polymer density, N_A: Avogadro's number, m_0: the monomer molecular weight, D: the distance between grafting sites)

Using the above equations, the grafting density was estimated to be 0.28 chains/nm^2 and the distance between grafting sites should be approximately 2.14 nm.

Experiments using Sacrificial Initiator

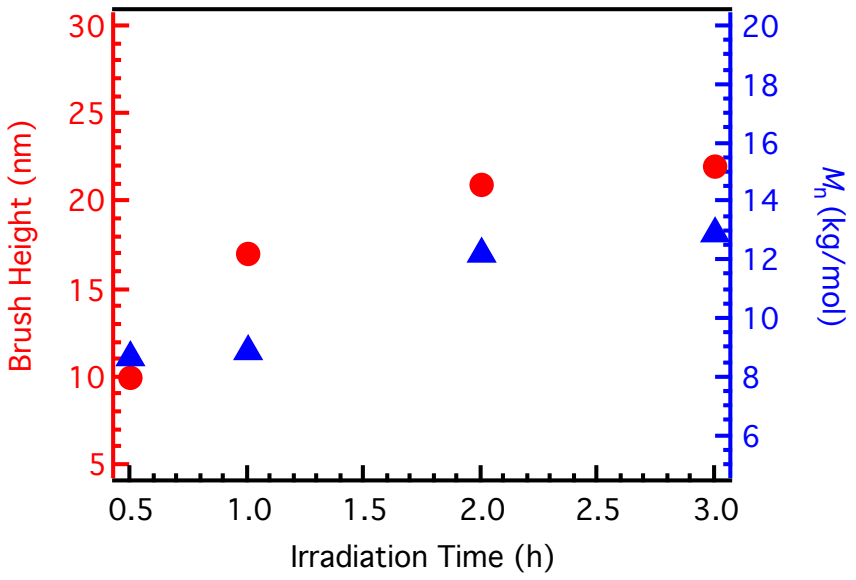

Figure S12. Plot depicting change in polymer brush height and free polymer M_n as a function of irradiation time (h).

A 10×10 mm ATRP initiator-functionalized silicon substrate was placed on top of a glass plate. A stock solution containing PTH (5.1 mg, 18.7 µmol, 5 mol%), methyl methacrylate (MMA) (40 µL, 0.37 mmol), ethyl ∝-bromoisobutyrate in DMA (38.4 µL, 0.37 µmol, 1.88 mg/mL) was prepared in a glass vial. 50 µL of this solution was pipetted onto the silicon substrate without any deoxygenation. Following this, a glass cover slip was placed on top of the solution to form a thin layer in contact with the substrate. The wafer was placed below a 405 nm collimated LED and irradiated for 0.5 hours. The reaction solution was collected for SEC analysis to determine the number-average molar mass (M_n) of free polymer in the solution. The substrate was cleaned by washing thoroughly with CH_2Cl_2 and then dried under a stream of nitrogen. Polymer brush height was measured by optical reflectometry. This

synthetic procedure was followed to obtain time points at 1, 2 and 3 hours. Polymer brush thicknesses and the number-average molar mass of free polymers increase with longer irradiation times.

Synthesis of Ir-Complex-containing Copolymer Brushes

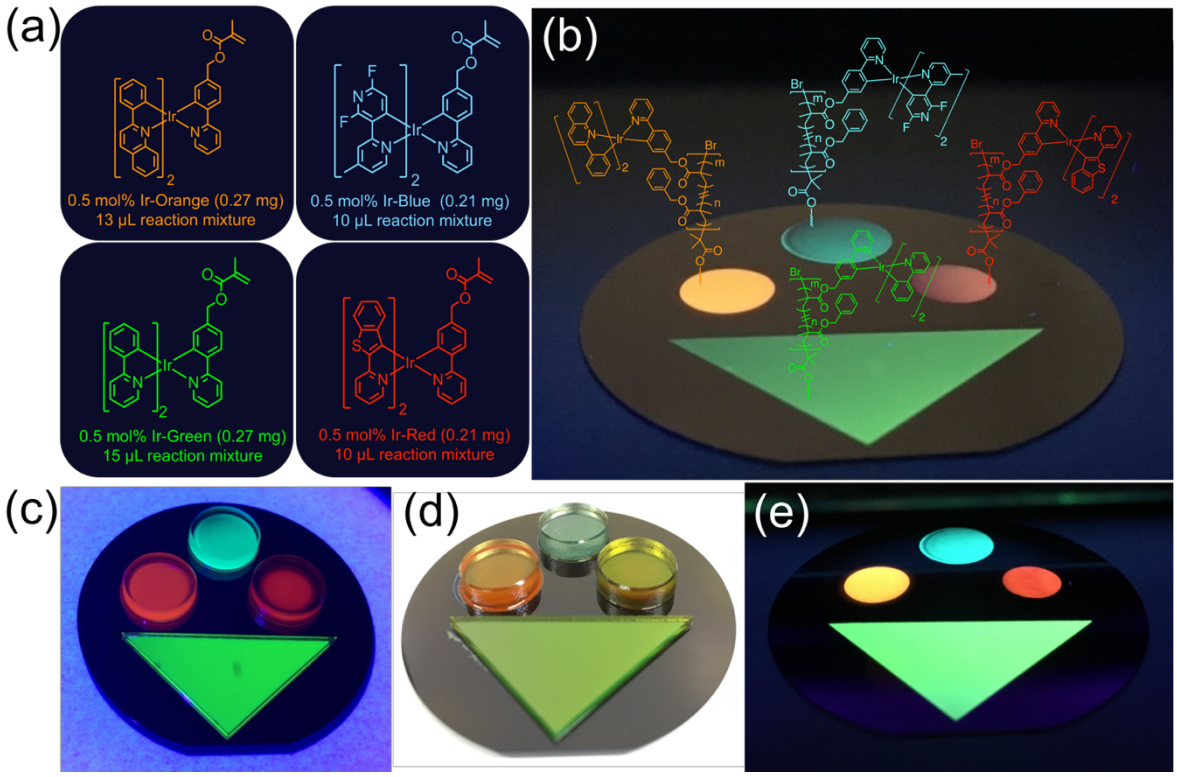

Figure S13. Copolymerization of benzyl methacrylate and Ir-complex on a 2-inch ATRP initiator-functionalized silicon wafer using different cover slips under ambient conditions. (a) Chemical structures of the different Ir-complexes and the corresponding amount of Ir-complex used during brush-growth. (b) Digital image of the four copolymer brushes under UV-irradiation with the corresponding chemical structures for each polymer brush provided. (c) Photoluminescence during light-mediated polymerization under 405 nm

LED excitation. (d) Digital image of the actual setup after the polymerization. (e) Photoluminescence (λ_{ex} = 254 nm) of the four different polymer brush films.

The Ir-blue solution was prepared by mixing Ir-blue (1.26 mg, 1.48 μmol, 0.5 mol%), BnMA (50 μL, 0.30 mmol), PTH (4.06 mg, 14.8 μmol, 5 mol%), and 11.4 μL DMA in a vial. To prepare the other Ir-complex solutions, the amount of PTH, BnMA and DMA was kept constant, using 1.11 mg (1.48 μmol, 0.5 mol%) Ir-green, 1.28 mg (1.48 μmol, 0.5 mol%) Ir-red, and 1.26 mg (1.48 μmol, 0.5 mol%) Ir-orange for the respective mixtures. Then, 15 μL of the Ir-green solution was pipetted onto a 2-inch diameter ATRP initiator-functionalized silicon substrate directly without any deoxygenation, followed by placement of a triangle-shaped glass cover slip on top of the solution to form a thin layer in contact with the substrate. Subsequently, 13 μL of the Ir-orange solution was pipetted onto the same wafer and a 0.5-inch diameter glass cover slip was placed on top of the solution. Then, 10 μL of the Ir-red solution with a 0.5-inch diameter glass and 10 μL of the Ir-blue solution with a 0.5-inch diameter glass were prepared on the same wafer, respectively. The wafer was placed below a 405 nm LED for 2 hours in the presence of air. The substrate was submerged in CH_2Cl_2 and the glass cover slips were removed. Then, the substrate was rinsed with CH_2Cl_2 and dried under a stream of nitrogen, revealing four different colored emissive polymer brushes on one 2-inch silicon wafer, as observed under 254 nm UV excitation.

Sequential Polymerization of DMAEMA-MTEMA-DMAEMA-MTEMA

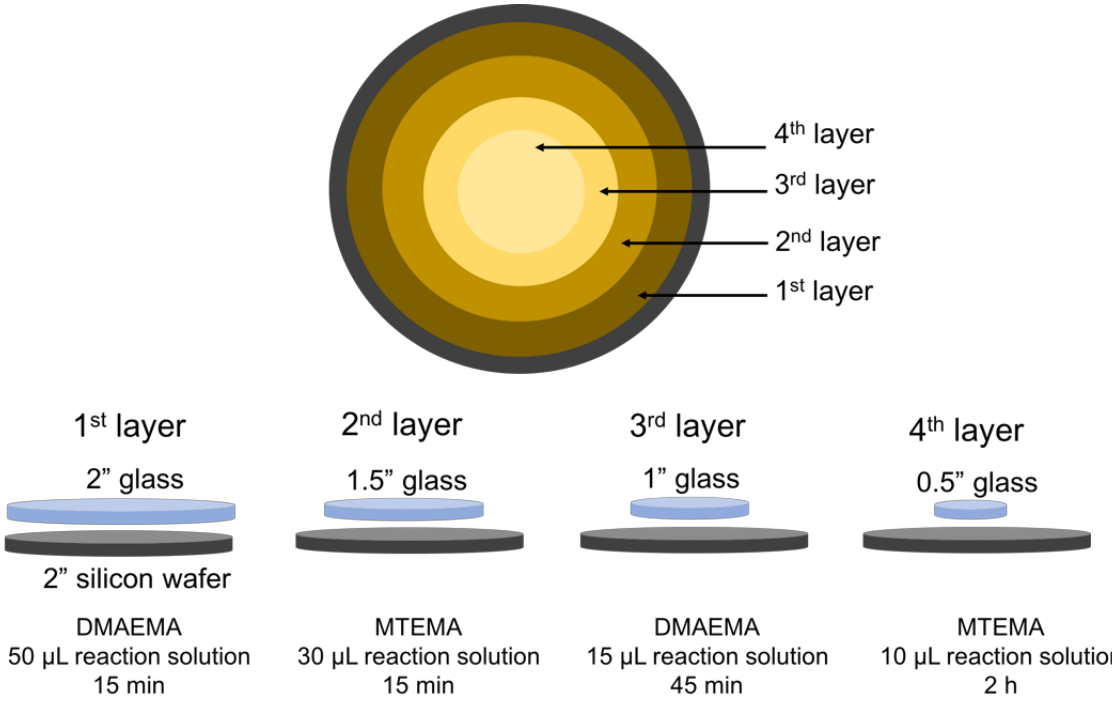

Figure S14. Schematic representation for the sequential polymerization of DMAEMA-MTEMA-DMAEMA-MTEMA under ambient conditions on a 2-inch ATRP initiator-functionalized silicon wafer.

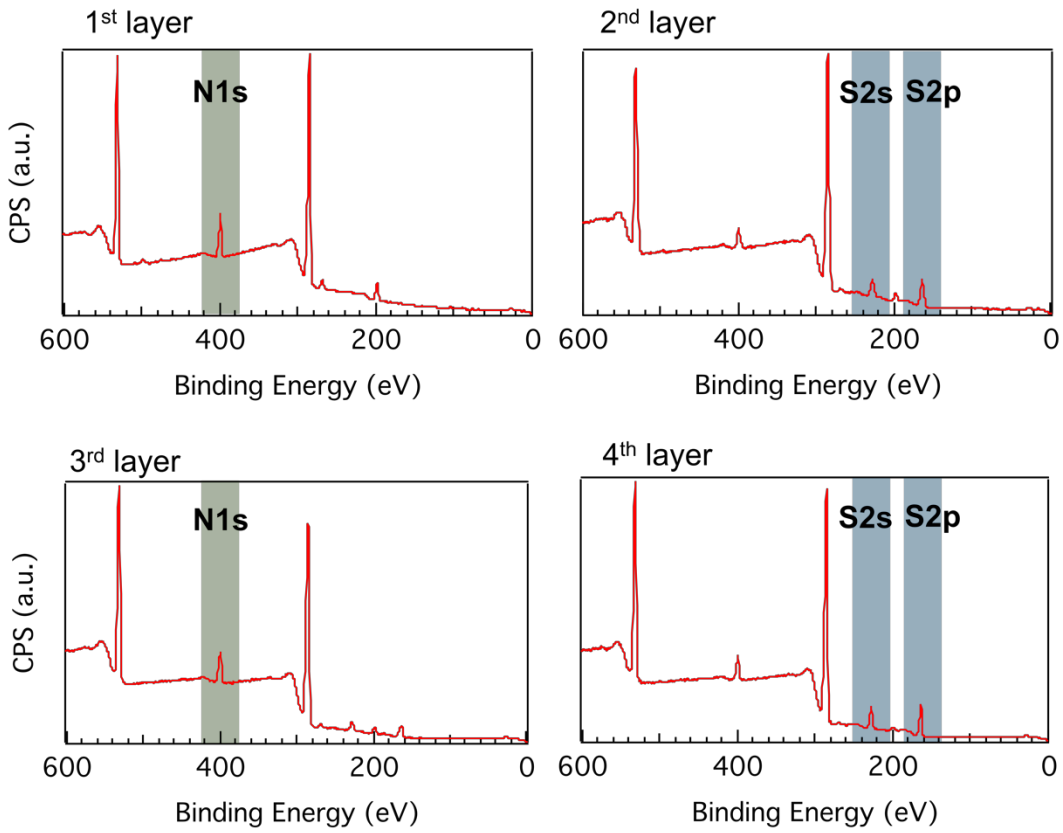

Figure S15. XPS highlighting elements unique to each layer; nitrogen (N1s) for first layer and third layer and sulfur (S2s and S2p) for second layer and fourth layer in Figure 5.

A homogeneous solution containing PTH (8.11 mg, 29.5 μmol, 5 mol%), DMAEMA (100 μL, 0.59 mmol), and 25 μL DMA was prepared, and 50 μL was pipetted onto a 2-inch diameter ATRP initiator-functionalized silicon substrate directly without any deoxygenation. Then, a 2-inch diameter glass was placed on top of the solution to form a thin layer in contact with the substrate. The wafer was placed below a 405 nm collimated LED for 15 minutes in the presence of air. Then, the substrate was cleaned with CH_2Cl_2 and dried under a stream of nitrogen. Subsequently, a homogeneous solution containing PTH (8.11 mg, 29.5 μmol, 5 mol%), MTEMA (91 μL, 0.59 mmol) and 34.1 μL DMA was prepared and 30 μL was pipetted

onto the P(DMAEMA) functionalized silicon substrate. Then, a 1.5-inch diameter glass was placed on top of the solution. The wafer was placed below a 405 nm collimated LED for 15 minutes in the presence of air. The substrate was cleaned with CH_2Cl_2 and then dried under a stream of nitrogen. To prepare the third and fourth layer of the polymer brushes, the synthetic procedure was repeated using 15 μL of the DMAEMA solution with a 1-inch diameter glass cover slip for 45 minutes of irradiation and 10 μL of the MTEMA solution with a 0.5-inch diameter glass cover slip for 2 hours of irradiation, respectively. The substrate was cleaned with CH_2Cl_2 and dried under a stream of nitrogen. Brush height was determined by optical reflectometry indicating the increase of polymer brush thickness going from 14 nm to 31 nm to 42 nm to 50 nm for 1st layer to 2nd layer to 3rd layer to 4th layer of polymer brushes, respectively. XPS confirmed the change in monomer functionality through the emergence of an N1s peak at a binding energy of BE_{N1s} = 399.48 eV indicative of the 1st layer of P(DMAEMA). For the 2nd layer, the peak intensity for N1s decreased, and S2s and S2p peaks at BE_{S2s} = 227.48 and BE_{S2p} = 163.48 eV appeared, indicating the presence of P(MTEMA). For the 3rd layer and 4th layer, the intensity similarly varied for N1s and S2s and S2p peaks, again indicating the presence of P(DMAEMA) and P(MTEMA) layers, respectively.

Sequential Polymerization of DMAEMA-BnMA-DMAEMA-BnMA

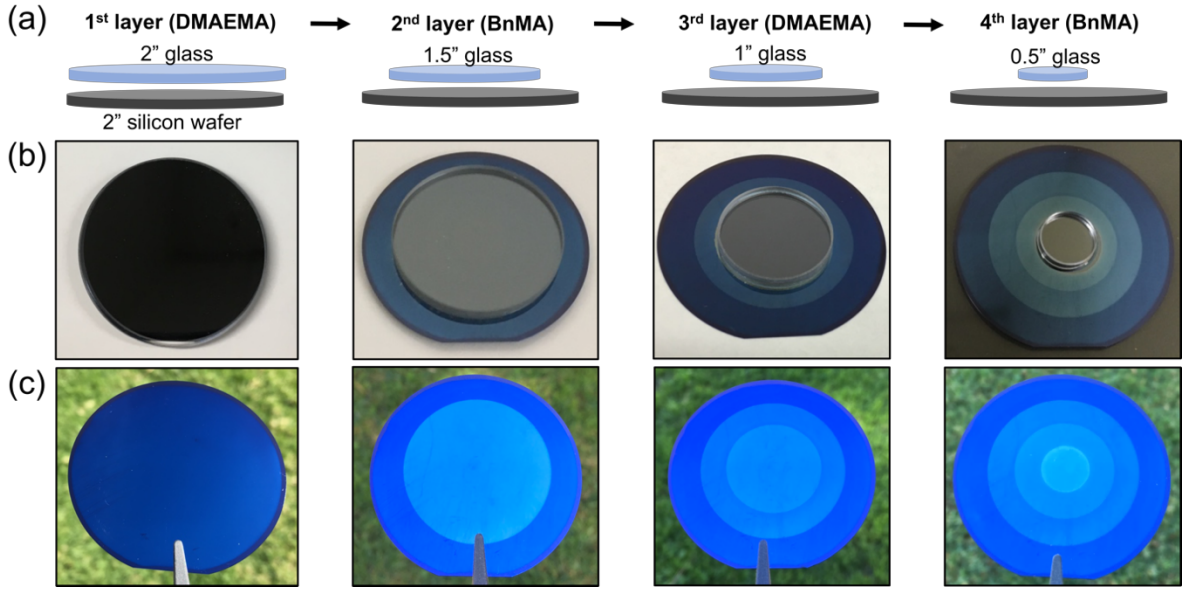

Figure S16. Sequential polymerization of DMAEMA-BnMA-DMAEMA-BnMA under ambient conditions (a) Graphical representation of the stepwise synthesis, (b) Corresponding digital images of the actual setup. (c) Digital images of polymer brushes on a 2-inch ATRP initiator-functionalized silicon wafer during stepwise brush growth.

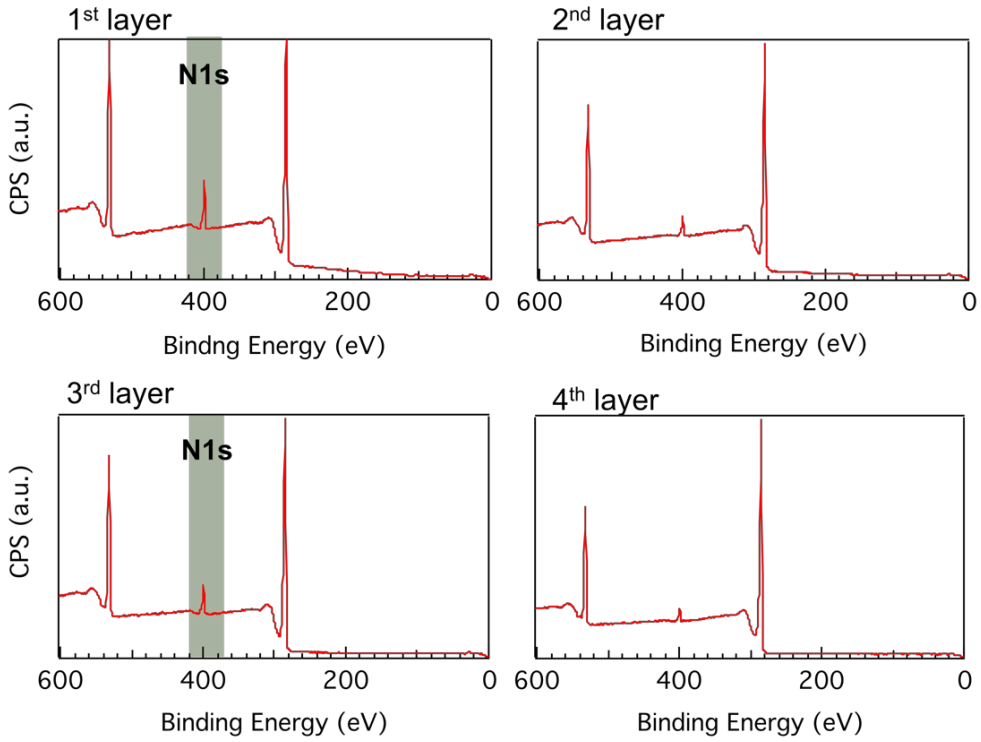

Figure S17. XPS highlighting the variable intensity of the nitrogen (N1s) signal for each layer of of DMAEMA-BnMA-DMAEMA-BnMA.

A homogeneous solution containing PTH (4.90 mg, 17.8 μmol, 5 mol%), DMAEMA (60 μL, 0.36 mmol), and 15.4 μL DMA was prepared, and 50 μL was pipetted onto a 2-inch diameter ATRP initiator-functionalized silicon substrate directly without any deoxygenation. Then, a 2-inch diameter glass was placed on top of the solution to form a thin layer in contact with the substrate. The wafer was placed below a 405 nm collimated LED for 15 minutes in the presence of air. Then, the substrate was cleaned with CH_2Cl_2 and dried under a stream of nitrogen. Subsequently, a homogeneous solution containing PTH (4.87 mg, 17.7 μmol, 5 mol%), BnMA (60 μL, 0.35 mmol) and 15 μL DMA was prepared and 30 μL was pipetted onto the P(DMAEMA) functionalized silicon substrate. Then, a 1.5-inch diameter glass was

placed on top of the solution. The wafer was placed below a 405 nm collimated LED for 30 minutes in the presence of air. The substrate was cleaned with CH_2Cl_2 and then dried under a stream of nitrogen. To prepare the third and fourth layer of the polymer brushes, the synthetic procedure was repeated using 15 μL of the DMAEMA solution with a 1-inch diameter glass cover slip for 30 minutes of irradiation, and 10 μL of the BnMA solution with a 0.5-inch diameter glass cover slip for 1 hour of irradiation, respectively. The substrate was cleaned with CH_2Cl_2 and dried under a stream of nitrogen. Brush height was determined by optical reflectometry indicating the increase of polymer brush thickness going from 16 nm to 30 nm to 36 nm to 50 nm for 1^{st} layer to 2^{nd} layer to 3^{rd} layer to 4^{th} layer of polymer brushes, respectively. XPS indicated the change in monomer functionality through the emergence of varied N1s signal intensity for the alternating P(DMAEMA) and P(BnMA) layers.

Sequential Polymerization of DMAEMA-MTEMA

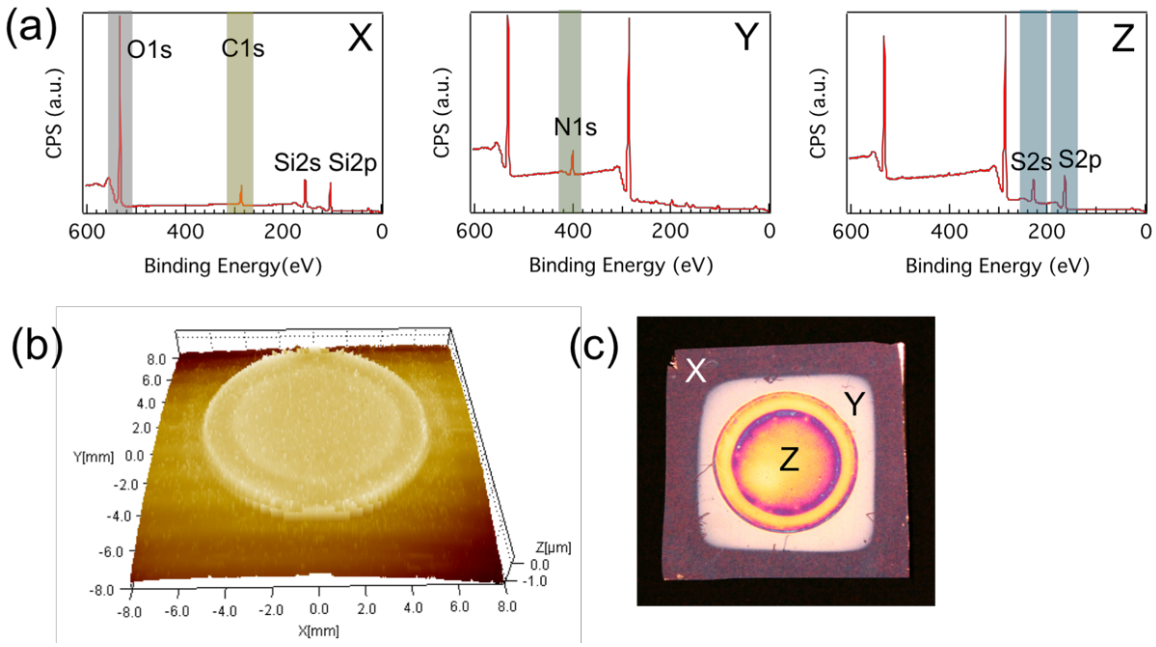

Figure S18. Sequential polymerization of DMAEMA-MTEMA brushes with two different shapes (square first layer and circular second layer). (a) XPS, identifying elements unique to each layer; nitrogen (N1s) for square first layer and sulfur (S2s and S2p) for circular second layer. (b) Profilometry indicating 3-dimensional patterned polymer brushes. (c) Digital micrograph showing 3 regions on the sample: initiator (X), P(DMAEMA) brushes (Y), and DMAEMA-MTEMA brushes (Z).

An 18×18 mm ATRP initiator-functionalized silicon substrate was placed on top of a glass plate. A homogeneous solution containing PTH (3.26 mg, 11.9 μmol, 1 mol%), DMAEMA (200 μL, 1.19 mmol), and 51.5 μL DMA was prepared and pipetted onto the silicon substrate directly until it was completely covered without any deoxygenation. Then, an 18×18 mm glass

cover slip was placed on top of the solution to form a thin layer in contact with the substrate. The wafer was placed below a 405 nm collimated LED for 2 hours in the presence of air. The substrate was washed with CH_2Cl_2 and then dried under a stream of nitrogen. The film thickness was measured to be 52 nm with optical reflectometry. Subsequently, a new solution mixture containing PTH (3.57 mg, 13.0 μmol, 1 mol%), MTEMA (200 μL, 1.30 mmol), and 75 μL DMA was prepared and pipetted onto the silicon substrate functionalized with 52 nm thick P(DMAEMA) brushes. Then, a circular glass cover slip (12 mm diameter) was placed on top of the solution to form a thin layer in contact with the substrate. The wafer was placed below a 405 nm collimated LED for 15 hours in the presence of air. The substrate was cleaned using Soxhlet extraction with CH_2Cl_2 for 24 h and then dried under a stream of nitrogen. Optical reflectometry indicated the overall brush thickness inside the circle was 136 nm, corresponding to an 84 nm increase in brush height. Profilometry confirmed the 3-dimensional topology with a central circular area of P(MTEMA) brush on top of a square region of P(DMAEMA) brush, and an "edge effect" zone (Figure S18c). Furthermore, XPS (Figure S18a) confirms a change in monomer functionality through the emergence of an N1s peak, corresponding to the bottom P(DMAEMA) layer, and S2s and S2p peaks for the second P(MTEMA) layer.

Sequential Polymerization of Patterned Polymer Brushes

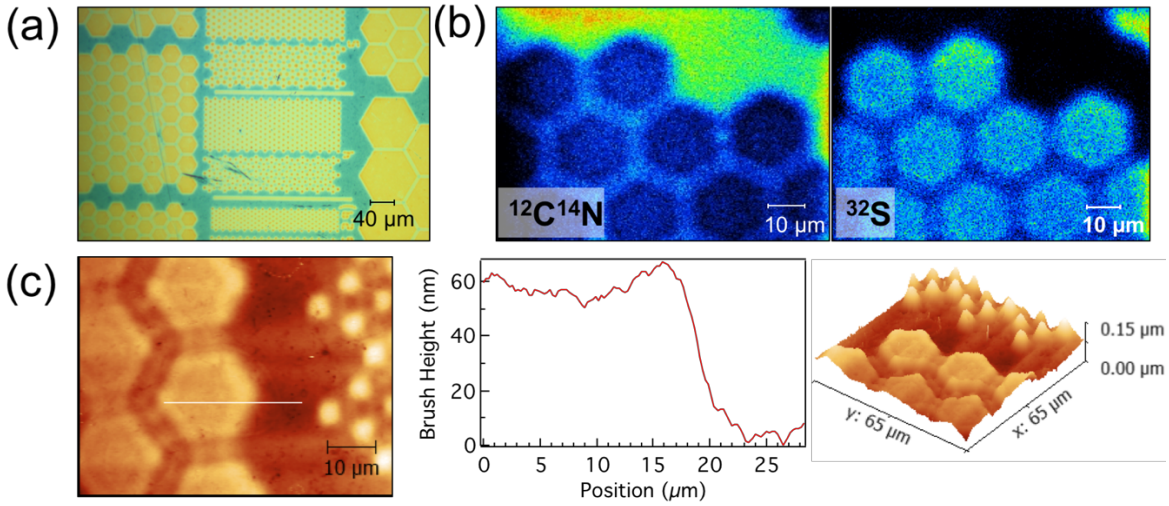

Figure S19. Patterned P(MTEMA) brushes on top of the uniform P(DMAEMA) layer, grown under ambient conditions (a) Optical-microscopy image of patterned polymer brushes (b) SIMS elemental maps for carbon-nitrogen (m/z = 26), highlighting P(DMAEMA) for the first layer and sulfur (m/z = 32) for the patterned P(MTEMA) (c) AFM topography image, height profile, and 3D image of patterned polymer brushes.

A 7×7 mm ATRP initiator-functionalized silicon substrate was placed on top of a glass plate. A homogeneous solution containing PTH (3.26 mg, 11.9 μmol, 1 mol%), DMAEMA (200 μL, 1.19 mmol), and 51.5 μL DMA was prepared and pipetted onto the silicon substrate directly until it was completely covered without any deoxygenation. Then, an 18×18 mm glass cover slip was placed on top of the solution to form a thin layer in contact with the substrate, while also filling the space underneath the glass cover slip. The wafer was placed below a 405 nm collimated LED for 2 hours in the presence of air. The substrate was washed with CH_2Cl_2

and then dried under a stream of nitrogen. The film thickness was measured to be 50 nm with optical reflectometry. Subsequently, a homogeneous solution containing PTH (3.57 mg, 13.0 μmol, 1 mol%), MTEMA (200 μL, 1.30 mmol), and 75 μL DMA was prepared and pipetted onto the silicon substrate containing uniform 50 nm thick P(DMAEMA) brushes. Then, a photomask containing polygons was placed on top of the solution to form a thin layer in contact with the substrate. The wafer was placed below a 405 nm collimated LED for 5 hours in the presence of air. The substrate was cleaned using Soxhlet extraction with CH_2Cl_2 for 24 h and then dried under a stream of nitrogen. The patterned polymer brushes were clearly visible by optical microscopy. SIMS elemental mapping of carbon-nitrogen and sulfur indicate successful reinitiation for the patterned polymer brushes. AFM was used to image surface topography, showing brush heights of 60 nm, corresponding to the patterned P(MTEMA) and generated 3D image.

^{1}H NMR spectra

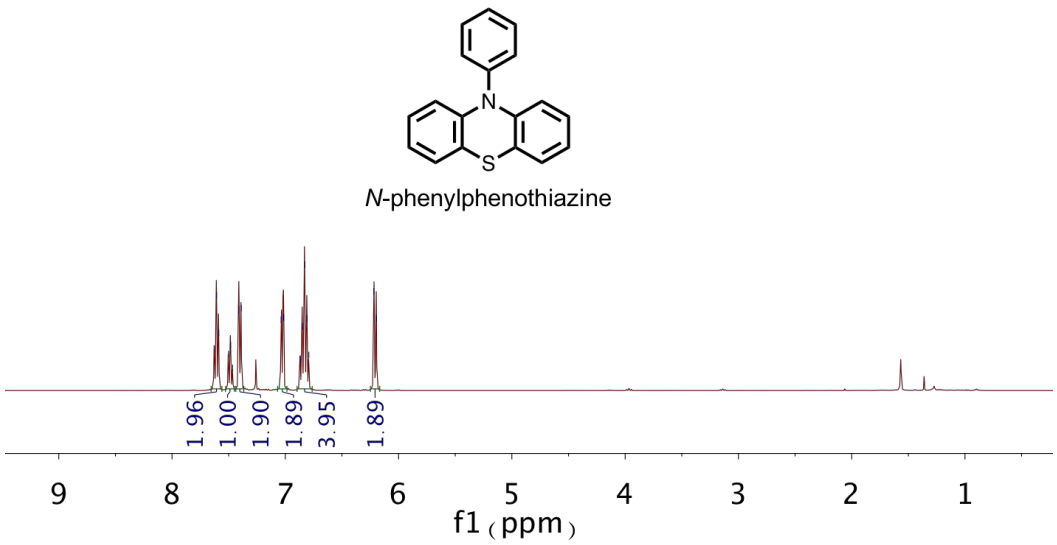

Figure S20. ^{1}H NMR in $CDCl_3$ of *N*-phenylphenothiazine (PTH).

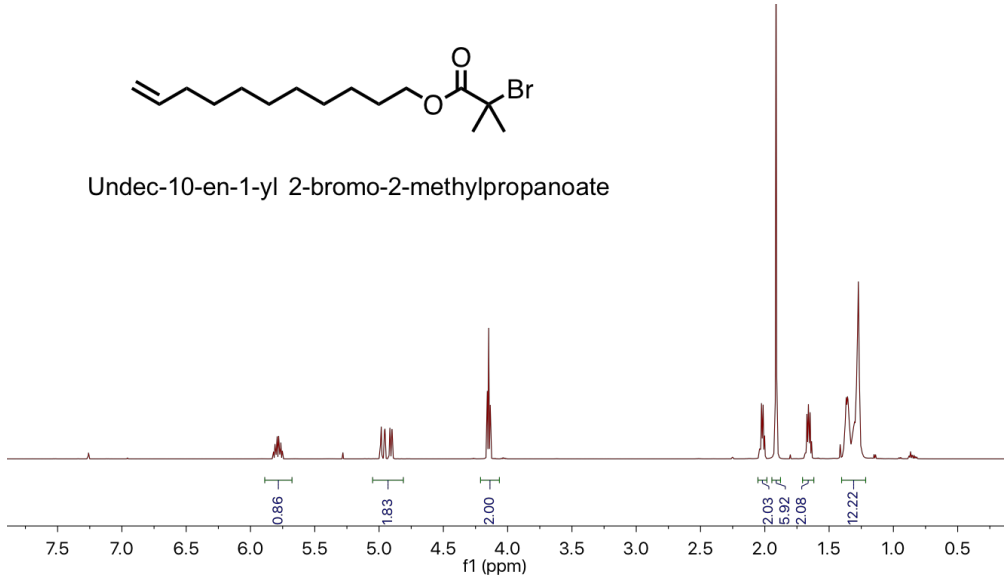

Figure S21. ^{1}H NMR in $CDCl_3$ of undec-10-en-1-yl 2-bromo-2-methylpropanoate.

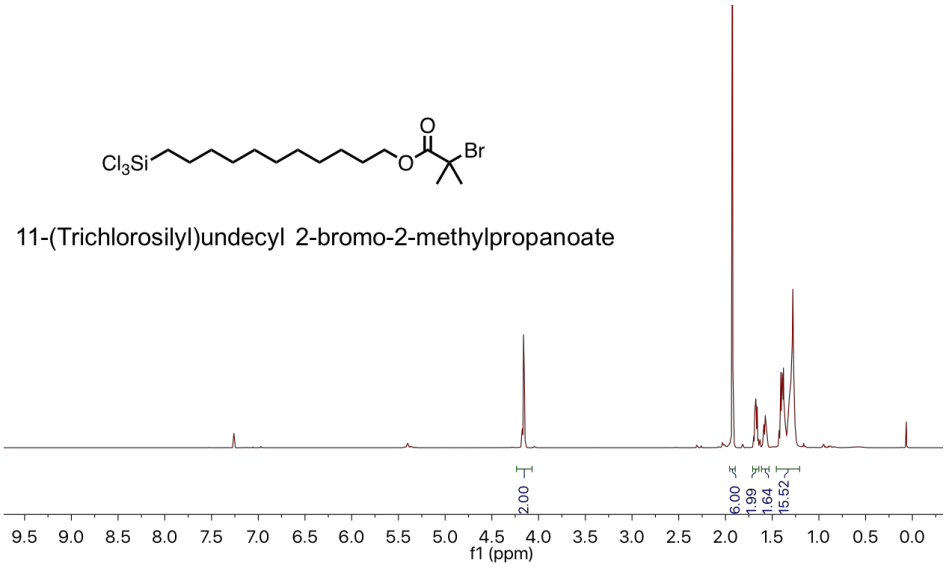

Figure S22. ^{1}H NMR in $CDCl_3$ of 11-(trichlorosilyl)undecyl 2-bromo-2-methylpropanoate**.**

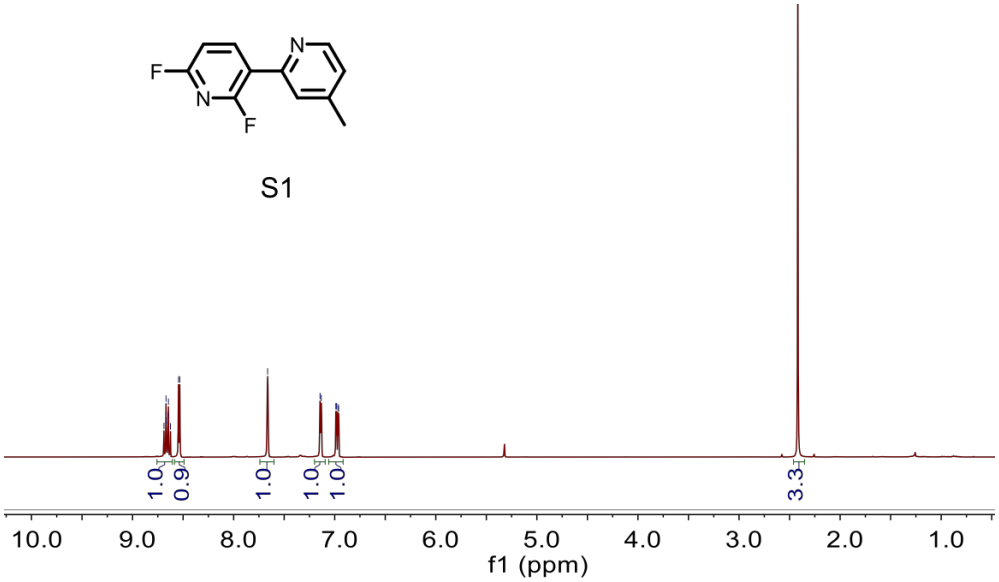

Figure S23. ^{1}H NMR in CD_2Cl_2 of S1**.**

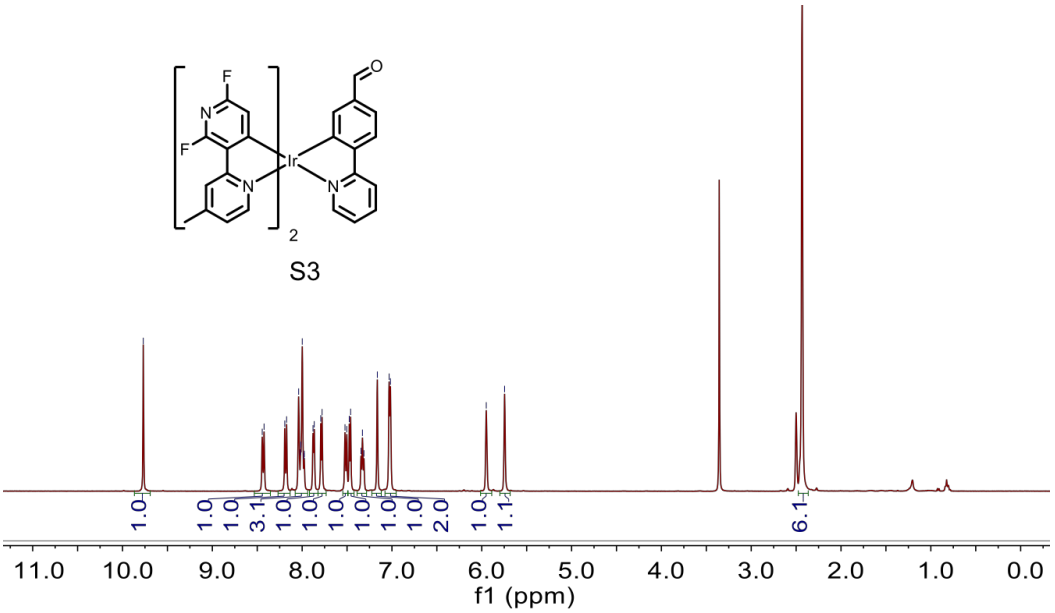

Figure S24. ^{1}H NMR in DMSO-d_6 of S3**.**

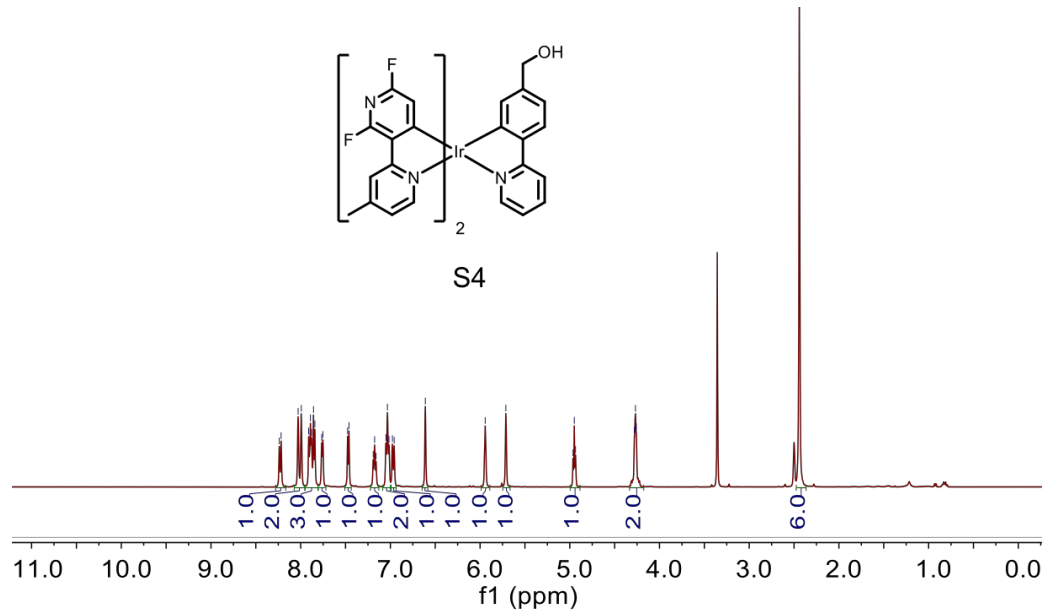

Figure S25. ^{1}H NMR in DMSO-d_6 of S4**.**

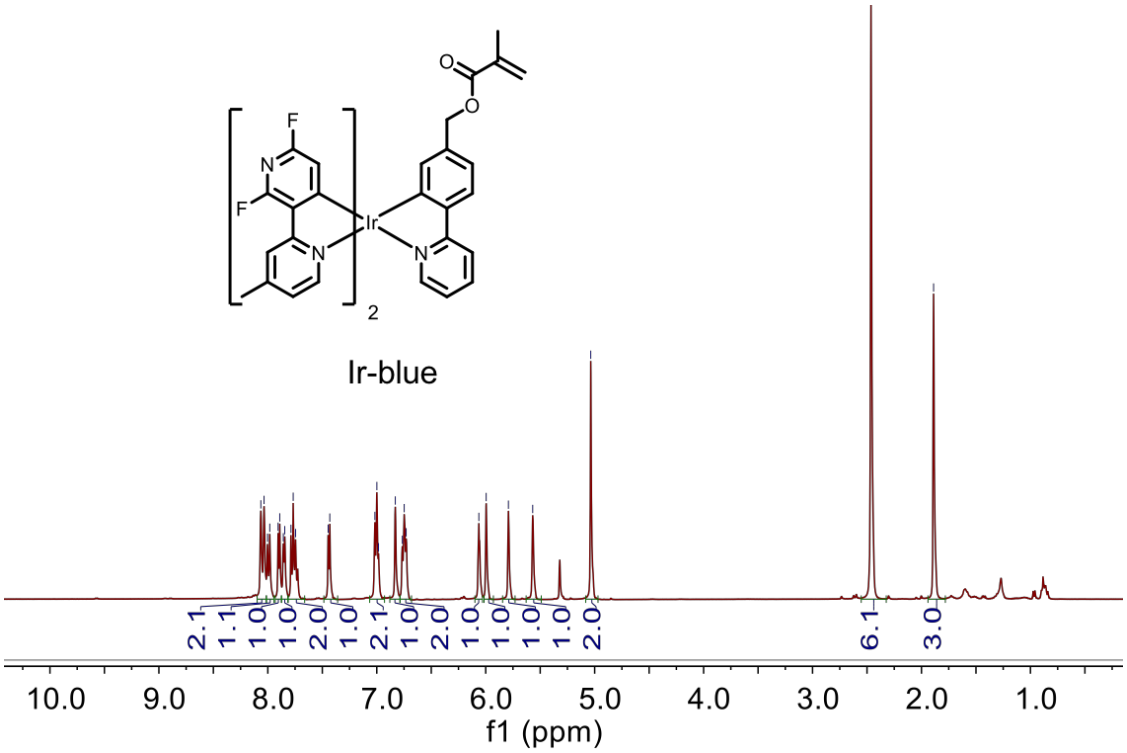

Figure S26. ^{1}H NMR in CD_2Cl_2 of Ir-blue**.**

3.6 References

1) R. Barbey, L. Lavanant, D. Paripovic, N. Schüwer, C. Sugnaux, S. Tugulu, H.-A. Klok, *Chem. Rev*. **2009**, *109*, 5437-5527.
2) S. Edmondson, V. L. Osborne, W. T. S. Huck, *Chem. Soc. Rev.* **2004**, *33*, 14-22.
3) W.-L. Chen, R. Cordero, H. Tran, C. K. Ober, *Macromolecules* **2017**, *50*, 4089-4113.
4) C. Schuh, S. Santer, O. Prucker, J. Rühe, *Adv. Mater*. **2009**, *21*, 4706-4710; e) B. Li, B. Yu, Q. Ye, F. Zhou, *Acc. Chem. Res.* **2015**, *48*, 229-237.
5) X. Xiong, L. Xue, J. Cui, *ACS Macro Lett.* **2018**, *7*, 239-243.
6) Y. N. Yuksekdag, T. N. Gevrek, A. Sanyal, *ACS Macro Lett.* **2017**, *6*, 415-420.
7) H. Ma, J. Hyun, P. Stiller, A. Chilkoti, *Adv. Mater.* **2004**, *16*, 338-341.
8) U. Bog, A. de los Santos Pereira, S. L. Mueller, S. Havenridge, V. Parrillo, M. Bruns, A. E. Holmes, C. Rodriguez-Emmenegger, H. Fuchs, M. Hirtz, *ACS Appl. Mater. Interfaces* **2017**, *9*, 12109-12117.
9) M. Ezzat, C.-J. Huang, *RSC Adv.* **2016**, *6*, 61695-61702.
10) J. A. Howarter, J. P. Youngblood, *Adv. Mater.* **2007**, *19*, 3838-3843.
11) L. Ionov, N. Houbenov, A. Sidorenko, M. Stamm, S. Minko, *Adv. Funct. Mater.* **2006**, *16*, 1153-1160.
12) T. Chen, R. Ferris, J. Zhang, R. Ducker, S. Zauscher, *Prog. Polym. Sci*. **2010**, *35*, 94-112.
13) I. Tokareva, S. Minko, J. H. Fendler, E. Hutter, *J. Am. Chem. Soc.* **2004**, *126*, 15950-15951.
14) M. Chen, W. H. Briscoe, S. P. Armes, J. Klein, *Science* **2009**, *323*, 1698-1701.
15) J. Pyun, T. Kowalewski, K. Matyjaszewski, *Macromol. Rapid Commun*. **2003**, *24*, 1043-1059.

16) M. Baum, W. J. Brittain, *Macromolecules* **2002**, *35*, 610-615.

17) M. Husseman, E. E. Malmström, M. McNamara, M. Mate, D. Mecerreyes, D. G. Benoit, J. L. Hedrick, P. Mansky, E. Huang, T. P. Russell, C. J. Hawker, *Macromolecules* **1999**, *32*, 1424-1431.

18) C. Konn, F. Morel, E. Beyou, P. Chaumont, E. Bourgeat-Lami, *Macromolecules* **2007**, *40*, 7464-7472.

19) R. R. Shah, D. Merreceyes, M. Husemann, I. Rees, N. L. Abbott, C. J. Hawker, J. L. Hedrick, *Macromolecules* **2000**, *33*, 597-605.

20) X. Fan, L. Lin, J. L. Dalsin, P. B. Messersmith, *J. Am. Chem. Soc.* **2005**, *127*, 15843-15847.

21) C. Scott, B. Mitrovic, S. Eastwood, G. Kinsel, *Polymer* **2014**, *55*, 3551-3556.

22) R. Dong, S. Krishnan, B. a. Baird, M. Lindau, C. K. Ober, *Biomacromolecules* **2007**, *8*, 3082-3092.

23) M. Y. Paik, Y. Xu, A. Rastogi, M. Tanaka, Y. Yi, C. K. Ober, *Nano Lett*. **2010**, *10*, 3873-3879.

24) F. Zhou, Z. Zheng, B. Yu, W. Liu, W. T. S. Huck, *J. Am. Chem. Soc.* **2006**, *128*, 16253-16258.

25) T. Chen, R. Jordan, S. Zauscher, *Soft Matt*. **2011**, *7*, 5532-5535.

26) S. J. Ahn, M. Kaholek, W. K. Lee, B. LaMattina, T. H. LaBean, S. Zauscher, *Adv. Mat.* **2004**, *16*, 2141-2145.

27) A. Sangsuwan, B. Narupai, P. Sae-ung, S. Rodtamai, N. Rodthongkum, V. P. Hoven, *Anal. Chem*. **2015**, *87*, 10738-10746.

28) B. Narupai, J. E. Poelma, C. W. Pester, A. J. McGrath, E. P. Toumayan, Y. Luo, J. W. Kramer, P. G. Clark, P. C. Ray, C. J. Hawker, *J. Polym. Sci. Part A: Polym. Chem*. **2016**, *54*, 2276-2284.

29) J. E. Poelma, B. P. Fors, G. F. Meyers, J. W. Kramer, C. J. Hawker, *Angew. Chem. Int. Ed.* **2013**, *52*, 6844-6848; *Angew. Chem*. **2013**, *125*, 6982-6986.

30) C. W. Pester, B. Narupai, K. M. Mattson, D. P. Bothman, D. Klinger, K. W. Lee, E. H. Discekici, C. J. Hawker, *Adv. Mater.* **2016**, *28*, 9292-9300.

31) N. J. Treat, H. Sprafke, J. W. Kramer, P. G. Clark, B. E. Barton, J. Read de Alaniz, B. P. Fors, C. J. Hawker, *J. Am. Chem. Soc.* **2014**, *136*, 16096-16101.

32) E. H. Discekici, C. W. Pester, N. J. Treat, J. Lawrence, K. M. Mattson, B. Narupai, E. P. Toumayan, Y. Luo, A. J. McGrath, P. G. Clark, J. Read de Alaniz, C. J. Hawker, *ACS Macro Lett.* **2016**, *5*, 258-262.

33) X. Pan, C. Fang, M. Fantin, N. Malhotra, W. Y. So, L. A. Peteanu, A. A. Isse, A. Gennaro, P. Liu, K. Matyjaszewski*, J. Am. Chem. Soc.* **2016**, *138*, 2411-2425.

34) K. Matyjaszewski, D. Hongchen, W. Jakubowski, J. Pietrasik, A. Kusumo, *Langmuir* **2007**, *23*, 4528-4531.

35) G. J. Dunderdale, C. Urata, D. F. Miranda, A. Hozumi, *ACS Appl. Mater. Interfaces* **2014**, *6*, 11864-11868.

36) T. Zhang, Y. Du, J. Kalbacova, R. Schubel, R. D. Rodriguez, T. Chen, D. R. T. Zahn, R. Jordan, *Polym. Chem.* **2015**, *6*, 8176-8183.

37) B. P. Harris, A. T. Metters, *Macromolecules* **2006**, *39*, 2764-2772.

38) R. Jordan, A. Ulman, J. F. Kang, M. H. Rafailovich, J. Sokolov, *J. Am. Chem. Soc.* **1999**, *121*, 1016-1022.

39) Z. A. Page, B. Narupai, C. W. Pester, R. Bou Zerdan, A. Sokolov, D. S. Laitar, S. Mukhopadhyay, S. Sprague, A. J. McGrath, J. W. Kramer, P. Trefonas, C. J. Hawker, *ACS Cent. Sci.* **2017**, *3*, 654-661.

4. Low Temperature, Rapid Copolymerization of Acrylic Acid and Sodium Acrylate in Water

4.1 Abstract

Controlled polymerization of poly(acrylic acid) in aqueous solution is a major challenge requiring design of scalable, industry-oriented syntheses that afford modest molar mass and dispersity control without long reaction times and environmentally demanding conditions. In response, this report presents the rapid copolymerization of acrylic acid and sodium acrylate using an inexpensive and scalable protocol based on thermal initiation of simple mixtures containing an alkyl iodide and sodium iodide in water.

4.2 Introduction

Poly(acrylic acid) (PAA) and related copolymers are widely used in industry for the production of adhesives, superabsorbents, scale inhibitors, and coatings.[1-2] Despite its breadth of use, the direct synthesis of PAA is not straightforward; the high reactivity of acrylic acid in conventional free-radical polymerization (FRP) generally leads to high molar masses, broad molar mass distributions, and uncontrolled crosslinking in many cases.[2-3] This synthetic challenge is often at odds with imparting optimal material performance, which is obtained for well-defined materials. For example, reducing dispersity in low molar mass PAA has been shown to significantly enhance the stability of titania and calcite dispersions.[4]

Controlled radical polymerization (CRP) techniques, including atom transfer radical polymerization (ATRP),[5] nitroxide-mediated radical polymerization (NMP),[6] and reversible addition fragmentation chain transfer (RAFT)[7] polymerization are highly valued as a means to prepare functional polymers of predefined molecular weight and dispersity ($Đ$). Although ATRP can polymerize a wide range of monomers, this technique has limitations with acidic monomers such as meth/acrylic acid. This is primarily due to ligand protonation at low pH and competitive coordination of the carboxylate groups to the catalytic metal center.[8] An alternative strategy for the synthesis of well-defined PAA is to polymerize *tert*-butyl acrylate (*t*-BA) via ATRP followed by acidic deprotection of the *tert*-butyl esters. However, the post-polymerization modification and purification steps render this strategy cumbersome.[9-10] Although NMP[11] and RAFT[12-14] can directly polymerize acrylic acid, these techniques are characterized by long reaction times, stringent conditions, and costly reagents, all of which are undesirable from a commercial standpoint. Alternative techniques such as precipitation polymerization in supercritical carbon dioxide,[15-16] organocobalt-mediated polymerization[17]

and cyanoxyl-mediated polymerization[18] also enable the preparation of PAA, but the requirements of specific catalysts and specialized equipment limit wide-spread implementation.

Consequently, a key challenge for acidic monomers is the design of environmentally-friendly, industry-oriented syntheses that can afford molar mass and dispersity control without forgoing the economic scalability and high conversion characteristic of free-radical chemistry. In the present work, we investigate the direct synthesis of PAA in aqueous solution without the need for expensive or synthetically taxing reagents or protocols. We show that in the presence of iodoacetonitrile, sodium iodide (NaI) and conventional radical initiators, acrylic acid copolymerizes with its sodium salt to afford PAA with moderate control over molecular weight and narrowed molar mass distribution (Scheme 1). Significantly, the polymerization exhibits high conversion and comparable kinetics to conventional FRP. We hypothesize that side reactions (e.g., deleterious chain transfer to polymer and termination) are mitigated via degenerative chain transfer events to the added alkyl iodide, leading to moderate molecular weight control based on the initial molar ratio of monomer to chain transfer agent (CTA).[23] This fast, economical, and industry-oriented synthesis utilizes inexpensive salts with water as a cost-effective and green solvent.

The strategy, inspired by reports on controlled iodine chain transfer systems from Goto[19-22] and Matyjaszewski,[23-24] benefits from radical processes that are well-known in organic synthesis and are most efficient for alkyl iodides.[25] We postulate that the elementary reactions of polymerization (initiation, propagation, and termination) can be supplemented with degenerative chain transfer events to an added alkyl iodide, thus forming iodine-capped

dormant species that forestall side reactions and lower both molar mass and dispersity via a reduced number of active radicals.[23]

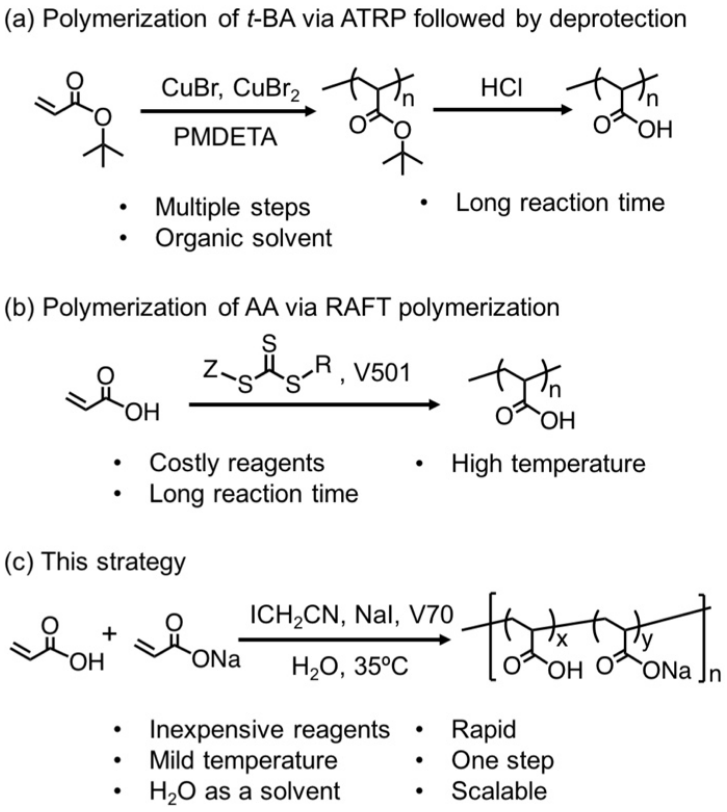

Scheme 1. Previously reported (a) two-step synthetic pathway for PAA,[9] (b) direct polymerization of AA via RAFT polymerization,[14] and (c) this work copolymerizing acrylic acid and sodium acrylate in water at mild temperature.

4.3 Results and Discussion

In preliminary experiments, the direct polymerization of pure acrylic acid was examined (90 wt% monomer in water, Table 1, entry 1) using iodoform as a chain transfer agent and

2,2'-azobis(4-methoxy-2,4-dimethylvaleronitrile) (V70) as a thermal initiator. It was encouraging to note that ~45% monomer conversion was obtained after 16 hours under these conditions. To accurately estimate the molar mass and dispersity (*Đ*), the crude poly(acrylic acid) was purified by dialysis and subsequently methylated via reaction with trimethylsilyl diazomethane in methanol (see Experimental section for details). Methylation render the product soluble in organic solvents, enabling the molecular weight determination via conventional calibration analysis using size exclusion chromatography (SEC) eluting with chloroform. Estimates of the number-average molar mass (M_n) and dispersity were 7800 g/mol and 1.6, respectively indicating a significant improvement in molecular weight control relative to crosslinked or branched materials obtained via conventional free radical chemistry. Higher conversions and increased molecular weights could be obtained at lower monomer wt%, however no control over the polymerization process was observed.

Table 1. The polymerization of acrylic acid with iodoform as a chain transfer agent in water.

entry	wt% monomer in water[a]	% conv.[b]	M_n (exp) (g/mol)[c]	$Đ$[c]
1	90	45	7800	1.58
2	80	40	4700	1.37
3	50	88	10000	2.00
4	30	>95	40000	4.00
5[a]	60	90	35000	2.32

All polymerizations were performed in water at 40 °C for ca. 16-23 hours using AA (60 eq.), NaI (1.5 eq.), V70 (0.25 eq.) and iodoform as the CTA (1.0 eq.) unless otherwise noted. aThe polymerization was performed in water at rt using a 1:1 ratio of AA to NaA for 5 minutes. bConversion was calculated from 1H-NMR analysis of

crude product. cThe molar mass and Đ of methylated PAA samples were estimated from SEC analysis relative to PMMA standards using chloroform as eluent.

To address this lack of control and increase the reaction kinetics, the copolymerization of acrylic acid (AA) and sodium acrylate (NaA) mixtures were subsequently examined. This strategy is based on enhancing the rate of polymerization (R_p) and overall monomer conversion by exploiting the known sensitivity of R_p for acrylic acid to both the ionic strength and pH of the medium.[14,26-28] In addition, the general copolymerization of AA with a co-monomer has been previously shown to increase control over the growing copolymer.[31-33] In stark contrast to pure acrylic acid, the 1:1 comonomer mixture of AA and NaA was notably exothermic and after only 5 minutes the polymerization mixture increased significantly in viscosity with near-quantitative conversion (≥90%) being observed. Following methylation, SEC analysis showed increased molar mass and dispersity (M_n = 35000 g/mol, $Đ$ = 2.3, Table 1, entry 5) when compared to the corresponding acrylic acid homopolymerization using iodoform as the CTA. Given the improved rate of reaction, we hypothesized that control may improve using iodoacetonitrile as an alternative CTA. This reasoning is driven by the increased solubility of iodoacetonitrile in aqueous solutions, thus mitigating challenges of iodine transfer from the CTA. Indeed, using iodoacetonitrile as the CTA with the 1:1 comonomer mixture of AA and NaA results in a reduced molar mass and dispersity (M_n = 12000 g/mol, $Đ$ = 1.7), consistent with improved control (Table S2, entry 1). Additional syntheses performed at a fixed monomer:iodoacetonitrile ratio with increased content of AA in the monomer feed (70–90 mol% AA and 30-10 mol% NaA), afforded moderately-defined materials with only minor broadening of molar mass distributions ($Đ \approx 2.0–2.3$) and increased M_n (14000–27000 g/mol) (Table 2, entries 2-4) showing the potential for monomer mixtures

and specifically, a 50:50 mixture. These results are also in-line with previous reports indicating sensitivity of the polymerization rate to varied degrees of neutralization of the acrylic acid monomer.[14,26-27]

Table 2. Copolymerization of AA and NaA mixtures of varied composition with iodoacetronitrile as a chain transfer agent.

entry	Fraction of AA (mol%)	% conv.[a]	M_n (exp) (g/mol)[b]	$Đ$[b]
1	50	90	12000	1.71
2	70	>95	14000	2.21
3	80	85	27000	1.99
4	90	>95	25000	2.29

All polymerizations were performed in water (33 wt% monomer) at 35 °C for *ca.* 21-24 hours using monomer (60 eq.), NaI (1.5 eq.), V70 (0.25 eq.) and iodoacetronitrile as the CTA (1.0 eq.) unless otherwise noted. [a]Conversion was calculated from ^{1}H-NMR analysis of crude product. [b]The molar mass and $Đ$ of methylated PAA samples were estimated from SEC analysis relative to PS standards using chloroform as eluent.

A series of control experiments were then conducted to give further insight into the role of each component in the polymerization via their systematic removal from the starting polymerization mixture (Table 3, entries 2–4). Of particular note was the observation that in the absence of the initiator V70, no polymerization was observed even in the presence of iodoacetonitrile and NaI (Table 3, entry 3). Conversely, conducting the polymerization in the absence of iodoacetonitrile leads to gelation within minutes indicating its necessary function as a CTA (Table 3, entry 4). Finally, although omission of NaI results in comparable monomer conversion (95%), the methylated PAA product exhibited significantly higher molar mass and dispersity (M_n = 20000 g/mol, $Đ$ = 2.0) than the corresponding polymerization conducted with

NaI (Figure S1, Table 3, entry 1-2). These results suggest that NaI may moderate polymer growth and enhance the efficiency of chain transfer to iodoacetonitrile.

Table 3. The control experiments of copolymerization of AA and NaA in water.

entry	[CTA]:[NaI]:[V70]	% conv.[a]	M_n (exp) (g/mol)[b]	$Đ$[b]
1	[1]:[1.5]:[0.25]	90	12000	1.71
2	[1]:[0]:[0.25]	95	20000	2.04
3	[1]:[1.5]:[0]	<5	-	-
4	[0]:[1.5]:[0.25]	Gels within minutes	-	-

All polymerizations were performed in water (33 wt% monomer) using AA (30.0 eq.), NaA (30.0 eq.) at 35 °C for *ca.* 21 hours. [a]Conversion was calculated from ^{1}H-NMR analysis of crude product. [b]The molar mass and *Đ* of methylated PAA samples were estimated from SEC analysis relative to PS standards using chloroform as eluent.

The rapid reaction (<5 minutes) of these AA/NaA mixtures prompted a thorough investigation of the polymerization process. As can be seen in Figure 1, after a short incubation period (~2-3 minutes), rapid monomer conversion that plateaus at ~90% is observed with an associated spike in the internal reaction temperature to ca. 100 °C (external bath temperature of 35 °C). This rate acceleration arises from the large enthalpy of polymerization for acrylic acid/sodium acrylate and the compounded effects of a high monomer concentration resulting in poor heat dissipation.[29-30] This excessive heat generation is of particular importance for implementation of this chemistry at increased scale and to address this challenge, additional experiments investigating the role of water as a diluent to suppress thermal runaway were

conducted. In these systems, individual reaction temperatures were monitored during polymerization using an immersed temperature probe with figure 1 mapping monomer conversion (estimated via ^{1}H-NMR analysis of discrete samples withdrawn periodically under argon) onto the recorded temperature profiles obtained during the course of polymerization for varied concentrations of monomer. Significantly, as the monomer content is reduced to 33 wt%, a sharp temperature spike is not observed. Instead a gradual increase in internal reaction temperature to 60 °C is observed with high conversions still being achieved within 10 minutes. The effects of rate acceleration on the polymerization could be further controlled by decreasing the monomer concentration to 25 and 15 wt% (Figure 1c-d, respectively). In these cases, minimal temperature increases are observed with ~90% monomer conversion occurring within 2-3 hours. Observed plateaus in conversion are likely attributable to the increased solution viscosity or to the "gel effect", which limits the final extent of reaction under the effectively isothermal conditions achieved at 25 and 15 wt% monomer. Most importantly, it should be noted that all monomer concentrations produced copolymers of comparable molar mass ($M_n \approx 11000–18000$ g/mol) and moderate dispersities ($Đ < 2$) as estimated via SEC of the methylated products (Table S1).

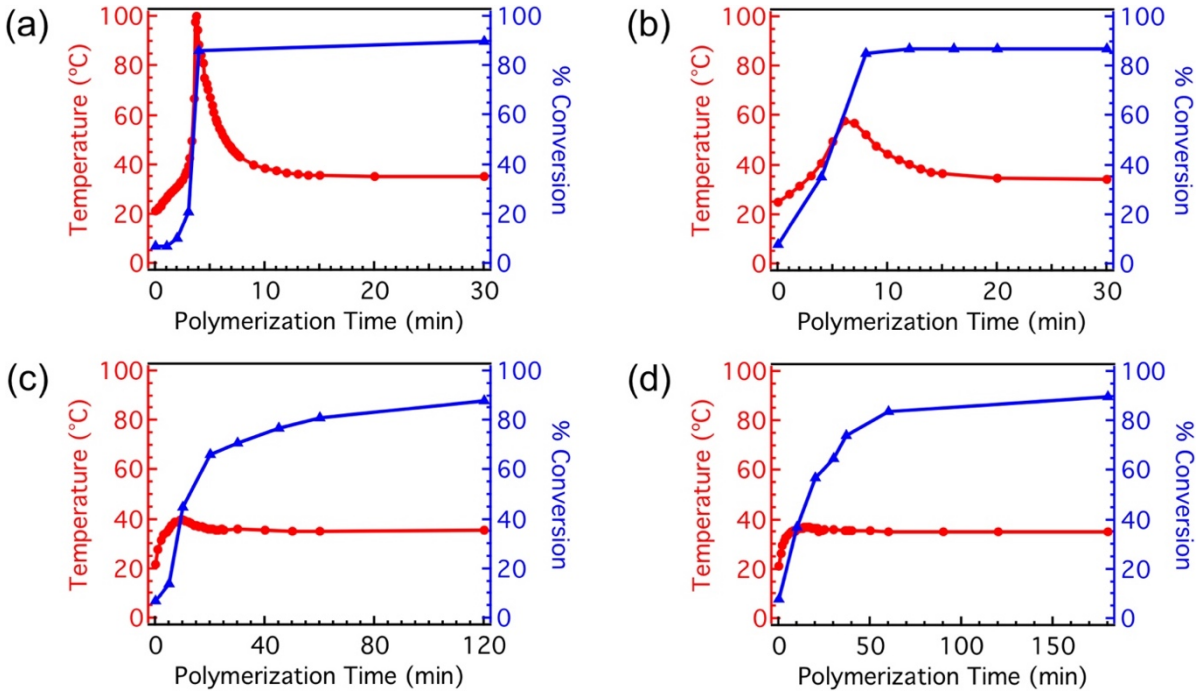

Figure 1. Reaction temperature (red circle) and conversion (blue triangle) profiles of the polymerization measured for 1:1 monomer mixtures of AA and NaA polymerized at concentrations (a) 50, (b) 33, (c) 25, and (d) 15 wt% monomer in water.

The previously highlighted experiments employ V70 to thermally generate radicals due to its relatively low decomposition temperature (10 hours half-life decomposition temperature of 30 °C). The influence of temperature on the polymerization process was therefore explored through the use of alternative thermal initiators such as 2,2'-azobis(2-methylpropionitrile) (AIBN) or 4,4'-azobis(4-cyanopentanoic acid) (V501). Although AIBN and V501 differ in solubility, both initiators undergo homolysis at elevated temperatures when compared to V70 (10 hours half-life decomposition temperatures of 65 °C and 70 °C respectively). For both AIBN and V501, polymerization at 70 °C resulted in high monomer conversion (>95%) with

comparable molar mass distributions (M_n = 12000 g/mol, $Đ$ = 1.5, see Table S2) to the products obtained at 35 °C using V70. These results illustrate the versatility of this technique and associated tolerance to alternative radical sources and elevated reaction temperatures. In addition, it is worth noting that implementation of this chemistry at increased scale (ca. 10 grams of monomer) also results in high monomer conversion (>95%) with comparable molar mass and molar mass distributions (M_n = 7700 g/mol, $Đ$ = 1.9, details provided in the SI) to laboratory scale (1-2 grams) under the same conditions.

In contrast to traditional free radical processes, low molar mass products were obtained with this process and the molecular weights could be correlated to the monomer:iodoacetonitrile molar ratios. Figure 2 displays the corresponding SEC chromatograms of the methylated PAA copolymers in chloroform produced by varying initial monomer-to-CTA ratios. As the monomer-to-CTA ratio increased from 8:1 to 90:1, the relative molar masses systematically increased from 4000 g/mol to 16000 g/mol with dispersities consistently below 2.0 (Table 4). While these results indicate moderate molar mass control, they do not show full agreement between the product molar mass and the targeted values, suggesting that the iodine transfer events are not quantitative.

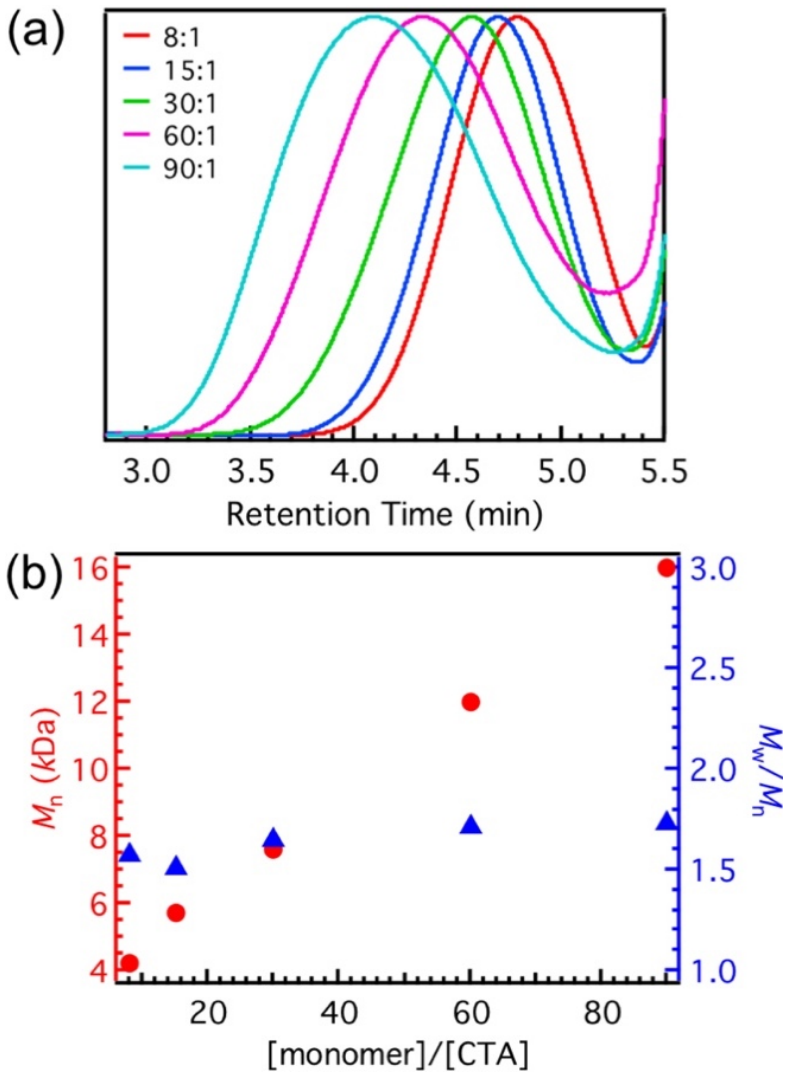

Figure 2. (a) SEC traces of methylated PAA products synthesized, and (b) dependence of estimated molar mass (red circle) and Đ (M_w/M_n, blue triangle) on the initial monomer:CTA ratio.

Table 4. Result summary for the synthesis of PAA-*co*-PNaA of varied molar mass.

entry	monomer:CTA[a]	% conv.[b]	M_n (exp) (g/mol)[c]	$Đ$[c]
1	8:1	95	4200	1.57
2	15:1	94	5700	1.51
3	30:1	>95	7600	1.65
4	60:1	90	12000	1.71
5	90:1	95	16000	1.73

All polymerizations were performed in water (33 wt% monomer) at 35 °C for *ca.* 20 hours using a 1:1 ratio of AA to NaA, NaI (1.5 eq.), V70 (0.25 eq.) and iodoacetonitrile as the CTA (1.0 eq). [a]Molar ratio of monomer-to-CTA. [b]Conversion was calculated from ^{1}H-NMR analysis of crude product. [c]The molar mass and $Đ$ of methylated PAA samples were estimated from SEC analysis relative to PS standards using chloroform as eluent.

4.4 Conclusion

In conclusion, the rapid, low temperature synthesis of poly(acrylic acid) was successfully achieved in concentrated aqueous solution through the copolymerization of acrylic acid and sodium acrylate. Parameters such as nature of the iodo-CTA, presence of NaI and monomer wt% systematically influence the kinetics and molar mass distribution of the product copolymers. This procedure represents a user-friendly system for the scalable synthesis of poly(acrylic acid) and holds promise for an environmentally-friendly process that can be tailored for other acidic monomer and co-monomer mixtures.

4.5 Supporting Information

General Reagent Information. Acrylic acid (Acros Organics, 98%, extra pure, stabilized), sodium acrylate (Sigma Aldrich, 97%), iodoacetonitrile (Alfa Aesar, 97%), iodoform (Alfa Aesar, 99%), (trimethylsilyl)diazomethane (Sigma Aldrich, 2 M solution in diethyl ether), 2,2'-azobis(4-methoxy-2,4-dimethylvaleronitrile) (V70, Wako Specialty Chemicals), 4,4'-azobis(4-cyanopentanoic acid) (V501, Acros Organics, 97%), 2,2'-azobis(2-methylpropionitrile) (AIBN, Sigma Aldrich, 98%) and NaI (Fisher Scientific, 99%) were used as received.

General Analytical Information. Nuclear magnetic resonance spectra were recorded on a Varian 400, 500 or 600 MHz spectrometer. Size exclusion chromatograohy (SEC) was performed on a Waters 2690 separation module equipped with a Waters 2410 refractive index detector eluting with 0.25% trimethylamine in chloroform and calibrated relative to poly(methyl methacrylate) standards or a Waters Acquity Advanced Polymer Characterization (APC) equipped with Acquity UPLC refractive index detector eluting with 0.25% trimethylamine in chloroform and calibrated relative to polystyrene standards.

General procedure for the copolymerization of acrylic acid and sodium acrylate

NaI (43.7 mg, 0.3 mmol, 1.5 eq.), deionized water (1.9 mL), sodium acrylate (NaA) (548.1 mg, 5.8 mmol, 30.0 eq.) and acrylic acid (AA) (0.4 mL, 5.8 mmol, 30.0 eq.) were added sequentially to a 20 mL scintillation vial equipped with a stir bar. Iodoacetonitrile (ICH2CN) (14.1 μL, 0.2 mmol, 1.0 eq.) and V70 (15.0 mg, 0.05 mmol, 0.25 eq.) were then added, and the vial was sealed with a septum-cap. The reaction solution was degassed by purging with argon for 15 minutes. The vial was then transferred to a heating block and stirred at 35 °C. The polymerization was stopped by opening the vial to expose the crude mixture to air. A small aliquot of the crude mixture was taken for NMR analysis to determine monomer conversion.

Purification of copolymer product

The crude product was diluted and then filtered through a 0.45 μm cellulose acetate membrane. The product was dialyzed against 1.0 M HCl using cellulose ester dialysis tubing (molecular weight cut-off (MWCO) = 100 – 500 g/mol) for 24 hours, and then against deionized water for 48 hours. After lyophilization, the polymer product was isolated as a white powder of purified PAA.

Methylation of copolymer product

To a 4 mL vial equipped with a magnetic stir bar, 20.0 mg of purified polymer and 1.0 mL methanol were added. 1.0 mL of trimethylsilyl diazomethane solution (2.0 M in diethyl ether) was added to the reaction mixture dropwise over 10 minutes at 0 ˚C. Then, the solution was left stirring overnight at room temperature. Acetic acid was added to quench the unreacted trimethylsilyl diazomethane before removing all the solvent and most volatile organic

residuals under reduced pressure. The polymer was then re-dissolved in chloroform for SEC analysis to estimate the molar mass and *Đ* of the methylated PAA product.

General procedure for the polymerization of acrylic acid

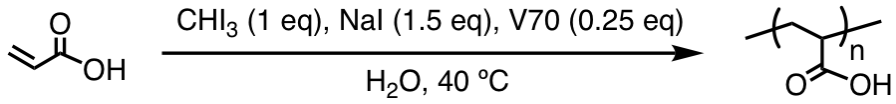

Iodoform (76.6 mg, 0.2 mmol, 1.0 eq.), NaI (43.7 mg, 0.3 mmol, 1.5 eq.), V70 (15.0 mg, 0.05 mmol, 0.25 eq.), deionized water (90 µL) and acrylic acid (AA) (800 µL, 11.7 mmol, 60.0 eq.) were added to a 4 mL vial equipped with a stir bar, and the vial was sealed with a septum-cap. The reaction solution was degassed by purging with Argon for 10 min. Then, the vial was transferred to a heating block and stirred at 40 °C and the polymerization was allowed to proceed for 16 hours. Afterwards the polymerization was stopped by opening the vial to expose the crude mixture to air. A small aliquot of the crude mixture was taken for NMR analysis to determine monomer conversion.

Purification and methylation of polymer product *(using AA as a monomer)*

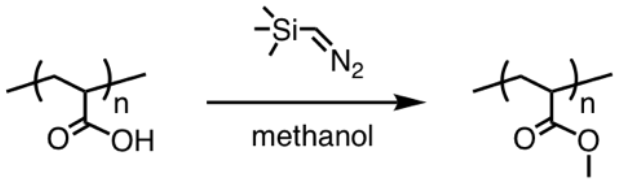

The crude product was diluted and filtered through a 0.45 µm cellulose acetate membrane. The product was dialyzed against deionized water using cellulose ester dialysis

tubing (MWCO = 100 – 500) for 48 hours. After lyophilization, the product was isolated as a slightly yellow powder of purified PAA (using iodoform as a chain transfer agent). The purified PAA product was methylated using trimethylsilyl diazomethane rendered the product polymer soluble in organic solvents, enabling conventional calibration analysis via size exclusion chromatography (SEC) eluted with chloroform, according to a previously published procedure.

Control experiments

NaI (43.7 mg, 0.3 mmol, 1.5 eq.), deionized water (1.9 mL), sodium acrylate (NaA) (548.1 mg, 5.8 mmol, 30.0 eq.) and acrylic acid (AA) (0.4 mL, 5.8 mmol, 30.0 eq.) were added sequentially to a 20 mL vial equipped with a stir bar. Iodoacetonitrile (ICH_2CN) (14.1 μL, 0.2 mmol, 1.0 eq.) and V70 (15.0 mg, 0.05 mmol, 0.25 eq.) were added and the vial was sealed with a septum-cap. The reaction solution was degassed by purging with argon for 15 minutes. The vial was then transferred to a heating block and stirred at 35 °C, and the polymerization was allowed to proceed for 21 hours. Afterwards the polymerization was stopped by opening the vial to expose the crude mixture to air. A small aliquot of the crude mixture was taken for NMR analysis to determine monomer conversion. The product was purified and methylated following the same procedure. The molar mass and $Đ$ of methylated PAA product were determined by SEC eluted with chloroform. The control experiments were performed as presented above, without the addition of NaI (Table 3, entry 2), V70 (Table 3, entry 3) and iodoacetonitrile (Table 3, entry 4).

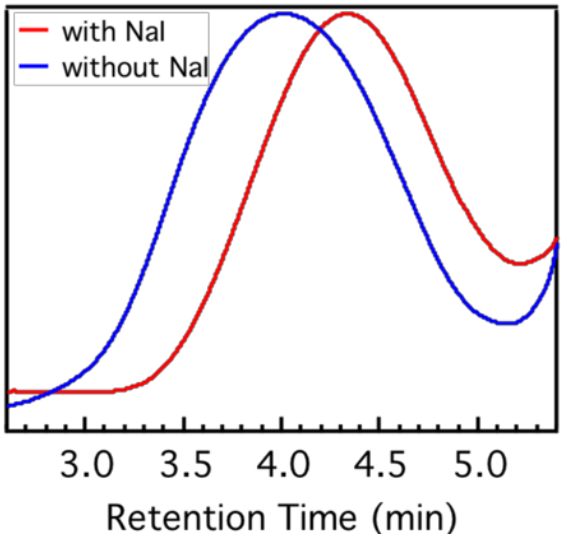

Figure S1. SEC chromatograms of the methylated PAA samples in the presence (red) and in the absence (blue) of NaI.

Copolymerization of varied monomer composition

NaI (43.7 mg, 0.3 mmol, 1.5 eq.), deionized water (1.9 mL), sodium acrylate (NaA) (548.1 mg, 5.8 mmol, 30.0 eq.) and acrylic acid (AA) (0.4 mL, 5.8 mmol, 30.0 eq.) were added sequentially to a 20 mL vial equipped with a stir bar. Iodoacetonitrile (ICH_2CN) (14.1 μL, 0.2 mmol, 1.0 eq.) and V70 (15.0 mg, 0.05 mmol, 0.25 eq.) were added, and the vial was sealed with a septum-cap. The reaction solution was degassed by purging with argon for 15 minutes. Then, the vial was transferred to a heating block and stirred at 35 °C and the polymerization was allowed to proceed for 21 hours. Afterwards the polymerization was stopped by opening the vial to expose the crude mixture to air. A small aliquot of the crude mixture was taken for NMR analysis to determine monomer conversion. The molar mass and $Đ$ of methylated PAA product were determined by SEC eluted with chloroform. For other monomer contents, the synthetic procedure was repeated except the content of AA in the monomer feed varied from 70–90 mol% as the monomer:iodoacetonitrile ratio was fixed.

Varying concentration of monomer in water

NaI (87.0 mg, 0.6 mmol, 1.5 eq.), deionized water (1.9 mL), sodium acrylate (NaA) (1.1 g, 11.7 mmol, 30.0 eq.) and acrylic acid (AA) (0.8 mL, 11.7 mmol, 30.0 eq.) were added sequentially to a 20 mL vial equipped with a stir bar. Iodoacetonitrile (ICH_2CN) (28 μL, 0.4 mmol, 1.0 eq.) and V70 (30.0 mg, 0.1 mmol, 0.25 eq.) were added, and the vial was sealed with a septum-cap. The reaction solution was degassed by purging with Argon for 15 minutes. The temperature probe was placed in the reaction solution to track the temperature during the polymerization. The vial was transferred to a heating block and stirred at 35 °C. The temperature was recorded every second and aliquots were taken from the polymerization mixture for NMR analysis to determine monomer conversion during the polymerization. For other monomer concentrations (15–33 wt% monomer in water), the polymerization procedure was followed as the concentration of monomers (AA and NaA) in water varied. The product was purified and methylated following the same procedure. The molar mass and $Đ$ of the methylated PAA product were determined by SEC eluted with chloroform.

Table S1. Copolymerization of AA and NaA mixture of varied overall monomer concentration (wt%) in water

entry	wt% monomer in water	conversion (%)[a]	M_n (exp) (g/mol)[b]	$Đ^b$
1	50	90	14000	1.64
2	33	87	11000	1.84
3	25	88	18000	1.48
4	15	94	12000	1.94

All polymerizations were performed in water at 35 °C, using AA (30.0 eq.), NaA (30.0 eq.), iodoacetonitrile (1.0 eq.), NaI (1.5 eq.), V70 (0.25 eq.). The polymerization was stopped after 30 minutes

(entry 1 and 2), 2 hours (entry 3) and 5 hours (entry 4). [a]Conversion was calculated by ^{1}H-NMR. [b]The molar mass and $Đ$ of methylated PAA samples were obtained from SEC analysis relative to PS standards using chloroform as eluent.

Synthesis of P(AA-*co*-NaA) at elevated temperature

NaI (43.7 mg, 0.3 mmol, 1.5 eq.), deionized water (1.9 mL), sodium acrylate (NaA) (548.1 mg, 5.8 mmol, 30.0 eq.) and acrylic acid (AA) (0.4 mL, 5.8 mmol, 30.0 eq.) were added sequentially to a 20 mL vial equipped with a stir bar. Iodoacetonitrile (ICH_2CN) (14.1 μL, 0.2 mmol, 1.0 eq.) and AIBN (8.0 mg, 0.05 mmol, 0.25 eq.) were added, and the vial was then sealed with a septum-cap. The reaction solution was degassed by purging with argon for 15 minutes. The vial was transferred to a heating block and stirred at 70 °C, and the polymerization was allowed to proceed for 19 hours. The polymerization was stopped by opening the vial to expose the crude mixture to air. A small aliquot of the crude mixture was taken for NMR analysis to determine monomer conversion. The molar mass and $Đ$ of methylated PAA product were determined by SEC eluted with chloroform. For other radical initiators, the synthetic procedure was repeated except V501 was substituted for AIBN as the free radical initiator.

Table S2. Copolymerization of AA and NaA in water using other radical initiators at elevated temperature

entry	radical initiator	temperature (°C)	conversion (%)[a]	M_n (exp) (g/mol)[b]	$Đ^b$
1	V70	35	90	12000	1.71
2	AIBN	70	>95	12000	1.53
3	V501	70	>95	11000	1.54

All polymerizations were performed for 19-21 hours using AA (30.0 eq.), NaA (30.0 eq.), iodoacetonitrile (1.0 eq.), NaI (1.5 eq.), radical initiator (0.25 eq.) (33 wt% monomer in water). [a]Conversion was calculated by ^{1}H-NMR. [b]The molar mass and *Đ* of methylated PAA samples were obtained from SEC analysis relative to PS standards using chloroform as eluent.

10-gram scale synthesis of P(AA-*co*-NaA)

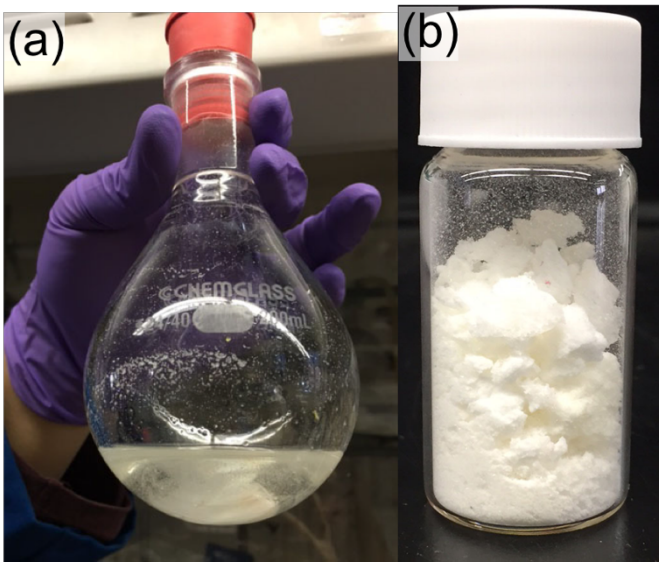

Figure S2. (a) Photo showing the 10-gram scale synthesis of P(AA-*co*-NaA) at the end of the polymerization. (b) Photo showing the crude mixture after lyophilizing as a white powder.

Acrylic acid (AA) (4.0 mL, 4.2 g, 5.8 mmol, 30.0 eq.), sodium acrylate (NaA) (5.5 g, 5.8 mmol, 30.0 eq.), NaI (440 mg, 0.3 mmol, 1.5 eq.) and deionized water (19 mL) were sequentially added to a 250 mL round bottom flask with a stir bar. Iodoacetonitrile (ICH_2CN) (140 μL, 1.9 mmol, 1.0 eq.) was added and the flask was then sealed with a septum. The reaction solution was degassed by purging with argon for 30 minutes, and V70 (150 mg, 0.5 mmol, 0.25 eq.) was then added under Argon atmosphere. The reaction flask was transferred to an oil bath and stirred at 35 °C and the polymerization was allowed to proceed for 22 hours. The polymerization was stopped by exposing the crude mixture to air. A small aliquot of the crude mixture was taken for NMR analysis to determine monomer conversion. The crude mixture was lyophilized to give a white powder (yield: 10 g, 99%). The product was purified and methylated following the same procedure. The molar mass and $Đ$ of methylated PAA product were determined by SEC eluted with chloroform.

Variation of molar mass of P(AA-*co*-NaA)

NaI (328 mg, 2.2 mmol, 1.5 eq.), deionized water (1.9 mL), sodium acrylate (NaA) (548.1 mg, 5.8 mmol, 4.0 eq.) and acrylic acid (AA) (0.4 mL, 5.8 mmol, 4.0 eq.) were added sequentially to a 20 mL vial equipped with a stir bar. Iodoacetonitrile (ICH_2CN) (105 μL, 1.5 mmol, 1.0 eq.) and V70 (112 mg, 0.4 mmol, 0.25 eq.) were added, and the vial was sealed with a septum-cap. The reaction solution was degassed by purging with Argon for 15 minutes. Then the vial was transferred to a heating block and stirred at 35 °C, and the polymerization was allowed to proceed for 20 hours. The polymerization was stopped by opening the vial to expose the crude mixture to air. A small aliquot of the crude mixture was taken for NMR analysis to determine monomer conversion. For other monomer-to-iodoacetonitrile ratios, the

polymerization procedure was followed with the total molar equivalents of monomers (AA and NaA) to ICH_2CN varied from 15, 30, 60 to 90, and fixed quantities of monomer and solvent. The product was purified and methylated following the same procedure. The molar mass and $Đ$ of methylated PAA product were determined by SEC eluted with chloroform.

4.6 References

1) K.F. Fazende, M. Phachansitthi, J. D. Mota-Morales, J. A. Pojman, *J. Polym. Sci. Part A: Polym. Chem*. **2017**, *55*, 4046-4050.
2) T. Spychaj, *Prog. Org. Coat.* **1989**, *17*, 71-88.
3) M. R. J., C. Gerardo, M. Paola, Y. M. M., G.-S. Manuel, V. J. R. and G. L. M., *Macromol. React. Eng.* **2011**, *5*, 223-231.
4) J. Loiseau, N. Doërr, J. M. Suau, J. B. Egraz, M. F. Llauro, C. Ladavière and J. Claverie, *Macromolecules* **2003**, *36*, 3066-3077.
5) K. Matyjaszewski and J. Xia, *Chem. Rev*. **2001**, *101*, 2921-2990.
6) C. J. Hawker, A. W. Bosman and E. Harth, *Chem. Rev.* **2001**, *101*, 3661-3688.
7) G. Moad, E, Rizzardo, S. H. Thang, *Chem. Asian J.* **2013**, *8*, 1634-1644.
8) M. Fantin, A. A. Isse, A. Venzo, A. Gennaro and K. Matyjaszewski, *J. Am. Chem. Soc*. **2016**, *138*, 7216-7219.
9) K. A. Davis and K. Matyjaszewski, *Macromolecules* **2000**, *33*, 4039-4047.
10) Z. A. Page, R. Bou Zerdan, W. R. Gutekunst, A. Anastasaki, S. Seo, A. J. McGrath, D. J. Lunn, P. G. Clark and C. J. Hawker, *J. Polym. Sci. Part A: Polym. Chem*. **2016**, *54*, 801-807.
11) L. Couvreur, C. Lefay, J. Belleney, B. Charleux, O. Guerret and S. Magnet, *Macromolecules* **2003**, *36*, 8260-8267.
12) C. Ladavière, N. Dörr and J. P. Claverie, *Macromolecules* **2001**, *34*, 5370-5372.
13) J. Ji, L. Jia, L. Yan and P. R. Bangal, *J. Macromol. Sci, Part A*. **2010**, *47*, 445-451.
14) I. Chaduc, A. Crepet, O. Boyron, B. Charleux, F. D'Agosto and M. Lansalot, *Macromolecules* **2013**, *46*, 6013-6023.

15) T. J. Romack, E. E. Maury and J. M. DeSimone, *Macromolecules* **1995**, *28*, 912-915.

16) Q. Xu, B. Han and H. Yan, *Polymer* **2001**, *42*, 1369-1373.

17) C.-H. Peng, M. Fryd and B. B. Wayland, *Macromolecules* **2007**, *40*, 6814-6819.

18) D. Grande, R. Guerrero and Y. Gnanou, *J. Polym. Sci. Part A: Polym. Chem*. **2004**, *43*, 519-533.

19) J. Sarkar, L. Xiao and A. Goto, *Macromolecules* **2016**, *49*, 5033-5042.

20) L. Xiao, K. Sakakibara, Y. Tsujii and A. Goto, *Macromolecules* **2017**, *50*, 1882-1891.

21) A. Goto, A. Ohtsuki, H. Ohfuji, M. Tanishima and H. Kaji, *J. Am. Chem. Soc*. **2013**, *135*, 11131-11139.

22) C.-G. Wang and A. Goto, *J. Am. Chem. Soc*. **2017**, *139*, 10551-10560.

23) S. G. Gaynor, J.-S. Wang and K. Matyjaszewski, *Macromolecules* **1995**, *28*, 8051-8056.

24) M. C. Iovu and K. Matyjaszewski, *Macromolecules* **2003**, *36*, 9346-9354.

25) K. Matyjaszewski, S. Gaynor and J.-S. Wang, *Macromolecules* **1995**, *28*, 2093-2095.

26) R. A. Scott and N. A. Peppas, *AIChE Journal* **1997**, *43*, 135-144.

27) S. Khanlari and M. A. Dubé, *J. Macromol. Sci, Part A*. **2015**, *52*, 587-592.

28) M. Uhniat, R. Sikorski and L. Woroszilo, *Polym. Sci. U.S.S.R.* **1981**, *23*, 2622-2627.

29) M. G. Cáceres, G. C. G., V. S. E., M. R. J., V. J. R. and G. L. M., *Macromol. React. Eng.* **2017**, *11*, 1600049.

30) M. Daniel, P. Martina, K. Rodrigo, S. Nathalie and P. J. Carlos, *Macromol. Symp.* **2016**, *368*, 49-59.

31) U. Capasso Palmiero, A. Chovancová, D. Cuccato, G. Storti, I. Lacík and D. Moscatelli, *Polymer* **2016**, *98*, 156-164.

32) L. Couvreur, B. Charleux, O. Guerret and S. Magnet, *Macromol. Chem. Phys.* **2003**, *204*, 2055-2063.

33) D. Benoit, V. Chaplinski, R. Braslau and C. J. Hawker, *J. Am. Chem. Soc*. **1999**, *121*, 3904-3920.

5. Conclusion and Outlook

5.1 Conclusion

Controlled radical polymerization techniques have benefited greatly in the synthesis of polymers with predefined molecular weight and dispersity. The ability to precisely control polymer brush growth has enabled applications ranging from anti-fogging, anti-fouling, chemical sensing to biomedical applications. In this dissertation, surface-initiated polymerization has been introduced in Chapter 1 using atom transfer radical polymerization technique. Moreover, photoinduced polymerization has also been described with the ability to provide excellent spatial and temporal control over polymer brush growth. The development of metal-free photoredox catalyst and oxygen tolerance in controlled radical polymerization have also been discussed. In addition, the polymerization of acrylic acid has been introduced.

In Chapter 2, a new synthetic strategy to prepare hierarchical comb brush architectures is reported. Linear copolymer brushes of methyl methacrylate and 2-hydroxyethyl methacrylate were prepared via light-mediated polymerization using *fac*-[$Ir(ppy)_3$] as a photoredox catalyst. Subsequently, the bromide chain ends were deactivated with ethyl vinyl ether by light-mediated atom transfer radical addition. Then, 2-hydroxyethyl methacrylate side chains are functionalized with initiators for a secondary polymerization affording branched polymer brush architectures.

In Chapter 3, the fabrication of well-defined, multifunctional polymer brushes under ambient conditions using microliter volumes is described. This facile strategy uses light-

mediated metal-free atom transfer radical polymerization coupled with simple glass cover slips. *N*-phenylphenothiazine acts as both an oxygen scavenger and photoredox catalyst for the polymerization. The glass cover slip serves as a vertical barrier for oxygen diffusion resulting in excellent spatial control over polymer brush growth allowing the fabrication of multiple polymer brushes simultaneously on the same silicon wafer.

In Chapter 4, copolymerization of acrylic acid and sodium acrylate in water at mild temperature is reported. This system is designed for environmentally-friendly and industry-oriented syntheses to afford poly(acrylic acid) with moderate control over molar mass and dispersity. The polymerization uses monomer mixture with alkyl iodide and sodium iodide as mediators in water without expensive reagents exhibiting high conversion in a short period of time. The parameters such as thermal initiators, alkyl iodides, monomer concentrations, fraction of acrylic acid in monomer mixture have been studied. This polymerization represents user-friendly and scalable synthesis for poly(acrylic acid).

5.2 Future directions and outlook

The development of synthetic strategies in this dissertation demonstrates the practicality and versatility which can be useful for a wide range of applications. It will encourage further multidisciplinary investigation in the area of chemistry, biotechnology and material science. For example, the development of polymer brush growth on a variety of substrates (glass, plastic, membrane) including flexible or curved surfaces are of particular interest and could benefit from the synthetic strategies presented in this dissertation. Moreover, the study of area-selective polymer brush growth on heterogeneous substrates such as metal/Si surfaces could be useful for self-aligning material deposition for nanoelectronic devices. The selective deposition on the vertical surface of 3D nanostructures is also interesting and could be

beneficial to atomic layer deposition applications. In addition, the development of polymer brush growth via photoinduced cationic polymerization and photoinduced electron transfer reversible addition fragmentation chain transfer polymerizations can expand the monomer scope allowing a variety of materials to be obtained. Finally, the synthetic strategy for poly(acrylic acid) presented in this dissertation can be tailored for other acidic monomers which is difficult to prepare using other polymerization techniques.

Appendix A

Engineering Surfaces through Sequential Stop-Flow Photopatterning[3]

[3] Reproduced with permission: Pester, C. W.; **Narupai, B.**; Mattson, K. M.; Bothman, D. P.; Klinger, D.; Lee, K. W.; Discekici, E. H.; Hawker, C. J. "Engineering Surfaces through Sequential Stop-Flow Photopatterning." *Adv. Mater.* **2016,** *28*, 9292-9300. DOI: 10.1002/adma.201602900. Copyright 2016, Wiley. License Number: 4440481396870.

ADVANCED MATERIALS
www.advmat.de

Materials Views
www.MaterialsViews.com

Engineering Surfaces through Sequential Stop-Flow Photopatterning

Christian W. Pester, Benjaporn Narupai, Kaila M. Mattson, David P. Bothman, Daniel Klinger, Kenneth W. Lee, Emre H. Discekici, and Craig J. Hawker**

Dedicated to Prof. Edward J. Kramer

Polymer films are scientifically and industrially relevant for a broad collection of applications, ranging from marine paints[1] and biomedical devices[2] to flame-retardant coatings.[3] Their fabrication typically involves physisorption-based techniques,[4] such as spray-, dip- or spin-coating, which modify surface properties uniformly. While effective, these physisorption strategies do not provide the ability to pattern films, inherently limiting polymer coatings to a single functionality or physical property.

To address this limitation, the covalent attachment of polymers has emerged as a viable strategy for the preparation of multifunctional surfaces, either by grafting polymers to, or growing them from a surface via surface-initiated controlled radical polymerization (SI-CRP).[5,6] Here, external regulation of SI-CRP,[6–10] e.g., via light, plays a crucial role in controlling the distribution of surface functional groups.[11–13] Such topographically and/or chemically patterned polymer brushes are valuable for a plethora of interdisciplinary applications.[14–20] For example, they allow fabrication of "intelligent" substrates which selectively adapt to their environment on the microscale or nanoscale[21] through spatial control of wetting,[22] mechanical,[23–25] biological,[26–28] or electronic[29] properties. A series of recent reviews highlight both the capabilities and drawbacks of current 2D and 3D polymer brush patterning techniques.[14–20]

Polymer brushes can be patterned via either "bottom-up"[13,30–34] or "top-down"[35,36] strategies. Soft lithography[37–39] is a prominent example for a contact-based bottom-up approach: elastomeric stamps are used to print patterns of polymerization initiators, which can subsequently be amplified via SI-CRP. In contrast, top-down strategies, e.g., e-beam lithography, locally remove either surface-anchored initiators (prior to SI-CRP), or previously grown polymer brushes. As a result, chemical patterning of surfaces with polymer brushes traditionally requires iterative: i) initiator deposition, ii) pattern amplification via SI-CRP, and iii) polymer chain end deactivation. These multiple steps (plus related rinsing and cleaning steps) are repeated for each additional polymeric species, rapidly increasing the amount of required processing steps for even simple patterned surfaces. Such repetitive methodologies are therefore challenging,[40] creating a demand for more efficient and less complicated fabrication strategies.

An ideal process would combine the benefits of: i) a synthetically facile, high throughput approach with ii) the ability to create multiple levels of patterning via a continuous process. In analogy with traditional photolithography, light represents a mild non-contact stimulus capable of mediating numerous chemical reactions.[5,7–9,32,33,41–45] In tandem with a variety of additional post polymerization functionalization procedures,[46] photochemistry also allows the spatially controlled incorporation and immobilization of an array of different functional units on surfaces.

Here, the combination of stopped-flow techniques[47] and reduction photolithography is decribed,[48] to engineer a modular platform for sequential photochemical reactions in a continuous manner. This facilitates chemical surface patterning through successive exchange of reactants within a stop-flow cell, while providing significant flexibility to exchange light sources, and/or spatially decoupled photomasks. **Scheme 1** illustrates such a photochemical sequence: Spatially controlled photopolymerization, followed by exchange of the solution within the stop-flow cell, and then secondary functionalization of polymer brushes, in this case by light-mediated removal of the active terminal bromine chain end. During this entire process, neither wafer nor photomask are moved, which allows spatial confinement of functionalization exclusively to regions where polymer brushes were previously grown. As a direct consequence, adjacent surface-grafted polymerization initiators remain untouched, affording hierarchical chemical patterning on uniformly functionalized

Dr. C. W. Pester, B. Narupai, K. M. Mattson, E. H. Discekici, Prof. C. J. Hawker
Materials Research Laboratory (MRL)
University of California, Santa Barbara
Santa Barbara, CA 93106, USA
E-mail: pester@mrl.ucsb.edu; hawker@mrl.ucsb.edu
Dr. C. W. Pester, Prof. C. J. Hawker
Materials Department
University of California, Santa Barbara
Santa Barbara, CA 93106, USA
B. Narupai, K. M. Mattson, E. H. Discekici, Prof. C. J. Hawker
Department of Chemistry and Biochemistry
University of California, Santa Barbara
Santa Barbara, CA 93106, USA
Dr. D P. Bothman
Department of Mechanical and Environmental Engineering
University of California, Santa Barbara
Santa Barbara, CA 93106, USA
Prof. D. Klinger
Institut für Pharmazie
Freie Universität Berlin
14195 Berlin, Germany
K. W. Lee
Department of Physics
University of California
Santa Barbara, CA 93106, USA

DOI: 10.1002/adma.201602900

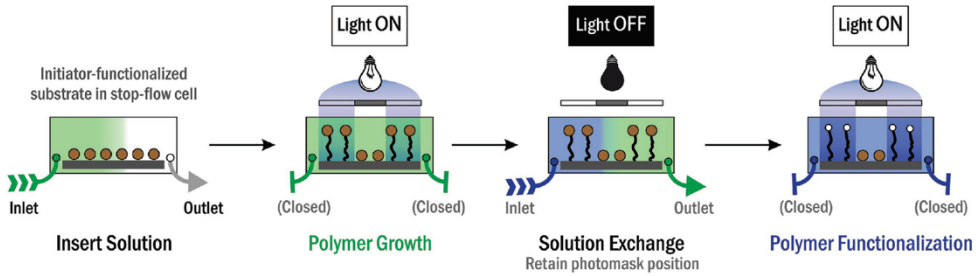

Scheme 1. Concept of solution-exchange lithography. Enclosing a substrate in a stop-flow cell allows for in situ exchange of reactants and execution of successive chemical reactions at precisely the same location. Illustrated here is light-mediated growth of polymer brushes followed by solution exchange and subsequent, spatially controlled passivation of the active polymer chain ends.

substrates. This renders repetitive initiator deposition and related cleaning/treatment steps unnecessary and results in economic and environmental advantages. Ultimately, this solution-exchange lithography concept streamlines the production of chemically patterned surfaces and affords access to hierarchically structured substrates, all from uniform initiating layers.

The experimental setup involves an array of lenses to optically reproduce 1:1, magnify, or reduce and project an inkjet-printed photomask onto a substrate positioned inside a stop-flow cell (see **Figure 1**). This stop-flow cell was readily scaled to accommodate large wafers of Ø = 7.6 cm (3 in.) diameter, enhancing both the relevance and potential of this process, with the immediate proximity between cover glass and substrate allowing capillary forces to uniformly spread the reactants over the surface (see Figure S1, Supporting Information). This uniform spreading allows production of homogeneous uniform polymer brush films with thicknesses of up to 120 ± 2 nm as determined by optical reflectometry. Reduction projection reproduces the image from an original photomask on a surface with reduced size. This concept facilitates alignment and/or stacking of multiple patterns by eye, paving a path toward complex microscopic patterns from macroscopic photomasks. The ratio of the focal lengths of the two lenses (f_1 and f_2) determines the linear reduction factor (LRF) = f_1/f_2, which could readily be adjusted by simply exchanging lenses. For this work, focal lengths of f_1 = 500 mm and f_2 = 100 mm were used, resulting in optical reduction by a factor of five (area reduction to 1/25th of the original photomask). This spatial decoupling (separating) of the photomask(s) from the substrate has a number of benefits. The noncontact-based nature allows use of inexpensively produced, inkjet-printed photomasks. If desired, simple *x*,*y*-translation of the substrate stage allows lateral repetition of either a single or multiple patterns. In addition, all processing steps, including chemical reactions, rinsing, and drying can be performed without removing the substrate from its original position. This allows successive, spatially well-defined (photo)chemical reactions to be performed sequentially from uniform initiating layers, including but not limited to both traditional[10] and light-mediated controlled radical polymerization,[5,7–9,32,33,41,42] dehalogenation,[43] thiol-ene coupling,[49,50] and atom transfer radical addition.[44,45] As an added benefit, the stop-flow cell is sealed from the surrounding environment and is readily filled via cannula transfer. This enables oxygen-sensitive reactions to be performed under simple conditions, without the need for a glove box or other Schlenk-technique related equipment (see the Experimental Section).

Figure 2 demonstrates the potential of this setup for the controlled radical photopolymerization[8,13,32] growth of patterned poly(methyl methacrylate) (poly(MMA)) brushes with high spatial fidelity (see Figure 2b,e, and Figure S2, Supporting Information). The resulting topographical patterning was revealed

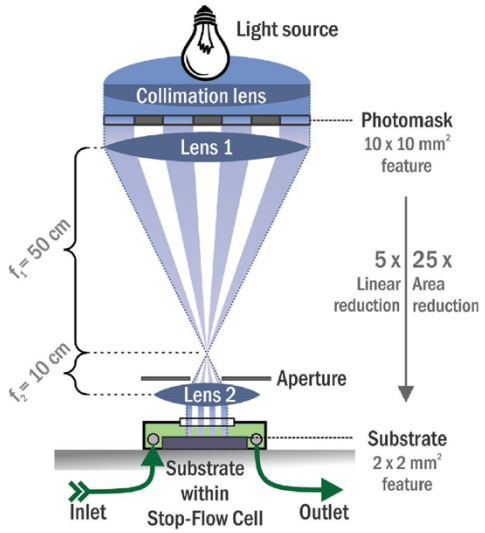

Figure 1. Schematic of solution-exchange lithography. An array of lenses is used to project the pattern of a photomask onto a substrate that is enclosed in a stop-flow cell. At focal lengths of f_1 = 50 cm and f_2 = 10 cm, this projector reduces features of the photomask image by a linear reduction factor of LRF = 5 (25× reduction in area) and reproduces them on the surface. Spatially decoupling the stop-flow cell from the photomask allows exchange of solutions while retaining the exact position of the photomask, enabling sequential stop-flow photochemistry.

ADVANCED MATERIALS
www.advmat.de
Materials Views
www.MaterialsViews.com

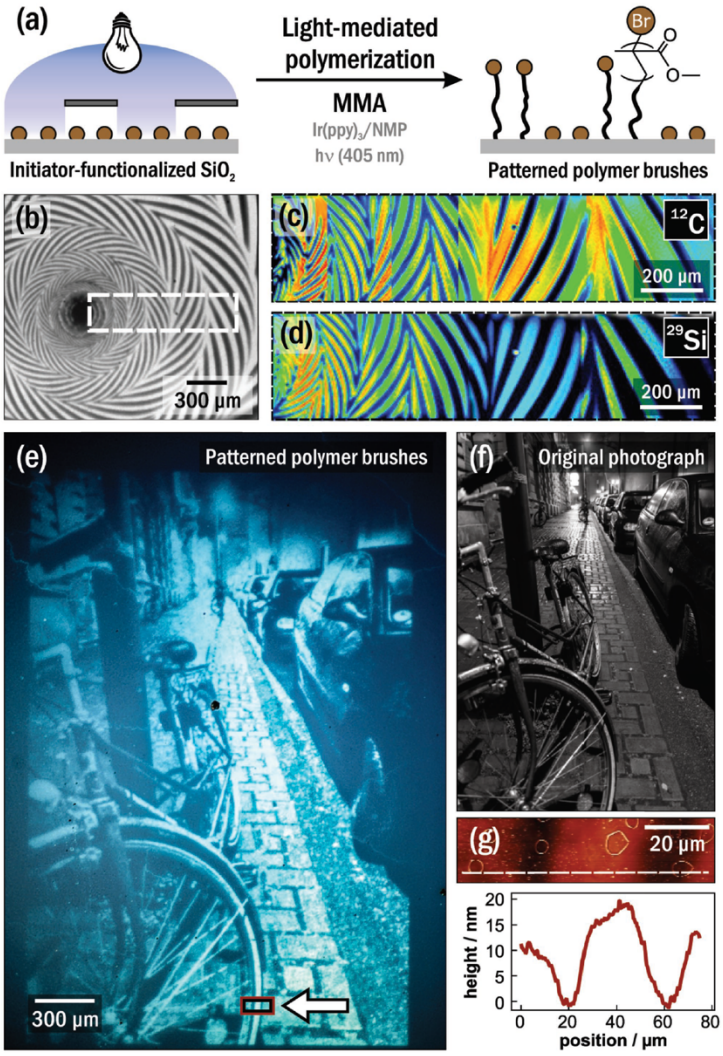

Figure 2. a) Schematic of light-mediated controlled radical polymerization of methyl methacrylate (MMA) by irradiation of an initiator-functionalized SiO_2 substrate through a binary photomask. The brown circles indicate the polymerization initiators. For clarity, both the detailed projection setup (see Figure 1) and the stop-flow cell (see Scheme 1) are omitted. b) Optical-microscopy image of poly(MMA) brushes (light) on SiO_2 (dark). The dashed rectangle in (b) indicates where the secondary-ion mass-spectrometry element maps of carbon (m/z =12 (c)) and silicon (m/z = 29 (d)) fragments were obtained. e,f) A patterned poly(MMA) brush reproduction (e) of an original photograph (f), which was taken by C. W. Pester. The reproduction illustrates the achievable spatial resolution and complexity. The original photomask was reproduced on the substrate at 1/25th its original size, allowing for the production of multiple different polymer-brush-height gradients in close proximity and in a single polymerization step. g) Atomic force microscopy image of the square area indicated in (e), and the corresponding line cut (dashed line) indicates a polymer brush height of up to 20 nm.

by optical microscopy and atomic force microscopy (AFM), which showed a patterned polymer brush thickness of 20 nm after 30 min of light-mediated controlled radical polymerization (see Figure 2g and the Experimental Section). In secondary-ion mass spectrometry (SIMS), carbon (m/z = 12, poly(MMA)) fragment maps further indicated successful reproduction of the

original photomask image (see Figure 2c). Correspondingly, silicon ($m/z = 29$) was detected exclusively in regions of the silicon dioxide (SiO_2) substrate where the photomask blocked the light and no polymer was grown (see Figure 2d). At LRF = 5, the total area of the resulting reduced pattern (2 mm × 2 mm) was 4% of the original inkjet-printed photomask (10 mm × 10 mm). The smallest obtainable line features are a function of both initial feature sizes and optical reduction. For the experiments described herein, features as small as 2 µm were obtained (see Figure 2b). As previously reported, simple variation of either polymerization time and/or photon flux may be used to target different brush heights, and a majority of polymer chain ends remain active for additional functionalization or further growth.[13,32,33] The rate of polymer brush growth is a function of the distance between the substrate and light source (d_{LED}), as well as the intensity of the incident light.[33] For the experiments depicted in this report, we utilized constant substrate-to-light source distances of $d_{LED} = f_1 + f_2 = 600$ mm (for the projection of patterns), or $d_{LED} = 15$ mm (for the growth of uniform polymer brush layers). At $d_{LED} = 600$ mm, we could regulate light intensities between 6.88 and 173.6 µW mm^{-2} (confined to a spot size of 0.25 cm^2), which would allow for modulation of the polymerization kinetics if desired.[33] The polymer brush patterns described in this contribution were all produced using an intensity of 5.6 µW mm^{-2} at $d_{LED} = 600$ mm, which afforded linear polymer brush growth (see Figure S3, Supporting Information) This patterning approach was shown to be compatible with both conventional photomasks as well as with inkjet-printed overhead transparencies (see Figure 2b,e), affording the reproduction of arbitrarily complex patterns and manufacturing of surfaces combining numerous polymer brush height gradients on a single substrate.

The ability to exchange reactants in situ while retaining the position of the photomask is a significant advantage when chemically patterning polymer brushes. The use of sequential photochemical reactions allows preparation of chemically versatile surfaces, as demonstrated in the following by preparation of binary polymer brush patterns. Such binary patterned substrates offer lateral combination of different functional materials with contrasting physical properties and represent an intriguing pathway toward surfaces which selectively adapt to their environment.[21] However, in conventional processes, the preparation of binary polymer brushes with microscale feature sizes requires tedious and iterative deposition of initiator patterns, subsequent pattern amplification (via SI-CRP), followed by chain end passivation (vide supra).[38] To the best of our knowledge, no established method has been capable of fabricating binary patterned brushes from uniform initiator layers.In contrast, the setup described herein allows for the preparation of binary brushes from a uniform initiating layer via sequential stop-flow photochemistry. Eliminating the repetitive initiator deposition steps not only facilitates processing, but also prevents related chemical contamination. **Figure 3**a illustrates the formation of such a chemically patterned, binary surface with disparate wetting properties. Initially, patterned poly(ethylene glycol) methacrylate (PEGMA) brushes were grown by irradiation through a photomask. AFM indicated a thickness of the patterned polymer brushes of 13 nm after 15 min of irradiation at $\lambda = 405$ nm through a photomask. Then, without moving the photomask, reactants within the stop-flow cell were exchanged and a solution of a highly reducing photocatalyst was inserted to promote spatially controlled dehalogenation of the polymer brush chain end.[43] Because the photomask remains in its original position, this subsequent, light-mediated passivation reaction is locally confined to where the initial PEGMA polymerization occurred. The poly(PEGMA) brushes are therefore selectively deactivated and cannot participate in subsequent polymerizations. Surface-bound polymerization initiators that did not participate in the initial polymerization remain active and allow a third sequential reaction to be performed, i.e., growth of 1*H*,1*H*,2*H*,2*H*-perfluorooctyl methacrylate (PFOMA) polymer brushes via atom transfer radical polymerization (ATRP). Optical microscopy (Figure 3b–d) and SIMS (Figure 3e,f) confirmed the topographical and binary chemical nature of the resulting substrate with fluorine ($m/z = 19$, poly(PFOMA)) and oxygen ($m/z = 16$, poly(PEGMA)) fragment maps matching the positive and negative representation of the original photomask, respectively. These binary patterns were also accessible by substituting the dehalogenation step (cf. Figure 3a) with spatially controlled chain end passivation via atom transfer radical addition (see Figure S6, Supporting Information),[44,45] highlighting the compatibility of this platform with a range of light-mediated reactions.

The preparation of binary hydrophilic poly(PEGMA) and hydrophobic poly(PFOMA) brushes from incompatible monomers further serves to demonstrate the breadth of accessible materials. Their significantly contrasting wetting properties are evident from their water contact angles, $\theta_{PEGMA} = 61°$ and $\theta_{PFOMA} = 120°$, which, according to the Young–Dupré equation, correspond to surface energies of $W_{poly(PEGMA)} = 0.11$ J m^{-2} and $W_{poly(PFOMA)} = 0.04$ J m^{-2}, respectively (see Figure S5, Supporting Information).[51] Spatially confined, hydrophilic poly(PEGMA) regions are observed to selectively swell upon rising humidity (see Figure 3c), increasing the poly(PEGMA) brush height and promoting localized water droplet formation, i.e., selective wetting (Figure 3d). The synthesis of such continuous binary patterns from uniform initiating layers offers significant opportunities and directly relies on the ability to exchange reactants in situ, allowing for sequential photochemical procedures while retaining the position of the photomask.

In addition to the exchange of solutions, the modular nature of this strategy also allows substitution of photomasks and/or light sources during the modification of a single substrate. This feature is illustrated by successively performing a series of photochemical reactions while exchanging both the photomask and the light source (i.e., the wavelength). Initially, a 51.1 ± 0.5 nm thick, homogeneous poly(PEGMA-*co*-VMA) (where VMA is vinyl methacrylate), 50:50 mol%) copolymer brush layer was grown by uniformly irradiating the substrate for 10 min. X-ray photoelectron spectroscopy (XPS) confirmed the targeted 50 mol% incorporation of vinyl functionalities (see the Supporting Information). Without changing the position of the substrate, the reactants within the stop-flow cell were exchanged and a subsequent thiol-ene coupling reaction was performed. **Figure 4**a illustrates radical addition of a hydrophobic 1*H*,1*H*,2*H*,2*H*-perfluorodecanethiol (PFDT) across

ADVANCED MATERIALS
www.advmat.de
www.MaterialsViews.com

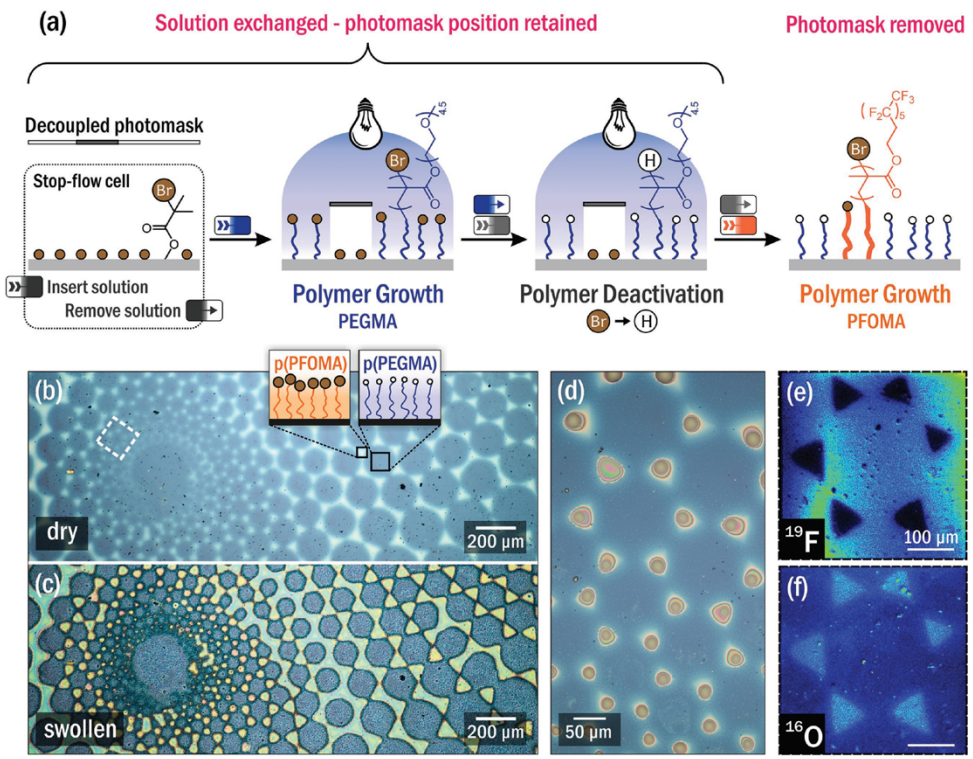

Figure 3. a) Formation of binary brushes via a cascade of sequential photochemical reactions. The substrate is enclosed in the stop-flow cell throughout this process. For clarity, we omitted displaying the stop-flow cell and the projection setup (compare with Figure 1). Photopolymerization of PEGMA is followed by light-mediated dehalogenation (local deactivation of polymer brush chain ends). The photomask remains in place while reactant solutions are exchanged. Lastly, the photomask is removed and PFOMA is polymerized via atom transfer radical polymerization. The color-coded boxes above the arrows indicate the experimental procedure of inserting or removing reactant solution. b) Optical bright-field image of dry binary polymer brushes. c) Lateral combination of hydrophilic and hydrophobic properties allows for selective swelling in a high humidity environment. d) Water droplets are formed exclusively in hydrophilic regions. e,f) Secondary-ion mass spectrometry indicates spatial confinement of fluorine (e) and oxygen (f) fragments, providing additional evidence for the chemically binary nature of the surface. The ^{16}O and ^{19}F maps obtained from the dashed white rectangular region in (b) represent the positive and negative of the original photomask, respectively.

the pendant vinyl functionalities present in the hydrophilic poly(PEGMA-*co*-VMA) copolymer brush. As a result, a novel surface-tethered bottle brush architecture with statistically distributed side arms of different polarities was obtained. XPS indicated the appearance of both fluorine and sulfur peaks and allowed quantitative determination of the efficiency of the thiol-ene reaction (≈79 % yield) within the outermost 10 nm of the polymer brush (see Figure 4b–d and Supporting Information). Highlighting the ability of this modular platform to exchange light sources, thiol-ene coupling was successfully performed both under UV (λ = 365 nm)[49] as well as under visible-light (λ = 405 nm) irradiation (see the Experimental Section).[50]

Traditionally, patterning with materials of such distinctly dissimilar polarities, i.e., PEGMA and PFDT, is considered difficult. For example, the initial polymer brush may render the substrate too hydrophobic (or hydrophilic) for uniform wetting and subsequent, spatially controlled functionalization. Here, this challenge is mitigated by the immediate proximity of the cover glass, which allows capillary action to serve as the driving force to uniformly spread the reactants over the substrate. Indeed, as illustrated in **Figure 5**a, PFDT is readily incorporated with spatial control by irradiation of a poly(PEGMA-*co*-VMA) coated substrate through a photomask. In optical microscopy (see Figure 5b), darker areas can be identified as PFDT-functionalized poly(PEGMA-*co*-VMA/PFDT) bottlebrushes. The addition of PFDT into the polymer brush backbone locally increases density (and brush height) to yield optical contrast. Optical reflectometry and AFM indicated a localized increase in polymer brush thickness from 60.2 ± 3.0 nm to a total bottlebrush height of 70.0 ± 3.1 nm. Chemical patterning was

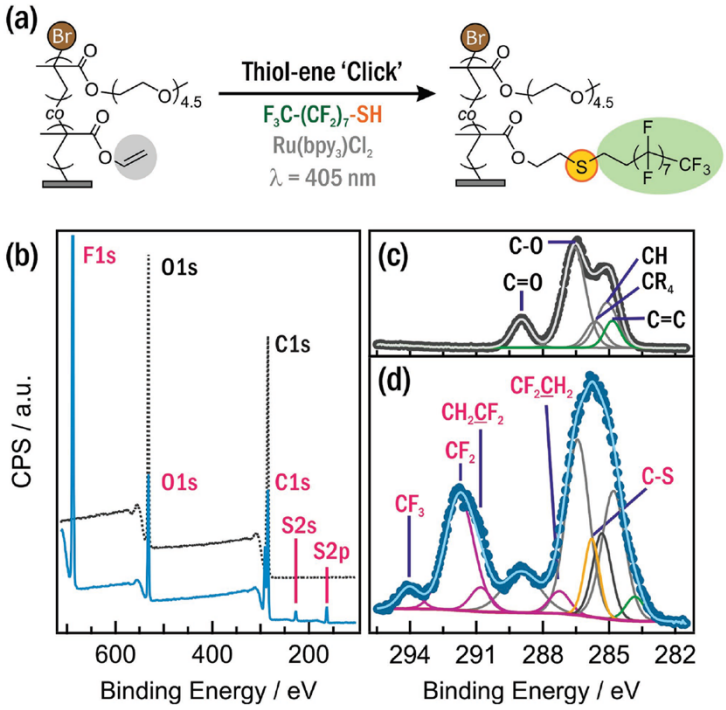

Figure 4. a) Light-mediated thiol-ene coupling of pendant vinyl groups in poly(PEGMA-*co*-VMA) polymer brushes with 1*H*,1*H*,2*H*,2*H*-perfluorodecanethiol (PFDT) to form bottlebrush architectures with hydrophilic and hydrophobic sidearms. b) Fluorine (F1s) and sulfur (S2s and S2p) peaks in the X-ray photoelectron spectrum indicate successful formation of poly(PEGMA-*co*-VMA/PFDT) bottlebrushes. The dashed gray and solid blue lines correspond to the initial and the thiol-ene treated film, respectively. High-resolution XPS carbon C1s scans of both c) the initial and d) thiol-ene functionalized film. A sum of Gaussian bell curves (solid lines) was used to fit experimental data (bullets) and quantify binding energies and ratios of individual chemical components.

verified by mapping fluorine (m/z = 19, Figure 5b, inset) fragments in SIMS, which were detected exclusively where PFDT was incorporated into the polymer brush.

A key advantage of this experimental setup is the capability to hierarchically pattern substrates from uniform initiator monolayers (vide supra). Notably, sequential functionalization is now also possible on previously grown (uniform or patterned) polymer brushes, enhancing the scope of accessible substrates and materials. This benefit is illustrated by chain-extending patterned poly(PEGMA-*co*-VMA/PFDT) bottlebrushes with methyl methacrylate (MMA) to form poly(PEGMA-*co*-VMA/PFDT)-*b*-poly(MMA) diblock architectures (see Figure 5a). Starting from the spiral pattern shown in Figure 5b, exchange of both the solution and the photomask allowed a second, different pattern to be fabricated on the initial polymer brush surface. Optical microscopy (Figure 5c) confirmed the presence of two patterns, corresponding to the initial thiol-ene patterned spiral (cf. Figure 5b), superimposed by poly(MMA) rectangles. Demonstrating the chemical and topographical possibilities, this surface combines three monomers, one thiol-ene functionalization, and two different patterns. Significantly, the resulting four, distinct polymer brush architectures, each with discrete chemical properties, were obtained by only three sequential photochemical processing steps from a uniform initiating layer.

In conclusion, this contribution illustrates the versatility and modular nature of solution-exchange lithography as a novel platform for surface patterning. This approach circumvents the need for repetitive initiator deposition, as is common in many conventional techniques, and allows preparation of patterned surfaces with large topographical and chemical variety from uniform initiating monolayers. Key to these advances is the ability to exchange reaction solutions in situ, leading to homogeneous wetting of substrates with solutions of vastly contrasting polarity. Eliminating the necessity to remove the substrate between individual processing steps enables successive reactions to be performed in the same location with microscale resolution. In addition, all procedures, including oxygen-sensitive reactions, can now be performed in a closed stop-flow cell and without the necessity of a glove box, while

ADVANCED MATERIALS
www.advmat.de
www.MaterialsViews.com

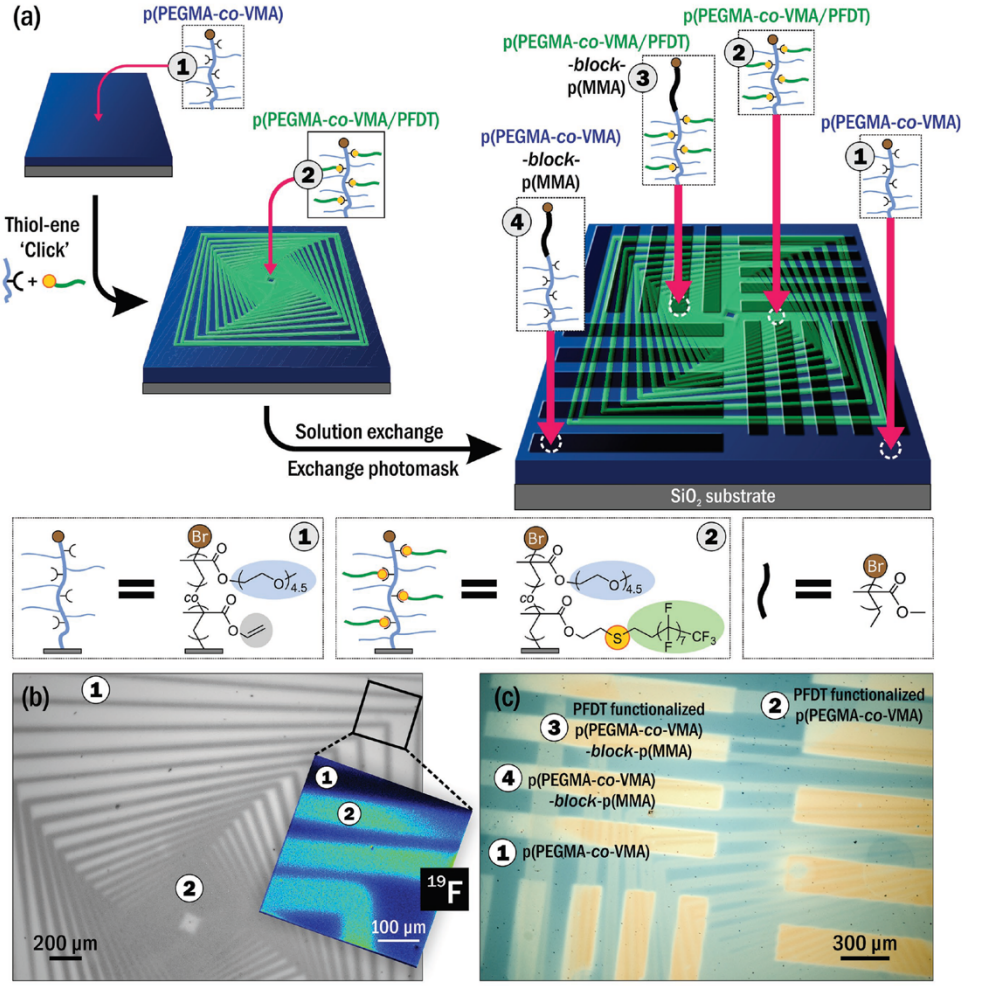

Figure 5. a) Schematic of sequential, different photochemical reactions performed without tampering with the substrate. A homogeneous poly(PEGMA-*co*-VMA) (**1**) copolymer layer was grown, then locally functionalized via thiol-ene "click" chemistry (see Figure 4) to form poly(PEGMA-*co*-VMA/PFDT) bottlebrushes (**2**). b) Both optical microscopy and ^{19}F secondary-ion mass spectrometry maps (inset) confirm the resulting chemical "spiral" pattern. The light and dark areas in the optical image correspond to the initial poly(PEGMA-*co*-VMA) brush layer and PFDT-functionalized bottlebrushes, respectively. Subsequently, while leaving the substrate in place, both the solution and the photomask were exchanged. Chain extension via spatially controlled photopolymerization of methyl methacrylate (MMA) results in a rectangular pattern of poly(PEGMA-*co*-VMA/PFDT)-*b*-poly(MMA) (**3**) and poly(PEGMA-*co*-VMA)-*b*-poly(MMA) (**4**) diblock regions. c) Optical microscopy showed the overlay of two distinctly dissimilar patterns and confirmed the formation of hierarchical 3D polymer brushes. The optical image of the resulting hierarchical 3D polymer brushes showed both the initial thiol-ene spiral pattern (cf. b), and the rectangular poly(MMA) pattern.

the decoupling of photomask and wafer allows the use of inexpensive, inkjet-printed overhead transparencies as photomasks, significantly reducing both time and cost related to fabrication of standard photomasks. We believe the platform described herein offers a facile strategy for the highly reproducible and streamlined production of topographically- and chemically diverse patterned polymer brush surfaces from uniform initiating layers.

Experimental Section

General Reagent and Setup Information: Silicon substrates with 100 nm oxide were purchased from Silicon Quest International. Monomers and other chemicals were obtained from Sigma–Aldrich and, unless otherwise noted, used without further purification. The stop-flow cell was custom designed. All projector parts, including light source, posts, holders, and lenses where obtained by Thorlabs. Thorlabs Olympus BX & IX series (λ = 365 and 405 nm) collimated light-emitting diodes (LEDs) were used for all light-mediated reactions. LED light intensities were modulated by a Thorlabs LED D1B T-cube driver and measured by a Newport optical power/energy meter model 842 PE with a Newport 884-IGR OD3 attenuator.

General Procedure for Oxygen-Free Filling of the Cell: The reagent solution was placed in a reaction vial and degassed by passing a continuous stream of dry argon through the solution. The outlet was connected to the stop-flow cell, while simultaneously purging the reaction chamber. After 10 min of sparging both solution and the stop-flow cell, the reagent was transferred into the stop-flow cell via a cannula transfer process. The required time for this filling process can be adjusted by regulating the pressure of the inert gas. Experimentally, slow filling (approx. 30 s) has proven most successful for uniform substrate wetting. Finally, the outlet and inlet valves were closed (in that order) and the stop-flow cell was left to react for a given amount of time (with either the light source on or off). For multistep processes, the chamber was rigorously rinsed with 10 mL of *N*-methyl-2-pyrrolidone (NMP) and 20 mL dichloromethane (DCM) (unless noted otherwise) between individual steps.

Light-Mediated Polymerization and Dehalogenation: Wafer preparation and immobilization of α-bromoisobutyrate (initiating species) on silicon substrates was performed following previously published procedures.[32] Unless otherwise noted, all light-mediated polymerizations were carried out at a light intensity of 5.6 μW mm^{-2} and in a 1:4 v/v mixture of catalyst solution (1.2 mg mL^{-1} tris[2-phenylpyridinato-C^2,*N*]iridium(III) (*fac*-Ir(ppy)$_3$) in NMP) to monomer, as previously reported.[32] Dehalogenation reactions were performed according to previously reported conditions[43] by flooding the chamber with dehalogenation solution and irradiation for 4 h with λ = 405 nm light.

ATRP of 1H,1H,2H,2H-Perfluorodecyl Methacrylate: Inhibitor was removed from 1*H*,1*H*,2*H*,2*H*-perfluorooctyl methacrylate (PFOMA) by flowing the monomer through a short plug of basic alumina. PFOMA (708 μL, 2.45 mmol) and *N*,*N*,*N*′,*N*″,*N*″-pentamethyldiethylenetriamine (PMDETA) (63 μL, 0.3 mmol) were dissolved in 10 mL of *N*,*N*-dimethylformamide (DMF). The solution was sparged under stirring and argon flow for 30 min before transfer to a second, previously degassed vial containing 28 mg (0.2 mmol) copper(I) bromide (CuBr). The resulting PFOMA/PMDETA/CuBr/DMF solution was sparged for another 30 min before transfer into previously degassed vials containing the SiO_2 substrates. The polymerization was terminated by opening the vial to air, followed by repeated rinsing of the wafers with DMF and DCM.

UV Thiol-ene "Click" Reaction of 1H,1H,2H,2H-Perfluorodecanethiol: PEGMA (average M_n = 300 g mol^{-1}) and VMA were copolymerized (1:1 mol%) via (Ir(ppy)$_3$)-catalyzed polymerization on functionalized SiO_2 wafers according the method described above. Thiol-ene coupling was carried out between the surface-anchored vinyl moieties in the backbone of the polymer brushes and 1*H*,1*H*,2*H*,2*H*-perfluorodecanethiol (PFDT) by flooding the stop-flow cell with a solution of PFDT (0.9 mL, 3.1 mmol), 2,2-dimethoxy-2-phenylacetophenone (DMPA) (30 mg, 0.12 mmol), and butylated hydroxytoluene (BHT) (15 mg, 0.07 mmol) in 1.35 mL chlorobenzene and irradiation with λ = 365 nm light for 2 h.

Visible-Light-Mediated Thiol-ene Click Reaction of 1H,1H,2H,2H-Perfluorodecanethiol: Modifying a previously published method,[50] within the stop-flow cell, a uniformly covered a 50:50 mol% statistical copolymer brush composed of PEGMA and VMA (thickness 51.1 ± 0.5 nm) with was covered with a solution of PFDT (0.8 mL, 2.8 mmol), tris(2,2′-bipyridal) ruthenium(II)chloride hexahydrate (Ru(bpy)$_3$Cl$_2$, 0.6 mg, 0.8 mmol), and 4-decylaniline (2 mg, 8.6 mmol) in 2.5 mL NMP. Irradiation with λ = 405 nm light afforded patterned substrates after 30 min at 79% yield (as determined by XPS, see Supporting Information).

Instrumentation and Analysis: Film thicknesses were measured with a Filmetrics F20 by setting silicon oxide (100 nm) as the first layer and the polymer brush as the second layer. Optical images were captured with a Nikon Ellipse E600 optical microscope. Tapping mode atomic force images were recorded using a MFP-3D system (Asylum Research, Santa Barbara, CA). The measurements were conducted using commercial Si cantilevers. XPS was performed using a Kratos Axis Ultra Spectrometer (Kratos Analytical, Manchester, UK) with a monochromatic aluminum K_α X-ray source (1486.6 eV) operating at 225 W under a vacuum of 10^{-8} Torr. Charge compensation was carried out by injection of low-energy electrons into the magnetic lens of the electron spectrometer. The analyzer pass energy was set at 20 eV for high-resolution spectra, and data were recorded at intervals of 0.05 eV. Survey spectra were recorded at 80 eV pass energy. Spectra were analyzed using CasaXPS v.2.3.16 software (Casa Software Ltd.). Unless noted otherwise, XPS spectra were normalized with respect to the carbonyl peak at a binding energy of 288.96 eV. SIMS imaging was performed using a Cameca IMS 7*f* system (Cameca SAS, Gennevilliers, France). A 10 kV Cs+ ion beam and 5 kV negative sample potential were used, for a total impact energy of 15 kV. The 150 pA primary beam was focused to a spot size of approximately 1 μm, and rastered over a 400 μm × 400 μm area. Images of negatively charged secondary ions were typically collected for 20 to 60 s, depending on signal strength. The approximate film etching rate during imaging was 4 Å min^{-1}. The reported contact angles were measured using an OCA 15Pro optical contact-angle measuring instrument (Dataphysics). A 1 μL droplet of deionized water was deposited on the samples and allowed to equilibrate for ≈10 s. Then, the shape of droplet was modeled as a truncated sphere. The reported contact angles are the angles between the tangent and the base of the truncated sphere at the liquid–solid–vapor triple line.

Supporting Information

Supporting Information is available from the Wiley Online Library or from the author.

Acknowledgements

The authors dedicate this work to the late Prof. Edward J. Kramer. C.W.P. acknowledges the Alexander von Humboldt Foundation for financial support. This work was in part supported by the MRSEC Program of the National Science Foundation under Award No. DMR 1121053, the Office of Naval Research (ONR) through Award No. N000141110325, and the Institute for Collaborative Biotechnologies through Grant No. W911NF-09-0001 from the U.S. Army Research Office. K.M.M. and E.H.D. thank the NSF Graduate Research Fellowship for funding. B.N. thanks the Development and Promotion of Science and Technology Talents Project, Royal Government of Thailand Fellowship for funding. B.N., K.M.M., and C.J.H. also thank the PREM program of the National Science Foundation (DMR-1205194) for partial support. The authors thank Dr. Thomas E. Mates for help with acquisition of SIMS data, and Dr. Yair Kaufmann for determination of contact angles. The authors also appreciate fruitful discussions with Dr. Lewis Manring and Prof. Ryan Hayward.

Received: June 1, 2016
Revised: July 14, 2016
Published online: September 12, 2016

[1] E. Almeida, T. C. Diamantino, O. de Sousa, *Prog. Org. Coatings* **2007**, *59*, 2.
[2] H. Murata, B. J. Chang, O. Prucker, M. Dahm, J. Ruhe, *Surf. Sci.* **2004**, *570*, 111.
[3] S. Liang, N. M. Neisius, S. Gaan, *Prog. Org. Coatings* **2013**, *76*, 1642.

[4] K. Norrman, A. Ghanbari-Siahkali, N. B. Larsen, *Annu. Rep. Prog. Chem., Sect. C* **2005**, *101*, 174.
[5] B. Zhao, W. J. Brittain, *Prog. Polym. Sci.* **2000**, *25*, 677.
[6] R. Barbey, L. Lavanant, D. Paripovic, N. Schüwer, C. Sugnaux, S. Tugulu, H. Klok, *Chem. Rev.* **2009**, *109*, 5437.
[7] F. A. Leibfarth, K. M. Mattson, B. P. Fors, H. A. Collins, C. J. Hawker, *Angew. Chem., Int. Ed.* **2013**, *52*, 199.
[8] B. P. Fors, C. J. Hawker, *Angew. Chem., Int. Ed.* **2012**, *51*, 8850.
[9] S. Dadashi-Silab, M. Atilla Tasdelen, Y. Yagci, *J. Polym. Sci., Part A: Polym. Chem.* **2014**, *52*, 2878.
[10] K. Matyjaszewski, J. Xia, *Chem. Rev.* **2001**, *101*, 2921.
[11] Z. Nie, E. Kumacheva, *Nat. Mater.* **2008**, *7*, 277.
[12] O. Azzaroni, *J. Polym. Sci., Part A: Polym. Chem.* **2012**, *50*, 3225.
[13] C. W. Pester, J. E. Poelma, B. Narupai, S. N. Patel, G. M. Su, T. E. Mates, Y. Luo, C. K. Ober, C. J. Hawker, E. J. Kramer, *J. Polym. Sci., Part A: Polym. Chem.* **2016**, *54*, 253.
[14] B. Li, B. Yu, Q. Ye, F. Zhou, *Acc. Chem. Res.* **2015**, *48*, 229.
[15] M. E. Welch, C. K. Ober, *J. Polym. Sci., Part B: Polym. Phys.* **2013**, *51*, 1457.
[16] X. Zhou, X. Liu, Z. Xie, Z. Zheng, *Nanoscale* **2011**, *3*, 4929.
[17] T. Chen, I. Amin, R. Jordan, *Chem. Soc. Rev.* **2012**, *41*, 3280.
[18] U. Schmelmer, A. Paul, A. Küller, M. Steenackers, A. Ulman, M. Grunze, A. Gölzhäuser, R. Jordan, *Small* **2007**, *3*, 459.
[19] A. Olivier, F. Meyer, J. M. Raquez, P. Damman, P. Dubois, *Prog. Polym. Sci.* **2012**, *37*, 157.
[20] T. Wu, K. Efimenko, J. Genzer, *J. Am. Chem. Soc.* **2002**, *124*, 9394.
[21] S. Minko, D. Usov, E. Goreshnik, M. Stamm, *Macromol. Rapid Commun.* **2001**, *22*, 206.
[22] E. Wischerhoff, K. Uhlig, A. Lankenau, H. G. Börner, A. Laschewsky, C. Duschl, J.-F. Lutz, *Angew. Chem., Int. Ed.* **2008**, *47*, 5666.
[23] J. Buensow, T. S. Kelby, W. T. S. Huck, *Acc. Chem. Res.* **2010**, *43*, 466.
[24] O. Azzaroni, B. Trappmann, P. Van Rijn, F. Zhou, B. Kong, W. T. S. Huck, *Angew. Chem., Int. Ed.* **2006**, *45*, 7440.
[25] F. Zhou, P. M. Biesheuvel, E. Y. Choi, W. Shu, R. Poetes, U. Steiner, W. T. S. Huck, *Nano Lett.* **2008**, *8*, 725.
[26] P. M. Mendes, *Chem. Soc. Rev.* **2008**, *37*, 2512.
[27] N. Ayres, *Polym. Chem.* **2010**, *1*, 769.
[28] Q. Wei, T. Becherer, S. Angioletti-Uberti, J. Dzubiella, C. Wischke, A. T. Neffe, A. Lendlein, M. Ballauff, R. Haag, *Angew. Chem., Int. Ed.* **2014**, *53*, 8004.
[29] K. Wolski, M. Szuwarzyński, M. Kopeć, S. Zapotoczny, *Eur. Polym. J.* **2015**, *65*, 155.
[30] R. D. Piner, J. Zhu, F. Xu, S. Hong, C. A. Mirkin, *Science* **1999**, *283*, 661.
[31] W. Eck, V. Stadler, W. Geyer, M. Zharnikov, A. Gölzhäuser, M. Grunze, *Adv. Mater.* **2000**, *12*, 805.
[32] J. E. Poelma, B. P. Fors, G. F. Meyers, J. W. Kramer, C. J. Hawker, *Angew. Chem., Int. Ed.* **2013**, *52*, 6844.
[33] E. H. Discekici, C. W. Pester, N. J. Treat, J. Lawrence, K. M. Mattson, B. Narupai, E. P. Toumayan, Y. Luo, A. J. McGrath, P. G. Clark, J. Read de Alaniz, C. J. Hawker, *ACS Macro Lett.* **2016**, *5*, 258.
[34] M. Kaholek, W. K. Lee, B. LaMattina, K. C. Caster, S. Zauscher, *Nano Lett.* **2004**, *4*, 373.
[35] A. Rastogi, M. Y. Paik, M. Tanaka, C. K. Ober, *ACS Nano* **2010**, *4*, 771.
[36] S. Sun, M. Montague, K. Critchley, M.-S. Chen, W. J. Dressick, S. D. Evans, G. J. Leggett, *Nano Lett.* **2006**, *6*, 29.
[37] G. M. Whitesides, Y. Xia, *Angew. Chem., Int. Ed.* **1998**, *37*, 551.
[38] F. Zhou, Z. Zheng, B. Yu, W. Liu, W. T. S. Huck, *J. Am. Chem. Soc.* **2006**, *128*, 16253.
[39] S. Alom Ruiz, C. S. Chen, *Soft Matter* **2007**, *3*, 168.
[40] M. Steenackers, R. Jordan, A. Küller, M. Grunze, *Adv. Mater.* **2009**, *21*, 2921.
[41] P. Xiao, J. Zhang, F. Dumur, M. A. Tehfe, F. Morlet-Savary, B. Graff, D. Gigmes, J. P. Fouassier, J. Lalevée, *Prog. Polym. Sci.* **2015**, *41*, 32.
[42] J. Lalevée, S. Telitel, P. Xiao, M. Lepeltier, F. Dumur, F. Morlet-Savary, D. Gigmes, J. P. Fouassier, *Beilstein J. Org. Chem.* **2014**, *10*, 863.
[43] K. M. Mattson, C. W. Pester, W. R. Gutekunst, A. T. Hsueh, E. H. Discekici, Y. Luo, B. V. K. J. Schmidt, A. J. McGrath, P. G. Clark, C. J. Hawker, unpublished.
[44] B. P. Fors, J. E. Poelma, M. S. Menyo, M. J. Robb, D. M. Spokoyny, J. W. Kramer, J. H. Waite, C. J. Hawker, *J. Am. Chem. Soc.* **2013**, *135*, 14106.
[45] J. D. Nguyen, J. W. Tucker, M. D. Konieczynska, C. R. J. Stephenson, *J. Am. Chem. Soc.* **2011**, *133*, 4160.
[46] R. M. Arnold, D. L. Patton, V. V. Popik, J. Locklin, *Acc. Chem. Res.* **2014**, *47*, 2999.
[47] D. Dendukuri, S. S. Gu, D. C. Pregibon, T. A. Hatton, P. S. Doyle, *Lab Chip* **2007**, *7*, 818.
[48] H. Wu, T. W. Odom, G. M. Whitesides, *Anal. Chem.* **2002**, *74*, 3267.
[49] C. E. Hoyle, C. N. Bowman, *Angew. Chem., Int. Ed.* **2010**, *49*, 1540.
[50] J. Xu, C. Boyer, *Macromolecules* **2015**, *48*, 520.
[51] L. Makkonen, *Langmuir* **2000**, *16*, 7669.

Appendix B

Novel Strategy for Photopatterning Emissive Polymer Brushes for Organic Light Emitting Diode Applications[4]

[4] Page, Z. A.; **Narupai, B**.; Pester, C. W.; Bou Zerdan, R.; Sokolov, A.; Laitar, D. S.; Mukhopadhyay, S.; Sprague, S.; McGrath, A. J.; Kramer, J. W.; Trefonas, P.; Hawker, C. J. "Novel Strategy for Photopatterning Emissive Polymer Brushes for Organic Light Emitting Diode Applications." *ACS Cent. Sci.* **2017,** *3*, 654-661. DOI: 10.1021/acscentsci.7b00165.

ACS central science

Research Article

http://pubs.acs.org/journal/acscii

Novel Strategy for Photopatterning Emissive Polymer Brushes for Organic Light Emitting Diode Applications

Zachariah A. Page,[†] Benjaporn Narupai,[†,‡] Christian W. Pester,[†] Raghida Bou Zerdan,[†] Anatoliy Sokolov,[§] David S. Laitar,[§] Sukrit Mukhopadhyay,[§] Scott Sprague,[§] Alaina J. McGrath,[†] John W. Kramer,[§] Peter Trefonas,[⊥] and Craig J. Hawker*[,†,‡]

[†]Materials Research Laboratory and [‡]Department of Chemistry and Biochemistry, University of California Santa Barbara, California 93106, United States

[§]The Dow Chemical Company, Midland, Michigan 48674, United States

[⊥]The Dow Electronic Materials Company, 455 Forest Street, Marlborough, Massachusetts 01752, United States

Supporting Information

ABSTRACT: A light-mediated methodology to grow patterned, emissive polymer brushes with micron feature resolution is reported and applied to organic light emitting diode (OLED) displays. Light is used for both initiator functionalization of indium tin oxide and subsequent atom transfer radical polymerization of methacrylate-based fluorescent and phosphorescent iridium monomers. The iridium centers play key roles in photocatalyzing and mediating polymer growth while also emitting light in the final OLED structure. The scope of the presented procedure enables the synthesis of a library of polymers with emissive colors spanning the visible spectrum where the dopant incorporation, position of brush growth, and brush thickness are readily controlled. The chain-ends of the polymer brushes remain intact, affording subsequent chain extension and formation of well-defined diblock architectures. This high level of structure and function control allows for the facile preparation of random ternary copolymers and red−green−blue arrays to yield white emission.

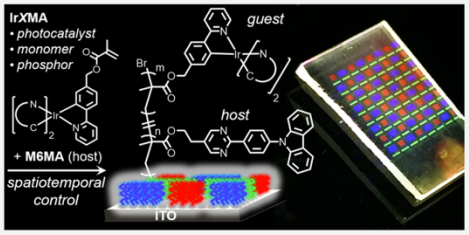

INTRODUCTION

Organic light emitting diode (OLED) displays are among the most energy-efficient two-dimensional display technologies and can be found in everyday appliances, including smartphones, laptops, and televisions.[1,2] However, the efficiency of OLED displays is offset by the cost of production, in part, due to the use of evaporative deposition processes.[3,4] While solution-based methods are attractive alternatives that grant access to low-cost, large area, and high throughput fabrication (e.g., spin-coating, roll-to-roll, etc.), these approaches inherently suffer from limited patterning capabilities. A major challenge is the development of a simple method to generate phosphorescent OLED arrays using solution-based processes.

Display technology often relies on the use of white light to render colored images. Traditionally, white light is obtained by blending red, green, and blue (RGB) emission, which, through clever engineering, can be achieved using a variety of device architectures and pixel layouts.[5−10] Although a number of methods to achieve emissive patterned OLED arrays from solution have been developed, practical limitations such as fabrication complexity, singlet-only emission, scalability issues, low feature resolution, and the use of undesirable reagents have prevented commercialization.[11−15] For example, printing and lithographic techniques require either complex equipment or numerous iterative processing steps,[11−14] while photo-cross-linking is more rapid, but utilizes intense ultraviolet (UV) radiation and photoinitiators[15−19] that contaminate the emissive layer (EML) in an OLED device.

State-of-the-art solution-based patterning procedures achieve spatial resolution either by physically separating the emissive materials during deposition (printing/lithography) or by UV-cross-linking. For the latter approach, the irradiated area is rendered insoluble, which, after washing away un-cross-linked material, allows for subsequent deposition. In contrast to these multistep procedures, surface-initiated growth of polymer brushes has been used for nonpatterned semiconducting[20−23] and patterned insulating polymers[24−29] with a variety of external stimuli being used to provide spatial control.[30,31] In particular, surface initiated atom transfer radical polymerization (SI-ATRP) catalyzed by photoactive Ir(III) phosphors can be used to pattern polymer brushes using visible light,[32] and the "living" nature of this process permits hierarchical patterning of block copolymer brush architectures with submicron feature resolution.[26]

Received: April 16, 2017
Published: June 7, 2017

DOI: 10.1021/acscentsci.7b00165
ACS Cent. Sci. 2017, 3, 654−661

Scheme 1. General Route to Graft Emissive Polymer Brushes from ITO[a]

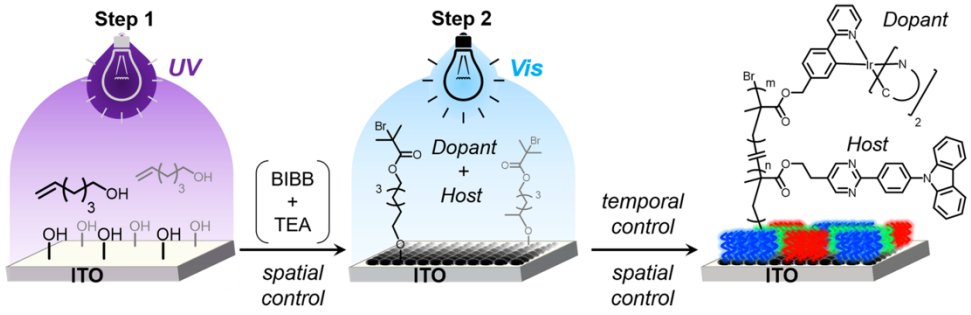

[a]Step 1: functionalization of ITO with 5-hexenol using UV light followed by acylation with α-bromoisobutyryl bromide (BIBB). Step 2: growth of electronically active polymer brushes with visible light.

Significantly, Ir(III) complexes are also widely used as dopants in semiconducting host matrices for OLED devices based on high photoluminescence quantum yield (PLQY), stability, short triplet (T_1) state lifetimes, and spectral tunability from blue to near-infrared.[33−35] In addition, covalent attachment of the Ir(III) complexes to the host mitigates phase separation to further improve device longevity.[36−38]

Here we introduce novel Ir(III) photocatalysts to grow patterned, electronically active, polymer brushes from indium tin oxide (ITO) substrates (Scheme 1). Notably, the Ir(III) species initially acts as a photocatalyst to initiate/mediate polymerization of the brush architectures and then as a covalently bound phosphorescent dopant for patterned OLED devices with a carbazole-based host.[39] Spatiotemporal control, color mixing through copolymerization, chain extension to diblock polymer brushes, and white emission from a red, green, blue pixel array are demonstrated using this novel methodology. As a final demonstration, functional multicolored OLEDs are fabricated to highlight the utility of these materials in next generation display technologies.

■ RESULTS AND DISCUSSION

The host repeat unit, termed **M6MA**, was selected to be a carbazole-phenyl-pyrimidine moiety covalently attached to a polymerizable methacrylate group. **M6MA**, shown in Scheme 2a, was conveniently prepared in four steps from commercial starting materials.[39] To fully address the potential of white light generation, a library of dopant comonomers with emission spanning the visible spectrum, in particular RGB, were prepared, as shown in Scheme 2b. The heteroleptic and functional Ir(III) complexes were synthesized following initial Nonoyama chemistry[40] to prepare the μ-dichloro bridged dimer (**1**), reaction with silver triflate (AgOTf), and coupling with 4-(pyridine-2-yl)benzaldehyde to yield a range of aldehyde derivatives, **2**. Reduction of **2** provides the corresponding hydroxymethyl derivatives (**3**), followed by acylation with methacryloyl chloride to provide the desired iridium monomers, **IrXMA**, where the C^N ligand, **X**, dictates the triplet (T_1) energy and thus emission color. Specifically, **X** represents difluorophenylpyridine (dfppy), phenylpyridine (ppy), phenylquinoline (pq), or benzothiophenylpyridine (btp) (Scheme 2). Copolymerizations of **M6MA** and **IrXMA** under standard radical conditions confirmed monomer compatibility and allowed for basic photophysical characterization of the resultant soluble polymers. The copolymers were found to have unique emission profiles dictated by the **IrXMA** comonomer, granting access to turquoise (dfppy), green (ppy), orange (pq), and red (btp) phosphorescence, while homopolymers of **M6MA** provide deep

Scheme 2. Chemical Structures for (a) M6MA and (b) IrXMA Monomers[a]

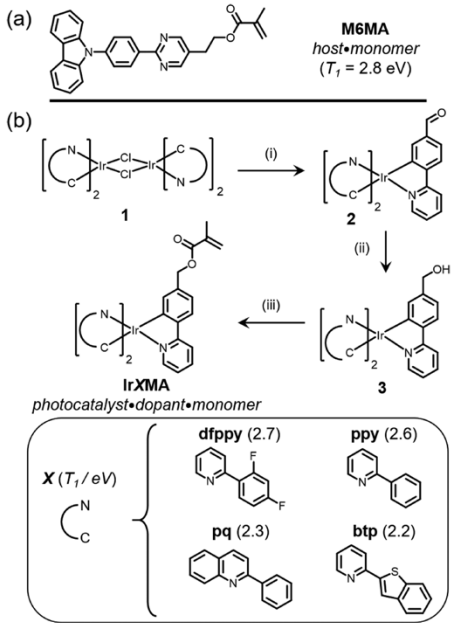

[a]Synthesis of IrXMA, reagents and conditions: (i) AgOTf, 4-(2-pyridyl)benzaldehyde, DMA, 130 °C, 30%. (ii) $NaBH_4$, DCM/EtOH, rt, > 90%. (iii) Methacryloyl chloride, DCM, 0 °C → rt, > 90%. Ligands, their acronyms, and experimental triplet energies provided (bottom).

DOI: 10.1021/acscentsci.7b00165
ACS Cent. Sci. 2017, 3, 654−661

blue fluorescence. It should be noted that the high photoluminescence quantum yield (PLQY ≈ 30−70%) values for the copolymers suggests random monomer incorporation, which mitigates radiative quenching pathways (Table S2).

After establishing monomer compatibility under radical polymerization conditions and examination of the photophysics of the resultant soluble copolymers, an analogous "grafting-from" procedure for polymer brush formation was investigated. Because of its established utility as a transparent electrode in optoelectronic applications, ITO was chosen as the substrate for SI-ATRP. While ITO can be functionalized with silanes and phosphonic acids, these reactions are nonselective.[41] As a result, a photochemical strategy involving the radical coupling with alkenes was chosen, which also provides spatial control.[42,43] Irradiation of ITO with 254 nm UV light in the presence of 5-hexenol followed by acylation of the alcohol functionalized ITO with α-bromoisobutyryl bromide (BIBB) provides initiation sites covalently attached to the surface (Scheme 1, step 1).[44] Surface functionalization was confirmed through X-ray photoelectron spectroscopy (XPS), revealing both bromine and carbonyl functionalities (Figure S11).

Initially, **M6MA** homopolymer brushes were grafted from the initiator-functionalized ITO, using small amounts of $Ir(ppy)_3$ (0.005 mol %) photocatalyst and visible light. The resulting brushes emitted a bright blue fluorescence under UV excitation, characteristic of poly(**M6MA**) thin films measured in our previous study.[39] Since larger quantities of Ir(III) are typically incorporated into the emissive layer of efficient OLEDs, substituting the $Ir(ppy)_3$ photocatalyst with a higher mol % of the **IrXMA** comonomer (1−12 mol %) was considered to be a facile replacement. Indeed, the use of visible light to grow the copolymers provides a library of ITO-tethered brushes having turquoise, green, orange, and red phosphorescence directly matching the analogous soluble polymer samples (Figures 1 and S7). The use of unfunctionalized ITO under the same reaction conditions confirmed that nonspecific polymer adsorption does not occur. The utility of larger quantites of photocatalyst, as is the case for copolymerizations with **IrXMA**, had the added benefit of reducing the amount of light required to elicit brush growth by 1−2 orders of magnitude compared with analogous homopolymer brush growth (Figure S12).[45] Photoluminescence profiles of copolymer brushes (3 mol % **IrXMA**) reveal peak emission wavelengths ranging from 490 to 600 nm with little-to-no residual blue fluorescence from the host, indicative of efficient energy transfer to the Ir(III) dopants. This efficient energy transfer is attributed to the high triplet energy (T_1) of the **M6MA** host ($T_1 \approx 2.8$ eV),[39] relative to the **IrXMA** dopants ($T_1 \lesssim 2.7$ eV) (Tables S1 and S2). XPS was then used to confirm the chemical composition for the five different brushes, with distinct peaks for all brushes. For example, F 1s signals were only observed for poly(**M6MA**-*co*-**IrdfppyMA**) brushes as expected (Figure S13). In addition, indium and tin signals were below detection limits, suggesting uniform coverage with thicknesses exceeding ∼10 nm.

Control of Ir(III) incorporation (i.e., host:dopant ratio) in the emissive layer is critical to overall OLED device performance. To test whether dopant incorporation could be controlled, five different copolymer brushes were grown uniformly on ITO using variable amounts of **IrppyMA** (0, 1, 3, 6, and 12 mol %). XPS was used to determine the chemical composition of the resulting brushes, showing a clear increase in the Ir $4f_{7/2}$ and Ir $4f_{5/2}$ signals at binding energies of 60 and 63 eV, respectively, as the **IrppyMA** loading was increased (Figure 2). Notably, the atomic percent of

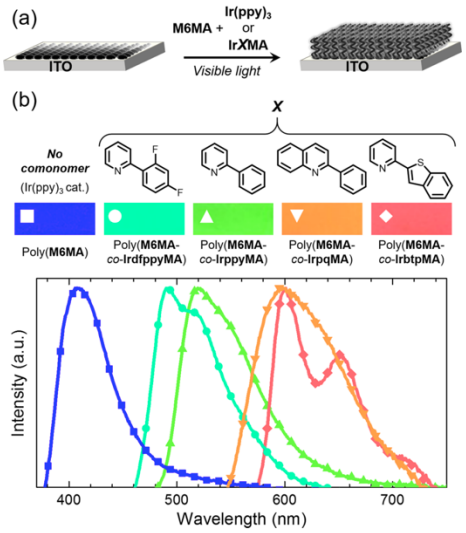

Figure 1. Polymer brushes grafted from ITO using $Ir(ppy)_3$ (0.005 mol %) as the photocatalyst for poly(**M6MA**) and 3 mol % **IrXMA** for copolymers. (a) Schematic representation of grafting from procedure; initiator functionalized ITO to polymer brushes. (b) Chemical structures for C^N ligands (**X**) of **IrXMA** and corresponding photoluminescence profiles. Rectangles are images of the polymer brushes on ITO under 365 nm excitation (Figure S14 for full images).

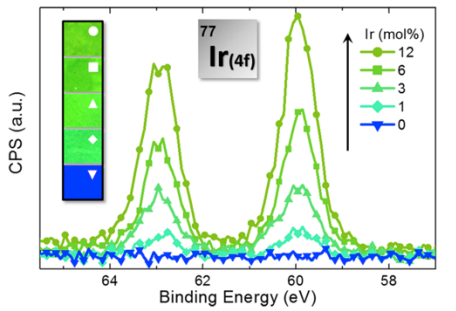

Figure 2. XPS overlay of poly(**M6MA**-*co*-**IrppyMA**) brushes with varied Ir dopant content showing high resolution Ir $4f_{7/2}$ and Ir $4f_{5/2}$ signals at 60 and 63 eV, respectively. Photoluminescence images of the corresponding brushes under 365 nm excitation are provided as an inset.

Ir, relative to carbon, oxygen, and nitrogen, was in good agreement with the expected values (Figure S15). Additionally, photoluminescence measurements on the four copolymer samples reveal a bathochromic shift and broadening of emission for higher **IrppyMA** loadings, which can be observed in the photoluminescence images provided as an inset in Figure 2, and more clearly in the emission profiles given in Figure S16. The noted red-shift and broadening upon increasing dopant content is consistent with the analogous spun-cast soluble polymer samples,[39] indicating that this methodology allows for polymer

DOI: 10.1021/acscentsci.7b00165
ACS Cent. Sci. 2017, 3, 654−661

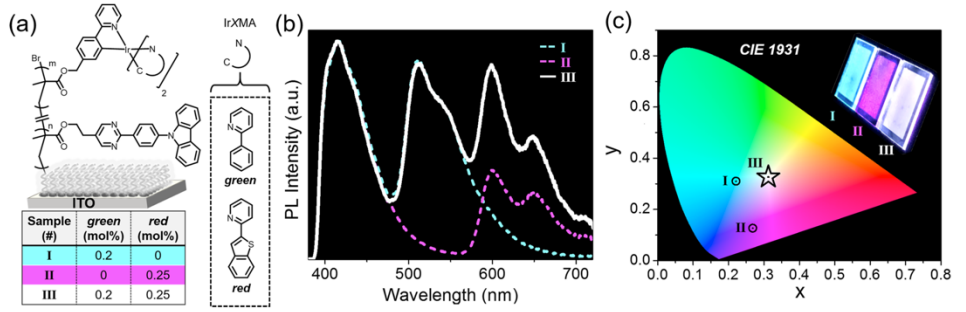

Sample (#)	green (mol%)	red (mol%)
I	0.2	0
II	0	0.25
III	0.2	0.25

Figure 3. White emission from copolymer brushes on ITO. (a) Chemical structures and composition for **I**, poly(**M6MA**-*co*-**IrppyMA**), **II**, poly(**M6MA**-*co*-**IrbtpMA**), and **III** poly(**M6MA**-*co*-**IrppyMA**-*co*-**IrbtpMA**). (b) Photoluminescence profiles showing contributions from red, green, and blue emission for the different copolymer brushes. (c) CIE 1931 coordinates for **I** $(x, y) = (0.22, 0.31)$, **II** $(x, y) = (0.27, 0.13)$, and **III** $(x, y) = (0.31, 0.33)$. Inset is a digital image of the polymer brushes under 365 nm excitation.

brushes with specific dopant content and tunable optical performance to be easily fabricated.

An interesting feature of this copolymer brush strategy is that precise control over dopant concentration makes the generation of white light possible by carefully tuning the composition of red, green, and blue emitting components during random copolymerization (Figure 3a). To demonstrate this ability, we sought to directly obtain white emission by copolymerizing **IrbtpMA** and **IrppyMA** with **M6MA**. In this manner, red and green dopants are copolymerized at low concentration with **M6MA**, allowing for the blue fluorescence from **M6MA** to also be present. Indeed, by carefully tuning the feed ratio of the two **IrXMA** comonomers relative to **M6MA**, white emission was achieved, shown as **sample III** in Figure 3b (Figure S17 for optimization of ternary copolymerizations) with color (x, y) coordinates of (0.31, 0.33) being measured using photoluminescence spectroscopy and matching the white point following 1931 Commission Internationale de L'Éclairage (CIE) guidelines (Figure 3c). It is particularly noteworthy that removing either the red (**I**) or green (**II**) components highlights the respective contribution from each emitter, providing insight into the mechanism of energy transfer within the three component copolymer (**III**) (Figure S18). The difference in peak height for the red emission in **II** and **III** is anticipated, given overlap between the **IrppyMA** emission and **IrbtpMA** absorption, which lends to radiative energy transfer (Figure S18). Visually, there is a dramatic difference between the observable emission colors between **I**, **II**, and **III**, given minute changes in dopant concentrations, as shown in the digital images given as an inset in Figure 3c. This behavior further illustrates the facile emission tunability that is provided with this platform, along with the ability to generate white light for low energy solid-state lighting applications.

For multicolored pixel arrays, the ability to regulate grafting position (e.g., spatial control) is critical and has not been accomplished with electronically active brushes. To investigate this feature, surface patterning using photomasks was examined for either the UV initiator functionalization step (Scheme 1, step 1) or during the visible light-induced polymerization step (Scheme 1, step 2). A chrome coated quartz photomask with transparent rectangular windows (Figure S3, mask 1) was utilized for spatially resolving both light-driven surface chemistries (Figure 4a,b). Significantly, the resulting brushes were spatially resolved in both cases with a notable difference in color for the two reflectance images shown in Figure 4, likely arising from differences in brush height. To further compare both methods, a cross-sectional average of the emission intensity was measured and revealed improved uniformity when employing the photomask during the polymerization process (step 2). Given the superior spatial control achieved during polymer brush growth, this approach was used for all subsequent studies. Moreover, this methodology can be used to provide polymer brush patterns with resolution down to the micron level (Figures 4c and S19), outcompeting state-of-the-art pixels achieved via evaporative deposition ($\sim 5 \times 5\ \mu m^2$).[2,46] These small feature sizes are of particular interest for microdisplay applications, where decreasing pixel dimensions are required to enhance image resolution.[18,47−49]

Since the thickness of each layer in an OLED stack is critical to performance, brush thickness versus time was investigated by patterning poly(**M6MA**) brushes that were grown for different lengths of time followed by analysis with atomic force microscopy (AFM) (details given in the Supporting Information). In Figure 5a the boxed regions are reflectance images, with their center denoted by a cross that corresponds to the specific thickness on the axis, while a 2-point color gradient in between each boxed region was generated from the respective L*,a*,b* color space values as a representation of the theoretical color for any given thickness (Table S4). The distinct color variations for small changes in brush thickness allows for rapid determination of brush height by simply observing the color of reflected white light. In addition, from these results emerged clear evidence for temporal control and direct correlation between polymerization time and brush thickness (Figure S23). To test whether phosphorescent brushes could be grown with temporal control, 6 mol % **IrppyMA** was copolymerized with **M6MA**. The color from reflectance imaging suggests that brush thickness increases with irradiation time, which was further confirmed using AFM of scratched films (Figure 5b). Moreover, the increase in observable emission intensity over time correlates with an increase in brush thickness (Figure 5 inset, bottom). This ability to control copolymer brush formation using only an Ir-functionalized comonomer is significant and illustrates that the generation of phosphorescent pixels of any color on the order of microns in the x, y dimensions and nanometers in the z dimension is possible using this approach.

DOI: 10.1021/acscentsci.7b00165
ACS Cent. Sci. 2017, 3, 654−661

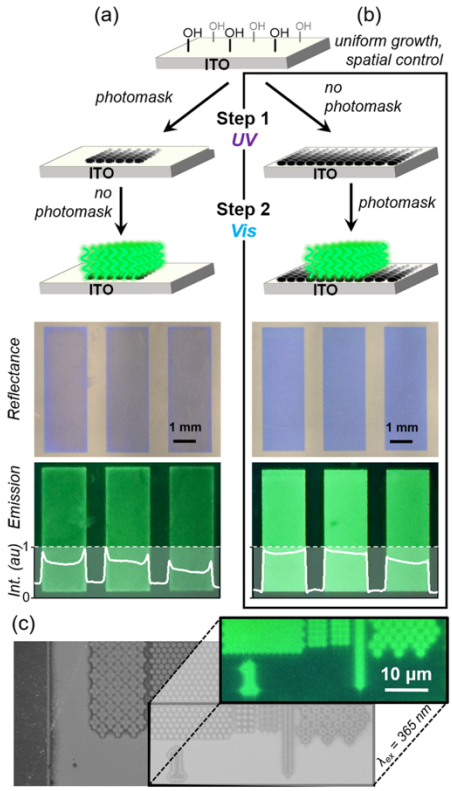

Figure 4. Spatial control for poly(**M6MA**-*co*-**IrppyMA**) brushes containing ~6 mol % **IrppyMA**, after irradiation through a chrome coated quartz photomask at either (a) step 1 (UV) or (b) step 2 (vis). Schematic representation of the functionalization (top) and corresponding reflectance and photoluminescence images. The inset represents normalized emission intensity as a cross-sectional average, showing improved uniformity and spatial control when employing the photomask at step 2. (c) Micron feature resolution obtained by photopatterned polymer grafting (step 2), showing microscopy images (grayscale reflectance and photoluminescence inset, λ_{ex} = 365 nm).

The most efficient OLEDs to date are multilayers, including a hole transport layer (HTL), electron blocking layer (EBL), emissive layer (EML), hole blocking layer (HBL), and electron transport layer (ETL), making it a necessity to extrapolate beyond the copolymer brushes generated herein to act as an EML. Advantageously, the surface-bound brushes are robust, allowing for subsequent layer deposition to achieve multilayered architectures. Alternatively, the "living" nature of the controlled photoATRP process allows for multiblock brush formation, given the presence of active bromide chain-ends. To this point, diblock copolymer architectures with two electronically active blocks were fabricated, both with thicknesses controlled through irradiation time. As a proof of principle, poly(**M6MA**) was grown uniformly on ITO as the first block, followed by growth of patterned copolymers containing **M6MA** and **IrbtpMA** (10 mol

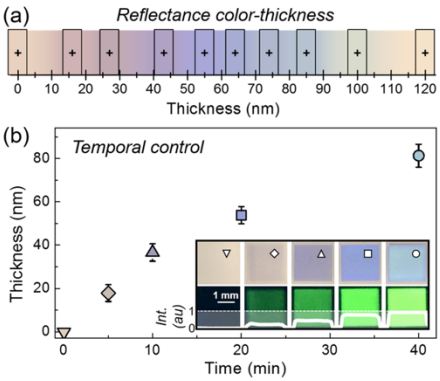

Figure 5. Temporal control over polymer brush growth on ITO. (a) Reflectance color-brush thickness correlation for poly(**M6MA**) determined using AFM and (b) growth of poly(**M6MA**-*co*-**IrppyMA**) over time, using 6 mol % **IrppyMA**. Inset shows reflectance (top) and photoluminescence (bottom, λ_{ex} = 365 nm) images, with normalized emission intensity as a cross-sectional average, demonstrating increased brightness with brush height.

%), to yield poly(**M6MA**-*b*-(**M6MA**-*co*-**IrbtpMA**)) brushes (Figure 6a). The chain extension is evident from photoluminescence spectroscopy, with the appearance of a red emission peak at ~600 nm (Figure 6b). Additionally, reflectance microscopy shows two distinct colors for the first block,

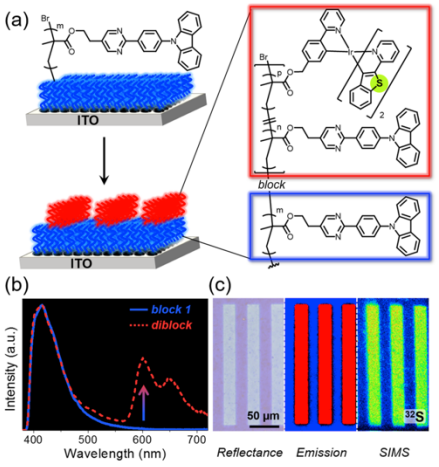

Figure 6. Diblock polymer brushes. (a) Schematic representation for diblock brush growth, and chemical structures for poly(**M6MA**), block 1, and poly(**M6MA**-*b*-(**M6MA**-*co*-**IrbtpMA**)), diblock. (b) Overlaid photoluminescence spectra before (blue solid line) and after (red dashed line) diblock brush growth. (c) Reflectance, emission, and SIMS images (from left to right) of the 20 × 200 μm^2 diblock copolymers. ^{32}S signal detected with SIMS, with increasing counts in going from blue to red.

DOI: 10.1021/acscentsci.7b00165
ACS Cent. Sci. 2017, 3, 654−661

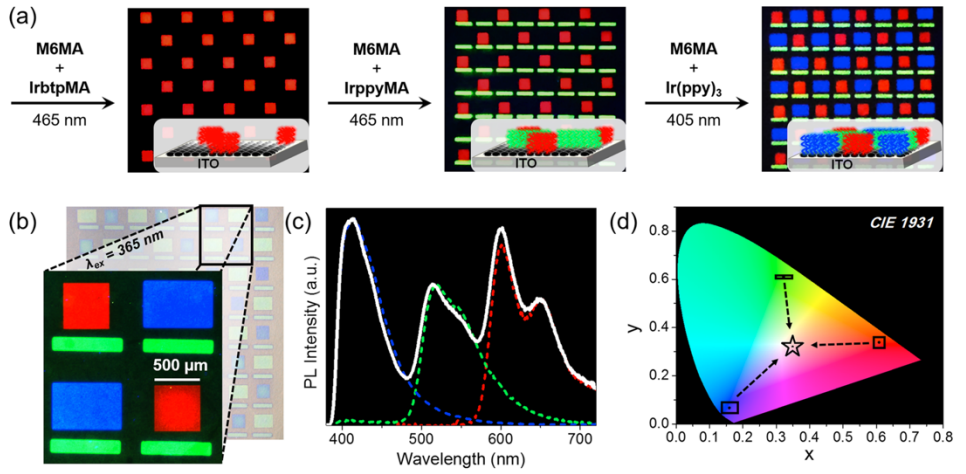

Figure 7. Generation of a red, green, and blue pixel array (PenTile RGBG format) on ITO through stepwise photopolymerizations using three different aligned photomasks. (a) Photoluminescence images (λ_{ex} = 365 nm) of the three step RGBG array fabrication, going from red (poly(**M6MA**-*co*-**IrbtpMA**); 500 × 500 μm^2), to green (poly(**M6MA**-*co*-**IrppyMA**); 125 × 750 μm^2), to blue (poly(**M6MA**); 500 × 750 μm^2) pixels. Schematic representations provided as insets. (b) Reflectance microscopy image and enlarged photoluminescence microscopy image (λ_{ex} = 365 nm) of the array. (c) Photoluminescence profile of the pixel array overlaid with individual RGB emission profiles. (d) CIE 1931 coordinates for the sum emission profile, (x, y) = (0.35, 0.32), shown as the white trace in "c" along with the individual red, (x, y) = (0.61, 0.34), green, (x, y) = (0.32, 0.61), and blue, (x, y) = (0.16, 0.07), coordinates.

poly(**M6MA**), and the diblock copolymer, correlating to a total thickness of ∼45 and 85 nm, respectively (Figure 6c). Photoluminescence microscopy indicates that the dopant resides solely in the 20 × 200 μm^2 rectangles (distinct red emission; Figure 6c), which was further confirmed with secondary ion mass spectrometry (SIMS), detecting the sulfur atoms (^{32}S) present in the **btp** ligand (Figure 6c). To demonstrate versatility, this procedure was also used to generate other diblock copolymer brushes (**M6MA**-*b*-(**M6MA**-*co*-**IrppyMA**)) (Figure S25).

The high degree of spatial control was further illustrated by the preparation of multicolored pixel arrays that are utilized in direct-lit display applications. The PenTile RGBG array of pixels used in active matrix OLEDs and plasma displays was chosen to showcase this methodology (Figure 7). Three chrome-coated glass photomasks were fabricated to contain different sized transparent rectangles for red, green, and blue pixels (masks 9–11, Figure S3), while a substrate holder composed of black Delrin and stainless still pins (Figure S2) was fabricated and used to align the masks. Sequentially, poly(**M6MA**-*co*-**IrbtpMA**), poly(**M6MA**-*co*-**IrppyMA**), and poly(**M6MA**) brushes were grown from ITO, providing red, green, and blue emissive rectangles, respectively (Figure 7a). Figure 7b shows a photoluminescence microscope image of the sample under 365 nm excitation, demonstrating well-defined features for the RGBG arrangement. The total photoluminescence output from the array was measured in an integrating sphere by exciting with UV light to determine the emission profile (Figure 7c) and chromaticity (Figure 7d).

Comparing the photoluminescence profiles for each individual pixel reveals good overlap with the sum "white" emission, demonstrating that it is simply a combination of the three different pixels, as would be the case in a direct-lit display. The chromaticity from the emission profile was generated following CIE guidelines, providing (x, y) coordinates of (0.35, 0.32), which is near the white point, as defined by illuminant DL65, (x, y) = (0.31, 0.33). Figure 7d also shows the individual CIE 1931 coordinates for red, green, and blue, which exhibits the underlying color mixing process that results in the "white" emission. The multicolored patterning clearly demonstrates that this new methodology is an effective way to fabricate pixel arrays from solution for OLED display applications.

As a final demonstration, monochromatic (Figure S27) and multicolored OLED devices were fabricated using the "grafting-from" procedure. Figure 8a provides a schematic representation of the multicolored device, with an architecture (from bottom up) of ITO/EML/HBL/ETL/EIL/Al, where ITO is the anode, polymer brushes comprise the EML, 5-(4-([1,1′-biphenyl]-3-yl)-6-phenyl-1,3,5-triazin-2-yl)-7,7-diphenyl-5,7-dihydroindeno-[2,1-*b*]carbazole acts as the HBL, 2,4-bis(9,9-dimethyl-9*H*-fluoren-2-yl)-6-(naphthalen-2-yl)-1,3,5-triazine comprises the

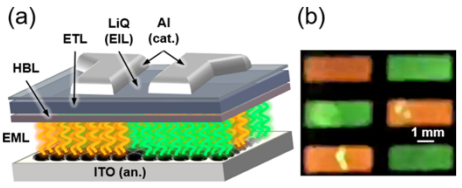

Figure 8. Multicolored OLED composed of poly(**M6MA**-*co*-**IrpqMA**) and poly(**M6MA**-*co*-**IrppyMA**) as the orange and green emitting regions, respectively. (a) Device architecture fabricated from the bottom up: ITO/EML/HBL/ETL/LiQ/Al. (b) Photograph showing electroluminescence of device under forward bias.

DOI: 10.1021/acscentsci.7b00165
ACS Cent. Sci. 2017, 3, 654–661

ETL, 8-hydroxy quinolinato lithium (LiQ), the electron injection layer (EIL), and aluminum (Al), the cathode. Two polymer brushes, poly(**M6MA**-*co*-**IrpqMA**), orange emitter, and poly(**M6MA**-*co*-**IrppyMA**), green emitter, were grafted from six ITO pixels on one glass substrate using low intensity visible irradiation through two chrome-coated glass photomasks (masks 16 and 17, Figure S3). Applying forward bias on a fully fabricated device prototype led to observable electroluminescence for all six pixels and two distinct colors (orange and green) as shown in Figure 8b. Current−voltage−light (JVL) device characterization was not performed owing to poor device lifetime/stability at voltages with observable light emission. Typically, the onset of light emission was observed between 8 and 9 V with images of pixel emission taken between 10 and 13 V. Short circuit formation was the primary failure mechanism between 8 and 13 V of potential. The high driving voltage is attributed to the lack of a hole injection layer, as well as a need for further material/device optimization. Significantly, turn-on of all six pixels suggests excellent brush coverage/uniformity with the potential of this platform for OLED display applications being clearly demonstrated by the ability to fabricate multicolored emissive devices.

CONCLUDING REMARKS

Electronically active and multicolored phosphorescent pixel arrays with remarkable control over size, shape, and architecture were demonstrated using a solution based approach. More specifically, low energy visible light could be used to graft patterned emissive polymer brushes from initiator functionalized ITO. Novel iridium monomers bearing a pendent methacrylate were synthesized and utilized for the dual purpose of catalyzing/mediating controlled radical polymerization and harnessing triplet energy through phosphorescence. The grafting of semiconducting methacrylate-based brushes using photoATRP provided emission spanning the visible spectrum, from blue to red, dictated by the C^N ligand (**X**) on the iridium complex. Moreover, the Ir(III) dopant content within the brushes was controlled by the monomer feed ratio, which allowed for white emission from RGB copolymer brushes. The facile fabrication of RGB pixel arrays for white emission and a working multicolored OLED prototype showcased the utility of this methodology for display applications. This novel platform opens up numerous multidisciplinary research opportunities, including the synthetic development of monomers for improved hole transport, the fabrication of functional nonlinear surfaces for improved light out-coupling, and pixel feature reduction for high resolution microdisplay applications.

ASSOCIATED CONTENT

Supporting Information

The Supporting Information is available free of charge on the ACS Publications website at DOI: 10.1021/acscentsci.7b00165.

Experimental details and further characterization (PDF)

AUTHOR INFORMATION

Corresponding Author

*E-mail: hawker@mrl.ucsb.edu.

ORCID

Craig J. Hawker: 0000-0001-9951-851X

Notes

The authors declare no competing financial interest.

ACKNOWLEDGMENTS

We thank the MRSEC program of the National Science Foundation (DMR 1121053) and The Dow Chemical Company through the Dow Materials Institute at UCSB for financial support. The authors acknowledge the use of the Microfluidics Laboratory and NCF Cleanroom within the California NanoSystems Institute. We thank Dr. David Bothman for help with photomask and substrate holder design and Dr. David Devore (Dow) for insightful discussions. C.W.P. acknowledges the Alexander von Humboldt foundation for financial support.

REFERENCES

(1) Gao, H.-Y.; Yao, Q.-X.; Liu, P.; Zheng, Z.-Q.; Liu, J.-C.; Zheng, H.-D.; Zeng, C.; Yu, Y.-J.; Sun, T.; Zeng, Z.-X. Latest Development of Display Technologies. *Chin. Phys. B* **2016**, *25* (9), 094203.

(2) OLED Microdisplays: Technology and Applications. In *OLED Microdisplays: Technology and Applications*; Templier, F., Ed.; Wiley-ISTE, 2014; pp 231−246.

(3) Diao, Y.; Shaw, L.; Bao, Z.; Mannsfeld, S. C. B. Morphology Control Strategies for Solution-Processed Organic Semiconductor Thin Films. *Energy Environ. Sci.* **2014**, *7*, 2145−2159.

(4) Ho, S.; Liu, S.; Chen, Y.; So, F. Review of Recent Progress in Multilayer Solution-Processed Organic Light-Emitting Diodes. *J. Photonics Energy* **2015**, *5* (1), 057611.

(5) Wu, Z.; Ma, D. Recent Advances in White Organic Light-Emitting Diodes. *Mater. Sci. Eng., R* **2016**, *107*, 1−42.

(6) Gather, M. C.; Köhnen, A.; Meerholz, K. White Organic Light-Emitting Diodes. *Adv. Mater.* **2011**, *23* (2), 233−248.

(7) D'Andrade, B. W.; Forrest, S. R. White Organic Light-Emitting Devices for Solid-State Lighting. *Adv. Mater.* **2004**, *16* (18), 1585−1595.

(8) Wu, S.; Li, S.; Sun, Q.; Huang, C.; Fung, M.-K. Highly Efficient White Organic Light-Emitting Diodes with Ultrathin Emissive Layers and a Spacer-Free Structure. *Sci. Rep.* **2016**, *6*, 25821.

(9) Kim, J. W.; You, S.; Kim, N. H.; Yoon, J.-A.; Cheah, K. W.; Zhu, F. R.; Kim, W. Y. Study of Sequential Dexter Energy Transfer in High Efficient Phosphorescent White Organic Light-Emitting Diodes with Single Emissive Layer. *Sci. Rep.* **2015**, *4*, 7009.

(10) Reineke, S.; Lindner, F.; Schwartz, G.; Seidler, N.; Walzer, K.; Lüssem, B.; Leo, K. White Organic Light-Emitting Diodes with Fluorescent Tube Efficiency. *Nature* **2009**, *459* (7244), 234−238.

(11) Pardo, D. A.; Jabbour, G. E.; Peyghambarian, N. Application of Screen Printing in the Fabrication of Organic Light-Emitting Devices. *Adv. Mater.* **2000**, *12* (17), 1249−1252.

(12) Choi, J.; Kim, D.; Yoo, P. J.; Lee, H. H. Simple Detachment Patterning of Organic Layers and Its Application to Organic Light-Emitting Diodes. *Adv. Mater.* **2005**, *17* (2), 166−171.

(13) Oh, S.; Park, S. K.; Kim, J. H.; Cho, I.; Kim, H.; Park, S. Y. Patterned Taping: A High-Efficiency Soft Lithographic Method for Universal Thin Film Patterning. *ACS Nano* **2016**, *10*, 3478−3485.

(14) Jung, S.-H.; Kim, J.-J.; Kim, H.-J. High Performance Inkjet Printed Phosphorescent Organic Light Emitting Diodes Based on Small Molecules Commonly Used in Vacuum Processes. *Thin Solid Films* **2012**, *520* (23), 6954−6958.

(15) Muller, C. D.; Falcou, A.; Reckefuss, N.; Rojahn, M.; Wiederhirn, V.; Rudati, P.; Frohne, H.; Nuyken, O.; Becker, H.; Meerholz, K. Multi-Colour Organic Light-Emitting Displays by Solution Processing. *Nature* **2003**, *421*, 829−833.

(16) Scheler, E.; Strohriegl, P. Three Color Random Fluorene-Based Oligomers for Fast Micrometer-Scale Photopatterning. *Chem. Mater.* **2010**, *22*, 1410−1419.

(17) Gather, B. M. C.; Köhnen, A.; Falcou, A.; Becker, H.; Meerholz, K. Solution-Processed Full-Color Polymer Organic Light-Emitting Diode Displays Fabricated by Direct Photolithography. *Adv. Funct. Mater.* **2007**, *17*, 191−200.

(18) Ventsch, F.; Gather, M. C.; Meerholz, K. Towards Organic Light-Emitting Diode Microdisplays with Sub-Pixel Patterning. *Org. Electron.* **2010**, *11*, 57−61.

DOI: 10.1021/acscentsci.7b00165
ACS Cent. Sci. 2017, 3, 654−661

(19) Derue, L.; Olivier, S.; Tondelier, D.; Maindron, T.; Geffroy, B.; Ishow, E. All-Solution-Processed Organic Light-Emitting Diodes Based on Photostable Photo-Cross-Linkable Fluorescent Small Molecules. *ACS Appl. Mater. Interfaces* **2016**, *8*, 16207−16217.
(20) Doubina, N.; Jenkins, J. L.; Paniagua, S. A.; Mazzio, K. A.; MacDonald, G. A.; Jen, A. K. Y.; Armstrong, N. R.; Marder, S. R.; Luscombe, C. K. Surface-Initiated Synthesis of poly(3-Methylthiophene) from Indium Tin Oxide and Its Electrochemical Properties. *Langmuir* **2012**, *28* (3), 1900−1908.
(21) Huddleston, N. E.; Sontag, S. K.; Bilbrey, J. A.; Sheppard, G. R.; Locklin, J. Palladium-Mediated Surface-Initiated Kumada Catalyst Polycondensation: A Facile Route towards Oriented Conjugated Polymers. *Macromol. Rapid Commun.* **2012**, *33* (24), 2115−2120.
(22) Beryozkina, T.; Boyko, K.; Khanduyeva, N.; Senkovskyy, V.; Horecha, M.; Oertel, U.; Simon, F.; Stamm, M.; Kiriy, A. Grafting of Polyfluorene by Surface-Initiated Suzuki Polycondensation. *Angew. Chem., Int. Ed.* **2009**, *48* (15), 2695−2698.
(23) Snaith, H. J.; Whiting, G. L.; Sun, B.; Greenham, N. C.; Huck, W. T. S.; Friend, R. H. Self-Organization of Nanocrystals in Polymer Brushes. Application in Heterojunction Photovoltaic Diodes. *Nano Lett.* **2005**, *5* (9), 1653−1657.
(24) Yan, J.; Pan, X.; Schmitt, M.; Wang, Z.; Bockstaller, M. R.; Matyjaszewski, K. Enhancing Initiation Efficiency in Metal-Free Surface-Initiated Atom Transfer Radical Polymerization (SI-ATRP). *ACS Macro Lett.* **2016**, *5* (6), 661−665.
(25) Narupai, B.; Poelma, J. E.; Pester, C. W.; McGrath, A. J.; Toumayan, E. P.; Luo, Y.; Kramer, J. W.; Clark, P. G.; Ray, P. C.; Hawker, C. J. Hierarchical Comb Brush Architectures via Sequential Light-Mediated Controlled Radical Polymerizations. *J. Polym. Sci., Part A: Polym. Chem.* **2016**, *54* (15), 2276−2284.
(26) Pester, C. W.; Narupai, B.; Mattson, K. M.; Bothman, D. P.; Klinger, D.; Lee, K. W.; Discekici, E. H.; Hawker, C. J. Engineering Surfaces through Sequential Stop-Flow Photopatterning. *Adv. Mater.* **2016**, *28*, 9292−9300.
(27) Discekici, E. H.; Pester, C. W.; Treat, N. J.; Lawrence, J.; Mattson, K. M.; Narupai, B.; Toumayan, E. P.; Luo, Y.; McGrath, A. J.; Clark, P. G.; Read De Alaniz, J.; Hawker, C. J. Simple Benchtop Approach to Polymer Brush Nanostructures Using Visible-Light-Mediated Metal-Free Atom Transfer Radical Polymerization. *ACS Macro Lett.* **2016**, *5* (2), 258−262.
(28) Li, B.; Yu, B.; Ye, Q.; Zhou, F. Tapping the Potential of Polymer Brushes through Synthesis. *Acc. Chem. Res.* **2015**, *48* (2), 229−237.
(29) Poelma, J. E.; Fors, B. P.; Meyers, G. F.; Kramer, J. W.; Hawker, C. J. Fabrication of Complex Three-Dimensional Polymer Brush Nanostructures through Light-Mediated Living Radical Polymerization. *Angew. Chem., Int. Ed.* **2013**, *52* (27), 6844−6848.
(30) Leibfarth, F. A.; Mattson, K. M.; Fors, B. P.; Collins, H. A.; Hawker, C. J. External Regulation of Controlled Polymerizations. *Angew. Chem., Int. Ed.* **2013**, *52*, 199−210.
(31) Li, B.; Yu, B.; Huck, W. T. S.; Liu, W.; Zhou, F. Electrochemically Mediated Atom Transfer Radical Polymerization on Nonconducting Substrates: Controlled Brush Growth through Catalyst Diffusion. *J. Am. Chem. Soc.* **2013**, *135*, 1708−1710.
(32) Fors, B. P.; Hawker, C. J. Control of a Living Radical Polymerization of Methacrylates by Light. *Angew. Chem., Int. Ed.* **2012**, *51* (35), 8850−8853.
(33) Lamansky, S.; Djurovich, P.; Murphy, D.; Abdel-Razzaq, F.; Lee, H. E.; Adachi, C.; Burrows, P. E.; Forrest, S. R.; Thompson, M. E. Highly Phosphorescent Bis-Cyclometalated Iridium Complexes: Synthesis, Photophysical Characterization, and Use in Organic Light Emitting Diodes. *J. Am. Chem. Soc.* **2001**, *123* (18), 4304−4312.
(34) Ulbricht, C.; Beyer, B.; Friebe, C.; Winter, A.; Schubert, U. S. Recent Developments in the Application of Phosphorescent iridium(III) Complex Systems. *Adv. Mater.* **2009**, *21*, 4418−4441.
(35) Deng, Y.-L.; Cui, L.-S.; Liu, Y.; Wang, Z.-K.; Jiang, Z.-Q.; Liao, L.-S. Solution-Processable Iridium Phosphors for Efficient Red and White Organic Light-Emitting Diodes with Low Roll-Off. *J. Mater. Chem. C* **2016**, *4*, 1250−1256.
(36) Sudhakar, M.; Djurovich, P. I.; Hogen-Esch, T. E.; Thompson, M. E. Phosphorescence Quenching by Conjugated Polymers. *J. Am. Chem. Soc.* **2003**, *125*, 7796−7797.
(37) Sandee, A. J.; Williams, C. K.; Evans, N. R.; Davies, J. E.; Boothby, C. E.; Kohler, A.; Friend, R. H.; Holmes, A. B. Solution-Processible Conjugated Electrophosphorescent Polymers. *J. Am. Chem. Soc.* **2004**, *126*, 7041−7048.
(38) Poulsen, B. D. A.; Kim, B. J.; Ma, B.; Zonte, C. S.; Frechet, J. M. J. Site Isolation in Phosphorescent Bichromophoric Block Copolymers Designed for White Electroluminescence. *Adv. Mater.* **2010**, *22*, 77−82.
(39) Page, Z. A.; Chiu, C.-Y.; Narupai, B.; Laitar, D. S.; Mukhopadhyay, S.; Sokolov, A.; Hudson, Z. M.; Bou Zerdan, R.; McGrath, A. J.; Kramer, J. W.; Barton, B. E.; Hawker, C. J. Highly Photoluminescent Nonconjugated Polymers for Single-Layer Light Emitting Diodes. *ACS Photonics* **2017**, *4*, 631−641.
(40) Nonoyama, M. Benzo[h]quinolin-10-Yl-N Iridium(III) Complexes. *Bull. Chem. Soc. Jpn.* **1974**, *47*, 767−768.
(41) Pujari, S. P.; Scheres, L.; Marcelis, A. T. M.; Zuilhof, H. Covalent Surface Modification of Oxide Surfaces. *Angew. Chem., Int. Ed.* **2014**, *53* (25), 6322−6356.
(42) Li, Y.; Giesbers, M.; Gerth, M.; Zuilhof, H. Generic Top-Functionalization of Patterned Antifouling Zwitterionic Polymers on Indium Tin Oxide. *Langmuir* **2012**, *28* (34), 12509−12517.
(43) Li, Y.; Zuilhof, H. Photochemical Grafting and Patterning of Organic Monolayers on Indium Tin Oxide Substrates. *Langmuir* **2012**, *28* (12), 5350−5359.
(44) Huang, C.; Tassone, T.; Woodberry, K.; Sunday, D.; Green, D. L. Impact of ATRP Initiator Spacer Length on Grafting Poly(methyl Methacrylate) from Silica Nanoparticles. *Langmuir* **2009**, *25*, 13351−13360.
(45) Dolinski, N. D.; Page, Z. A.; Eisenreich, F.; Niu, J.; Hecht, S.; Read de Alaniz, J.; Hawker, C. J. A Versatile Approach for In Situ Monitoring of Photoswitches and Photopolymerizations. *ChemPhotoChem.* **2017**, *1*, 125−131.
(46) Chung, Y.; Murmann, B.; Selvarasah, S.; Dokmeci, M. R.; Bao, Z. Low-Voltage and Short-Channel Pentacene Field-Effect Transistors with Top-Contact Geometry Using Parylene-C Shadow Masks. *Appl. Phys. Lett.* **2010**, *96*, 133306.
(47) Ji, Y.; Ran, F.; Xu, H.; Shen, W.; Zhang, J. Improved Performance and Low Cost OLED Microdisplay with Titanium Nitride Anode. *Org. Electron.* **2014**, *15* (11), 3137−3143.
(48) Xie, G.; Xue, Q.; Chen, P.; Tao, C.; Zhao, C.; Lu, J.; Gong, Z.; Zhang, T.; Huang, R.; Du, H.; Xie, W.; Hou, J.; Zhao, Y.; Liu, S. Highly Efficient and Low-Cost Top-Emitting Organic Light-Emitting Diodes for Monochromatic Microdisplays. *Org. Electron.* **2010**, *11* (3), 407−411.
(49) Can, C.; Underwood, I. Compact and Efficient RGB to RGBW Data Conversion Method and Its Application in OLED Microdisplays. *J. Soc. Inf. Disp.* **2013**, *21* (3), 109−119.

DOI: 10.1021/acscentsci.7b00165
ACS Cent. Sci. 2017, 3, 654−661